

**SYNTHESIS AND PROPERTIES OF
MULTIFUNCTIONAL SINGLE MOLECULE MAGNETS**

MATHIEU GONIDEC

Doctoral Thesis

**Programa de doctorat en
Ciència de Materials**

**Supervised by David B. Amabilino
and Jaume Veciana Miró**

**Departament de Química
Facultat de Ciències**

2010

Memòria presentada per aspirar al Grau de Doctor per Mathieu Gonidec

Vist i plau,

Els directors,

Prof. David B. Amabilino

Prof. Jaume Veciana i Miró

Bellaterra, 07/07/2010



David B. AMABILINO i **Jaume VECIANA i MIRÓ**, investigadors principals del CSIC en el Institut de Ciència de Materials de Barcelona (ICMAB-CSIC)

CERTIFIQUEN

Que el **Mathieu GONIDEC**, Màster en Química Molecular i Supramolecular i Enginyer Superior Químic, va realitzar el treball d'investigació portant el títol: “**Synthesis and Properties of Multifunctional Single Molecule Magnets**”. Aquest treball s'ha desenvolupat en el marc del programa de doctorat en Ciència de Materials del departament de Química de la Universitat Autònoma de Barcelona.

I perquè consti, signen el present certificat.

Prof. David B. Amabilino

Prof. Jaume Veciana i Miró

Bellaterra, 7 de Juliol del 2010



ACKNOWLEDGEMENTS

The realization of this PhD Thesis was a long and studious task. For this reason, I would like to thank all the people that helped me during its realization, on a scientific, personal and financial basis.

I would like first to thank warmly my two directors David Amabilino and Jaume Veciana for giving me the opportunity to perform this work at the ICMAB and for believing in it from the beginning to the end. I would like to thank them especially for their guidance all the way through this work and for always finding time to be available when I needed advice and comfort, despite their always very busy schedule.

I would like to thank the institution that provided financial support to this work, the Marie Curie 6th Framework program for providing the funding allowing me to perform this work and to attend many conferences and meetings.

I would like to thank also all of those who worked in the groups during these four years, for their friendship and support, and for stoically bearing with me telling them about my work over and over again, for all of these reasons, thank you Adam, Alba, Amable, Angela B., Angela D., Carme, Cesar, Claudia, Concepció, Dani R., Dani V., Elena B., Elena L., Elena R., Elisa, Emi, Evelyn, Filippo, François, Ingrid, Inhar, Inma, Inna, Javi, Josep, Judit, Lise, Lourdes, Luca, Magalí, Malena, Maria C., Maria M., Marta, Nans, Neil, Nora, Nuria, Paco O., Paco V., Patrizia, Pepe, Raphael, Santi, Vega, Veronica, Victor, Vladimir, Wojciech. In such a long list I hope I didn't forget anyone and I present my most sincere apologies if I did.

During this PhD work, I had the opportunity to stay several weeks at Martin Schroeder's lab at the school of chemistry in Nottingham and I'd like to thank him for giving me this opportunity, I'd like to also warmly thank Jonathan McMaster and Steve Davies for greeting me in Nottingham and working with me during these short stays. Of course I'd like to thank all of the Students in Nottingham who made my life easier, helped me in the lab and kept me entertained, including Illich, Marco, Charlotte, Dorothée, Alex, Emma, Eduardo and Nacho.

I am very grateful to Fernando Luis for greeting me in his lab during one week in Zaragoza, for his company and for his efficiency, dedicating me 100% of his time during my stay in Zaragoza, and being always very available and efficient during the time it took us to properly analyze the results.

I would like to thank Roberto Biagi for the great experiments he performed and for his dedication to our project.

I would also like to thank Jordi Esquena for inviting me to do some measurements in his lab in Barcelona, and for helping me out with the interpretation of the results. Many thanks also to his student Àlex Vilchez who dedicated me a lot of his time in order to prepare and characterize my samples while he was already busy with his owns.

On a more personal basis, I would like to thank all of my friends in Barcelona, including my team, Castellans de Barcelona who introduced me to their ways of living and taught me their language. Being part of the team makes me feel part of this country, part of this region, it makes me feel I belong.

Of my first years here I would like to thank warmly Oli who moved to Catalunya from Strasbourg at the same time I did and made it easier to feel at ease in a new city that was at first full of strangers. I will always remember these weekends shared between Tarragona and Barcelona, discovering two new cities at a time, those were very good times.

I will always be grateful to my family for their support, and for shaping me into who I am over the years, for better or for worse! My grandparents, whose combined abilities probably helped me through this work, my parents, brothers and sisters who always encouraged me, cheering me up in the bad days, sharing the joys of the good ones and whose occasional visits made my life here all the merrier. And last but not least, I would like to thank “my” Isabel, for these years spent together, and for those to come, for her love and patience bearing with me trying to explain her Molecular Magnetism, Chemistry and all sorts of things, for overlooking my compulsive (and probably hereditary) need to check just about anything in a dictionary or on the internet at any moment. I would also like to apologize to her, to my colleagues and to anyone who has known me over the last few months for my bad temper during the writing of this PhD thesis, being the result of a stimulating but tiring and stressing work.

This work could not have been done without the participation and support of all of the above persons or institutions, so once again: **Thank You All.**

ABBREVIATIONS

AFM: Atomic Force Microscopy
CD: Circular Dichroism spectroscopy
CV: Cyclic Voltammetry
DBU: Diazabicyclo-undecene
DCC: Dicyclohexylcarbodiimide
DCM: Dichloromethane
DFT: Density Functional Theory
DMA: Dimethylacetamide
DMAP: Dimethylaminopyridine
DMF: Dimethylformamide
DMSO: Dimethylsulfoxide
DSC: Differential Scanning Calorimetry
EPR: electron Paramagnetic Resonance
FT-IR: Fourier Transform-Infra Red spectroscopy
HOPG: Highly Oriented Pyrolytic Graphite
LDI-TOF-MS: Laser Desorption Ionization Time of Flight Mass Spectrometry
m.p.: melting point
M.W.: Molecular Weight
MCD: Magnetic Circular Dichroism
MFM: Magnetic Force Microscopy
NMR: Nuclear Magnetic Resonance
POM: Polarizing Optical Microscopy
QTM: Quantum Tunneling of Magnetization
SAM: Self-Assembled Monolayer
SAXS: Small Angle X-ray Scattering
SCE: Saturated Calomel Electrode
SMM: Single Molecule Magnet
SP-STM: Spin Polarized-Scanning Tunneling Microscopy
SQUID: Superconducting Quantum Interference Device
THF: Tetrahydrofuran
UHV: Ultra High Vacuum
UV-Vis: Ultra Violet-Visible absorption spectroscopy
VSM: Vibrating Sample Magnetometer
XAS: X-ray Absorption Spectroscopy
XMCD: X-ray Magnetic Circular Dichroism

TABLE OF CONTENT

CHAPTER 1

Introduction	1
1-1 Magnetism: Historical perspective	1
1-2 Magnetization hysteresis	2
1-3 Molecular magnetic materials	3
1-4 Single-Molecule Magnets	5
1-4-1 $[\text{Mn}_{12}\text{O}_{12}(\text{CH}_3\text{COO})_{16}(\text{H}_2\text{O})_4]$ or Mn_{12}ac	5
1-4-2 Quantum tunneling of magnetization in Mn_{12}ac	8
1-4-3 Structural disorder in Mn_{12}ac	11
1-4-4 Dilute-solution experiments	12
1-4-5 Other single-molecule magnets based on transition metals	14
1-4-5-1 Manganese clusters	14
1-4-5-2 Iron clusters	17
1-5 Single-ion magnets	19
1-5-1 Recent SMMs based on single metal ions	20
1-5-1-1 Lanthanide polyoxometalates	20
1-5-1-2 A SMM based on a single iron (II) metal ion	22
1-5-2 Double-decker lanthanide complexes	24
1-5-2-1 Magnetic properties of double-decker lanthanide complexes	24
1-5-2-2 Physico-chemical properties of double-decker phthalocyanine lanthanide complexes	31
1-6 Applications with single-molecule magnets	34
Bibliography	36

CHAPTER 2

Objectives	41
-------------------	-----------

CHAPTER 3

Synthesis of double-decker phthalocyanine terbium complexes	43
3-1 Introduction	43
3-2 Synthesis of phthalonitriles	44
3-2-1 Preparation of substituted phthalonitriles from 1,2-dibromocatechol	44
3-2-2 Functionalization of 4,5-dichlorophthalonitrile with alkylthiolates	49
3-2-3 Preparation of functionalized phthalonitriles from 4,5-dichlorophthalic acid	51
3-3 Synthesis of metal free phthalocyanines	54
3-4 Synthesis of double-decker phthalocyanine complexes	57
3-4-1 Two-step synthesis of double-decker phthalocyanine complexes	58
3-4-2 One-step synthesis of double-decker phthalocyanine complexes	61
3-4-3 Synthesized complexes used for magnetic characterizations	64

Bibliography	66
--------------	----

CHAPTER 4

Magnetic behavior of three redox states of a SMM in solution	67
4-1 Introduction	67
4-2 Redox chemistry of complexes ${}^i\text{Pc}_2\text{Tb}$ and ${}^{C15}\text{Pc}_2\text{Tb}$	68
4-2-1 Spectroelectrochemistry of complex ${}^i\text{Pc}_2\text{Tb}$ (${}^i\text{Pc}_2\text{Tb}$)	70
4-2-2 Spectroelectrochemistry of complex ${}^{C15}\text{Pc}_2\text{Tb}$	79
4-3 Magnetic circular dichroism set-up	81
4-4 Magnetic circular dichroism measurements	84
4-4-1 Preparation and characterization of the samples	84
4-4-2 MCD spectra of three redox states of complex ${}^i\text{Pc}_2\text{Tb}$	86
4-4-3 Magnetization data from MCD measurements	89
4-4-3-1 Magnetization hysteresis of three redox states of complex ${}^i\text{Pc}_2\text{Tb}$ studied by MCD	89
4-4-3-2 Magnetic relaxation of three redox states of complex ${}^i\text{Pc}_2\text{Tb}$ studied by MCD	95
4-5 Conclusions	103
Bibliography	103

CHAPTER 5

Magnetic behavior of a double-decker complex on graphite	105
5-1 Introduction	105
5-2 Synthesis of the double-decker complexes ${}^i\text{Pc}_2\text{Tb}$, ${}^{C15}\text{Pc}_2\text{Tb}$ and ${}^{C22}\text{Pc}_2\text{Tb}$	107
5-3 Dropcasting the double-decker complexes ${}^i\text{Pc}_2\text{Tb}$, ${}^{C15}\text{Pc}_2\text{Tb}$ and ${}^{C22}\text{Pc}_2\text{Tb}$ on graphite	109
5-3-1 Dropcasting of ${}^i\text{Pc}_2\text{Tb}$ from toluene	109
5-3-2 Surface deposition of ${}^{C15}\text{Pc}_2\text{Tb}$	115
5-3-3 Surface deposition of ${}^{C22}\text{Pc}_2\text{Tb}$	118
5-3-3-1 Atomic force microscopy measurements on a monolayer of ${}^{C22}\text{Pc}_2\text{Tb}$ on HOPG	118
5-3-3-2 Magnetic force microscopy measurements on a monolayer of ${}^{C22}\text{Pc}_2\text{Tb}$ on HOPG	119
5-4 Magnetic characterizations of double-decker terbium complexes deposited on HOPG	121
5-4-1 Magnetic behavior of a bulk sample of ${}^i\text{Pc}_2\text{Tb}$	123
5-4-2 Magnetic behavior of a monolayer of ${}^i\text{Pc}_2\text{Tb}$ deposited on HOPG	126
5-4-2-1 Magnetic behavior of the neutral complex $[{}^i\text{Pc}_2\text{Tb}]^0$ on HOPG	126
5-4-2-2 Magnetic behavior of the anionic complex $[{}^i\text{Pc}_2\text{Tb}]^-$ on HOPG	129
5-5 Conclusions	133
Bibliography	134

CHAPTER 6

A liquid crystalline single-molecule magnet	135
6-1 Introduction	135
6-2 Synthesis and characterization of the studied compound	136
6-3 Study of the mesomorphic behaviors of compounds 22 and 27	141

6-4 Processing of the liquid crystalline complex 27 and preparation of samples with different supramolecular structures	146
6-5 Study of the magnetic properties of materials deriving from 27 with different supramolecular structures.	151
6-5-1 Temperature dependent ac magnetic susceptibility measurements	151
6-5-2 Frequency dependent ac magnetic susceptibility measurements	156
Bibliography	166
CHAPTER 7	
Experimental	169
7-1 Techniques and instruments	169
7-2 Reactants and chromatography	171
7-3 Synthesis and characterization	171
CHAPTER 8	
Conclusions	199
APPENDIX I	
Magnetic circular dichroism	201
APPENDIX II	
X-ray magnetic circular dichroism	207
II-1 Definition and conventions	207
II-2 Principles and nomenclature	207
II-3 Chemical specificity	208
II-4 Detection methods	210
II-5 Sum rules	211
II-6 Conclusions	212
APPENDIX III	
ARTICLES	213

CHAPTER 1

INTRODUCTION

1-1 Magnetism: Historical perspective

Magnetism is one of the most important physical phenomena in the universe. It is ubiquitous in both natural and technological matters, from the earth's magnetic field to many components of electronic devices which are part and parcel of our everyday life. The first observation of a magnetic phenomenon is credited to Thales of Miletus, a philosopher of ancient Greece who accounted for the attraction of lodestone to iron as early as the 6th century B.C. At the time, lodestone, a naturally magnetized piece of magnetite (or Fe_3O_4), was found in Magnesia, in ancient Thessaly, Greece, which explains the origin of the word "magnet". On the other hand, in an article about the origin of the compass,^[1] Li Shu-hua credits the earliest description of an observation of the effect of magnetism in ancient China to a document written in the fourth century BC, the *Liu-che-tch'ouen-ts'ieou* that reads: "The lodestone makes iron come or it attracts it". In ancient Chinese, lodestone was called "ts'eu-che" which literally means "loving stone" or in French "pierre aimant" due to its attraction to iron, which by literal translation from the chinese is thought to be the origin of the French word for magnet: "aimant".

The observation of the attraction of lodestone to iron was repeated over centuries by an incredible number of scientists, who sometimes compared it to the love of the mother caring for her children,^[2] or to the attraction of newlyweds.^[3] But it took centuries for lodestone to pass from a scientific curiosity to an actual functional material. Indeed, it was not until the 12th century D.C. that the Chinese used a lodestone based compass for navigation, which was the first milestone of a long series of scientific discoveries leading to the exploitation of magnetism as a more general fundamental tool. Ever since the early example of the compass, magnetic materials have been little by little incorporated in our everyday life. Permanent magnets can be found in our hard-disk

[1] L. Shu-hua, *Isis* **1954**, 45, 175-196.

[2] L. Tche-tchen, *pen-ts'ao-kang-mou*, **1580**.

[3] G. B. Porta, *Natural Magick*, **1589**.

drives and credit cards as recording media and are also present in electromechanical transducer devices such as electric motors, audio speakers or microphones.

1-2 Magnetization hysteresis

A magnet is a material that can be magnetized and can present a permanent magnetic moment in the absence of any exterior magnetic field. The main characteristics of a magnet are the parameters of its hysteresis of magnetization, which are its remnant magnetization and its coercive field (see Figure 1-1).

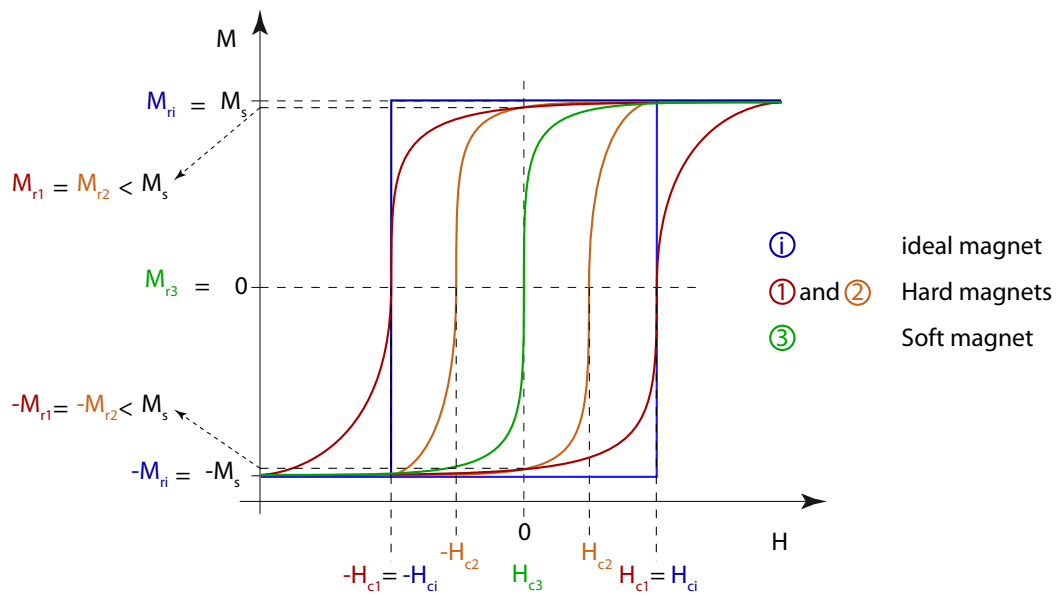


Figure 1-1. Magnetization hysteresis plots of four model magnets indicating their coercive fields H_c and remnant magnetizations M_r .

Magnets are in essence bistable systems which can be magnetized along one particular z direction or the opposite direction $-z$. When applying a sufficiently high magnetic field along z , magnets are magnetized at a saturation magnetization value M_s . When the external magnetic field is removed, hard magnets maintain a non zero permanent magnetization called remnant magnetization M_r . If one applies an external magnetic field along $-z$ then the magnet saturates at a magnetization value of $-M_s$ and when removing the magnetic field, the remnant magnetization value is now $-M_r$.

For an ideal magnet (see Figure 1-1) the magnitude of the remnant magnetization M_{ri} is equal to the saturation magnetization M_s , nevertheless in a real hard magnet, the remnant magnetization is usually lower than the saturation value and the value varies

from one magnet to the other. Simply put, the value of M_r is the relative amount of magnetization that the magnet maintains when in the absence of an external magnetic field.

In order to flip the magnetization of a hard magnet from positive to negative value, it is necessary to apply a magnetic field strong enough to destroy the cohesion of the magnet. The field at which such a flipping occurs is therefore called the coercive field. This is the other important parameter of the magnetization hysteresis curves of hard magnets. Finally, a soft magnet is a material that can be magnetized but shows no magnetization hysteresis, which translates into $H_c = 0$ and $M_r = 0$. Figure 1-1 illustrates the magnetization versus field curves obtained for an ideal magnet (i), two hard magnets with different values of H_c (1 and 2) and a soft magnet (3).

1-3 Molecular magnetic materials

While most of the applications of magnetic materials to date are based on bulk metals or metal oxides, a new field of research emerged, around the end of the 20th century, to investigate the properties of molecular magnetic materials.^[4-8] Initially, the research in molecular magnetic materials started with Magnetochemistry, which is a branch of chemistry which uses physical measurements, and more specifically magnetic techniques, to obtain structural and electronic information on simple paramagnetic systems.^[9] In the 1980s the potential for low cost processing and chemical tuning of molecular materials induced a shift to a new research field, the “Molecular Magnetism”,^[10] envisaged as an essentially multidisciplinary field that aims at combining the knowledge of chemists with those of theoretical chemists and physicists in order to design molecular magnetic materials and predict and rationalize their physical properties. The research activity of the field was conducted in several directions. While some groups investigated the possibility to obtain purely organic

[4] J. S. Miller and M. Drillon, *Magnetism: Molecules to Materials I, Models and Experiments*, Wiley-VCH, **2001**.

[5] J. S. Miller and M. Drillon, *Magnetism: Molecules to Materials II, Molecule-based Materials*, Wiley-VCH, **2001**.

[6] J. S. Miller and M. Drillon, *Magnetism: Molecules to Materials III, Nanosized Magnetic Materials*, Wiley-VCH, **2002**.

[7] J. S. Miller and M. Drillon, *Magnetism: Molecules to Materials IV*, Wiley-VCH, **2003**.

[8] J. S. Miller and M. Drillon, *Magnetism: Molecules to Materials V*, Wiley-VCH, **2005**.

[9] R. L. Carling, *Magnetochemistry*, Springer-Verlag, **1986**.

[10] O. Kahn, *Molecular Magnetism*, VCH Publishers, **1993**.

ferromagnets, others tried to push up the ordering temperatures, which are typically below the boiling point of liquid nitrogen.

The first examples of molecular ferro- and ferrimagnets were reported in the late 1980s. In 1987, Miller *et al.* reported that $[\text{Fe}(\text{C}_5\text{Me}_5)_2][\text{TCNE}]$ showed spontaneous ferromagnetic ordering below 4.5 K.^[11] Only one year later, Kahn *et al.* presented a new ferromagnetically ordering system at approximately the same temperature (4.6 K) based on bimetallic Cu(II)-Mn(II) chains.^[12]

The year 1991 saw two important breakthroughs. On one hand Manriquez *et al.* reported the first room temperature molecular magnet,^[13] $\text{V}(\text{TCNE})_2$, whose structure remains unknown to date. $\text{V}(\text{TCNE})_2$ orders ferrimagnetically above room temperature due to the antiferromagnetic coupling between the V^{2+} ions ($S = 3/2$) and the radical anions TCNE^- ($S = 1/2$). On the other hand, Tamura *et al.* reported the first all-organic ferromagnet,^[14] a compound of the well known nitronyl nitroxide family of stable radicals. While the compound ordered at only 0.6 K, it demonstrated the possibility to obtain molecular magnets in which the magnetic orbitals were purely of type s or p and not d or f as is the case for third and fourth row transition metals (3d or 4d), lanthanides (4f) and actinides (5f) used in classical bulk magnets. Nevertheless, these magnets are soft magnets with almost no coercive field due to the lack of anisotropy of the s and p orbitals. The highest ordering temperature in a purely organic magnet to date is 35 K,^[15] which is quite an improvement when compared to the compound by Kinoshita and coworkers, but is still too low to envisage any practical application as a permanent magnet.

Despite the novelty of preparing bulk molecular magnets ordering around room temperature, it was soon realized that one of the great advantages of molecular materials in magnetism is the possibility to control the dimensionality of the magnetic structure. Indeed, the control of the reaction conditions and the chemical nature of the compounds used to prepare molecular magnetic materials allows the preparation of strictly 3D bulk

[11] J. S. Miller, J. C. Calabrese, H. Rommelmann, S. R. Chittipeddi, J. H. Zhang, W. M. Reiff and A. J. Epstein, *J. Am. Chem. Soc.* **1987**, *109*, 769-781.

[12] O. Kahn, Y. Pei, M. Verdaguer, J. P. Renard and J. Sletten, *J. Am. Chem. Soc.* **1988**, *110*, 782-789.

[13] J. M. Manriquez, G. T. Yee, R. S. McLean, A. J. Epstein and J. S. Miller, *Science* **1991**, *252*, 1415-1417.

[14] M. Tamura, Y. Nakazawa, D. Shiomi, K. Nozawa, Y. Hosokoshi, M. Ishikawa, M. Takahashi and M. Kinoshita, *Chem. Phys. Lett.* **1991**, *186*, 401-404.

[15] F. Palacio, G. Antorrena, M. Castro, R. Burriel, J. Rawson, J. N. B. Smith, N. Bricklebank, J. Novoa and C. Ritter, *Phys. Rev. Lett.* **1997**, *79*, 2336.

ferro- or ferrimagnets, but also in lower dimensionalities, with 2D, 1D or strictly 0D magnetic materials, in which the magnetic interactions are propagated in a plane, in only one direction, or confined to an independent nanometric magnetic cluster. An extensive amount of research was done in order to prepare such materials, eventually leading to the discovery of the first compound exhibiting what was called “single-molecule magnet” behavior, which is the capacity of each individual molecule to retain a net magnetic moment below a critical blocking temperature in the absence of an external magnetic field.^[16]

1-4 Single-Molecule Magnets

1-4-1 $[\text{Mn}_{12}\text{O}_{12}(\text{CH}_3\text{COO})_{16}(\text{H}_2\text{O})_4]$ or Mn_{12}ac

It is unthinkable to write anything about single-molecule magnets (SMMs) without mentioning the archetypal molecule $[\text{Mn}_{12}\text{O}_{12}(\text{CH}_3\text{COO})_{16}(\text{H}_2\text{O})_4]$, from now on called Mn_{12}ac . Indeed, this system is both the first single-molecule magnet ever reported and the most studied one.

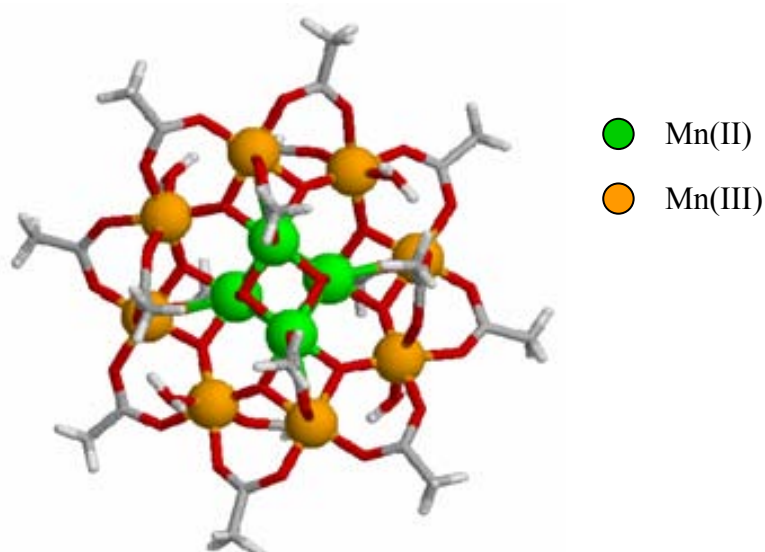


Figure 1-2. Crystal structure of the $[\text{Mn}_{12}\text{O}_{12}(\text{CH}_3\text{COO})_{16}(\text{H}_2\text{O})_4]$ complex.

Even though most authors do not mention it, the possibility of formation of an acetate dodecanuclear manganese complex was first proposed by Weinland and Fisher

^[16] D. Gatteschi, R. Sessoli and J. Villain, *Molecular Nanomagnets*, Oxford University Press, Oxford, **2006**.

in 1921.^[17] Nevertheless, the first synthesis and crystal structure of the Mn_{12}ac cluster as we know it was reported by Lis in 1980.^[18] At the time the author performed only dc magnetic measurements and limited his observations mostly to describing the structure of the cluster. Eight years later, Boyd *et al.* presented the magnetic properties of the benzoate equivalent of the Mn_{12} cluster,^[19] and concluded on the possibility to build bulk molecular magnetic materials using these complexes as a building block and finding a way to link them together. It was finally in 1991 that the true nature of Mn_{12}ac was recognized. When measuring the ac magnetic susceptibility of the cluster, Caneschi *et al.* noticed that the temperature dependant imaginary part of the ac magnetic susceptibility presented a peak whose position depended on the frequency of the applied field (see Figure 1-3).^[20] The presence of a peak in the imaginary part of the susceptibility meant that the complex was lagging with respect to the applied oscillating magnetic field, which in turn meant that it showed a slow magnetic relaxation below 10 K. Moreover, the fact that the position of the maximums of the peaks was frequency dependent allowed the researchers to discard the possibility that this was produced by a bulk magnetic ordering, and the complex was attributed a multiplet splitted $S = 10$ ground state with a zero field splitting parameter $D = -0.50 \text{ cm}^{-1}$.

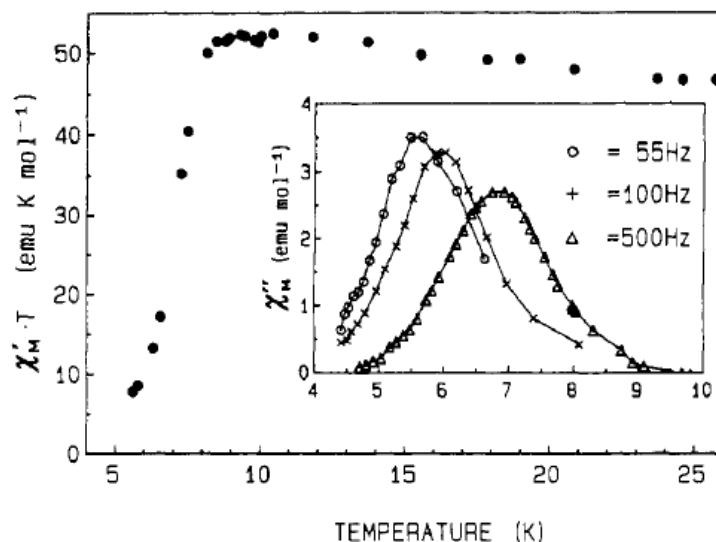


Figure 1-3. First ac magnetic susceptibility data recorded on Mn_{12}ac . The inset shows the imaginary part of the magnetic susceptibility vs. T measured at 55, 100 and 500 Hz.

[17] R. F. Weinland and G. Fischer, *Z. Anorg. Allg. Chem.* **1921**, 120, 161-180.

[18] T. Lis, *Acta Crystallog. B* **1980**, 36, 2042-2046.

[19] P. D. W. Boyd, Q. Li, J. B. Vincent, K. Folting, H. R. Chang, W. E. Streib, J. C. Huffman, G. Christou and D. N. Hendrickson, *J. Am. Chem. Soc.* **1988**, 110, 8537-8539.

[20] A. Caneschi, D. Gatteschi, R. Sessoli, A. L. Barra, L. C. Brunel and M. Guillot, *J. Am. Chem. Soc.* **1991**, 113, 5873-5874.

These values were confirmed a few years later by Sessoli *et al.* in an in depth study of the interactions in the cluster.^[21]

At the time, the authors pointed out that even though Mn_{12}ac was much smaller than the previously reported superparamagnets, it presented a similar behavior (temperature dependent blocking of the magnetic relaxation), and it was tempting to assume that the reason for its peculiar behavior laid in its high magnetic anisotropy originating from its high spin ground state and the anisotropy of the component metal ions.

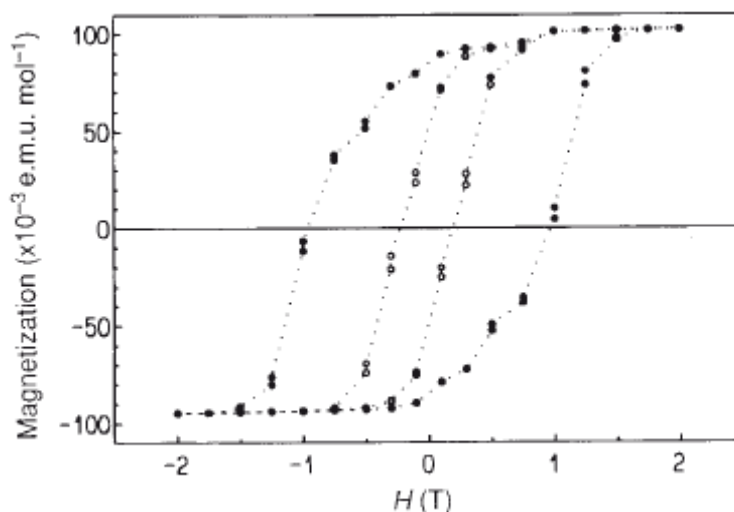


Figure 1-4. First magnetization hysteresis recorded on a polycrystalline sample of Mn_{12}ac .^[22]

The discovery of the slow magnetic relaxation in Mn_{12}ac was only the starting point. In 1993, it was shown that the complex shows magnetic hysteresis (see Figure 1-4) of purely molecular origin since no 3D ordering could be observed in either magnetization, susceptibility or specific heat measurements.^[22] The discovery of the possibility of magnetization hysteresis in a single-molecule, that is of the possibility of making single-molecule magnets, created quite an excitement, but more was to come since Mn_{12}ac was soon to provide the experimental observation of a quantum phenomenon: quantum tunneling of magnetization.

^[21] R. Sessoli, H. L. Tsai, A. R. Schake, S. Wang, J. B. Vincent, K. Folting, D. Gatteschi, G. Christou and D. N. Hendrickson, *J. Am. Chem. Soc.* **1993**, *115*, 1804-1816.

^[22] R. Sessoli, D. Gatteschi, A. Caneschi and M. A. Novak, *Nature* **1993**, *365*, 141-143.

1-4-2 Quantum tunneling of magnetization in Mn₁₂ac

Mn₁₂ac, like most single-molecule magnets to date, is a polynuclear transition metal cluster that combines a high spin ($S = 10$) ground state with a strong easy axis of magnetic anisotropy. In the case of Mn₁₂ac, the complex is made up of an outer ring of eight Mn(III) ions ($S = 2$) and a core of four Mn(II) ions ($S = 3/2$). The manganese ions of the outer ring are ferromagnetically coupled together, and so are the core manganese ions. Nevertheless, the core and the ring are coupled antiferromagnetically which altogether accounts for the $S = 10$ ground state (see Figure 1-5). The complex presents an axial symmetry, and it was shown that it presents a strong Ising anisotropy, which means that it presents an easy axis (or hard plane) of magnetization.

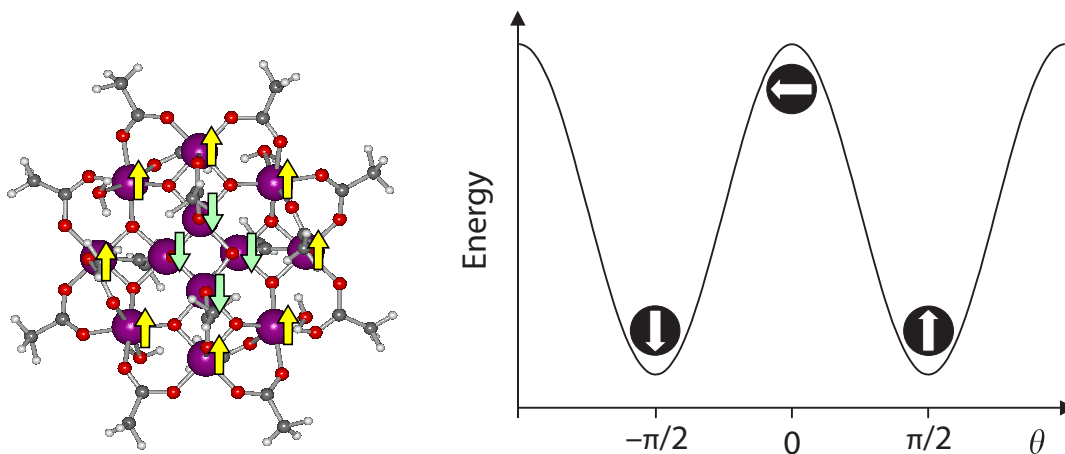


Figure 1-5. Magnetic structure of Mn₁₂ac (left) and the energy of a compound showing an Ising magnetic anisotropy as a function of the angle θ between the magnetization direction and the easy axis.

In a first approximation, the Mn₁₂ac complexes are described by the following Hamiltonian, taking into account the axial zero field splitting and the Zeeman splitting:

$$\mathcal{H} = -DS_z^2 - g\mu_B\mathbf{S}\cdot\mathbf{H}$$

Where D is the axial zero field splitting parameter, g is the g -factor of the compound, μ_B is the Bohr magneton, \mathbf{H} is the applied magnetic field, \mathbf{S} is the total spin of the system and S_z is its projection on the easy axis direction. The energies of the different m_s states are therefore given by the following expression:

$$E(m_s) = -Dm_s^2 - g\mu_B m_s H_z$$

Where H_z is the projection of the magnetic field on the easy axis direction and m_s are the spin microstates projected on the same axis. In zero field the Zeeman term is equal to zero and the energy diagram of the system is given in Figure 1-6.

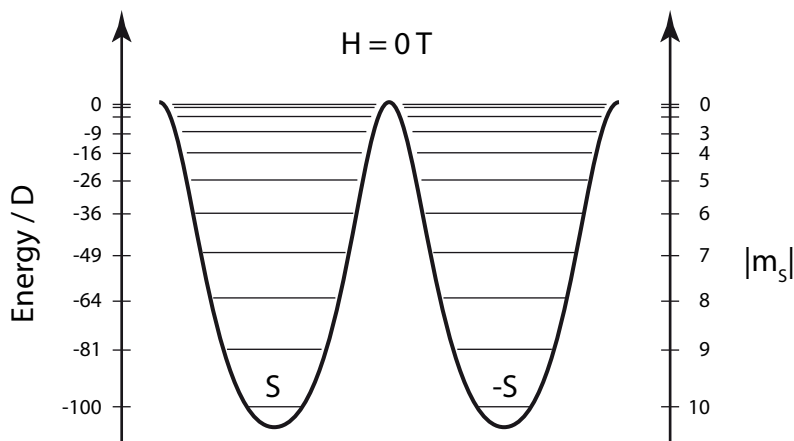


Figure 1-6. Energy diagram of the multiplets of the $S = 10$ compound in zero applied field.

In this situation the two states with quantum number S and $-S$ are equal in energy and the ground state is therefore degenerate and in principle the two states $m_s = S$ and $m_s = -S$ are equally populated.

On the contrary, when applying a component H_z along the easy axis of magnetization, the Zeeman term is non zero and the degeneracy is removed. In this case, the energies of one well are stabilized with respect to those of the other (Figure 1-7). The state $|S\rangle$ with $m_s = S$, is now metastable and it starts to depopulate to the benefit of the $|-S\rangle$ state with $m = -S$ which is now a true non degenerate ground state. The relaxation can occur in two ways. The compounds that are in a state $|S\rangle$ can overcome the anisotropy barrier by populating thermally the upper $|S+n\rangle$ states and therefore reach the state $|0\rangle$ and relax to the $|-S\rangle$ state in a thermally activated process following an Arrhenius-like behavior, with a relaxation rate τ^{-1} given by:

$$\tau^{-1} = \tau_0^{-1} \exp\left(-\frac{U_{\text{eff}}}{k_B T}\right)$$

Where U_{eff} is the effective barrier of reversal and k_B is the Boltzmann constant. Alternatively, if the applied magnetic component along the easy axis H_n is such that the $|S\rangle$ state coincides in energy with a $|-S+n\rangle$ state, then resonant tunneling occurs between the two states and the compounds in state $|S\rangle$ tunnel to state $|-S+n\rangle$ and relax

to the $|-S\rangle$ state. This process is called quantum tunneling of magnetization (QTM) and is a temperature independent process.

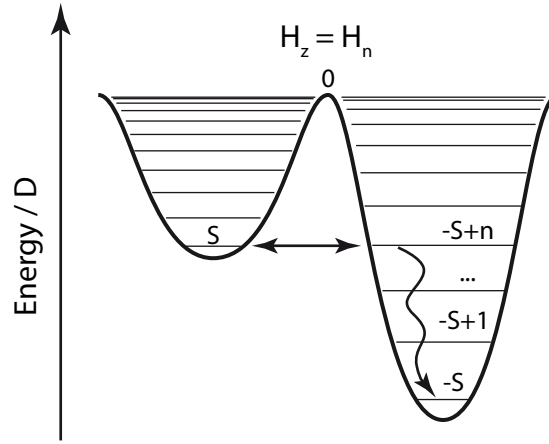


Figure 1-7. Energy diagram of the multiplets of the $S = 10$ compound applying a non zero magnetic field component H_n along the easy axis which makes the energy of the $|S\rangle$ and $|-S+n\rangle$ states coincide.

The occurrence of QTM happens at discrete values of magnetic field H_n for which the energies of $|m\rangle$ and $|-m+n\rangle$ are equal, which is given analytically by:

$$-Dm^2 - g\mu_B m H_n = -D(-m+n)^2 - g\mu_B(-m+n)H_n$$

$$-Dm^2 + D(-m+n)^2 = -g\mu_B(-2m+n)H_n$$

$$Dn(-2m+n) = -g\mu_B(-2m+n)H_n$$

Which finally simplifies as:

$$H_n = -Dn/g\mu_B$$

QTM occurs therefore at evenly spaced values of H which depend only on the zero field splitting parameter D and the g -factor of the compound. QTM provides an alternative route to the thermal relaxation of the superparamagnetic clusters, which was first evidenced in $Mn_{12}ac$ and translate in a staircase hysteresis curve of magnetization with a step at the values of H_n at which resonant tunneling occurs (see Figure 1-8). While the effect of QTM was already visible in the first recorded magnetization

hysteresis of Mn_{12}ac (see Figure 1-4),^[22] it was not identified at the time, and only a few years later was it recognized as such.^[23-27]

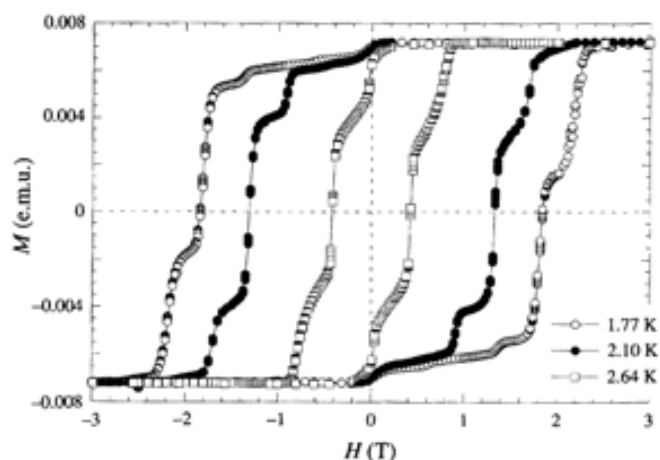


Figure 1-8. Magnetization hysteresis curve measured on a single-crystal of Mn_{12}ac measured at 1.77, 2.10 and 2.64 K.

In Mn_{12}ac the magnetization hysteresis curves (Figure 1-8) present steps that are evenly spaced by approximately 0.46 T, which corresponds to $D/g = 0.21 \text{ cm}^{-1}$ which is in good agreement with the values of D and g (0.5 cm^{-1} and 1.9, respectively) experimentally determined in an independent way from high field EPR experiments.^[21, 22] The steps can clearly be seen in Figure 1-8, and upon changing the temperature, the position of the steps is unchanged, but when lowering the temperature the hysteresis loop broadens and some steps that were so far undetectable can be observed.

1-4-3 Structural disorder in Mn_{12}ac

The Mn_{12} based SMMs (meaning, Mn_{12} clusters obtained by substitution of the acetate ligands by other carboxylates) often show the presence of two peaks in their ac magnetic susceptibility characteristics, implying the existence of a mixture of two species that are not magnetically equivalent and that show two different relaxation rates, one slower than the other.^[28-36] It has also been seen that by a simple ligand exchange

[23] J. R. Friedman, M. P. Sarachik, J. Tejada and R. Ziolo, *Phys. Rev. Lett.* **1996**, 76, 3830-3833.

[24] L. Thomas, F. Lioni, R. Ballou, D. Gatteschi, R. Sessoli and B. Barbara, *Nature* **1996**, 383, 145-147.

[25] J. R. Friedman, M. P. Sarachik, J. Tejada, J. Maciejewski and R. Ziolo, *J. Appl. Phys.* **1996**, 79, 6031-6033.

[26] D. Gatteschi and R. Sessoli, *Angew. Chem. Int. Ed.* **2003**, 42, 268-297.

[27] J. Tejada, R. F. Ziolo and X. X. Zhang, *Chem. Mater.* **1996**, 8, 1784-1792.

reaction or by changing the solvent in the coordination sphere of the cluster, its magnetic properties were notably affected.^[37] In particular, it was possible to obtain pairs of clusters exhibiting exclusively slow and fast relaxation rates, respectively, in which the difference was the carboxylate ligand or only the obtained solvate in the crystal structure. It was then possible to assign the two observed relaxation rates to the possibility of Jahn Teller isomerism in the coordination geometry of the Mn₁₂ derivative.^[30, 38, 39]

1-4-4 Dilute-solution experiments

While all of the experiments done on Mn₁₂ clusters presented here were done on the bulk solid material, either on a polycrystalline powder or on a single-crystal, the ultimate proof of the actual single-molecule magnet behavior of the Mn₁₂ clusters was to record the magnetic behavior of a collection of isolated complexes. The best way to do that was to dissolve them in a diamagnetic solvent and to record the magnetic behavior of the solutions. Indeed, in solution, the magnetic clusters are effectively separated from one another and should no longer interact.

-
- [28] H. J. Eppley, H.-L. Tsai, N. de Vries, K. Folting, G. Christou and D. N. Hendrickson, *J. Am. Chem. Soc.* **1995**, *117*, 301-317.
- [29] A. Cornia, A. C. Fabretti, R. Sessoli, L. Sorace, D. Gatteschi, A. L. Barra, C. Daiguebonne and T. Roisnel, *Acta Crystallogr C* **2002**, *58*, m371-373.
- [30] S. M. J. Aubin, Z. Sun, H. J. Eppley, E. M. Rumberger, I. A. Guzei, K. Folting, P. K. Gantzel, A. L. Rheingold, G. Christou and D. N. Hendrickson, *Inorg. Chem.* **2001**, *40*, 2127-2146.
- [31] D. Ruiz-Molina, P. Gerbier, E. Rumberger, D. B. Amabilino, I. A. Guzei, K. Folting, J. C. Huffman, A. Rheingold, G. Christou, J. Veciana and D. N. Hendrickson, *J. Mater. Chem.* **2002**, *12*, 1152-1161.
- [32] N. Domingo, P. Gerbier, J. Gomez, D. Ruiz-Molina, D. B. Amabilino, J. Tejada and J. Veciana, *Polyhedron* **2003**, *22*, 2355-2358.
- [33] P. Gerbier, N. Domingo, J. Gomez-Segura, D. Ruiz-Molina, D. B. Amabilino, J. Tejada, B. E. Williamson and J. Veciana, *J. Mater. Chem.* **2004**, *14*, 2455-2460.
- [34] M. Muntó, J. Gómez-Segura, J. Campo, M. Nakano, N. Ventosa, D. Ruiz-Molina and J. Veciana, *J. Mater. Chem.* **2006**, *16*, 2612-2617.
- [35] N. Domingo, F. Luis, M. Nakano, M. Muntó, J. Gómez, J. Chaboy, N. Ventosa, J. Campo, J. Veciana and D. Ruiz-Molina, *Physical Review B - Condensed Matter and Materials Physics* **2009**, *79*.
- [36] E. Terazzi, C. Bourgogne, R. Welter, J.-L. Gallani, D. Guillon, G. Rogez and B. Donnio, *Angew. Chem. Int. Ed.* **2008**, *47*, 490-495.
- [37] G. Aromi, S. M. J. Aubin, M. A. Bolcar, G. Christou, H. J. Eppley, K. Folting, D. N. Hendrickson, J. C. Huffman, R. C. Squire, H.-L. Tsai, S. Wang and M. W. Wemple, *Polyhedron* **1998**, *17*, 3005-3020.
- [38] Z. Sun, D. Ruiz, D. N. Hendrickson, N. R. Dilley, M. B. Maple, M. Soler, K. Folting, G. Christou and J. Ribas, *Chem. Commun.* **1999**, 1973-1974.
- [39] K. Awaga, Y. Suzuki, H. Hachisuka and K. Takeda, *J. Mater. Chem.* **2006**, *16*, 2516-2521.
- [40] N. Domingo, B. E. Williamson, J. Gomez-Segura, P. Gerbier, D. Ruiz-Molina, D. B. Amabilino, J. Veciana and J. Tejada, *Phys. Rev. B* **2004**, *69*, 052405.
- [41] E. J. L. McInnes, E. Pidcock, V. S. Oganessian, M. R. Cheesman, A. K. Powell and A. J. Thomson, *J. Am. Chem. Soc.* **2002**, *124*, 9219-9228.

The experiment was done by magnetic circular dichroism spectroscopy (see Appendix I) and showed that the MCD spectrum recorded on magnetized samples of a chiral Mn_{12}pro cluster (obtained from Mn_{12}ac by substitution of the acetate by (*S*)-chloropropionate) at 1.65 K when applying a ± 3 T magnetic field persisted partially once the field was removed. [33, 40, 41] In other words, the compound presented a remnant magnetization which was translated in a remnant MCD spectrum.

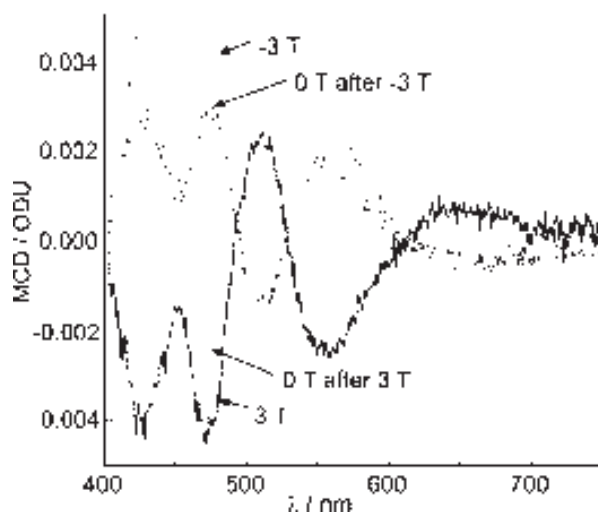


Figure 1-9. 1.65 K MCD spectra of Mn_{12}pro in 1:1 dichloromethane–toluene glass at an applied field of 3 and -3 T, and at 0 T after removing the applied fields.

This was also confirmed by recording the MCD signal versus field curves, which corresponded nicely to the magnetization hysteresis of the compound (see Figure 1-10).

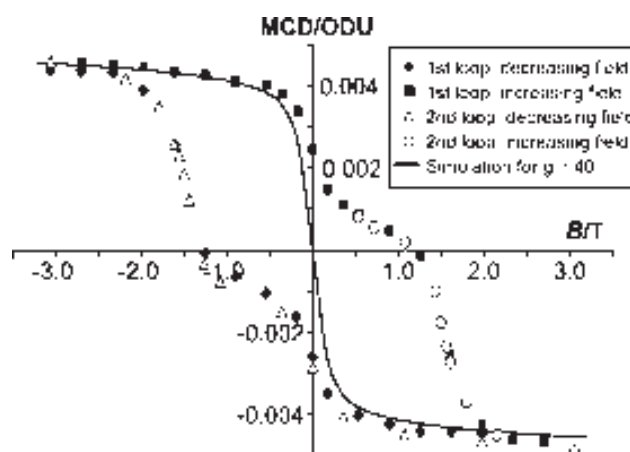


Figure 1-10. MCD hysteresis loop at 1.65 K for the 472 nm band of the Mn_{12}pro cluster in a 1:1 dichloromethane–toluene glass.

These experiments provided the ultimate proof that the magnetization hysteresis of Mn₁₂ compounds was an intrinsic behavior of the isolated clusters.

1-4-5 Other single-molecule magnets based on transition metals

Following the discovery of the Mn₁₂ clusters a great number of systems were prepared that showed SMM behavior. The number of hits searching for “single-molecule magnet” is of about a thousand, at a rate of more than one hundred papers each year since 2004. While a lot of new compounds have been synthesized, the general trends are the same, and most SMMs are still metallic clusters with a high spin ground state and a strong uniaxial anisotropy. While polynuclear SMMs of transition metal ions have been prepared in a variety of systems, including manganese, iron, V₄,^[42] and CrNi₆,^[43] an exhaustive list of all the studied compounds would be a long and not very interesting reading. For this reason, only some of the most studied and distinctive transition metal SMM clusters will be presented in this section.

1-4-5-1 Manganese clusters

Apart from the archetypal molecule Mn₁₂ac, a number of manganese clusters of various nuclearity were reported to function as single-molecule magnets.^[44, 45]

The smallest polynuclear transition metal SMMs found were those of the Mn₂ family.^[46, 47] These dinuclear manganese (III) Schiff base complexes allow for an easy modification of the properties by modifying the apical ligands and the chemical structure of Schiff bases. The ground state of the compounds were estimated to be S = 4, and the anisotropic zero field splitting varied from -0.3 to -1.03 cm⁻¹. The consequence of these parameters is that the blocking temperatures of the complexes are of the order of 3-5 K only at 10 kHz.

[42] S. L. Castro, Z. Sun, C. M. Grant, J. C. Bollinger, D. N. Hendrickson and G. Christou, *J. Am. Chem. Soc.* **1998**, *120*, 2365-2375.

[43] T. Mallah, C. Auburger, M. Verdagner and P. Veillet, *J. Chem. Soc., Chem. Commun.* **1995**, 61-62.

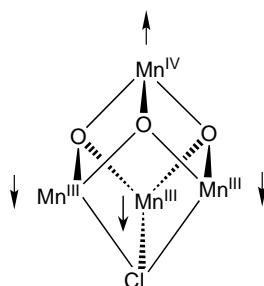
[44] E. K. Brechin, *Chem. Commun.* **2005**, 5141-5153.

[45] G. Rogez, B. Donnio, E. Terazzi, J.-L. Gallani, J.-P. Kappler, J.-P. Bucher and M. Drillon, *Adv. Mater.* **2009**, *21*, 4323-4333.

[46] Z. Lü, M. Yuan, F. Pan, S. Gao, D. Zhang and D. Zhu, *Inorg. Chem.* **2006**, *45*, 3538-3548.

[46] H. Miyasaka, R. Clérac, W. Wernsdorfer, L. Lecren, C. Bonhomme, K.-i. Sugiura and M. Yamashita, *Angew. Chem. Int. Ed.* **2004**, *43*, 2801-2805.

The slightly bigger tetranuclear manganese complex Mn_4 presents a distorted cubane structure.^[48-52]



The complex comprises three Mn(III) and one Mn(IV) ions in a trigonal pyramid disposition. The base consist of a Mn(III) triangle and above it lays the Mn(IV) ion. The lateral faces of the trigonal pyramid are capped by oxo bridges and the bottom face is capped by a chloride ion. The Mn(III) ions are coupled ferromagnetically together and the Mn(IV) ion is in antiferromagnetic configuration with respect to the other three ions which provides a ground state with $S = 9/2$. The originality of this complex with respect to the previously reported complex is that it is the first SMM with a half-integer spin ground state. This is important because it allowed to confirm that half-integer ground state SMMs could show quantum tunneling of magnetization.

Mn_4 was also shown to present a clear magnetization hysteresis (see Figure 1-11) but still at very low temperature (below 1 K). The zero field splitting parameter of Mn_4 was found to be -0.53 cm^{-1} which is almost the same as the one observed in $Mn_{12}ac$ (-0.46 cm^{-1}). Like in the case of $Mn_{12}ac$,^[22] the derivative of the magnetization hysteresis cycle was computed in order to appreciate the position of the QTM jumps in the M vs. H curve (Figure 1-11).

Many other higher nuclearity manganese clusters have been described to behave as single molecule magnets, like the Mn_{10} cluster of Barra *et al.*^[53] or the giant Mn_{84}

[48] S. M. J. Aubin, N. R. Dilley, L. Pardi, J. Krzystek, M. W. Wemple, L.-C. Brunel, M. B. Maple, G. Christou and D. N. Hendrickson, *J. Am. Chem. Soc.* **1998**, *120*, 4991-5004.

[49] A. Yamaguchi, H. Ishimoto, K. Awaga, J. S. Yoo, M. Nakano, D. N. Hendrickson, E. K. Brechin and G. Christou, *Physica B* **2000**, *284-288*, 1225-1226.

[50] S. Wang, M. S. Wemple, J. Yoo, K. Folting, J. C. Huffman, K. S. Hagen, D. N. Hendrickson and G. Christou, *Inorg. Chem.* **2000**, *39*, 1501-1513.

[51] J. Yoo, E. K. Brechin, A. Yamaguchi, M. Nakano, J. C. Huffman, A. L. Maniero, L.-C. Brunel, K. Awaga, H. Ishimoto, G. Christou and D. N. Hendrickson, *Inorg. Chem.* **2000**, *39*, 3615-3623.

[52] A. Bhattacharjee, Y. Miyazaki, M. Nakano, J. Yoo, G. Christou, D. N. Hendrickson and M. Sorai, *Polyhedron* **2001**, *20*, 1607-1613.

[53] A. L. Barra, A. Caneschi, D. Gatteschi, D. P. Goldberg and R. Sessoli, *J. Solid State Chem.* **1999**, *145*, 484.

cluster prepared by Tasiopoulos *et al.*^[54] The newest case of the series and perhaps one of the most promising family of compounds is that of the Mn₆.^[55-59]

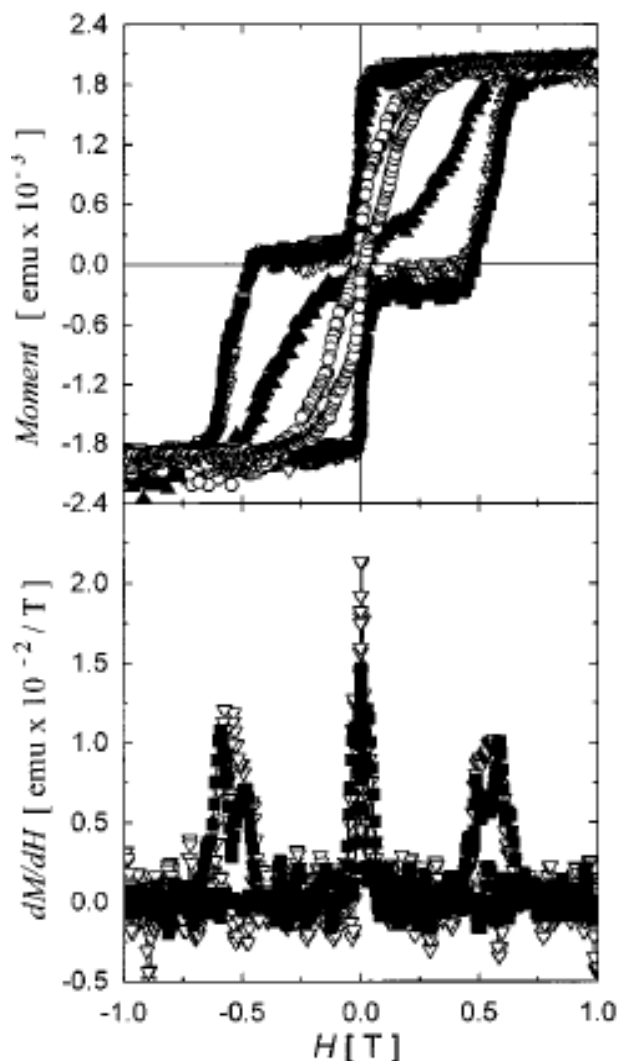


Figure 1-11. Magnetization hysteresis of a single crystal of Mn₄ measured at 0.900 (○), 0.706 (▲), 0.530 (▼) and 0.426 K (■). The bottom graph shows the derivatives of the hysteresis curves which indicate the field values at which QTM takes place.

^[54] A. J. Tasiopoulos, A. Vinslava, W. Wernsdorfer, K. A. Abboud and G. Christou, *Angew. Chem. Int. Ed.* **2004**, *43*, 2117-2121.

^[55] C. J. Milios, R. Inglis, R. Bagai, W. Wernsdorfer, A. Collins, S. Moggach, S. Parsons, S. P. Perlepes, G. Christou and E. K. Brechin, *Chem. Commun.* **2007**, 3476-3478.

^[56] C. J. Milios, R. Inglis, A. Vinslava, R. Bagai, W. Wernsdorfer, S. Parsons, S. P. Perlepes, G. Christou and E. K. Brechin, *J. Am. Chem. Soc.* **2007**, *129*, 12505-12511.

^[57] C. J. Milios, A. Vinslava, W. Wernsdorfer, S. Moggach, S. Parsons, S. P. Perlepes, G. Christou and E. K. Brechin, *J. Am. Chem. Soc.* **2007**, *129*, 2754-2755.

^[58] C. J. Milios, A. Vinslava, W. Wernsdorfer, A. Prescimone, P. A. Wood, S. Parsons, S. P. Perlepes, G. Christou and E. K. Brechin, *J. Am. Chem. Soc.* **2007**, *129*, 6547-6561.

^[59] C. J. Milios, A. Vinslava, P. A. Wood, S. Parsons, W. Wernsdorfer, G. Christou, S. P. Perlepes and E. K. Brechin, *J. Am. Chem. Soc.* **2006**, *129*, 8-9.

Indeed, the Mn_6 clusters hold the current record blocking temperature to date in SMMs with a 1000 Hz ac peak at approximately 7 K and a reported effective barrier height of 89 K.^[57] It is worth mentioning that despite the efforts made by a great number of chemist and physicists over the last 20 years, the Mn_6 cluster is the only polynuclear transition metal SMM to date that presents a higher effective barrier than the original Mn_{12}ac complex.

1-4-5-2 Iron clusters

Another transition metal that has been widely used to produce molecular magnetic materials is iron, which was used for instance to produce a variety of ferric wheels,^[60-63] and which of course has been used to produce a variety of SMMs.^[44, 64]

The first iron based SMM was an octanuclear iron(III) cluster, baptized as Fe_8 and synthesized in the early 1980s.^[65]

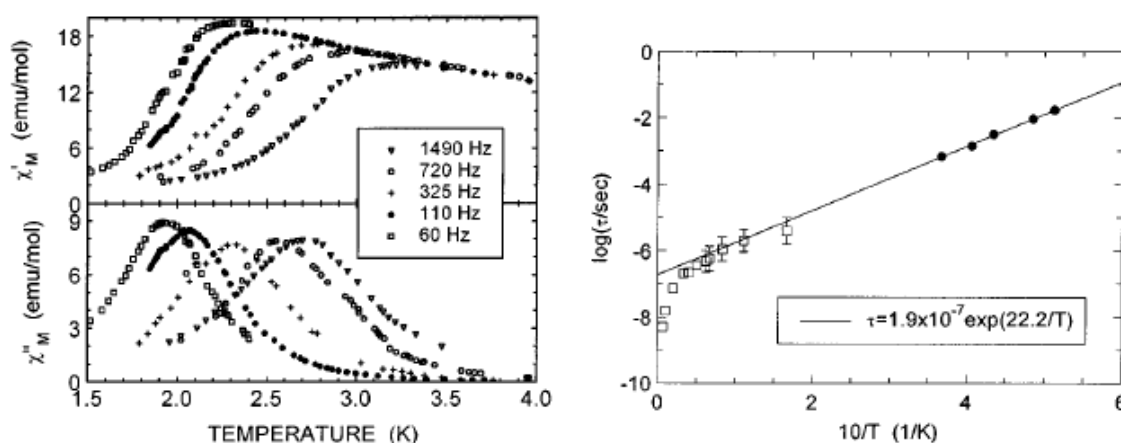


Figure 1-12. Ac magnetic susceptibility of Fe_8 as a function of temperature (left) and Arrhenius plot derived from the magnetic susceptibility data (black circles) and from Mössbauer measurements (squares).

It was reinvestigated in order to check for SMM behavior, and it was shown that indeed, Fe_8 presented a frequency dependent peak in its ac-magnetic susceptibility

[60] A. Caneschi, A. Cornia, A. C. Fabretti and D. Gatteschi, *Ang. Chem. Int. Ed.* **1996**, *34*, 2716-2718.

[61] A. Caneschi, A. Cornia and S. J. Lippard, *Angew. Chem. Int. Ed.* **1995**, *34*, 467-469.

[62] S. P. Watton, P. Fuhrmann, L. E. Pence, S. J. Lippard, A. Caneschi, A. Cornia and G. L. Abbati, *Angew. Chem. Int. Ed.* **1997**, *36*, 2774-2776.

[63] A. Caneschi, A. Cornia, A. C. Fabretti and D. Gatteschi, *Angew. Chem. Int. Ed.* **1999**, *38*, 1295-1297.

[64] D. Gatteschi, R. Sessoli and A. Cornia, *Chem. Commun.* **2000**, 725-732.

[65] K. Wieghardt, K. Pohl, I. Jibril and G. Huttner, *Angew. Chem. Int. Ed.* **1984**, *23*, 77-78.

demonstrating the slow magnetic relaxation, and an Arrhenius analysis showed its behavior as a superparamagnet (see Figure 1-12).^[66]

The complex, that presents a $S = 10$ ground state, like $Mn_{12}ac$, was shown to present an axial magnetic anisotropy with a zero field splitting parameter $D = -0.191 \text{ cm}^{-1}$ (compared to -0.5 cm^{-1} for $Mn_{12}ac$). While its behaviour is similar to $Mn_{12}ac$, its relaxation rate is a higher than that of $Mn_{12}ac$ in the same conditions. This example clearly illustrates that maintaining the ground state ($S = 10$), the compound that relaxes more slowly is the one having the bigger anisotropic zero field parameter D .

Another key SMM is the propeller-like Fe_4 system.^[67-71] The original $[Fe_4(OCH_3)_6dpm_6]$ (where $Hdpm = \text{dipivaloylmethane}$) presented an isotropic zero field splitting $D = -0.20 \text{ cm}^{-1}$ and a $S = 5$ ground state.

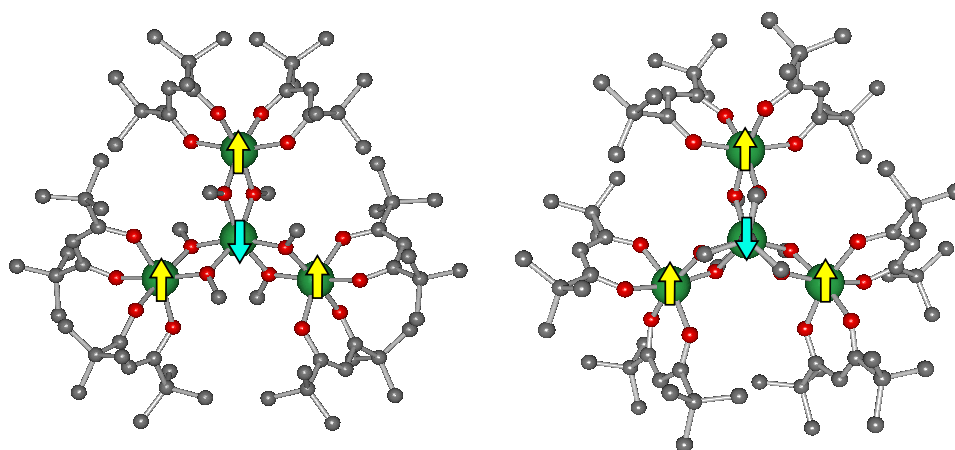


Figure 1-13. Magnetic and molecular structure of $[Fe_4(OCH_3)_6dpm_6]$ (left) and $[Fe_4(thme)_2dpm_6]$ (right)

Nevertheless, while the expected barrier height for these parameters was calculated to be of 7.2 K, the actual observed barrier height was estimated from the Arrhenius

^[66] A. L. Barra, P. Debrunner, D. Gatteschi, C. E. Schulz and R. Sessoli, *Europhys. Lett.* **1996**, *35*, 133-138.

^[67] A. L. Barra, A. Caneschi, A. Cornia, F. Fabrizi de Biani, D. Gatteschi, C. Sangregorio, R. Sessoli and L. Sorace, *J. Am. Chem. Soc.* **1999**, *121*, 5302-5310.

^[68] S. Accorsi, A.-L. Barra, A. Caneschi, G. Chastanet, A. Cornia, A. C. Fabretti, D. Gatteschi, C. Mortalò, E. Olivieri, F. Parenti, P. Rosa, R. Sessoli, L. Sorace, W. Wernsdorfer and L. Zoppi, *J. Am. Chem. Soc.* **2006**, *128*, 4742-4755.

^[69] A. Cornia, L. Gregoli, C. Danieli, A. Caneschi, R. Sessoli, L. Sorace, A.-L. Barra and W. Wernsdorfer, *Inorg. Chim. Acta* **2008**, *361*, 3481-3488.

^[70] A. Bouwen, A. Caneschi, D. Gatteschi, E. Goovaerts, D. Schoemaker, L. Sorace and M. Stefan, *J. Phys. Chem. B* **2001**, *105*, 2658-2663.

^[71] A. Cornia, A. C. Fabretti, P. Garrisi, C. Mortalò, D. Bonacchi, D. Gatteschi, R. Sessoli, L. Sorace, W. Wernsdorfer and A.-L. Barra, *Angew. Chem. Int. Ed.* **2004**, *43*, 1136-1139.

analysis of the ac magnetic susceptibility measurements to be of only 3.5 K, due to the efficiency of QTM in this compound.^[67]

Since $[\text{Fe}_4(\text{OCH}_3)_6\text{dpm}_6]$ was shown by EPR experiments to actually be structurally disordered,^[70] Cornia *et al.* decided to substitute the methoxy bridges by a tripodal ligand, 1,1,1-tris(hydroxymethyl)ethane (thme or H_3L^1), in order to make the compound more rigid and eliminate the lattice disorder, see the structure of the clusters in Figure 1-13. The new cluster still had an $S = 5$ ground state, but the zero field parameter was significantly increased from -0.20 cm^{-1} in $[\text{Fe}_4(\text{OCH}_3)_6\text{dpm}_6]$ to -0.445 cm^{-1} in $[\text{Fe}_4(\text{thme})_2\text{dpm}_6]$. Similarly, the effective barrier height was increased to 15.6 K.^[71]

Finally, Accorsi *et al.* introduced further modifications to the tripodal ligand used to prepare the cluster (see Figure 1-14), obtaining a whole family of clusters.^[68]

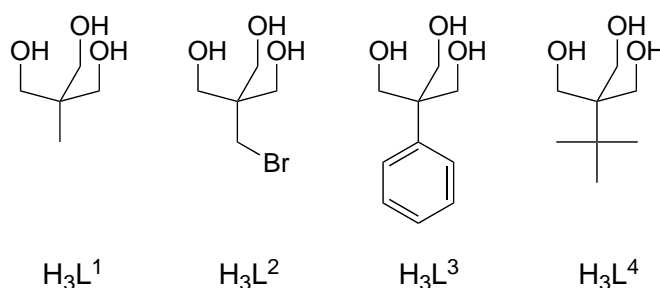


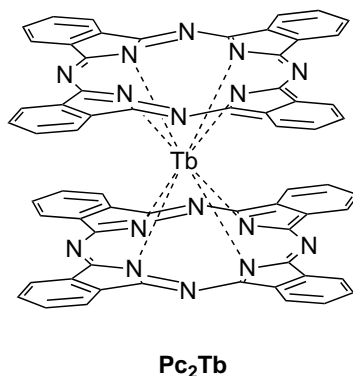
Figure 1-14. Family of tripodal ligands used for the preparation of the new family of Fe_4 clusters.

Out of all the clusters, those made with H_3L^1 , H_3L^2 and H_3L^3 were the best performing SMMs but their effective barrier height did not exceed 15-17 K, far from the reported value of 89 K of Mn_6 .

1-5 Single-ion magnets

The scientific community has dedicated countless efforts to the design and preparation of polynuclear transition metal clusters to try and discover new SMMs. The common goal for years was to obtain a cluster with a high magnetic anisotropy, and to achieve a high spin ground state by engineering the exchange coupling between the different transition metal ions constituting the clusters. Nevertheless, in the early 2000, this vision of single-molecule magnet was to be revised due to the appearance of the

first mononuclear SMM Pc_2Tb , described by Ishikawa *et al.*,^[72] in which obviously no intramolecular exchange coupling between metals could take place.



These new systems were first limited to double-decker lanthanide phthalocyanine complexes, and were extended only recently to lanthanide polyoxometalates and to the first mononuclear transition metal SMM, a high spin iron (II) complex. In this section, we will first review briefly the newest SMMs based on single magnetic ions and we will then discuss in more detail the history and the magnetic behavior of lanthanide phthalocyanine double-decker complexes.

1-5-1 Recent SMMs based on single metal ions

1-5-1-1 Lanthanide polyoxometalates

Recently, AlDamen *et al.* reported two families of monolanthanide polyoxometalates compounds^[73, 74] that behave as single-ion magnets: $[\text{Ln}(\text{W}_5\text{O}_{18})_2]^{9-}$ (for Ln = Tb, Dy, Ho, and Er) and $[\text{Ln}(\text{SiW}_{11}\text{O}_{39})_2]^{13-}$ (for Ln = Tb, Dy, Ho, Er, Tm and Yb). Out of all the prepared complexes, only the Ho and Er complexes of the form $[\text{Ln}(\text{W}_5\text{O}_{18})_2]^{9-}$ and the Dy, Ho, Er and Yb complexes of the form $[\text{Ln}(\text{SiW}_{11}\text{O}_{39})_2]^{13-}$ presented a slow magnetic relaxation characteristic of SMMs. Finally $[\text{Er}(\text{W}_5\text{O}_{18})_2]^{9-}$ was the only species exhibiting SMM behavior above 2 K. The symmetry of these polyoxometalate clusters is in principle the same as that of the double-decker lanthanide complexes (see Figure 1-16), providing a similar environment to the lanthanide ion.

^[72] N. Ishikawa, M. Sugita, T. Ishikawa, S.-y. Koshihara and Y. Kaizu, *J. Am. Chem. Soc.* **2003**, *125*, 8694-8695.

^[73] M. A. AlDamen, J. M. Clemente-Juan, E. Coronado, C. Martí-Gastaldo and A. Gaita-Ariño, *J. Am. Chem. Soc.* **2008**, *130*, 8874-8875.

^[74] M. A. AlDamen, S. Cardona-Serra, J. M. Clemente-Juan, E. Coronado, A. Gaita-Ariño, C. Martí-Gastaldo, F. Luis and O. Montero, *Inorg. Chem.* **2009**, *48*, 3467-3479.

It is worth noting that the Tb complexes of neither families present SMM behavior. This apparently surprising result was attributed to a slightly different geometry of the lanthanide ion in these clusters as that observed in phthalocyanine complexes.

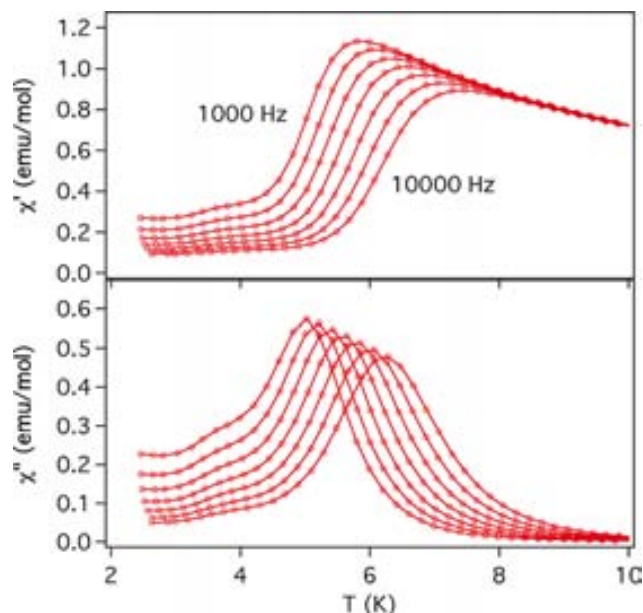


Figure 1-15. In phase (above) and out of phase (below) ac magnetic susceptibility of $[\text{Er}(\text{W}_5\text{O}_{18})_2]^{9-}$ measured at seven different frequencies between 1000 and 10000 Hz.

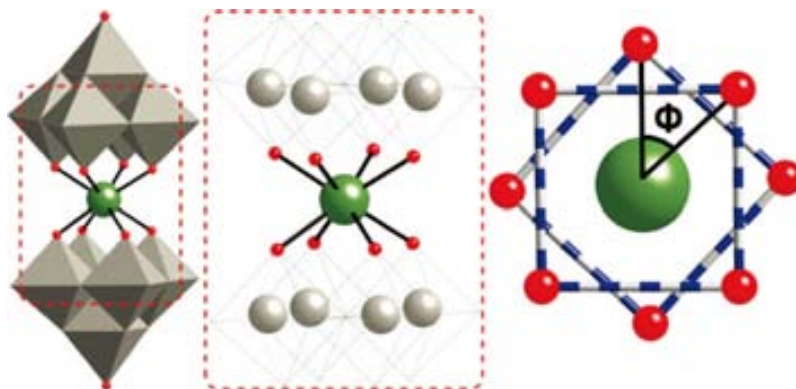


Figure 1-16. Structure of the $[\text{Er}(\text{W}_5\text{O}_{18})_2]^{9-}$ and projection of its coordination geometry

The main structural difference is the substitution of the nitrogen by oxygen atoms in the coordination sphere of the lanthanide and a slight compression of the square antiprism defined by the lanthanide ion and the eight oxygen atoms with respect to the geometry of Ishikawa's compounds. These slight differences are enough to completely perturb the ligand field splitting parameters and thus the energy level of the ground-state

multiplets. For instance, in the two new families of compounds, the Tb ion presents a $J = 0$ ground state.

1-5-1-2 A SMM based on a single iron (II) metal ion

The latest addition to the collection of SMMs based on a single metal ion is only very recent. Freedman *et al.* reported for the first time a single-ion magnet based on a transition metal ion, in this case iron(II).^[75]

The ground state of the complex, whose synthesis had been reported earlier by Harman *et al.*,^[76] was confirmed by dc magnetic susceptibility to be $S = 2$ and the high magnetic anisotropy caused by the orbital angular momentum of the high-spin ion makes this complex behave as a SMM.^[75] Such complexes have indeed been shown to present a very strong axial zero-field splitting of up to 50 cm^{-1} .^[77] In the present case, the complex presents a significant negative axial zero-field splitting $D = -39.6 \text{ cm}^{-1}$ and a small rhombic term $E = -0.41 \text{ cm}^{-1}$.

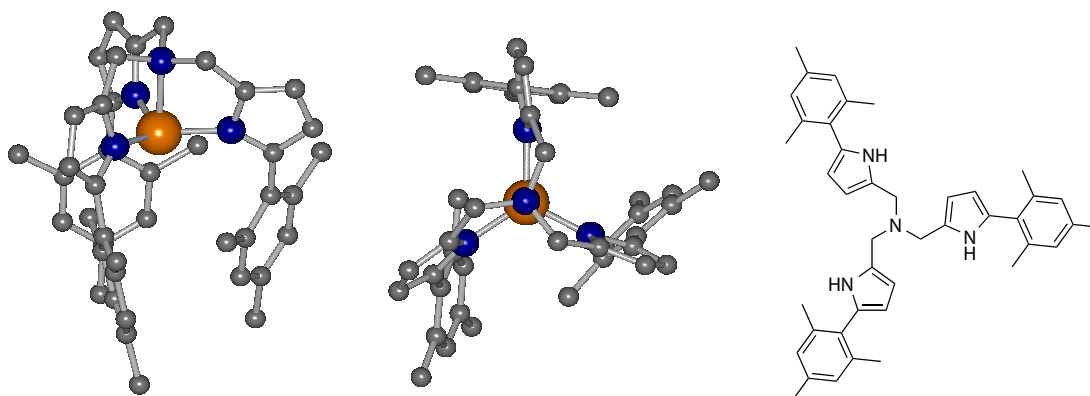


Figure 1-17. Structure of the high-spin iron(II) complex showing the trigonal prismatic geometry of the ion (left and center), and chemical structure of the tris(mesityl-pyrrolylmethyl)amine ligand (right).

^[75] D. E. Freedman, W. H. Harman, T. D. Harris, G. J. Long, C. J. Chang and J. R. Long, *J. Am. Chem. Soc.* **2010**, *132*, 1224-1225.

^[73] M. A. AlDamen, J. M. Clemente-Juan, E. Coronado, C. Martí-Gastaldo and A. Gaita-Ariño, *J. Am. Chem. Soc.* **2008**, *130*, 8874-8875.

^[74] M. A. AlDamen, S. Cardona-Serra, J. M. Clemente-Juan, E. Coronado, A. Gaita-Ariño, C. Martí-Gastaldo, F. Luis and O. Montero, *Inorg. Chem.* **2009**, *48*, 3467-3479.

^[76] W. H. Harman and C. J. Chang, *J. Am. Chem. Soc.* **2007**, *129*, 15128-15129.

^[75] D. E. Freedman, W. H. Harman, T. D. Harris, G. J. Long, C. J. Chang and J. R. Long, *J. Am. Chem. Soc.* **2010**, *132*, 1224-1225.

^[77] H. Andres, E. L. Bominaar, J. M. Smith, N. A. Eckert, P. L. Holland and E. Münck, *J. Am. Chem. Soc.* **2002**, *124*, 3012-3025.

Despite the good value of the axial zero-field splitting and the moderately high-spin ground state, the observed barrier height estimated from the Arrhenius analysis of the position of ac magnetic susceptibility peaks as a function of temperature and frequency of applied magnetic field was of only 42 cm^{-1} which is much lower than the theoretical value given by $|D|S^2 = 158 \text{ cm}^{-1}$.

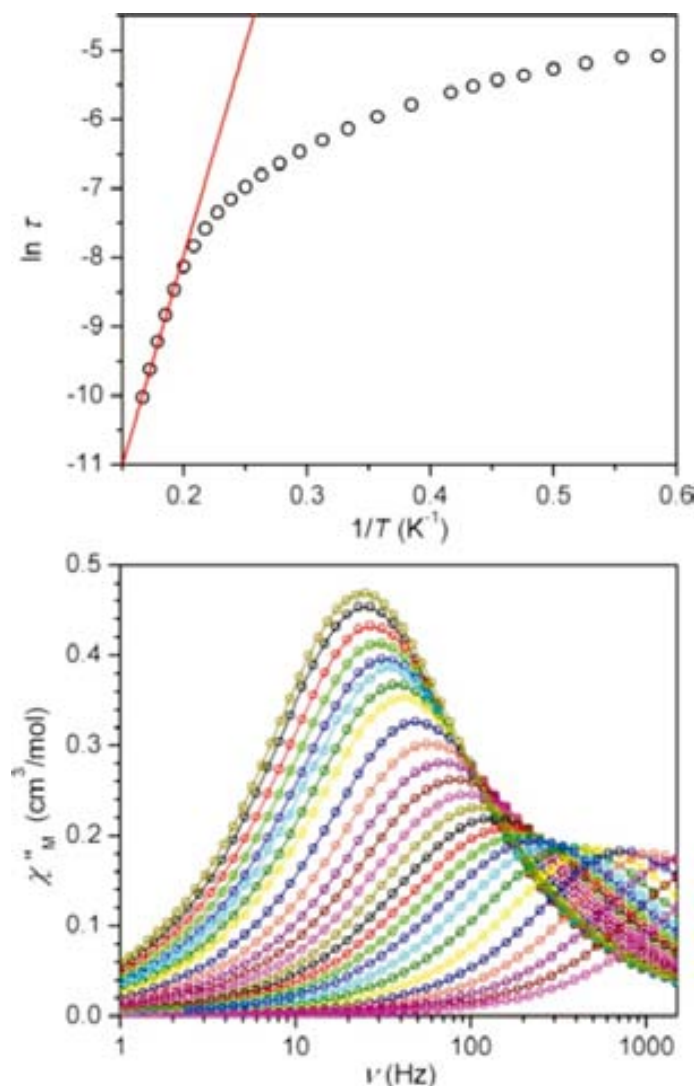


Figure 1-18. Arrhenius plot (above) obtained from the position of the frequency dependent out of phase magnetic susceptibility measurements done at temperatures between 1.7 and 6 K (below).

This low value, together with the strong non-linearity of the Arrhenius plot at low temperature (see Figure 1-18) strongly suggests the occurrence of quantum tunneling of magnetization as an alternative relaxation mechanism. This theory is also supported by the fact that the slow relaxation of magnetization is seen only when applying a dc magnetic field component that detunes the $\pm m_s$ states making the probability of

tunneling much lower. It is therefore probable that the absence of slow magnetic relaxation in a null applied dc field is due to the efficient tunneling between the ± 2 spin states.

1-5-2 Double-decker lanthanide complexes

1-5-2-1 Magnetic properties of double-decker lanthanide complexes

In 2002, after working with double and triple decker phthalocyanine complexes for several years,^[78-82] Ishikawa *et al.* established a new method to determine the ligand field parameters of a series of neutral triple decker lanthanide complexes by theoretical analysis of their magnetic susceptibility and their ^1H NMR spectra. Therefore, they could extract the energy diagram of the ground-state multiplets of the complexes.^[83] The method was then applied to the determination of the ligand-field parameters of the closed-shell anionic double-decker lanthanide complexes, extracting again the ground-state multiplets energy diagram (see Figure 1-19).^[84]

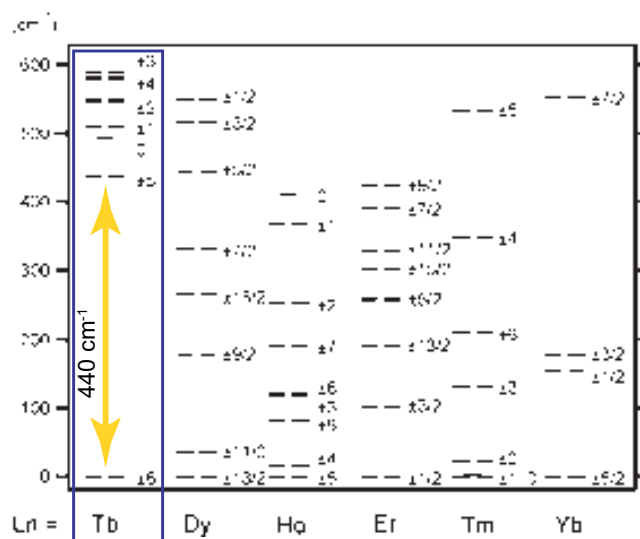


Figure 1-19. Energy diagram for the ground-state multiplets of $[\text{Pc}_2\text{Ln}]$ ($\text{Ln} = \text{Tb}, \text{Dy}, \text{Ho}, \text{Er}, \text{Tm},$ or Yb).

[78] N. Ishikawa and Y. Kaizu, *J. Phys. Chem.* **1996**, *100*, 8722-8730.

[79] N. Ishikawa, T. Okubo and Y. Kaizu, *Inorg. Chem.* **1999**, *38*, 3173-3181.

[80] N. Ishikawa and Y. Kaizu, *J. Phys. Chem. A* **2000**, *104*, 10009-10016.

[81] N. Ishikawa, *J. Porphyrins Phthalocyanines* **2001**, *5*, 87-101.

[82] N. Ishikawa, T. Iino and Y. Kaizu, *J. Am. Chem. Soc.* **2002**, *124*, 11440-11447.

[83] N. Ishikawa, T. Iino and Y. Kaizu, *J. Phys. Chem. A* **2002**, *106*, 9543-9550.

[84] N. Ishikawa, M. Sugita, T. Okubo, N. Tanaka, T. Iino and Y. Kaizu, *Inorg. Chem.* **2003**, *42*, 2440-2446.

Upon doing so, the energy diagram of the terbium(III) complex appeared to be a very appealing case. Indeed, the complex presents a $J = 6$ ground state, where $J = S + L$ is the total angular momentum, and the $m_J = 5$ multiplet was found to lay about 440 cm^{-1} or 633 K above the ground state, far too high to be populated thermally, which altogether predicted an outstanding behavior as a single-molecule magnet.

In order to demonstrate the SMM behavior of the $[\text{Pc}_2\text{Tb}]^-$ complex, the ac magnetic susceptibility was recorded on a pure sample and on a 2% solid solution of the magnetic complex in the isomorphous diamagnetic Yttrium(III) complex.^[72] As expected, the ac magnetic susceptibility of the complex showed a peak in the imaginary component at a much higher temperature than those observed for the previously described SMMs. Indeed, while Mn_{12}ac has an ac magnetic susceptibility peak at 6 K at an oscillating field of 100 Hz , $[\text{Pc}_2\text{Tb}]^-$ in the same conditions presents a peak at 33 K .

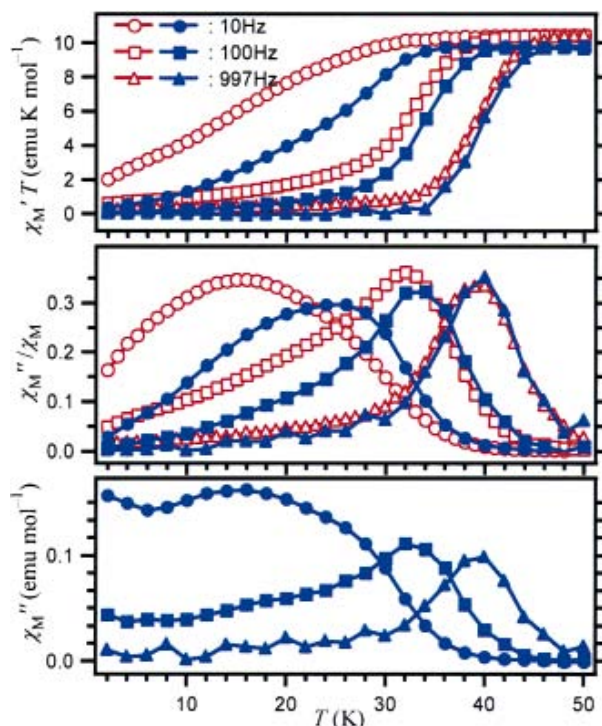


Figure 1-20. Real χ'_M (above) and imaginary χ''_M (middle and below) components of the ac magnetic susceptibility of $[\text{Pc}_2\text{Tb}]^-$ (open symbols) and of a 2% dilution of the same in the diamagnetic $[\text{Pc}_2\text{Y}]^-$ complex (solid symbols).

It is also interesting to notice that upon dilution, the characteristics of the complex were not lessened, but that on the contrary, the blocking temperature observed in the ac

^[72] N. Ishikawa, M. Sugita, T. Ishikawa, S.-y. Koshihara and Y. Kaizu, *J. Am. Chem. Soc.* **2003**, *125*, 8694-8695.

magnetic susceptibility curves were even increased. This was taken as a demonstration that the magnetic behavior was effectively an intramolecular one and that the weak intermolecular interactions were actually detrimental.

These data were completed later by magnetic hysteresis measurements done in the same solid solution conditions.^[85]

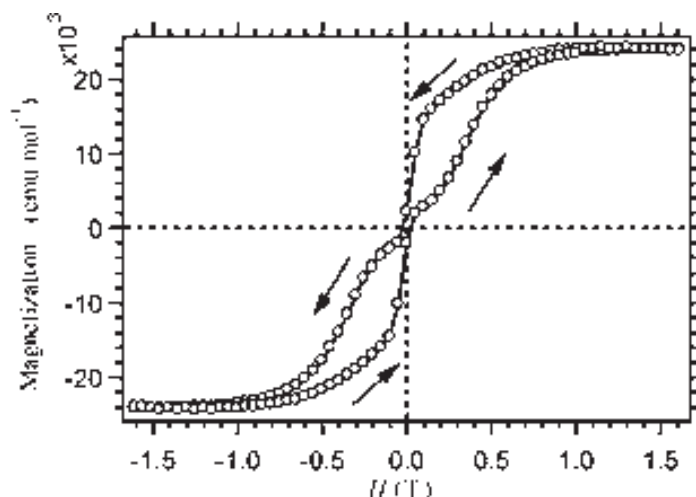


Figure 1-21. Magnetization vs field plot measured at 1.7 K for a powder sample of $[\text{Pc}_2\text{Tb}]^-\text{TBA}^+$ diluted at a concentration of 2% in $[\text{Pc}_2\text{Y}]^-\text{TBA}^+$

Despite the very high blocking temperature seen in the ac magnetic susceptibility of the $[\text{Pc}_2\text{Tb}]^-$ complex, the magnetization hysteresis was observed only at quite a low temperature (1.7 K), and it proved to be quite narrow close to zero-field (i.e. it presented a very small coercive field and a very small remnant magnetization). The magnetization hysteresis of the Dy complex was even narrower close to zero-field than that of the Tb complex.

The relaxation mechanisms involved in the $[\text{Pc}_2\text{Tb}]^-$ complexes were studied via Arrhenius analysis of the relaxation rate $1/\tau$ and the results are shown in Figure 1-22.

In a non-Kramer system, that is when there is an even number of electrons like in Tb^{3+} ($4f^8$), the relaxation time of the paramagnetic ion is given by the spin-lattice relaxation and obeys:^[86]

$$\tau^{-1} = R_d(h\nu)^3 \coth(h\nu/2kT) + R_{or} \Delta^3 [\exp(\Delta/kT) - 1]^{-1} + R_r T^7$$

^[85] N. Ishikawa, M. Sugita, T. Ishikawa, S.-y. Koshihara and Y. Kaizu, *J. Phys. Chem. B* **2004**, *108*, 11265-11271.

^[86] A. Abragam and B. Bleaney, *Electron Paramagnetic Resonance, Chapter 10*, Clarendon press, Oxford, **1970**.

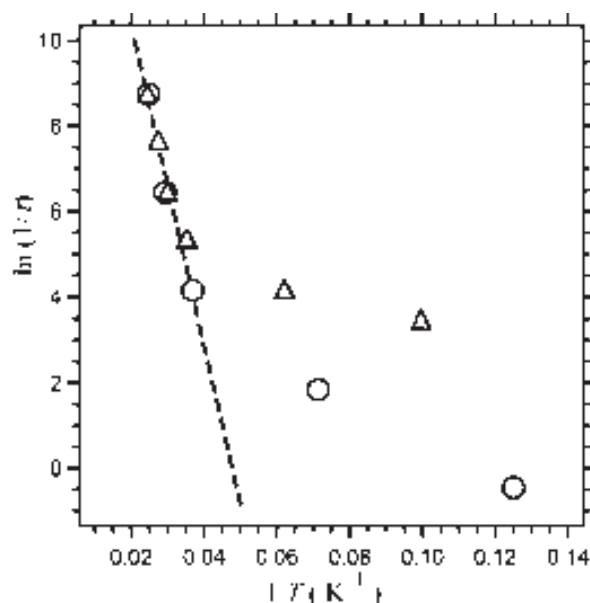


Figure 1-22. Arrhenius plot of $\ln(\tau^{-1})$ as a function of $1/T$ for the anionic terbium double-decker phthalocyanine complex (triangles) and the diluted sample of the same in the yttrium diamagnetic equivalent matrix (circles).

Where the first term corresponds to a direct spin-phonon coupling, the second term corresponds to an Orbach process (a two phonon process where the energy transferred to the lattice is given by the energy difference between the absorbed and emitted phonons for a low lying excited state) and the third one corresponds to a Raman process (a two phonon process where the energy transferred to the lattice is given by the energy difference between the absorbed and emitted phonons for a virtual excited state). The three type of processes are illustrated in Figure 1-23.

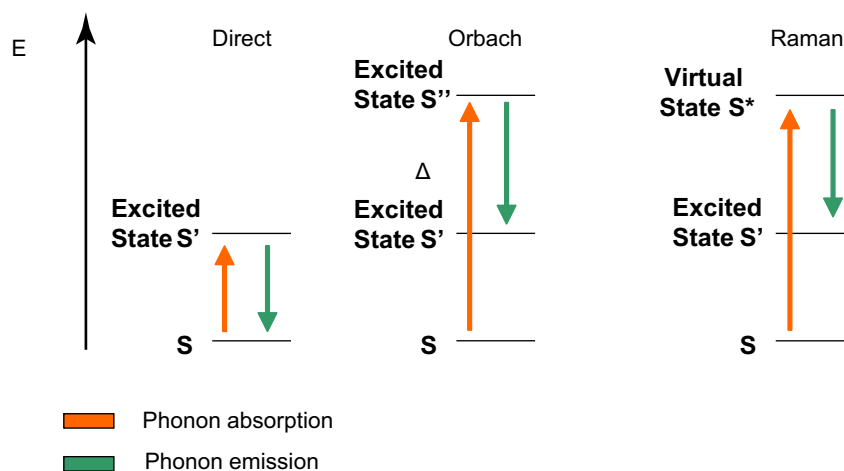


Figure 1-23. Illustration of the three spin-lattice relaxation mechanisms: the direct spin-phonon coupling, the Orbach process and the Raman process.

It was shown that at high temperature (above 25 K), the response of the complex response occurs through a thermally activated Orbach regime with an activation barrier of about 260 cm^{-1} which was consistent in principle with the order of magnitude of the difference in energy between the ground state $J = 6$ to the first excited state $J = 5$ (440 cm^{-1}). At lower temperatures, below 25 K, another process occurred which was attributed to either a Raman process or a direct spin-phonon coupling.

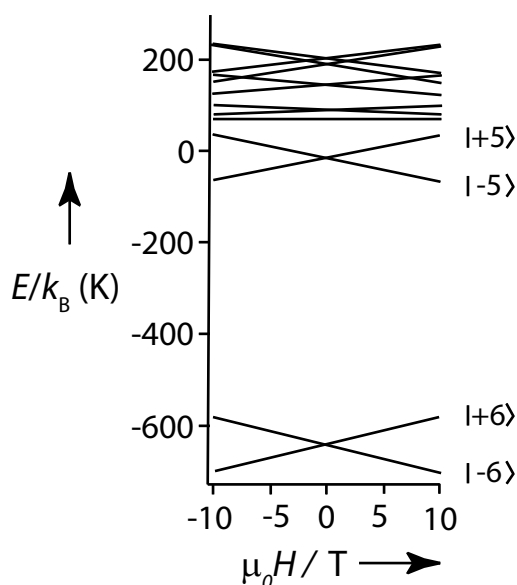


Figure 1-24. Zeeman energy diagram for the $J = 6$ ground-state multiplet

At the time, the authors concluded on the absence of quantum tunneling of magnetization steps in the magnetization hysteresis curve, and explained this absence by the huge energy difference between the ground-state and the first excited state of $J = 5$ (see Figure 1-24). Nevertheless, after recording a low temperature hysteresis of magnetization on a monocrystal of formula $\text{TBA}[\text{Pc}_2\text{Tb}_{0.02}\text{Y}_{0.98}]$, it was observed that the compound presents a staircase-like hysteresis, which is the trace of quantum tunneling of magnetization.^[87] Since the $J = 6$ and the $J = 5$ states are too far apart, the observed resonant tunneling could not be due to a transition between them. Instead, it was realized that terbium presents a nucleus with $I = 3/2$ in 100% natural abundance. Therefore, taking into account the interaction between the nucleus and the $4f^8$ system, the appropriate Hamiltonian for the system still contains the ligand field terms but one should add two additional terms corresponding to the hyperfine interaction $A_{\text{hf}}\mathbf{I}\mathbf{J}$ and the nuclear quadrupole interaction. Taking into account all of these parameters, it was

^[87] N. Ishikawa, M. Sugita and W. Wernsdorfer, *Angew. Chem. Int. Ed.* **2005**, *44*, 2931-2935.

therefore possible to assign the tunneling steps in the magnetization hysteresis curve to QTM between $|\pm J\rangle|\pm I\rangle$ substates of the $J = 6$ ground-state in the range of a few mK (see Figure 1-25). This nuclear spin driven quantum tunneling of magnetization was also demonstrated in a Holmium double-decker phthalocyanine complex.^[88]

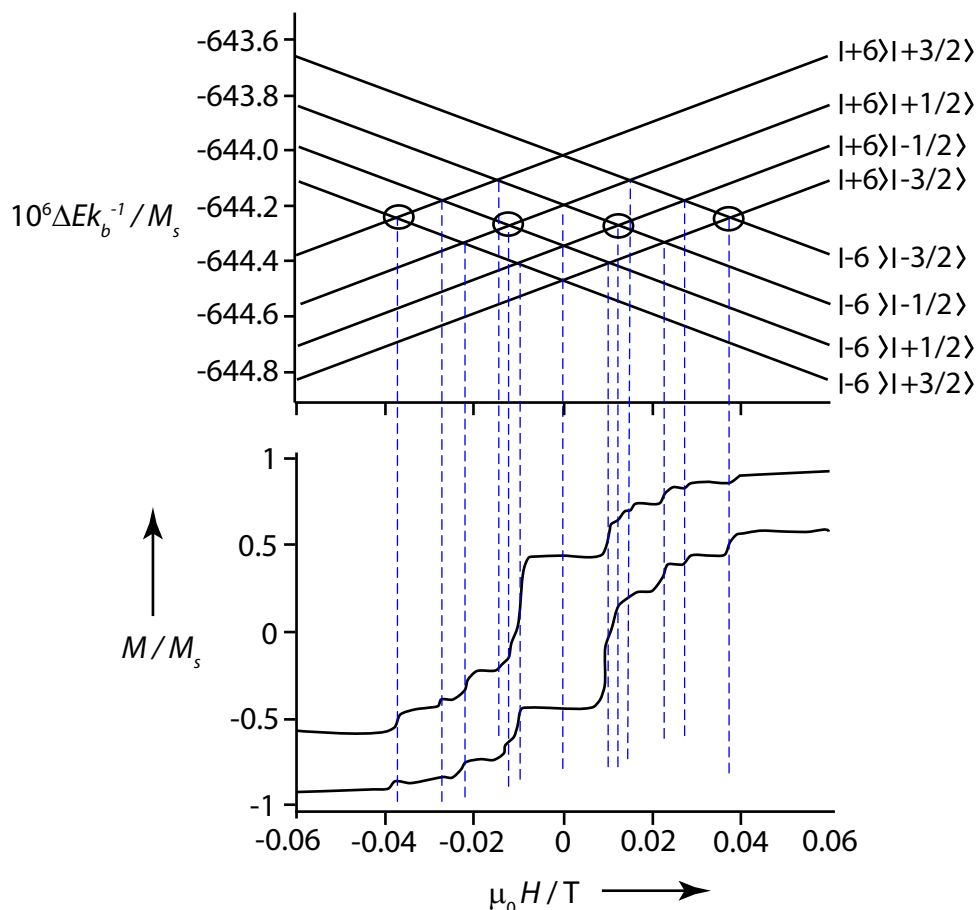


Figure 1-25. Zeeman energy diagram (above) taking into account the ligand field splitting, the hyperfine interaction and the quadrupole interaction. Magnetization hysteresis measured at 0.04 K (below)

Finally, in 2004, it was shown that the neutral species $[\text{Pc}_2\text{Tb}]^0$ which is the one electron oxidation product of $[\text{Pc}_2\text{Tb}]^-$ and therefore presents an unpaired electron delocalized over the whole complex and can be written as $[\text{Pc}^{2-} \text{Tb}^{3+} \text{Pc}^{\bullet-}]$, also presents single-molecule magnet behavior.^[89] Moreover, the neutral complex showed out of phase ac magnetic susceptibility peaks at higher temperature than the corresponding anionic compound (see Figure 1-26). This suggests that this oxidation state might be a

^[88] N. Ishikawa, M. Sugita and W. Wernsdorfer, *J. Am. Chem. Soc.* **2005**, *127*, 3650-3651.

^[89] N. Ishikawa, M. Sugita, N. Tanaka, T. Ishikawa, S.-y. Koshihara and Y. Kaizu, *Inorg. Chem.* **2004**, *43*, 5498-5500.

better single-molecule magnet than its parent anionic compound. Nevertheless, surprisingly, no hysteresis of magnetization was reported on this oxidation state at the beginning of the work toward this PhD thesis.

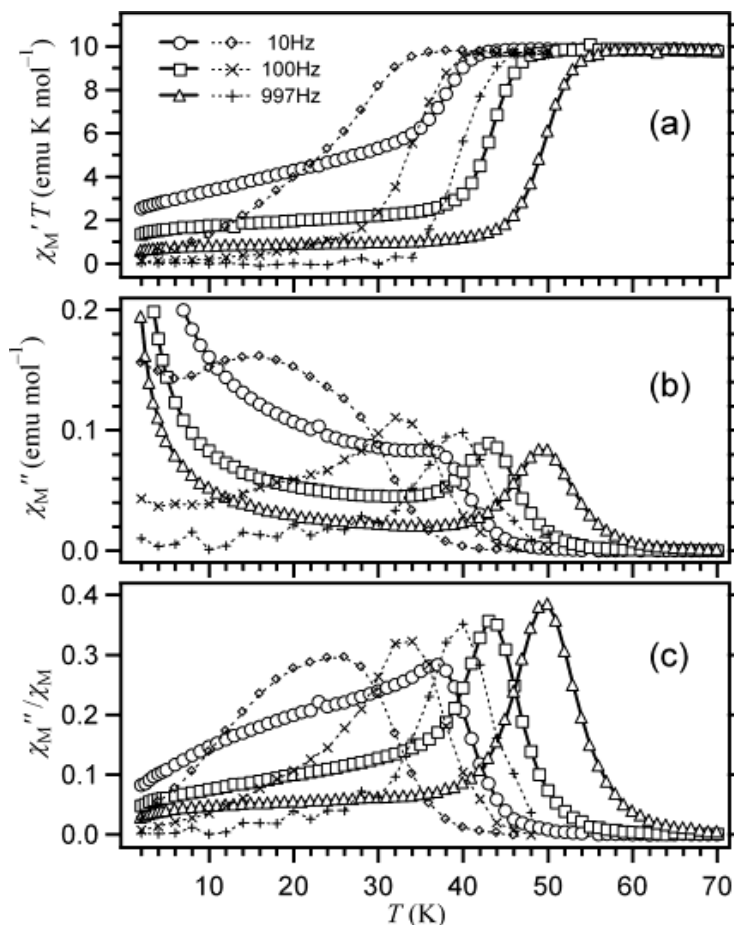


Figure 1-26. Real χ_M' (above) and imaginary χ_M'' (middle and below) components of the ac magnetic susceptibility of $[\text{Pc}_2\text{Tb}]^0$ (full line) and $[\text{Pc}_2\text{Tb}]^-$ (dotted line).

In principle, the double-decker complexes can be found in a variety of oxidation states, and at the beginning of this work, the magnetic behavior of the cationic state and the polyanionic states had not yet been studied either, and only the magnetic behavior of the cationic species has been reported since then,^[90, 91] showing a further increase in the temperature of the peaks of the out of phase ac magnetic susceptibility plots.

^[90] S. Takamatsu, T. Ishikawa, S.-y. Koshihara and N. Ishikawa, *Inorg. Chem.* **2007**, *46*, 7250-7252.
^[91] S. Takamatsu and N. Ishikawa, *Polyhedron* **2007**, *26*, 1859-1862.

1-5-2-2 Physico-chemical properties of double-decker phthalocyanine lanthanide complexes

While the SMM behavior of double-decker phthalocyanine lanthanide complexes have been reported only recently, these systems have been known for many years. Indeed the first synthesis of a lanthanide double-decker complex dates back to 1965,^[92] and the lutetium(III) complex was structurally characterized as early as 1985.^[93] Lutetium double-decker phthalocyanine complexes were also among the first molecular compounds behaving as semi-conductors,^[94-96] and have even been studied for field effect transistor applications.^[97, 98] In 1989, Belarbi *et al.* obtained a series of alkoxy functionalized double-decker phthalocyanine complexes and demonstrated their mesomorphic properties.^[99] The phase behavior of functionalized lanthanide double-decker phthalocyanine complexes would later be the subject of many articles, demonstrating the versatility of the property.^[100-103]

One of the most interesting reported characteristics of functionalized double-decker complexes towards nanotechnological applications is their ability to form well packed self-assembled monolayers over a graphite surface. This was demonstrated by STM experiments performed at the liquid-graphite interface (see Figure 1-27).^[104, 105]

-
- [92] I. S. Kirin, P. N. Moskalev and Y. A. Makashev, *Russ. J. Inorg. Chem.* **1965**, 1065-1066.
 [93] A. De Cian, M. Moussavi, J. Fischer and R. Weiss, *Inorg. Chem.* **1985**, *24*, 3162-3167.
 [94] M. Maitrot, G. Guillaud, B. Boudjema, J.-J. André, H. Strzelecka, J. Simon and R. Even, *Chem. Phys. Lett.* **1987**, *133*, 59-62.
 [95] P. Turek, P. Petit, J. J. Andre, J. Simon, R. Even, B. Boudjema, G. Guillaud and M. Maitrot, *J. Am. Chem. Soc.* **1987**, *109*, 5119-5122.
 [96] A. T. Chang and J.-C. Marchon, *Inorg. Chim. Acta* **1981**, *53*, L241-L243.
 [97] N. B. Chaure, J. L. Sosa-Sanchez, A. N. Cammidge, M. J. Cook and A. K. Ray, *Org. Elec.* **2010**, *11*, 434-438.
 [98] G. Chaidogiannos, F. Petraki, N. Glezos, S. Kennou and S. Nespurek, *Materials Science and Engineering: B* **2008**, *152*, 105-108.
 [99] Z. Belarbi, C. Sirlin, J. Simon and J. J. Andre, *J. Phys. Chem.* **1989**, *93*, 8105-8110.
 [100] C. F. van Nostrum, S. J. Picken, A.-J. Schouten and R. J. M. Nolte, *J. Am. Chem. Soc.* **1995**, *117*, 9957-9965.
 [101] K. Ban, K. Nishizawa, K. Ohta, A. M. van de Craats, J. M. Warman, I. Yamamoto and H. Shirai, *J. Mater. Chem.* **2001**, *11*, 321-331.
 [102] K. Binnemans and C. Gorller-Walrand, *Chem. Rev.* **2002**, *102*, 2303-2346.
 [103] A. G. Gurek, T. Basova, D. Luneau, C. Lebrun, E. Koltsov, A. K. Hassan and V. Ahsen, *Inorg. Chem.* **2006**, *45*, 1667-1676.
 [104] K. Binnemans, J. Slevén, S. De Feyter, F. C. De Schryver, B. Donnio and D. Guillon, *Chem. Mater.* **2003**, *15*, 3930-3938.
 [105] A. S. Klymchenko, J. Slevén, K. Binnemans and S. De Feyter, *Langmuir* **2006**, *22*, 723-728.
 [106] J. Gomez-Segura, I. Diez-Perez, N. Ishikawa, M. Nakano, J. Veciana and D. Ruiz-Molina, *Chem. Commun.* **2006**, 2866-2868.

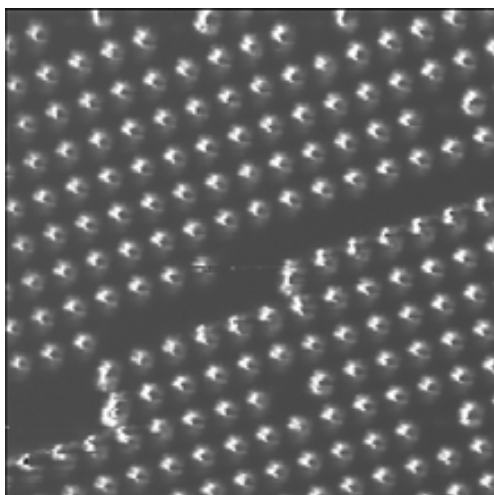


Figure 1-27. $40 \times 40 \text{ nm}^2$ STM image of a $[\text{Er}(\text{PcOC}_{12})_2]$ complex at the TCB-Graphite interface.

This combined with the single-molecule magnet behavior of the complex allows in principle to prepare a 2D-array of independent nanometric units, which could represent individual data bits of a hypothetical ultra high density storage device (albeit at very low temperature).

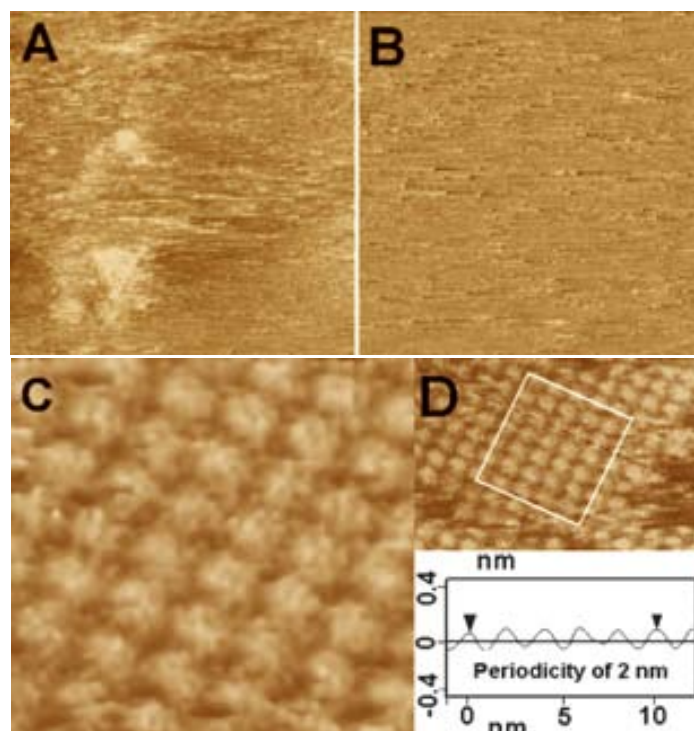


Figure 1-28. Large scale $500 \times 500 \text{ nm}^2$ STM image of the formed large aggregates after sample ageing (A). $80 \times 80 \text{ nm}^2$ detail showing no existence of ordered domains (B). High-resolution STM image of $8 \times 8 \text{ nm}$ scan area (C), where the phthalocyanine molecules can be clearly differentiated as bright spots. (D) Average section of the molecular layer.

It was nevertheless shown that such a monolayer of double-decker lanthanide phthalocyanine complexes bearing peripheral butyloxy substituents is not very stable in dry conditions, since after only 24 hours, the initial cubic phase disappears to form big aggregates (see Figure 1-28).^[106]

Finally, another interesting property of double-decker complexes is their electroactivity.^[107, 108] Indeed these complexes can be oxidized or reduced to a variety of oxidation states ranging from -5 to +2. This is yet another degree of freedom added to the possibilities of the system in order to study its magnetic behavior, since the magnetic properties of the different oxidation states are likely to be different from one another.

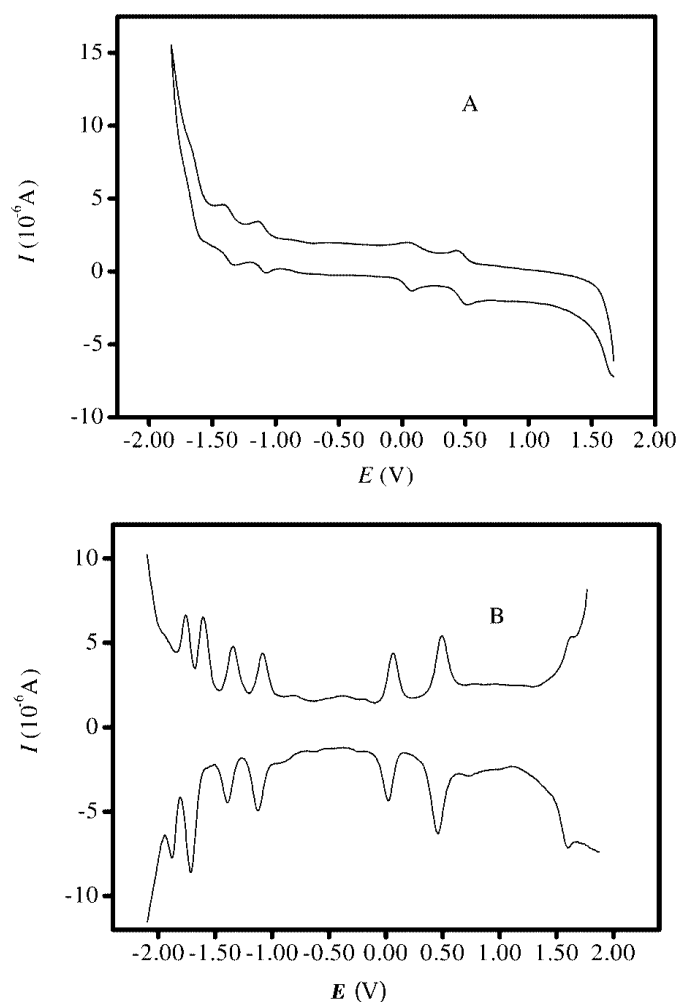


Figure 1-29. Cyclic voltammetry (A) and differential pulse voltammetry (B) of $\text{Y}(\text{Pc})_2$ in CH_2Cl_2 containing 0.1 M $[\text{Bu}_4\text{N}][\text{ClO}_4]$ at scan rates of 20 and 10 mV/s, respectively.

^[107] P. Zhu, F. Lu, N. Pan, Dennis P. Arnold, S. Zhang and J. Jiang, *Eur. J. Inorg. Chem.* **2004**, 2004, 510-517.

^[108] K. M. Kadish, T. Nakanishi, A. Gurek, V. Ahsen and I. Yilmaz, *J. Phys. Chem. B* **2001**, 105, 9817-9821.

It has already been shown above that Ishikawa and coworkers have reported how upon oxidation to the neutral complex, the magnetic properties of the anionic double-decker terbium phthalocyanine complex are strongly modified, and present a higher effective barrier.^[89]

1-6 Applications with single-molecule magnets

The research with single-molecule magnets is in constant expansion, while it was at first limited to the study of the bulk complexes, a lot of interest has been given lately to potential uses of these systems for fundamental and practical applications.

On a fundamental aspect, some interest has been given lately to magneto-chiral dichroism,^[109, 110] and chiral single-molecule magnets are ideal candidates for the observation of this phenomenon since they possess both natural chirality and an intrinsic lasting magnetic moment at the molecular level. While this effect has been measured recently in bulk chiral ferromagnets,^[111] it still has not been observed in single-molecule magnets.

On the other, the practical technological application of single-molecule magnets requires a control of their properties in interaction with a substrate.^[112] Indeed, a potential 2D storage device in which each molecule would be a bit of data would require it to be prepared as a stable 2D-array on a flat surface (the addressing and operating temperature of such a device are of course non-realistic at this stage), and after characterizing the behavior of SMMs in bulk, it is important to probe their properties when deposited on a substrate in order to check the persistence of the properties, which might as well be destroyed by the surface-molecule interaction. The preparation of surface supported SMMs is therefore a currently very active field of research, either by physisorption^[113-115] or chemical binding^[116-118] of the SMMs to a variety of substrates.

^[109] G. L. J. A. Rikken and E. Raupach, *Nature* **1997**, *390*, 493-494.

^[110] G. L. J. A. Rikken and E. Raupach, *Nature* **2000**, *390*, 932-935.

^[111] C. Train, R. Gheorghe, V. Krstic, L.-M. Chamoreau, N. S. Ovanesyan, G. L. J. A. Rikken, M. Gruselle and M. Verdaguer, *Nat. Mater.* **2008**, *7*, 729-734.

^[112] D. Gatteschi, A. Cornia, M. Mannini and R. Sessoli, *Inorg. Chem.* **2009**, *48*, 3408-3419.

^[113] L. Margheriti, M. Mannini, L. Sorace, L. Gorini, D. Gatteschi, A. Caneschi, D. Chiappe, R. Moroni, F. B. de Mongeot, A. Cornia, F. M. Piras, A. Magnani and R. Sessoli, *Small* **2009**, *5*, 1460-1466.

^[114] M. Mannini, D. Bonacchi, L. Zobbi, F. M. Piras, E. A. Speets, A. Caneschi, A. Cornia, A. Magnani, B. J. Ravoo, D. N. Reinhoudt, R. Sessoli and D. Gatteschi, *Nano Lett.* **2005**, *5*, 1435-1438.

After some failed attempts due to the instability Mn_{12} compounds when deposited on a Au surface,^[119] it was not until 2009 that the first magnetic characterization of a working SMM compound covalently bonded to a surface was reported,^[120] by covalently bonding an Fe_8 on gold via a long thioalkyl chain. It is worth mentioning that in this configuration, the compound is far enough from the surface not to be perturbed by it, but that packing of the SAM was not very efficient. Therefore, to date, no dense ordered self assembled monolayer of working SMMs on a surface have been described.

-
- [115] F. Pineider, M. Mannini, R. Sessoli, A. Caneschi, D. Barreca, L. Armelao, A. Cornia, E. Tondello and D. Gatteschi, *Langmuir* **2007**, *23*, 11836-11843.
- [116] G. G. Condorelli, A. Motta, M. Favazza, P. Nativo, I. L. Fragala and D. Gatteschi, *Chem. Eur. J.* **2006**, *12*, 3558-3566.
- [117] G. G. Condorelli, A. Motta, I. L. Fragala, F. Giannazzo, V. Raineri, A. Caneschi and D. Gatteschi, *Angew. Chem. Int. Ed.* **2004**, *43*, 4081-4084.
- [118] G. G. Condorelli, A. Motta, G. Pellegrino, A. Cornia, L. Gorini, I. L. Fragalà, C. Sangregorio and L. Sorace, *Chem. Mater.* **2008**, *20*, 2405-2411.
- [119] M. Mannini, P. Saintavit, R. Sessoli, C. Cartier dit Moulin, F. Pineider, M. A. Arrio, A. Cornia and D. Gatteschi, *Chem. Eur. J.* **2008**, *14*, 7530-7535.
- [120] M. Mannini, F. Pineider, P. Saintavit, C. Danieli, E. Otero, C. Sciancalepore, A. M. Talarico, M. A. Arrio, A. Cornia, D. Gatteschi and R. Sessoli, *Nat. Mater.* **2009**, *8*, 194-197.

Bibliography

- [1] L. Shu-hua, *Isis* **1954**, *45*, 175-196.
- [2] L. Tche-tchen, *pen-ts'ao-kang-mou*, **1580**.
- [3] G. B. Porta, *Natural Magick*, **1589**.
- [4] J. S. Miller, M. Drillon, *Magnetism: Molecules to Materials I, Models and Experiments*, Wiley-VCH, **2001**.
- [5] J. S. Miller, M. Drillon, *Magnetism: Molecules to Materials II, Molecule-based Materials*, Wiley-VCH, **2001**.
- [6] J. S. Miller, M. Drillon, *Magnetism: Molecules to Materials III, Nanosized Magnetic Materials*, Wiley-VCH, **2002**.
- [7] J. S. Miller, M. Drillon, *Magnetism: Molecules to Materials IV*, Wiley-VCH, **2003**.
- [8] J. S. Miller, M. Drillon, *Magnetism: Molecules to Materials V*, Wiley-VCH, **2005**.
- [9] R. L. Carling, *Magnetochemistry*, Springer-Verlag, **1986**.
- [10] O. Kahn, *Molecular Magnetism*, VCH Publishers, **1993**.
- [11] J. S. Miller, J. C. Calabrese, H. Rommelmann, S. R. Chittipeddi, J. H. Zhang, W. M. Reiff, A. J. Epstein, *J. Am. Chem. Soc.* **1987**, *109*, 769-781.
- [12] O. Kahn, Y. Pei, M. Verdaguer, J. P. Renard, J. Sletten, *J. Am. Chem. Soc.* **1988**, *110*, 782-789.
- [13] J. M. Manriquez, G. T. Yee, R. S. McLean, A. J. Epstein, J. S. Miller, *Science* **1991**, *252*, 1415-1417.
- [14] M. Tamura, Y. Nakazawa, D. Shiomi, K. Nozawa, Y. Hosokoshi, M. Ishikawa, M. Takahashi, M. Kinoshita, *Chem. Phys. Lett.* **1991**, *186*, 401-404.
- [15] F. Palacio, G. Antorrena, M. Castro, R. Burriel, J. Rawson, J. N. B. Smith, N. Bricklebank, J. Novoa, C. Ritter, *Phys. Rev. Lett.* **1997**, *79*, 2336.
- [16] D. Gatteschi, R. Sessoli, J. Villain, *Molecular Nanomagnets*, Oxford University Press, Oxford, **2006**.
- [17] R. F. Weinland, G. Fischer, *Z. Anorg. Allg. Chem.* **1921**, *120*, 161-180.
- [18] T. Lis, *Acta Crystallog. B* **1980**, *36*, 2042-2046.
- [19] P. D. W. Boyd, Q. Li, J. B. Vincent, K. Folting, H. R. Chang, W. E. Streib, J. C. Huffman, G. Christou, D. N. Hendrickson, *J. Am. Chem. Soc.* **1988**, *110*, 8537-8539.
- [20] A. Caneschi, D. Gatteschi, R. Sessoli, A. L. Barra, L. C. Brunel, M. Guillot, *J. Am. Chem. Soc.* **1991**, *113*, 5873-5874.
- [21] R. Sessoli, H. L. Tsai, A. R. Schake, S. Wang, J. B. Vincent, K. Folting, D. Gatteschi, G. Christou, D. N. Hendrickson, *J. Am. Chem. Soc.* **1993**, *115*, 1804-1816.
- [22] R. Sessoli, D. Gatteschi, A. Caneschi, M. A. Novak, *Nature* **1993**, *365*, 141-143.
- [23] J. R. Friedman, M. P. Sarachik, J. Tejada, R. Ziolo, *Phys. Rev. Lett.* **1996**, *76*, 3830-3833.
- [24] L. Thomas, F. Lioni, R. Ballou, D. Gatteschi, R. Sessoli, B. Barbara, *Nature* **1996**, *383*, 145-147.
- [25] J. R. Friedman, M. P. Sarachik, J. Tejada, J. Maciejewski, R. Ziolo, *J. Appl. Phys.* **1996**, *79*, 6031-6033.
- [26] D. Gatteschi, R. Sessoli, *Angew. Chem. Int. Ed.* **2003**, *42*, 268-297.
- [27] J. Tejada, R. F. Ziolo, X. X. Zhang, *Chem. Mater.* **1996**, *8*, 1784-1792.
- [28] H. J. Eppley, H.-L. Tsai, N. de Vries, K. Folting, G. Christou, D. N. Hendrickson, *J. Am. Chem. Soc.* **1995**, *117*, 301-317.

- [29] A. Cornia, A. C. Fabretti, R. Sessoli, L. Sorace, D. Gatteschi, A. L. Barra, C. Daiguebonne, T. Roisnel, *Acta Crystallogr C* **2002**, *58*, m371-373.
- [30] S. M. J. Aubin, Z. Sun, H. J. Eppley, E. M. Rumberger, I. A. Guzei, K. Folting, P. K. Gantzel, A. L. Rheingold, G. Christou, D. N. Hendrickson, *Inorg. Chem.* **2001**, *40*, 2127-2146.
- [31] D. Ruiz-Molina, P. Gerbier, E. Rumberger, D. B. Amabilino, I. A. Guzei, K. Folting, J. C. Huffman, A. Rheingold, G. Christou, J. Veciana, D. N. Hendrickson, *J. Mater. Chem.* **2002**, *12*, 1152-1161.
- [32] N. Domingo, P. Gerbier, J. Gomez, D. Ruiz-Molina, D. B. Amabilino, J. Tejada, J. Veciana, *Polyhedron* **2003**, *22*, 2355-2358.
- [33] P. Gerbier, N. Domingo, J. Gomez-Segura, D. Ruiz-Molina, D. B. Amabilino, J. Tejada, B. E. Williamson, J. Veciana, *J. Mater. Chem.* **2004**, *14*, 2455-2460.
- [34] M. Muntó, J. Gómez-Segura, J. Campo, M. Nakano, N. Ventosa, D. Ruiz-Molina, J. Veciana, *J. Mater. Chem.* **2006**, *16*, 2612-2617.
- [35] N. Domingo, F. Luis, M. Nakano, M. Muntó, J. Gómez, J. Chaboy, N. Ventosa, J. Campo, J. Veciana, D. Ruiz-Molina, *Physical Review B - Condensed Matter and Materials Physics* **2009**, *79*.
- [36] E. Terazzi, C. Bourgoigne, R. Welter, J.-L. Gallani, D. Guillon, G. Rogez, B. Donnio, *Angew. Chem. Int. Ed.* **2008**, *47*, 490-495.
- [37] G. Aromi, S. M. J. Aubin, M. A. Bolcar, G. Christou, H. J. Eppley, K. Folting, D. N. Hendrickson, J. C. Huffman, R. C. Squire, H.-L. Tsai, S. Wang, M. W. Wemple, *Polyhedron* **1998**, *17*, 3005-3020.
- [38] Z. Sun, D. Ruiz, D. N. Hendrickson, N. R. Dilley, M. B. Maple, M. Soler, K. Folting, G. Christou, J. Ribas, *Chem. Commun.* **1999**, 1973-1974.
- [39] K. Awaga, Y. Suzuki, H. Hachisuka, K. Takeda, *J. Mater. Chem.* **2006**, *16*, 2516-2521.
- [40] N. Domingo, B. E. Williamson, J. Gomez-Segura, P. Gerbier, D. Ruiz-Molina, D. B. Amabilino, J. Veciana, J. Tejada, *Phys. Rev. B* **2004**, *69*, 052405.
- [41] E. J. L. McInnes, E. Pidcock, V. S. Oganessian, M. R. Cheesman, A. K. Powell, A. J. Thomson, *J. Am. Chem. Soc.* **2002**, *124*, 9219-9228.
- [42] S. L. Castro, Z. Sun, C. M. Grant, J. C. Bollinger, D. N. Hendrickson, G. Christou, *J. Am. Chem. Soc.* **1998**, *120*, 2365-2375.
- [43] T. Mallah, C. Auberger, M. Verdagner, P. Veillet, *J. Chem. Soc., Chem. Commun.* **1995**, 61-62.
- [44] E. K. Brechin, *Chem. Commun.* **2005**, 5141-5153.
- [45] G. Rogez, B. Donnio, E. Terazzi, J.-L. Gallani, J.-P. Kappler, J.-P. Bucher, M. Drillon, *Adv. Mater.* **2009**, *21*, 4323-4333.
- [46] Z. Lü, M. Yuan, F. Pan, S. Gao, D. Zhang, D. Zhu, *Inorg. Chem.* **2006**, *45*, 3538-3548.
- [47] H. Miyasaka, R. Clérac, W. Wernsdorfer, L. Lecren, C. Bonhomme, K.-i. Sugiura, M. Yamashita, *Angew. Chem. Int. Ed.* **2004**, *43*, 2801-2805.
- [48] S. M. J. Aubin, N. R. Dilley, L. Pardi, J. Krzystek, M. W. Wemple, L.-C. Brunel, M. B. Maple, G. Christou, D. N. Hendrickson, *J. Am. Chem. Soc.* **1998**, *120*, 4991-5004.
- [49] A. Yamaguchi, H. Ishimoto, K. Awaga, J. S. Yoo, M. Nakano, D. N. Hendrickson, E. K. Brechin, G. Christou, *Physica B* **2000**, *284-288*, 1225-1226.
- [50] S. Wang, M. S. Wemple, J. Yoo, K. Folting, J. C. Huffman, K. S. Hagen, D. N. Hendrickson, G. Christou, *Inorg. Chem.* **2000**, *39*, 1501-1513.

- [51] J. Yoo, E. K. Brechin, A. Yamaguchi, M. Nakano, J. C. Huffman, A. L. Maniero, L.-C. Brunel, K. Awaga, H. Ishimoto, G. Christou, D. N. Hendrickson, *Inorg. Chem.* **2000**, *39*, 3615-3623.
- [52] A. Bhattacharjee, Y. Miyazaki, M. Nakano, J. Yoo, G. Christou, D. N. Hendrickson, M. Sorai, *Polyhedron* **2001**, *20*, 1607-1613.
- [53] A. L. Barra, A. Caneschi, D. Gatteschi, D. P. Goldberg, R. Sessoli, *J. Solid State Chem.* **1999**, *145*, 484.
- [54] A. J. Tasiopoulos, A. Vinslava, W. Wernsdorfer, K. A. Abboud, G. Christou, *Angew. Chem. Int. Ed.* **2004**, *43*, 2117-2121.
- [55] C. J. Milios, R. Inglis, R. Bagai, W. Wernsdorfer, A. Collins, S. Moggach, S. Parsons, S. P. Perlepes, G. Christou, E. K. Brechin, *Chem. Commun.* **2007**, 3476-3478.
- [56] C. J. Milios, R. Inglis, A. Vinslava, R. Bagai, W. Wernsdorfer, S. Parsons, S. P. Perlepes, G. Christou, E. K. Brechin, *J. Am. Chem. Soc.* **2007**, *129*, 12505-12511.
- [57] C. J. Milios, A. Vinslava, W. Wernsdorfer, S. Moggach, S. Parsons, S. P. Perlepes, G. Christou, E. K. Brechin, *J. Am. Chem. Soc.* **2007**, *129*, 2754-2755.
- [58] C. J. Milios, A. Vinslava, W. Wernsdorfer, A. Prescimone, P. A. Wood, S. Parsons, S. P. Perlepes, G. Christou, E. K. Brechin, *J. Am. Chem. Soc.* **2007**, *129*, 6547-6561.
- [59] C. J. Milios, A. Vinslava, P. A. Wood, S. Parsons, W. Wernsdorfer, G. Christou, S. P. Perlepes, E. K. Brechin, *J. Am. Chem. Soc.* **2006**, *129*, 8-9.
- [60] A. Caneschi, A. Cornia, A. C. Fabretti, D. Gatteschi, *Ang. Chem. Int. Ed.* **1996**, *34*, 2716-2718.
- [61] A. Caneschi, A. Cornia, S. J. Lippard, *Angew. Chem. Int. Ed.* **1995**, *34*, 467-469.
- [62] S. P. Watton, P. Fuhrmann, L. E. Pence, S. J. Lippard, A. Caneschi, A. Cornia, G. L. Abbati, *Angew. Chem. Int. Ed.* **1997**, *36*, 2774-2776.
- [63] A. Caneschi, A. Cornia, A. C. Fabretti, D. Gatteschi, *Angew. Chem. Int. Ed.* **1999**, *38*, 1295-1297.
- [64] D. Gatteschi, R. Sessoli, A. Cornia, *Chem. Commun.* **2000**, 725-732.
- [65] K. Wieghardt, K. Pohl, I. Jibril, G. Huttner, *Angew. Chem. Int. Ed.* **1984**, *23*, 77-78.
- [66] A. L. Barra, P. Debrunner, D. Gatteschi, C. E. Schulz, R. Sessoli, *Europhys. Lett.* **1996**, *35*, 133-138.
- [67] A. L. Barra, A. Caneschi, A. Cornia, F. Fabrizi de Biani, D. Gatteschi, C. Sangregorio, R. Sessoli, L. Sorace, *J. Am. Chem. Soc.* **1999**, *121*, 5302-5310.
- [68] S. Accorsi, A.-L. Barra, A. Caneschi, G. Chastanet, A. Cornia, A. C. Fabretti, D. Gatteschi, C. Mortalò, E. Olivieri, F. Parenti, P. Rosa, R. Sessoli, L. Sorace, W. Wernsdorfer, L. Zoppi, *J. Am. Chem. Soc.* **2006**, *128*, 4742-4755.
- [69] A. Cornia, L. Gregoli, C. Danieli, A. Caneschi, R. Sessoli, L. Sorace, A.-L. Barra, W. Wernsdorfer, *Inorg. Chim. Acta* **2008**, *361*, 3481-3488.
- [70] A. Bouwen, A. Caneschi, D. Gatteschi, E. Goovaerts, D. Schoemaker, L. Sorace, M. Stefan, *J. Phys. Chem. B* **2001**, *105*, 2658-2663.
- [71] A. Cornia, A. C. Fabretti, P. Garrisi, C. Mortalò, D. Bonacchi, D. Gatteschi, R. Sessoli, L. Sorace, W. Wernsdorfer, A.-L. Barra, *Angew. Chem. Int. Ed.* **2004**, *43*, 1136-1139.
- [72] N. Ishikawa, M. Sugita, T. Ishikawa, S.-y. Koshihara, Y. Kaizu, *J. Am. Chem. Soc.* **2003**, *125*, 8694-8695.
- [73] M. A. AlDamen, J. M. Clemente-Juan, E. Coronado, C. Martí-Gastaldo, A. Gaita-Ariño, *J. Am. Chem. Soc.* **2008**, *130*, 8874-8875.

- [74] M. A. AlDamen, S. Cardona-Serra, J. M. Clemente-Juan, E. Coronado, A. Gaita-Ariño, C. Martí-Gastaldo, F. Luis, O. Montero, *Inorg. Chem.* **2009**, *48*, 3467-3479.
- [75] D. E. Freedman, W. H. Harman, T. D. Harris, G. J. Long, C. J. Chang, J. R. Long, *J. Am. Chem. Soc.* **2010**, *132*, 1224-1225.
- [76] W. H. Harman, C. J. Chang, *J. Am. Chem. Soc.* **2007**, *129*, 15128-15129.
- [77] H. Andres, E. L. Bominaar, J. M. Smith, N. A. Eckert, P. L. Holland, E. Münck, *J. Am. Chem. Soc.* **2002**, *124*, 3012-3025.
- [78] N. Ishikawa, Y. Kaizu, *J. Phys. Chem.* **1996**, *100*, 8722-8730.
- [79] N. Ishikawa, T. Okubo, Y. Kaizu, *Inorg. Chem.* **1999**, *38*, 3173-3181.
- [80] N. Ishikawa, Y. Kaizu, *J. Phys. Chem. A* **2000**, *104*, 10009-10016.
- [81] N. Ishikawa, *J. Porphyrins Phthalocyanines* **2001**, *5*, 87-101.
- [82] N. Ishikawa, T. Iino, Y. Kaizu, *J. Am. Chem. Soc.* **2002**, *124*, 11440-11447.
- [83] N. Ishikawa, T. Iino, Y. Kaizu, *J. Phys. Chem. A* **2002**, *106*, 9543-9550.
- [84] N. Ishikawa, M. Sugita, T. Okubo, N. Tanaka, T. Iino, Y. Kaizu, *Inorg. Chem.* **2003**, *42*, 2440-2446.
- [85] N. Ishikawa, M. Sugita, T. Ishikawa, S.-y. Koshihara, Y. Kaizu, *J. Phys. Chem. B* **2004**, *108*, 11265-11271.
- [86] A. Abragam, B. Bleaney, in *Electron Paramagnetic Resonance*, Clarendon press, Oxford, **1970**.
- [87] N. Ishikawa, M. Sugita, W. Wernsdorfer, *Angew. Chem. Int. Ed.* **2005**, *44*, 2931-2935.
- [88] N. Ishikawa, M. Sugita, W. Wernsdorfer, *J. Am. Chem. Soc.* **2005**, *127*, 3650-3651.
- [89] N. Ishikawa, M. Sugita, N. Tanaka, T. Ishikawa, S.-y. Koshihara, Y. Kaizu, *Inorg. Chem.* **2004**, *43*, 5498-5500.
- [90] S. Takamatsu, T. Ishikawa, S.-y. Koshihara, N. Ishikawa, *Inorg. Chem.* **2007**, *46*, 7250-7252.
- [91] S. Takamatsu, N. Ishikawa, *Polyhedron* **2007**, *26*, 1859-1862.
- [92] I. S. Kirin, P. N. Moskalev, Y. A. Makashev, *Russ. J. Inorg. Chem.* **1965**, 1065-1066.
- [93] A. De Cian, M. Moussavi, J. Fischer, R. Weiss, *Inorg. Chem.* **1985**, *24*, 3162-3167.
- [94] M. Maitrot, G. Guillaud, B. Boudjema, J.-J. André, H. Strzelecka, J. Simon, R. Even, *Chem. Phys. Lett.* **1987**, *133*, 59-62.
- [95] P. Turek, P. Petit, J. J. Andre, J. Simon, R. Even, B. Boudjema, G. Guillaud, M. Maitrot, *J. Am. Chem. Soc.* **1987**, *109*, 5119-5122.
- [96] A. T. Chang, J.-C. Marchon, *Inorg. Chim. Acta* **1981**, *53*, L241-L243.
- [97] N. B. Chaure, J. L. Sosa-Sanchez, A. N. Cammidge, M. J. Cook, A. K. Ray, *Org. Elec.* **2010**, *11*, 434-438.
- [98] G. Chaidogiannos, F. Petraki, N. Glezos, S. Kennou, S. Nespurek, *Materials Science and Engineering: B* **2008**, *152*, 105-108.
- [99] Z. Belarbi, C. Sirlin, J. Simon, J. J. Andre, *J. Phys. Chem.* **1989**, *93*, 8105-8110.
- [100] C. F. van Nostrum, S. J. Picken, A.-J. Schouten, R. J. M. Nolte, *J. Am. Chem. Soc.* **1995**, *117*, 9957-9965.
- [101] K. Ban, K. Nishizawa, K. Ohta, A. M. van de Craats, J. M. Warman, I. Yamamoto, H. Shirai, *J. Mater. Chem.* **2001**, *11*, 321-331.
- [102] K. Binnemans, C. Gorller-Walrand, *Chem. Rev.* **2002**, *102*, 2303-2346.
- [103] A. G. Gurek, T. Basova, D. Luneau, C. Lebrun, E. Koltsov, A. K. Hassan, V. Ahsen, *Inorg. Chem.* **2006**, *45*, 1667-1676.

- [104] K. Binnemans, J. Sleven, S. De Feyter, F. C. De Schryver, B. Donnio, D. Guillon, *Chem. Mater.* **2003**, *15*, 3930-3938.
- [105] A. S. Klymchenko, J. Sleven, K. Binnemans, S. De Feyter, *Langmuir* **2006**, *22*, 723-728.
- [106] J. Gomez-Segura, I. Diez-Perez, N. Ishikawa, M. Nakano, J. Veciana, D. Ruiz-Molina, *Chem. Commun.* **2006**, 2866-2868.
- [107] P. Zhu, F. Lu, N. Pan, Dennis P. Arnold, S. Zhang, J. Jiang, *Eur. J. Inorg. Chem.* **2004**, *2004*, 510-517.
- [108] K. M. Kadish, T. Nakanishi, A. Gurek, V. Ahsen, I. Yilmaz, *J. Phys. Chem. B* **2001**, *105*, 9817-9821.
- [109] G. L. J. A. Rikken, E. Raupach, *Nature* **1997**, *390*, 493-494.
- [110] G. L. J. A. Rikken, E. Raupach, *Nature* **2000**, *390*, 932-935.
- [111] C. Train, R. Gheorghe, V. Krstic, L.-M. Chamoreau, N. S. Ovanesyan, G. L. J. A. Rikken, M. Gruselle, M. Verdager, *Nat. Mater.* **2008**, *7*, 729-734.
- [112] D. Gatteschi, A. Cornia, M. Mannini, R. Sessoli, *Inorg. Chem.* **2009**, *48*, 3408-3419.
- [113] L. Margheriti, M. Mannini, L. Sorace, L. Gorini, D. Gatteschi, A. Caneschi, D. Chiappe, R. Moroni, F. B. de Mongeot, A. Cornia, F. M. Piras, A. Magnani, R. Sessoli, *Small* **2009**, *5*, 1460-1466.
- [114] M. Mannini, D. Bonacchi, L. Zobbi, F. M. Piras, E. A. Speets, A. Caneschi, A. Cornia, A. Magnani, B. J. Ravoo, D. N. Reinhoudt, R. Sessoli, D. Gatteschi, *Nano Lett.* **2005**, *5*, 1435-1438.
- [115] F. Pineider, M. Mannini, R. Sessoli, A. Caneschi, D. Barreca, L. Armelao, A. Cornia, E. Tondello, D. Gatteschi, *Langmuir* **2007**, *23*, 11836-11843.
- [116] G. G. Condorelli, A. Motta, M. Favazza, P. Nativo, I. L. Fragala, D. Gatteschi, *Chem. Eur. J.* **2006**, *12*, 3558-3566.
- [117] G. G. Condorelli, A. Motta, I. L. Fragala, F. Giannazzo, V. Raineri, A. Caneschi, D. Gatteschi, *Angew. Chem. Int. Ed.* **2004**, *43*, 4081-4084.
- [118] G. G. Condorelli, A. Motta, G. Pellegrino, A. Cornia, L. Gorini, I. L. Fragalà, C. Sangregorio, L. Sorace, *Chem. Mater.* **2008**, *20*, 2405-2411.
- [119] M. Mannini, P. Sainctavit, R. Sessoli, C. Cartier dit Moulin, F. Pineider, M. A. Arrio, A. Cornia, D. Gatteschi, *Chem. Eur. J.* **2008**, *14*, 7530-7535.
- [120] M. Mannini, F. Pineider, P. Sainctavit, C. Danieli, E. Otero, C. Sciancalepore, A. M. Talarico, M. A. Arrio, A. Cornia, D. Gatteschi, R. Sessoli, *Nat. Mater.* **2009**, *8*, 194-197.

CHAPTER 2

OBJECTIVES

Taking into account the literature precedents exposed in the previous chapter, the four main objectives of this work were defined as follows:

1. The magnetic behavior of double-decker phthalocyanine lanthanide complexes has been studied only on the archetypal double-decker complexes Pc_2Ln , without substitution of the macrocyclic rings. By chemical modification of the phthalocyanine ligands, the first objective of this work was to: *Synthesize new functionalized double-decker phthalocyanine lanthanide complexes, in order to produce novel functional magnetic materials.*
2. The stability of physisorbed monolayers of previously reported double-decker phthalocyanine lanthanide complexes on graphite was poor, but there was a great deal of interest in being able to study the properties of these compounds immobilized on a surface. In order to be able to solve this problem, and approach the challenge of studying the properties of the compounds, the second objective of this work was to: *Synthesize long alkoxy chain functionalized double-decker phthalocyanine lanthanide complexes and to study the magnetic behavior of their self-assembled monolayers on graphite.*
3. The double-decker phthalocyanine lanthanide complexes can be oxidized or reduced to obtain a wide range of different species with redox states ranging from -5 to +3. The study of the magnetic behavior of those complexes have been almost limited so far to the mono-anionic complexes $[\text{Pc}_2\text{Ln}]^-$ and little was known on the magnetic behavior of the other oxidation states. For this reason, the third objective of this work was to: *Study the influence of the oxidation state of the double-decker phthalocyanine lanthanide complexes on their magnetic properties.*
4. Finally, the SMMs reported so far were known to be quite sensitive to the matrix arrangement in the solid phase and on the precise geometry of the coordination sphere of the magnetic ions. Moreover, some double-decker phthalocyanine complexes substituted with long alkyl chains present mesomorphic properties, which can be used as a tool to obtain a series of morphologically different solid

states of the same compound that may alter the magnetic properties through the intermolecular magnetic interactions. The fourth objective of this work was to: *Study the influence of the mesomorphic phases of a double-decker phthalocyanine lanthanide complex substituted with long alkyl chains on its magnetic properties.*

CHAPTER 3

SYNTHESIS OF DOUBLE-DECKER PHTHALOCYANINE TERBIUM COMPLEXES

3-1 Introduction

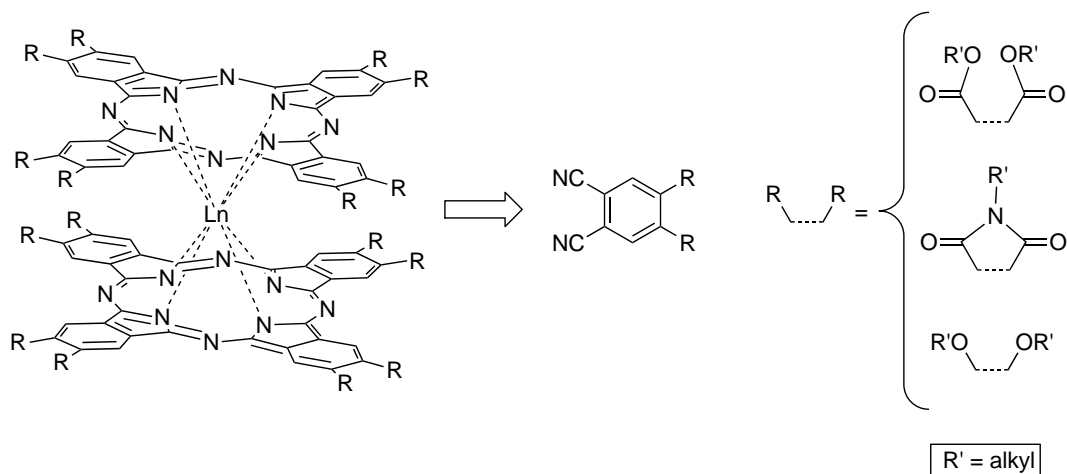
Double-decker phthalocyanine complexes have been known since 1965,^[1] and their synthesis has been described in a considerable amount of publications.^[2-11] During the course of this thesis, a variety of phthalocyanines and double-decker phthalocyanine complexes have been synthesized. While some synthetic details will be given in the next chapters, the present section aims at presenting the chemical methodologies used to prepare such compounds, to explain the synthetic choices or attempts that were made to do so, and to present the novel compounds that were prepared but have yet to be characterized magnetically.

The main synthetic goals of this PhD thesis were alkoxy substituted double-decker phthalocyanine lanthanide complexes and the electron deficient double-deckers bearing functions deriving from carboxylic groups such as alkyl imides and esters. The long alkoxy substituted complexes were prepared so as to provide a good interaction with a graphite surface in order to produce stable and organized self-assembled monolayers on this substrate. The electron deficient complexes, on the other hand, bearing either imide or ester functionalities, were prepared in order to induce a notable change in the electron density of the macrocyclic ring and therefore affect the magnetic properties of the corresponding complexes.

-
- [1] I. S. Kirin, P. N. Moskalev and Y. A. Makashev, *Russ. J. Inorg. Chem.* **1965**, 1065-1066.
[2] A. T. Chang and J.-C. Marchon, *Inorg. Chim. Acta* **1981**, 53, L241-L243.
[3] A. De Cian, M. Moussavi, J. Fischer and R. Weiss, *Inorg. Chem.* **1985**, 24, 3162-3167.
[4] Z. Belarbi, C. Sirlin, J. Simon and J. J. Andre, *J. Phys. Chem.* **1989**, 93, 8105-8110.
[5] A. Pondaven, Y. Cozien and M. L'Her, *New J. Chem.* **1992**, 16, 711-718.
[6] C. Cadiou, A. Pondaven, M. L'Her, P. Jehan and P. Guenot, *J. Org. Chem.* **1999**, 64, 9046-9050.
[7] N. Ishikawa and Y. Kaizu, *J. Phys. Chem. A* **2000**, 104, 10009-10016.
[8] M. Kocak, *J. Porphyrins Phthalocyanines* **2000**, 4, 742-744.
[9] K. Ban, K. Nishizawa, K. Ohta, A. M. van de Craats, J. M. Warman, I. Yamamoto and H. Shirai, *J. Mater. Chem.* **2001**, 11, 321-331.
[10] A. G. Gurek, V. Ahsen, D. Luneau and J. Pecaut, *Inorg. Chem.* **2001**, 40, 4793-4797.
[11] A. G. Gurek, T. Basova, D. Luneau, C. Lebrun, E. Koltsov, A. K. Hassan and V. Ahsen, *Inorg. Chem.* **2006**, 45, 1667-1676.

3-2 Synthesis of phthalonitriles

As shown in Scheme 3-1, the common precursors used for all of the phthalocyanine derivatives prepared in this PhD thesis are substituted phthalonitriles. Moreover it is worth mentioning that the prepared phthalonitriles all present a C-2 axis of symmetry in order to avoid obtaining mixtures of isomers. For this reason, the preparation of such phthalonitriles deserves special attention.



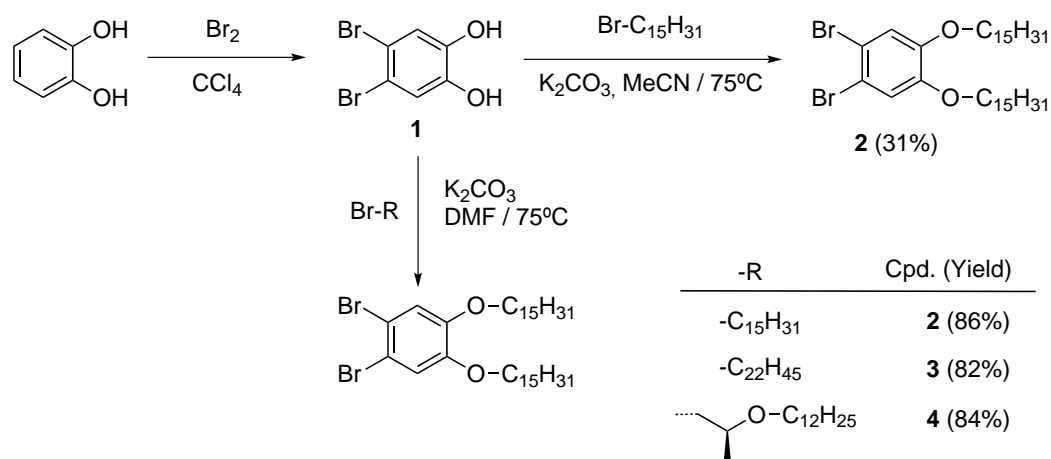
Scheme 3-1. Retrosynthetic scheme of the main target double-decker phthalocyanine lanthanide complexes bearing alkoxy substituents or electron attracting groups derived from carboxylic substituents.

3-2-1 Preparation of substituted phthalonitriles from 1,2-dibromocatechol

The preparation of alkoxy phthalonitriles is usually done from catechol in three steps. The first step corresponds to the bromination of catechol with molecular bromine, the second step comprises the alkylation of the brominated catechol in a basic medium, and finally the last step consists in the cyanation of 1,2-dibromo-1,2-bisalkoxybenzene.

The bromination of catechol was done following a described method on a multigram scale in good yields,^[12] and 1,2-dibromo-4,5-alkoxybenzene derivatives were prepared for various alkyl chains using the corresponding bromoalkyl derivative and a slight excess of K_2CO_3 (1.5 eq. with respect to the $-OH$ groups) in a warm polar solvent under a protective atmosphere of nitrogen (see Scheme 3-2). The first attempt with a 15 carbon linear alkyl chain using acetonitrile (MeCN) as a solvent provided the desired compound 1,2-dibromo-4,5-bis(pentadecyloxy)benzene (**2**) in a rather low yield of 31%.

^[12] M. Kohn, *J. Am. Chem. Soc.* **1951**, 73, 480.



Scheme 3-2. Synthesis of 1,2-dibromo-1,2-bisalkoxybenzenes **2**, **3** and **4**, employing MeCN or DMF as a solvent.

For this reason, to prepare the 22 carbon linear alkyl substituted derivative 1,2-dibromo-4,5-bisdocosyloxybenzene (**3**), in order to see if a slight change of polarity could affect the outcome for the reaction, N,N-dimethylformamide (DMF) was used as a solvent instead, achieving a higher yield (82 %). These optimized conditions were then used to prepare the chiral derivative 1,2-dibromo-4,5-bis((S)-2-(dodecyloxy)propoxy) benzene (**4**) in 84 % yield, and the synthesis of compound **2** was repeated in these conditions and was done on a multigram scale in high yield (86 %).

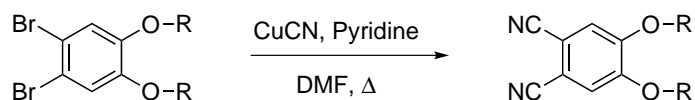
Once prepared, the 1,2-dibromo-1,2-bisalkoxybenzene derivatives were used for the preparation of the corresponding phthalonitriles by a cyanation reaction. Numerous attempts were made using the classical Rosenmund-von Braun's conditions. The Rosenmund-von Braun's reaction is the reaction of aryl halides with an excess of copper cyanide.^[13-15] This reaction can be done in the presence of pyridine as a catalyst and in refluxing DMF or without any solvent. Apart from the safety issues due to the use of a huge excess of cyanide, the reaction conditions tried never allowed clean reaction products to be obtained in a decent yield. One of the major problems of this reaction to prepare phthalonitriles is that in basic conditions in a polar solvent such as DMF, the transition metal ions like Cu⁺ can provoke the template tetramerization of the phthalonitriles formed in the course of the reaction to produce copper phthalocyanine. This is a strong limitation to the reaction, and for this reason the reactions had to be

[13] K. W. Rosenmund and E. Struck, *Berichte der deutschen chemischen Gesellschaft (A and B Series)* **1919**, 52, 1749-1756.

[14] J. von Braun and G. Manz, *Liebigs Ann. Chem.* **1931**, 488, 111-126.

[15] C. F. Koelsch and A. G. Whitney, *J. Org. Chem.* **1941**, 6, 795-803.

stopped when they just started to turn green in order to avoid the formation of copper phthalocyanine.



Scheme 3-3. The Rosenmund-von Braun's reaction applied to the synthesis of substituted phthalonitriles

For this reason, the final reaction mixtures always contained the unreacted dibromo aryl compounds, the bromocyanoaryl monosubstitution products, traces of copper phthalocyanine, other generic impurities that were identified by NMR as the 4-H-5-CN-aryl compounds and only small amounts of the desired phthalonitriles. The several attempts made with the Rosenmund-von Braun's reaction included changing the quantity of copper cyanide and pyridine, changing the reaction temperature and the solvent using compounds **2** or **3** as starting material. A summary of the tested conditions and the yields estimated by NMR of the crude mixture of product is given in Table 3-1.

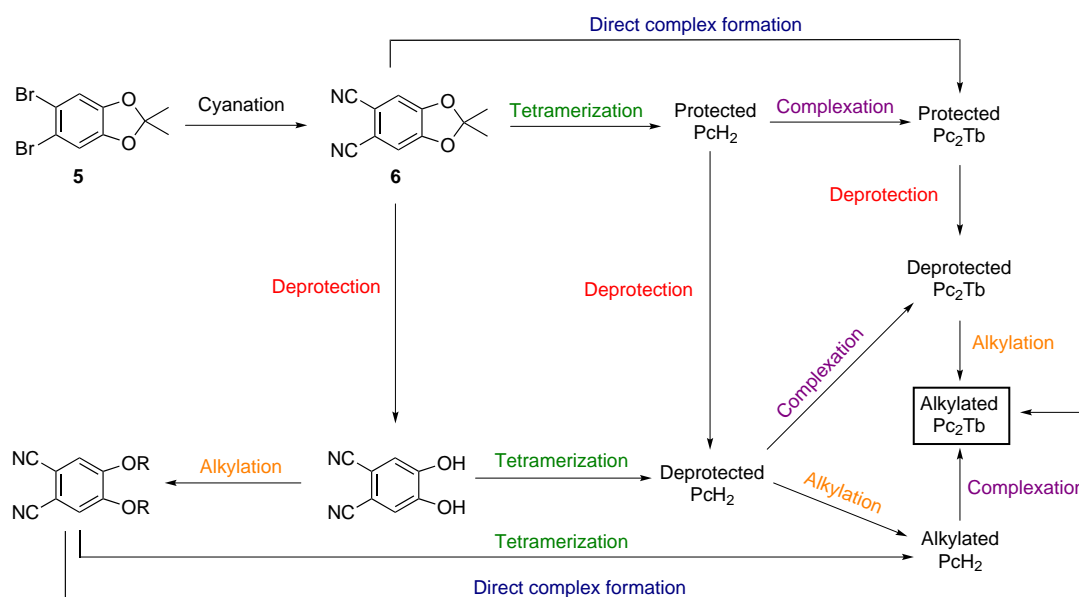
Table 3-1. Tested reaction conditions and corresponding yields of both the disubstituted and monosubstituted reaction products using the Rosenmund-von Braun cyanation reaction.

Starting compound	CuCN (eq.)	Pyridine (eq.)	Temperature (°C)	Time (h)	Solvent	Yield Ar(CN) ₂	Yield Ar(CN)Br
2	3	0.6	150	70	DMF	0	25
3	3	0.6	150	70	DMF	23	38
3	5.4	2.9	150	96	DMF	21	36
3	5	0	145	24	DMF	21	27
3	5	0	145	48	DMF	27	24
3	2.2	0	165	24	DMA	25	32

As a general observation, the phthalonitrile yield did not reach 30 % for any reaction conditions after changing the stoichiometry and the solvent and it was decided that an alternate pathway was mandatory if one wants to prepare on a large scale more valuable compounds such as the chiral phthalonitrile described later on, which requires six more steps to prepare and would require a better conversion methodology towards the phthalonitrile.

To solve this problem, the following synthetic alternative routes were designed (Scheme 3-4). Such routes require the preparation of a protected intermediate for all the alkoxy substituted phthalonitriles and an improvement of the cyanation method.

The previously reported acetal protected dibromocatechol (**5**)^[16, 17] was selected for this purpose. This protected dibromoaryl compound, was prepared with the idea of deprotecting the obtained compound at a later stage and functionalize then with the desired alkyl substituents.



Scheme 3-4. Possible reaction pathways from the acetal protected dibromoaryl derivative **5** to obtain the alkylation double-decker phthalocyanine terbium complexes

The possible synthetic strategies included introducing the desired alkoxy substituents after deprotection of the phthalonitrile or later on, after deprotection of the free base phthalocyanines or even directly of the double-decker complex.

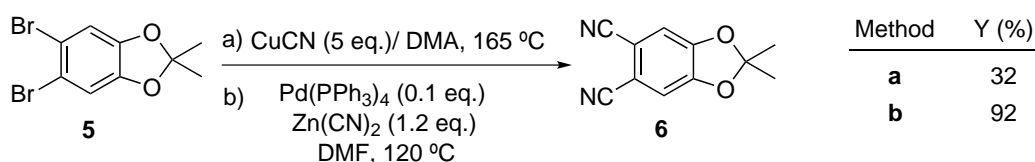
The common first step of these alternative strategies remains a cyanation process involving compound **5** as a starting material. While reproducing the conditions of Ivanov *et al.* (5 equivalents of CuCN, without pyridine and 3.5 h at 150 °C),^[16, 17] a very low yield of only 17% of **6** was obtained, together with the mononitrile derivative in 27% yield. The latter was reacted again with 1.2 equivalents of CuCN in DMA, achieving a global yield in phthalonitrile **6** of 39% over the two steps. The reaction was

[16] A. V. Ivanov, P. A. Svinareva, L. G. Tomilova and N. S. Zefirov, *Russ. Chem. Bull. Int. Ed.* **2001**, 50, 919-920.

[17] A. V. Ivanov, P. A. Svinareva, I. V. Zhukov, L. G. Tomilova and N. S. Zefirov, *Russ. Chem. Bull. Int. Ed.* **2003**, 52, 1562-1566.

repeated in refluxing DMA with almost stoichiometric quantities of CuCN (2.15 equivalents), with the effect of doubling the yield (32%). These moderately good conditions were encouraging enough to start working with the acetal protected species, but the improvement of the cyanation step was still of utmost interest.

The tandem zinc-palladium catalyzed cyanation reaction reported by Barret *et al.* was found to be a good alternative to the classical Rosenmund-von Braun cyanation reaction conditions.^[18] The reported conditions involved reacting a dibromo aryl derivative with 2.4 equivalents of zinc (II) cyanide and 0.5 equivalents of tetrakis(triphenylphosphine) palladium(0) in DMF at 85°C for 5 hours. The reaction was first tried on the acetal protected compound **5**, adapting the literature conditions. No phthalonitrile was obtained, and most of the starting material was recovered. The reaction was then tried again at higher temperature but changing strongly the stoichiometry. Thus, instead of using 0.5 equivalent of Pd[PPh₃]₄, the catalyst was used in only 0.1 equivalents (0.5 equivalents per Br group). Also, the amount of zinc (II) cyanide was reduced to almost stoichiometric conditions, using 1.2 equivalents (2.4 equivalents of cyanide) instead of the more than twofold excess used by Barrett *et al.* These conditions afforded a very high 83 % yield (using 154 mg of starting material) and was repeated on a multigram scale (3 g of starting material) affording yields of 85 and 92 % of 4,5-isopropylidenedioxyphthalonitrile (**6**).

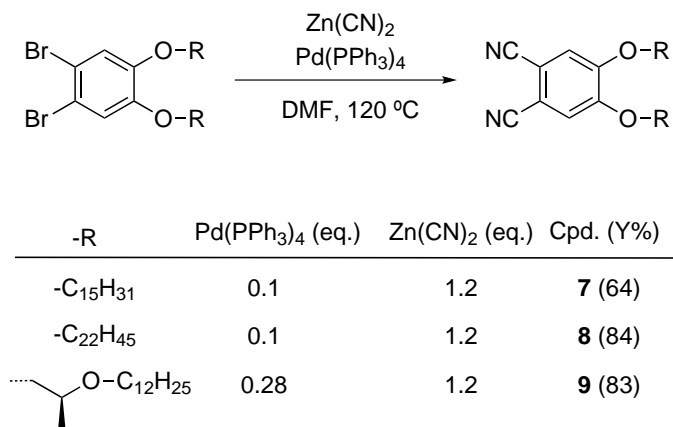


Scheme 3-5. Comparison of the Rosenmund-von Braun conditions (a) and the palladium(0) catalyzed conditions (b), together with the best yields obtained in both cases.

The excellent yields provided by employing these reaction conditions made it the method of choice throughout the rest of this work. It was used to prepare 1,2-dicyano-4,5-bis(pentadecyloxy)benzene (**7**) and 1,2-dicyano-4,5-bis(docosyloxy)benzene (**8**) in yields of 84 and 65%, respectively. The reaction was also applied to the preparation of 4,5-bis((S)-2-(dodecyloxy)propoxy)phthalonitrile (**9**) but surprisingly, in this case no conversion could be obtained with the standard conditions, possibly because of the

^[18] A. G. M. Barrett, G. R. Hanson, A. J. P. White, D. J. Williams and A. S. Micallef, *Tetrahedron* **2007**, *63*, 5244-5250.

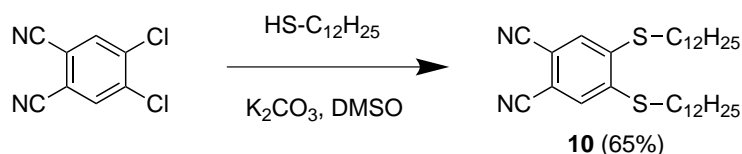
coordination of the ether groups to the metal. This problem was solved later on by incrementing the amount of catalyst to 0.28 equivalents, affording the desired chiral phthalonitrile **9** in 83% yield. The optimal reaction conditions and the best obtained yields are summarized in Scheme 3-6.



Scheme 3-6. Best yields and reaction conditions for the palladium catalyzed cyanation of three 4,5-alkoxy-1,2-dibromoaryls.

3-2-2 Functionalization of 4,5-dichlorophthalonitrile with alkylthiolates

In the previous section, the synthesis of a variety of phthalonitriles was reported, using 1,2-dibromocatechol as a precursor, and giving special emphasis to the necessary cyanation process. Nevertheless, it is also possible to obtain substituted phthalonitriles by functionalizing directly 4,5-dichlorophthalonitrile which is a commercially available product. A number of examples can be found in the literature, and usually involve the substitution of the aryl chloride by thiolates or aromatic alcoholates.^[11]



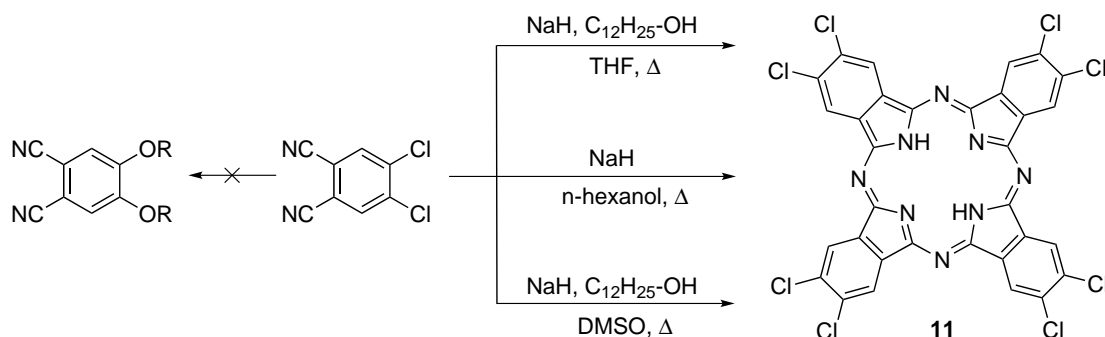
Scheme 3-7. Synthesis of 4,5-bis(dodecylthio)phthalonitrile (**10**) from 4,5-dichlorophthalonitrile.

A test reaction was done by reacting a slight excess of dodecan-1-thiol, using a total of 2.4 equivalents (i.e. 1.2 equivalents per Cl group) in the presence of a large excess of potassium carbonate (8.7 equiv.) in DMSO at room temperature. In these very mild

^[11] A. G. Gurek, T. Basova, D. Luneau, C. Lebrun, E. Koltsov, A. K. Hassan and V. Ahsen, *Inorg. Chem.* **2006**, *45*, 1667-1676.

conditions, the known phthalonitrile **10** was obtained in 12 hours in a decent 65 % yield (see Scheme 3-7).

The direct aromatic nucleophilic substitution of the aryl chlorides by thiolates is also reported with aromatic alcohols^[19, 20] but not with aliphatic alcohols. Nevertheless, we made a few trials with aliphatic alcohols as a new pathway to obtain disubstituted alkyloxy phthalonitriles. Taking into account that aliphatic alcohols are much more basic (pKa ~ 18) than aromatic alcohols or thiols (pKa ~ 10 and 12, respectively), the formation of the alcoholate to displace the aromatic chlorides requires a stronger base than K₂CO₃ (pKa ~ 12). For this reason we used sodium hydride (60 % in mineral oil) as a reagent.



Scheme 3-8. Failed attempts of synthesis of dialkoxy-phthalonitriles from 4,5-dichlorophthalonitrile, yielding the perchlorophthalocyanine **11** instead

The reaction was first tried in a variety of solvents and conditions, but the desired phthalonitriles could not be obtained. Upon warming-up of the reaction mixtures, a deep green color was always evolved which was found to be due to the formation of the corresponding octachloro substituted phthalocyanine derivative. Indeed the tetramerization of phthalonitriles is known to be done in polar solvents in the presence of alcoholates which is just the conditions tried for the substitution. The obtained compounds were practically insoluble in common solvents and were therefore not isolated. Nevertheless, the formation of **11** and a mixture of partially hydrogenated species was confirmed by LDI-TOF-MS, showing peaks at $m/z = 789.6$ and 810.6 D, corresponding to the molecular peak of [M⁻] and [NaM⁻], respectively (see Figure 3-1).

[19] D. Woehrlé, M. Eskes, K. Shigehara and A. Yamada, *Synthesis* **1993**, 194 - 196.

[20] M. J. Plater, A. Jeremiah and G. Bourhill, *J. Chem. Soc., Perkin Trans. 1* **2002**, 91 - 96.

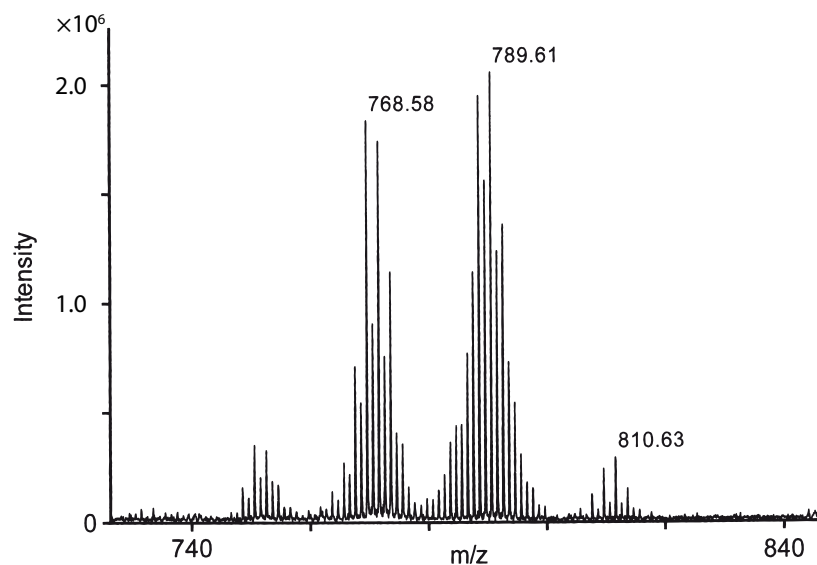
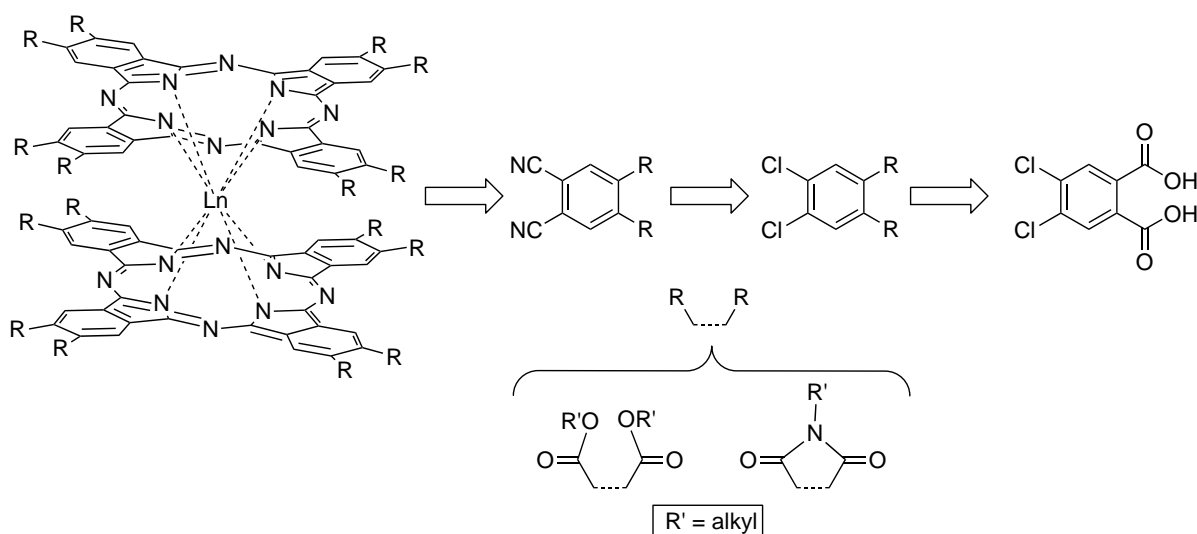


Figure 3-1. Negative polarity LDI-TOF mass spectrum of the mixtures of polychlorophthalocyanines obtained while trying to synthesize alkoxy phthalonitriles from dichlorophthalonitrile.

3-2-3 Preparation of functionalized phthalonitriles from 4,5-dichlorophthalic acid

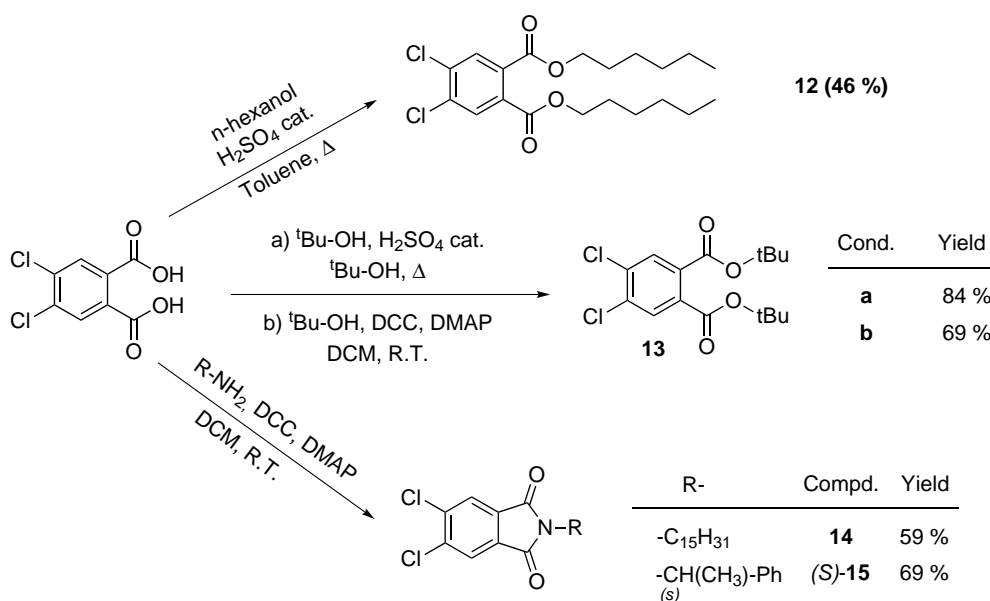


Scheme 3-9. Retrosynthetic scheme for the preparation of imide and ester functionalized double-decker phthalocyanine lanthanide complexes from 4,5-dichlorophthalic acid.

In order to vary the chemical substituents and in particular the electron density of the final phthalocyanines, amide and ester substituted phthalonitriles were prepared from

dichlorophthalic acid following up on the work of Tylleman *et al.* who prepared a series of ester substituted phthalocyanines.^[21]

The reported conditions of Tylleman *et al.* were first reproduced to prepare dihexyl-4,5-dichlorophthalate (**12**) in a moderate yield (46 %). In order to improve the yield of the reaction, an attempt was made using tert-butanol as both reagent and solvent, yielding di-tert-butyl-4,5-dichlorophthalate (**13**) in an excellent 84 % yield. But these conditions required the use of a large quantity of alcohol, and finally, this reaction was done again using the Steglich's esterification conditions,^[22] which is the reaction of the alcohol and the carboxylic acid in DCM at room temperature in the presence of a catalytic amounts of dimethylaminopyridine (DMAP) and almost stoichiometric amounts of N,N'-dicyclohexylcarbodiimide (DCC). The reaction proceeded in a 69 % yield, not as good as the 84 % of the thermally assisted acid catalyzed reaction, but required a smaller amount of the starting alcohol. Since the reaction of phthalic acid with primary amines is known to produce imides,^[23, 24] this method was also applied to the formation of the imide derivatives **14** (59 %) and (*S*)-**15** (69 %) by condensation of 1-pentadecylamine and (*S*)-1-phenylethylamine, respectively.



Scheme 3-10. Synthesis of the ester substituted compounds **12** and **13**, and of the imide derivatives **14** and (*S*)-**15**.

[21] B. Tylleman, R. Gomez-Aspe, G. Gbabode, Y. H. Geerts and S. Sergejev, *Tetrahedron* **2008**, *64*, 4155-4161.

[22] B. Neises and W. Steglich, *Angew. Chem. Int. Ed.* **1978**, *17*, 522-524.

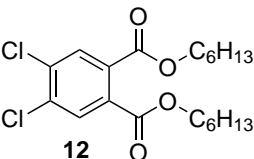
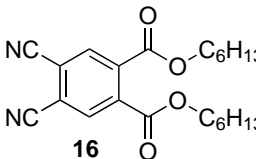
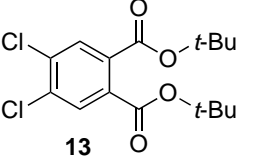
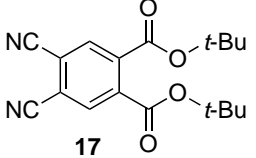
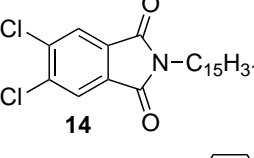
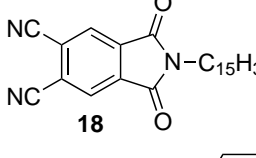
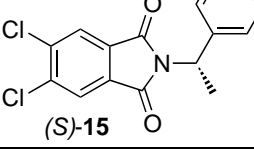
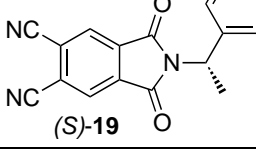
[23] M. Freund and H. Beck, *Berichte der deutschen chemischen Gesellschaft* **1904**, *37*, 1942-1946.

[24] B. Martin, H. Sekljic and C. Chassaing, *Org. Lett.* **2003**, *5*, 1851 - 1854.

The ester and imide functionalized phthalonitriles were prepared using the zinc-palladium catalyzed cyanation methodology. At first, the standard conditions using 1.1 equiv. of $\text{Zn}(\text{CN})_2$ and 0.1 equiv. of $\text{Pd}(\text{PPh}_3)_4$ were probed, but as in the case of the chiral phthalonitrile **9**, the amount of palladium catalyst had to be incremented for the reaction to work. After optimization, using a 0.2 equivalent of palladium catalyst the tert-butyl ester functionalized phthalonitrile **17**, the N-pentadecyl imide substituted phthalonitrile **18** and the chiral N-(S)-phenylethyl imide substituted phthalonitrile **19** were obtained in 32, 54 and 72 % yield, respectively. The amount of catalyst had to be incremented to 0.5 equivalents to obtain the hexyl ester substituted compound **16** in an excellent 86 % yield.

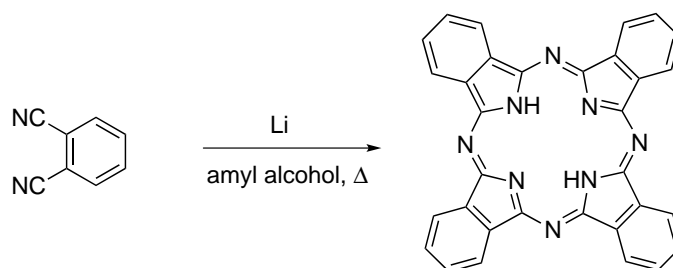
In these conditions, a family of novel phthalonitriles, substituted with electron-withdrawing groups, was prepared (see Table 3-2).

Table 3-2. Summary of the necessary amounts of palladium catalyst and the obtained conversion yields for the cyanation of compounds **12**, **13**, **14**, **S-15**.

Starting compound	$\text{Pd}(\text{PPh}_3)_4$ (eq.)	Product	Yield (%)
 12	0.5	 16	86
 13	0.2	 17	32
 14	0.2	 18	54
 (S)-15	0.2	 (S)-19	72

3-3 Synthesis of metal free phthalocyanines

The synthesis of metal free phthalocyanines is done by tetramerization of the corresponding phthalonitriles in a polar solvent and in the presence of a base. The classical conditions are those described by Barret, Frye and Linstead in 1938,^[25] in which lithium phthalocyanine is prepared as an intermediate from the phthalonitrile by refluxing the phthalonitrile in a freshly prepared 2M solution of lithium in amyl alcohol, and then the free base phthalocyanine is finally obtained by protolysis of the lithium complex.

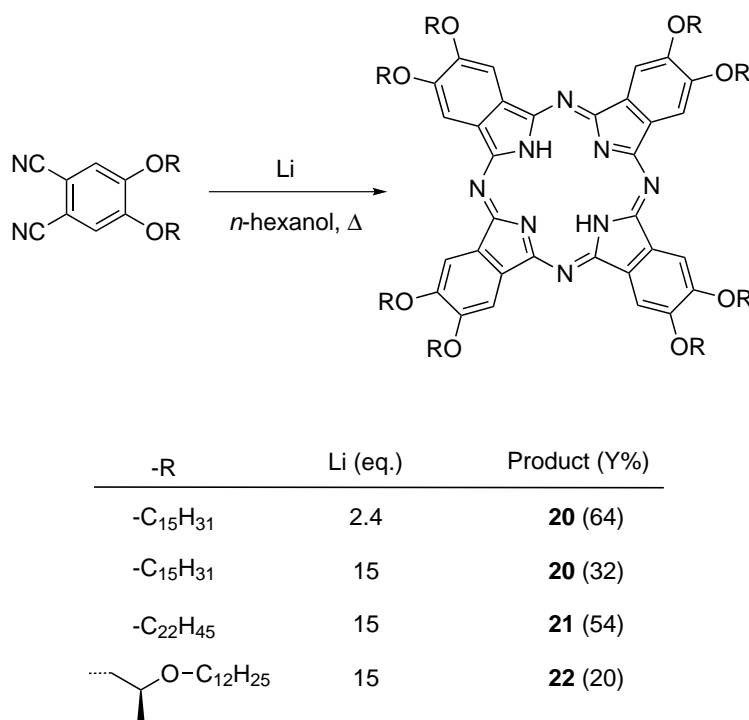


Scheme 3-11. Linstead's synthesis of phthalocyanine from phthalonitrile and lithium metal in amyl alcohol.

This method is widely used in the literature with some changes in the choice of the alcohol and usually provides good yields. In this work, we applied first this method using a tremendous excess of lithium in hexanol, because it was first tried on small quantities (for which it was necessary to introduce a bigger quantity of lithium due to partial reaction with air) and it was then scaled-up as it was. The initial standard procedure implied reacting the phthalonitriles with 15 equivalents of lithium hexanolate in hexanol, generated by reaction of elemental lithium with n-hexanol at 120 °C until complete dissolution. This method was applied to the preparation of octakis-pentadecyloxy-phthalocyanine (**20**), octakis-docosyloxy-phthalocyanine (**21**) and the chiral derivative 2,3,9,10,16,17,23,24-octakis-((S)-2-(dodecyloxy)propoxy)-phthalocyanine (**22**). The reaction yields were respectively 32, 54 and 20 %. While compound **21**, bearing 22 carbon linear alkyl chains, was synthesized in quite a good yield, the other two phthalocyanines were obtained in relatively poor yields. In order to check the influence of the quantity of lithium, the reaction was done again for compound **20** by first preparing a 2 M solution of lithium in n-hexanol and adding only 2.4 equivalent of

^[25] P. A. Barrett, D. A. Frye and R. P. Linstead, *J. Chem. Soc.* **1938**, 1157-1163.

lithium hexanolate in hexanol, without adding any more solvent despite the lack of fluidity of the mixture at room temperature. In this way, the pentadecyloxy substituted phthalocyanine **20** was obtained in 64 % yield which is the double of the yield obtained from the previous method (see Scheme 3-12).



Scheme 3-12. Synthesis of compounds **20**, **21** and **22** and corresponding yields as a function of the amount of elemental Li.

This method was also tried for the preparation of the hexyl-ester substituted phthalocyanine **23**, but as expected, the ester functions were partially saponified and the obtained deep blue reaction mixture was a complex mixture of compounds with saponified ester groups and decarboxylated compounds, as was shown by LDI-TOFMS (see Figure 3-2). No trace of the desired compound can be seen in the mass spectrum.

An alternative method was employed by analogy with the lanthanide acetate route towards double-decker phthalocyanine complexes, discussed later in this chapter, the ester substituted phthalonitrile was reacted with 1 equivalent of potassium acetate in the presence of one equivalent of diaza-bicyclo-undecene (DBU) in refluxing *n*-hexanol. Quite rapidly, the reaction mixture turned to a deep blue color indicating the formation of some phthalocyanine derivative. These conditions afforded the octa-hexylester-substituted phthalocyanine **23** in 34 % yield.

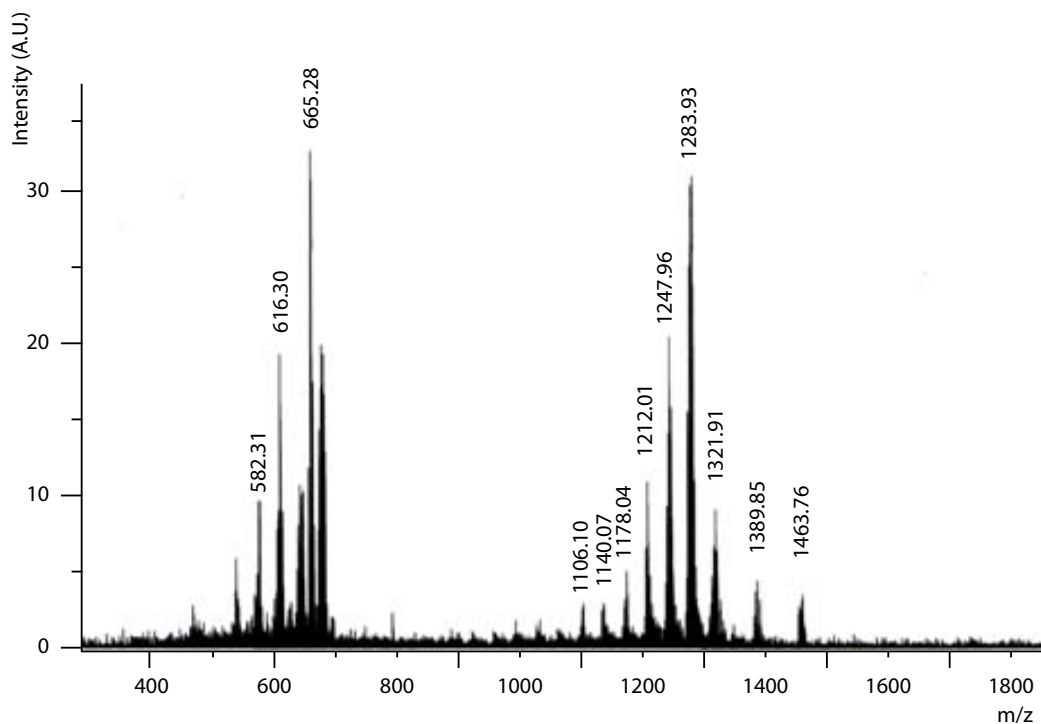


Figure 3-2. Negative polarity LDI-TOF mass spectrum of the obtained mixture of phthalocyanines when trying to synthesize the octa-ester substituted phthalocyanines using Linstead's conditions.

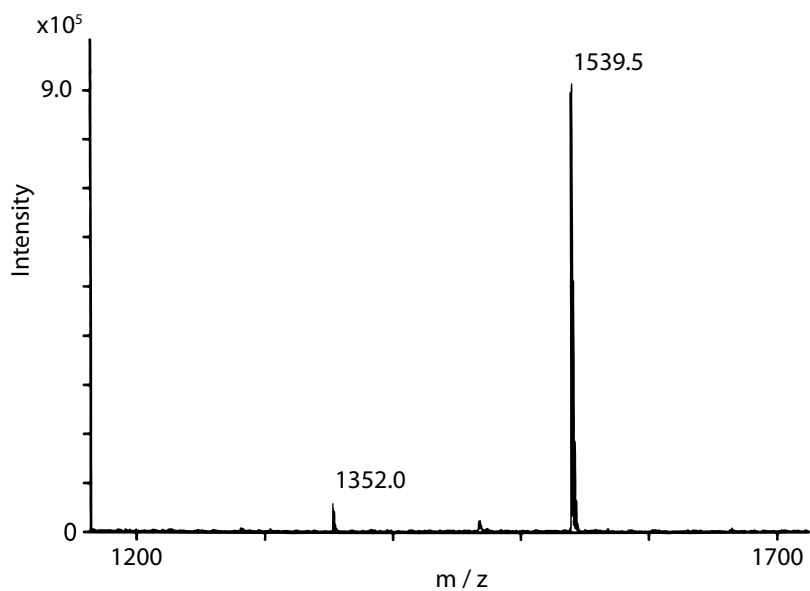
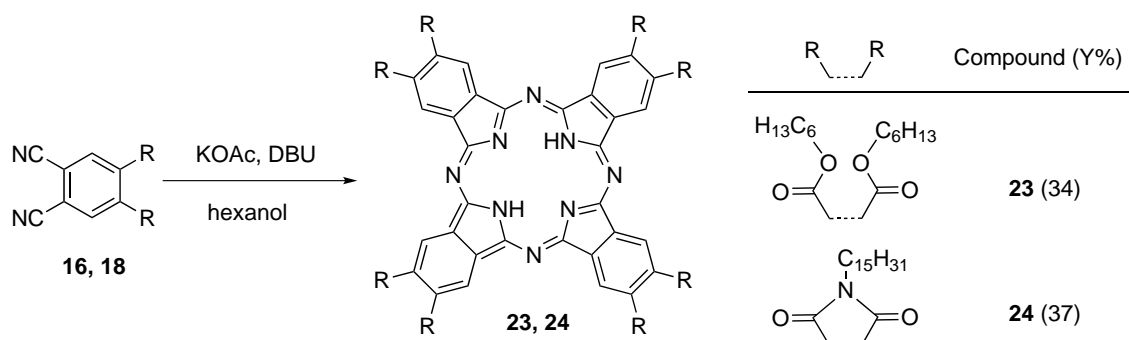


Figure 3-3. Negative polarity LDI-TOF mass spectrum of the hexyl ester substituted phthalocyanine **23** as obtained by refluxing **16** in the presence of potassium acetate and DBU in n-hexanol.

It is worth noting that this is the first direct synthesis of an octa-ester substituted free base phthalocyanine from the corresponding phthalonitrile since Barrett *et al.* could only prepare it by esterification of the corresponding octa-acid moiety.



Scheme 3-13. Synthesis of the ester and imide functionalized phthalocyanines **23** and **24**

Since the phthalimide functional groups can be hydrolyzed in the presence of a base in alcohols,^[26] the lithium amide conditions, involving the formation of alcoholate were discarded, and the milder KOAc-DBU conditions were also applied to the synthesis of tetrapentadecyl-29H,31H-2,3,9,10,16,17,23,24-phthalocyanine-tetradicarboximide (**24**) and the desired compound was obtained in a 37 % yield.

3-4 Synthesis of double-decker phthalocyanine complexes

The synthesis of double decker phthalocyanine lanthanide complexes can be done following two main routes (see Scheme 3-14).^[3, 4, 27-31] On one hand the complexes can be prepared in a one-step process directly from the corresponding phthalonitriles or they can be prepared by first synthesizing the free base phthalocyanine and then prepare the sandwich complexes by reacting them with lanthanide salts. In the course of this work, both approaches were followed depending on the substituents introduced on the periphery of the macrocycles.

^[26] S. Alibert-Fouet, I. Seguy, J.-F. Bobo, P. Destruel and H. Bock, *Chem. Eur. J.* **2007**, *13*, 1746-1753.

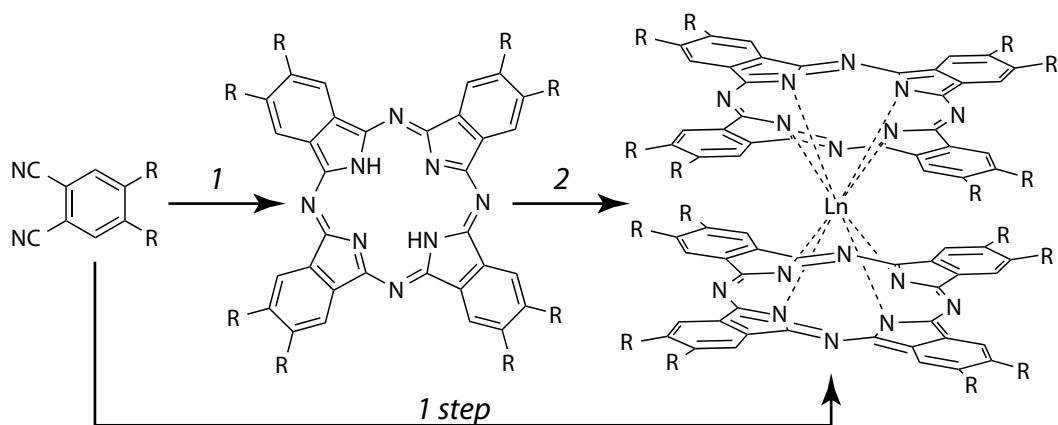
^[27] N. B. Chaure, J. L. Sosa-Sanchez, A. N. Cammidge, M. J. Cook and A. K. Ray, *Org. Elec.* **2010**, *11*, 434-438.

^[28] T. Gross, F. Chevalier and J. S. Lindsey, *Inorg. Chem.* **2001**, *40*, 4762-4774.

^[29] F. Nekelson, H. Monobe, M. Shiro and Y. Shimizu, *J. Mater. Chem.* **2007**, *17*, 2607-2615.

^[30] F. Nekelson, H. Monobe and Y. Shimizu, *Chem. Commun.* **2006**, 3874-3876.

^[31] F. Nekelson, H. Monobe and Y. Shimizu, *Mol. Cryst. Liq. Cryst.* **2007**, *479*, 205-211.



Scheme 3-14. Comparison of the one and two-steps approaches.

The main parameters used to determine which strategy to follow were the expected solubility of the free base phthalocyanine complexes and the chemical stability of the prepared compounds in the necessary reaction conditions.

3-4-1 Two-step synthesis of double-decker phthalocyanine complexes

Whenever possible, the preferred approach was to prepare the double-decker lanthanide complexes in a two-step synthetic route. First, the free base phthalocyanine were prepared and isolated, and then they were reacted with lanthanide salts in order to produce the corresponding lanthanide double-decker phthalocyanine complex. The reason why this method was preferred in a number of cases is because of the relative ease of purification of the free base phthalocyanine, as compared to the corresponding double-decker complexes.

Indeed, the one pot preparation of double-decker phthalocyanine lanthanide complexes usually affords mixtures of free base phthalocyanine, monophthalocyanine lanthanide complexes, double-decker complexes and if the mixture is heated for too long, it can also lead to the formation of triple-decker compounds, as can be seen by LDI-TOF-MS (see Figure 3-4). The separation of the latter mixture is not always so straightforward, given the fact that the double-decker complexes are quite acid and base sensitive and therefore the column chromatographies with SiO_2 have to be done carefully. For this reason, if the functionalized metal free phthalocyanine provides good solubility in common organic solvents, the two-step methodology is usually the best option.

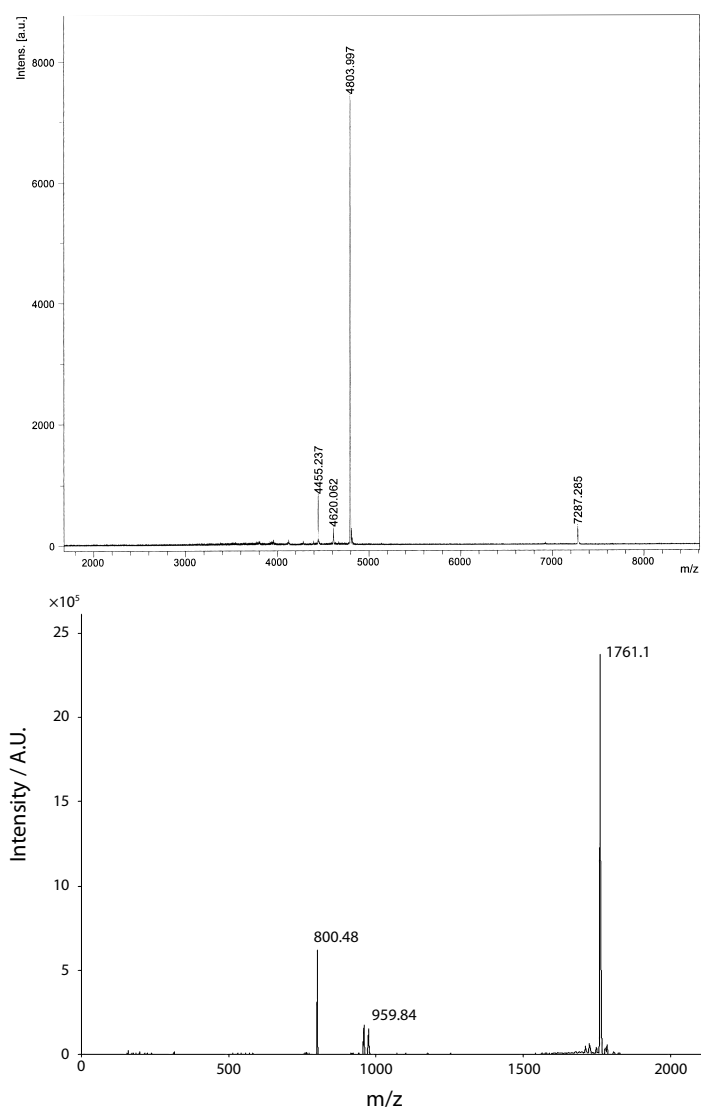
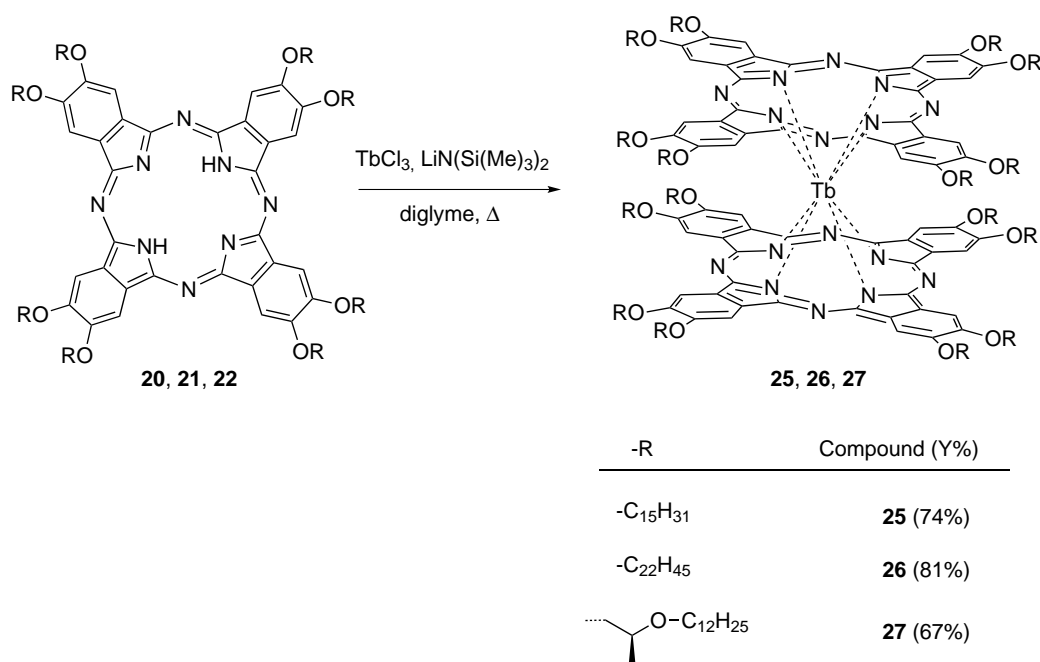


Figure 3-4. LDI-TOF spectra of the mixtures obtained in the one-step synthesis of **26** presenting the peaks of double- and triple decker complexes at $m/z = 4804.0$ and 7287.3 , respectively (above) and in the one-step synthesis of **28** presenting the peaks of the metal free phthalocyanine, the monophthalocyanine terbium complex and the double-decker complex at $m/z = 800.5$, 959.8 and 1761.1 , respectively.

The complexation reaction of metal free phthalocyanine with lanthanide salts to form double-decker complexes was studied in detail by Gross et al.,^[28] together with the possibility to prepare triple-decker complexes from the corresponding metal free phthalocyanines. The method consists in preparing in situ the activated lanthanide complex $\text{LnCl}[\text{N}(\text{SiMe}_3)_2]_2$ from anhydrous LnCl_3 (1 eq.) and $\text{Li-N}(\text{SiMe}_3)_2$ (2 eq.) in

^[28] T. Gross, F. Chevalier and J. S. Lindsey, *Inorg. Chem.* **2001**, *40*, 4762-4774.

diglyme at 0°C, and after adding the free base phthalocyanine (0.1-0.2 eq.) to the reaction mixture to heat the resulting solution at reflux temperature for 4-6 hours.



Scheme 3-15. Synthesis of complexes **25**, **26** and **27** from the corresponding metal free phthalocyanines **20**, **21** and **22**, respectively.

These conditions were used to synthesize the pentadecyloxy substituted complex **25**, the docosyloxy substituted complex **26** and the chiral alkoxy substituted complex **27** in very good yields of 74, 81 and 67%, respectively (see Scheme 3-15). Nevertheless, it was observed that this reaction requires a good control of the anhydrous conditions (properly dried Schlenk tubes, syringes, solvent and reagents) in order to work properly. Failing do so may result in the reaction not starting and requiring the addition of more lithium amide or more terbium salt. However if reproduced in rigorously dry conditions, the reaction proceeds smoothly in a few hours and can be monitored by UV-Vis spectroscopy.

The two-step method used to prepare phthalocyanine double-decker lanthanide complexes requires the use of a lithium amide, and since we have already shown how the ester and imide substituted phthalocyanines are incompatible with strong nucleophilic organic bases, the two-steps synthesis of these compounds was discarded.

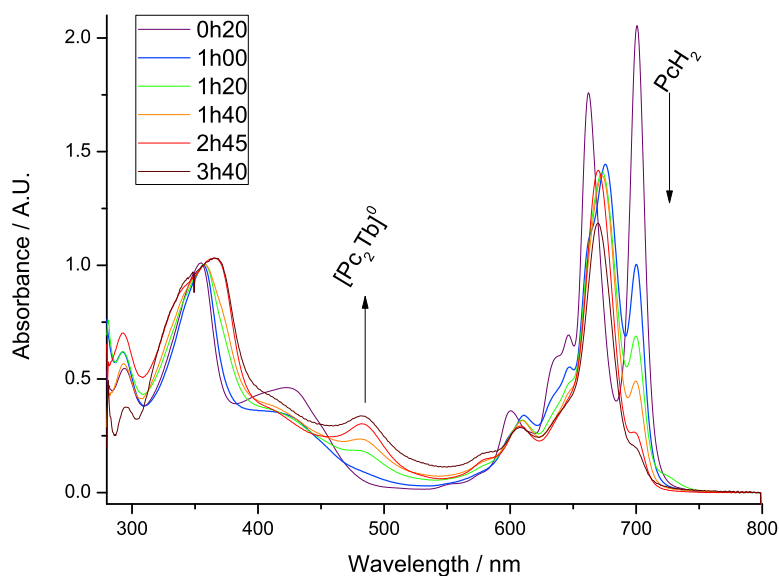


Figure 3-5. Qualitative evolution of the normalized UV-Vis spectra of the reaction mixture over time measured in toluene for the synthesis of **27**. During the course of the reaction, the band at 701 nm corresponding to the split Q-band of the metal-free phthalocyanine **22** gradually disappears while the band at 485 nm corresponding to the π -radical band of the neutral complex **27** gradually appears.

3-4-2 One-step synthesis of double-decker phthalocyanine complexes

In the case of the acetal complex **28**, the reaction was tried in the conditions of De Cian et al. using 1 equivalent of terbium(III)acetate, 8 equivalents of 4,5-isopropylidenedioxyphthalonitrile (**6**) and 4 equivalents of DBU.^[3] Surprisingly, only traces of phthalocyanines were obtained. Both the starting material **6** and the hydrated terbium acetate salt used in the reaction had been dried in vacuum, and the dry *n*-hexanol had been freshly distilled over sodium metal to ensure proper anhydrous conditions. It was not until several months had passed and after probing alternative reaction conditions that it was realized that lanthanide acetate hydrates cannot be dried by heating them in vacuum, since this leads to the formation of oxyacetates and oxides,^[32] which are not reactive under the conditions used for the formation of the double-deckers.

After consulting with Dr. Beatriz Ballesteros (Universidad Autónoma de Madrid) working with lutetium double-decker phthalocyanine complexes, it was confirmed that neither drying the lanthanide salts nor distilling the solvent was necessary. The best procedure was instead to use the lanthanide salts and the anhydrous grade solvent as

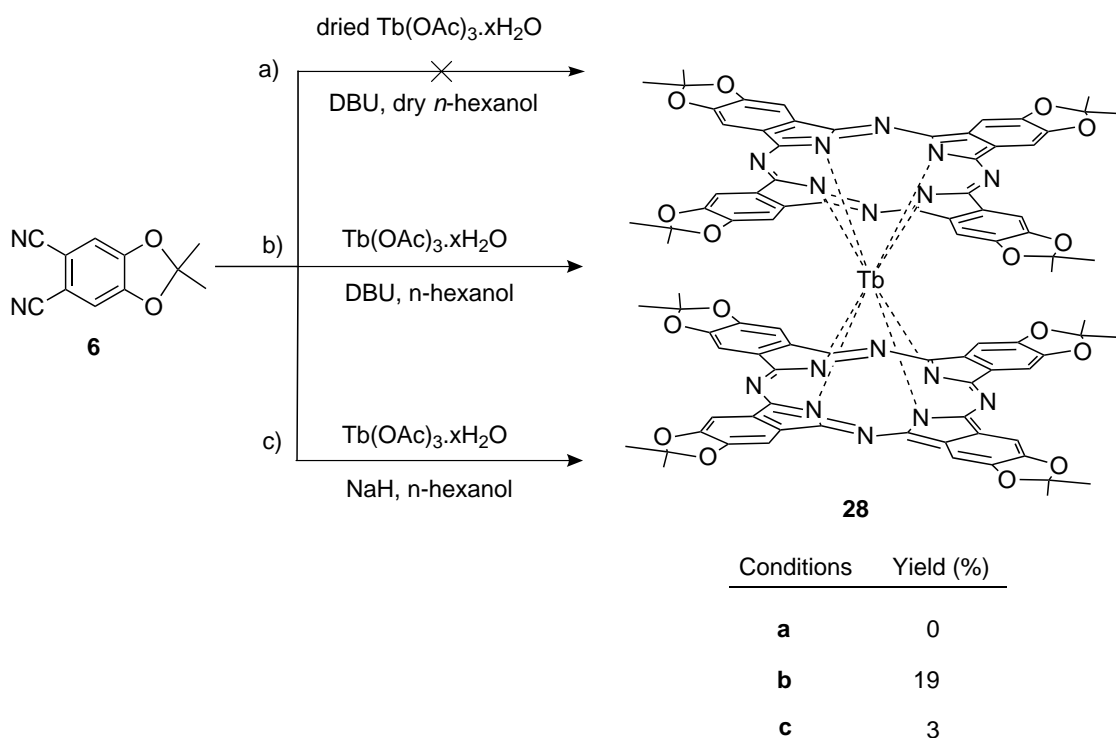
[3] A. De Cian, M. Moussavi, J. Fischer and R. Weiss, *Inorg. Chem.* **1985**, *24*, 3162-3167.

[32] *A Lanthanide Lanthology, Vol. I, A - L*, Molycorp, Inc., Mountain Pass, CA, U.S.A., **1993**. p.4

they came. After the reaction failed again, doubting about the quality of $\text{Tb}(\text{OAc})_3$ it was bought again from Sigma-Aldrich and used without any preliminary purification or drying. The reaction finally proceeded smoothly and afforded a moderate yield of 19%.

Due to the problems encountered in the reaction with DBU and $\text{Tb}(\text{OAc})_3$, and looking for an alternative, the DBU was substituted with sodium hydride in the same stoichiometry (see Scheme 3-16). Upon careful addition of NaH to a refluxing mixture of $\text{Tb}(\text{OAc})_3$ and the phthalonitrile **6** in *n*-hexanol, the solution instantly turned dark blue-green, which indicated the formation of phthalocyanines. The obtained reaction mixture contained mostly the acetal substituted free base phthalocyanine and only small quantities of the double-decker complex, not exceeding 3 % yield over several attempts.

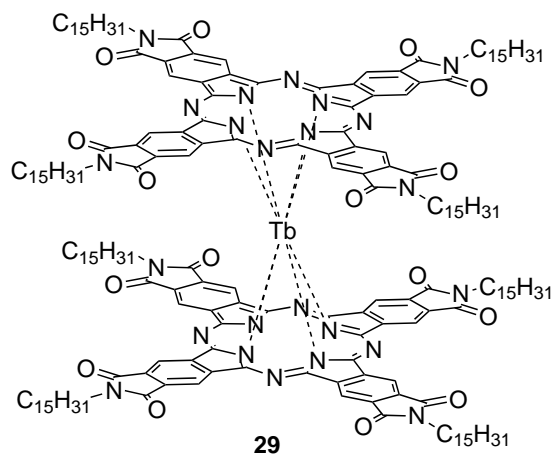
Despite the very low yield and the complicated purification of the mixture, this method was repeated several times in order to produce a few milligrams of complex **28**, until the problems with the DBU method were solved, after which this method was finally abandoned. It is nevertheless worth mentioning that while it does not provide high yields, it still stands as an existing alternative to the DBU method.



Scheme 3-16. Synthesis of the acetal protected double-decker phthalocyanine terbium complex **28**

Finally, the synthesis of the N-pentadecyl imide substituted double-decker phthalocyanine terbium complex **29** was done using the standard DBU method with a

yield of 37 %. The formation of compound **29** was confirmed by the LDI-TOF mass spectrometry (see Figure 3-6).



The UV-Vis spectrum of compound **29** measured in toluene was at first intriguing. Indeed it showed two broad bands in the Q-band region at 725 and 644 nm and did not show any band in the π -radical region of neutral double-decker complexes (around 460-490 nm).

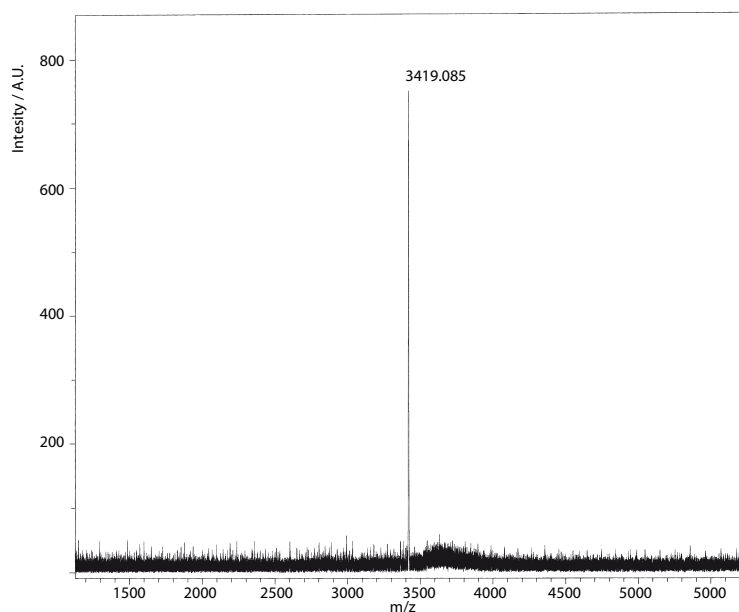


Figure 3-6. Negative polarity of the LDI-MS spectrum of the imide double-decker complex **29**

Nevertheless, upon treatment with iron perchlorate it could be oxidized, and the spectral features gradually changed to match that of a neutral double-decker complex (see Figure 3-7).

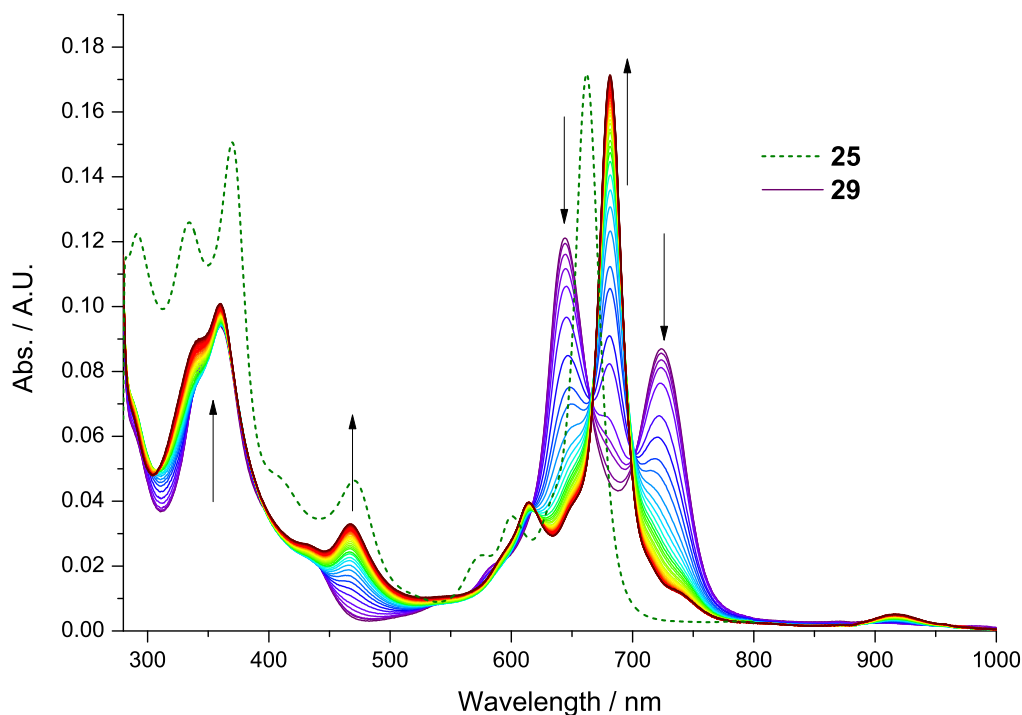


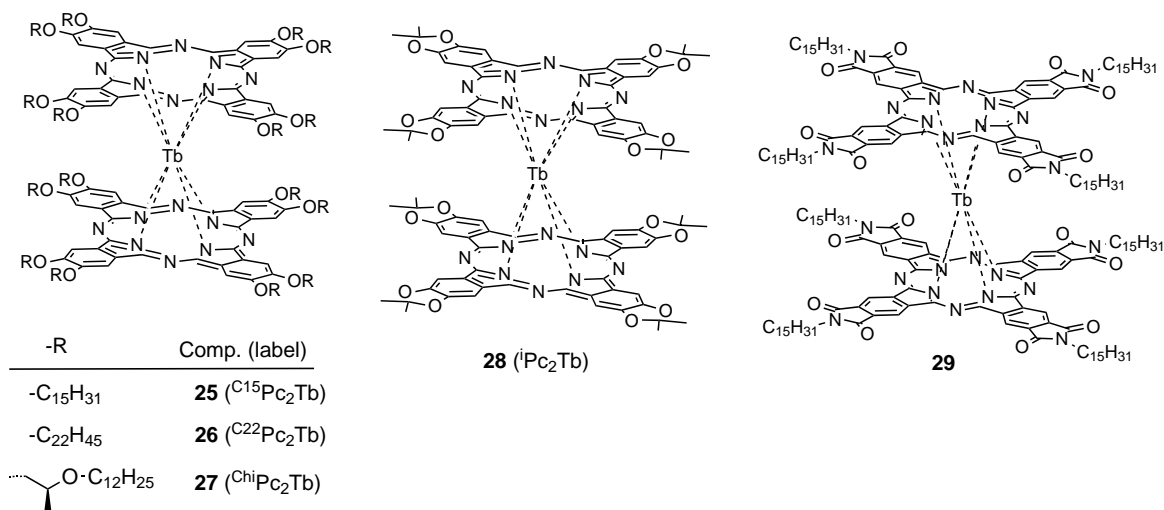
Figure 3-7. Evolution of the UV-Vis spectrum of a solution of the anionic complex **29** in toluene when oxidized to the neutral species by introduction of a small crystal of iron (III) perchlorate. The successive spectra (full lines) are measured at intervals of 2 minutes. The UV-Vis spectrum of the neutral pentadecyloxy substituted complex **25** (dotted line) is shown for comparison.

The Q-band of complex **29** is observed at 681 nm, which is at a slightly higher wavelength as compared to alkoxy functionalized double-decker complexes like complexes **25**, **26** and **27** which have Q-bands at *c.a.* 660-670 nm. Also, the splitting of the Soret bands is smaller (about 20 nm in complex **29** compared to 35 nm in complex **25**). The π -radical band on the contrary, is quite similar to that observed for complex **25** both in intensity and in energy, and is observed at 467 nm. It was therefore concluded that the complex, as it was synthesized, was in the anionic form, stabilized by the electron withdrawing imide groups, instead of the neutral form. It is worth noting that compound **29** is to the best of our knowledge the first octa-imide-substituted double-decker complex prepared until now.

Once well characterized this complex, it will be interesting to prepare and characterize a whole family of imide and ester double-decker phthalocyanine complexes in order to see the effect of these electron-withdrawing functional groups on the magnetic behaviors of the molecule.

3-4-3 Synthesized complexes used for magnetic characterizations

A total of five different double-decker complexes were synthesized during the course of the work towards this PhD thesis. Including the long alkoxy chains substituted complexes **25**, **26** and **27**, the known acetal protected complex **28** and the novel pentadecyl imide substituted complex **29**.



Scheme 3-17. Summary of the synthesized complexes **25**, **26**, **27**, **28** and **29** with the labels with which some of them will be named in the rest of this thesis.

Chapter 4 is dedicated to the electrochemical study of **28** (ⁱPc₂Tb) and the characterization of its magnetic behavior in solution in several oxidation states. In Chapter 5, the surface deposition of the alkoxy substituted complexes **25** (C¹⁵Pc₂Tb) and **26** (C²²Pc₂Tb), and of complex **28** (ⁱPc₂Tb) is studied, and the magnetic characterization of thick layers and monolayers of the neutral and anionic forms of **28** (ⁱPc₂Tb) are presented. Finally in Chapter 6, the liquid crystalline behavior of complex **27** (C^{hi}Pc₂Tb) is used to produce a variety of frozen solid phases, allowing to study the influence of the degree of order and of the matrix arrangement in the bulk solid phase on the magnetic behavior of the complex. Due to time limitations, the thorough characterization of the chemical and magnetic behavior of complex **29** is still a work in progress.

Bibliography

- [1] I. S. Kirin, P. N. Moskalev, Y. A. Makashev, *Russ. J. Inorg. Chem.* **1965**, 1065-1066.
- [2] A. T. Chang, J.-C. Marchon, *Inorg. Chim. Acta* **1981**, 53, L241-L243.
- [3] A. De Cian, M. Moussavi, J. Fischer, R. Weiss, *Inorg. Chem.* **1985**, 24, 3162-3167.
- [4] Z. Belarbi, C. Sirlin, J. Simon, J. J. Andre, *J. Phys. Chem.* **1989**, 93, 8105-8110.
- [5] A. Pondaven, Y. Cozien, M. L'Her, *New J. Chem.* **1992**, 16, 711-718.
- [6] C. Cadiou, A. Pondaven, M. L'Her, P. Jehan, P. Guenot, *J. Org. Chem.* **1999**, 64, 9046-9050.
- [7] N. Ishikawa, Y. Kaizu, *J. Phys. Chem. A* **2000**, 104, 10009-10016.
- [8] M. Kocak, *J. Porphyrins Phthalocyanines* **2000**, 4, 742-744.
- [9] K. Ban, K. Nishizawa, K. Ohta, A. M. van de Craats, J. M. Warman, I. Yamamoto, H. Shirai, *J. Mater. Chem.* **2001**, 11, 321-331.
- [10] A. G. Gurek, V. Ahsen, D. Luneau, J. Pecaut, *Inorg. Chem.* **2001**, 40, 4793-4797.
- [11] A. G. Gurek, T. Basova, D. Luneau, C. Lebrun, E. Koltsov, A. K. Hassan, V. Ahsen, *Inorg. Chem.* **2006**, 45, 1667-1676.
- [12] M. Kohn, *J. Am. Chem. Soc.* **1951**, 73, 480.
- [13] K. W. Rosenmund, E. Struck, *Berichte der deutschen chemischen Gesellschaft (A and B Series)* **1919**, 52, 1749-1756.
- [14] J. von Braun, G. Manz, *Liebigs Ann. Chem.* **1931**, 488, 111-126.
- [15] C. F. Koelsch, A. G. Whitney, *J. Org. Chem.* **1941**, 6, 795-803.
- [16] A. V. Ivanov, P. A. Svinareva, L. G. Tomilova, N. S. Zefirov, *Russ. Chem. Bull. Int. Ed.* **2001**, 50, 919-920.
- [17] A. V. Ivanov, P. A. Svinareva, I. V. Zhukov, L. G. Tomilova, N. S. Zefirov, *Russ. Chem. Bull. Int. Ed.* **2003**, 52, 1562-1566.
- [18] A. G. M. Barrett, G. R. Hanson, A. J. P. White, D. J. Williams, A. S. Micallef, *Tetrahedron* **2007**, 63, 5244-5250.
- [19] D. Woehrle, M. Eskes, K. Shigehara, A. Yamada, *Synthesis* **1993**, 194 - 196.
- [20] M. J. Plater, A. Jeremiah, G. Bourhill, *J. Chem. Soc., Perkin Trans. I* **2002**, 91 - 96.
- [21] B. Tylleman, R. Gomez-Aspe, G. Gbabode, Y. H. Geerts, S. Sergeyev, *Tetrahedron* **2008**, 64, 4155-4161.
- [22] B. Neises, W. Steglich, *Angew. Chem. Int. Ed.* **1978**, 17, 522-524.
- [23] M. Freund, H. Beck, *Berichte der deutschen chemischen Gesellschaft* **1904**, 37, 1942-1946.
- [24] B. Martin, H. Sekljic, C. Chassaing, *Org. Lett.* **2003**, 5, 1851 - 1854.
- [25] P. A. Barrett, D. A. Frye, R. P. Linstead, *J. Chem. Soc.* **1938**, 1157-1163.
- [26] S. Alibert-Fouet, I. Seguy, J.-F. Bobo, P. Destruel, H. Bock, *Chem. Eur. J.* **2007**, 13, 1746-1753.
- [27] N. B. Chaure, J. L. Sosa-Sanchez, A. N. Cammidge, M. J. Cook, A. K. Ray, *Org. Elec.* **2010**, 11, 434-438.
- [28] T. Gross, F. Chevalier, J. S. Lindsey, *Inorg. Chem.* **2001**, 40, 4762-4774.
- [29] F. Nekelson, H. Monobe, M. Shiro, Y. Shimizu, *J. Mater. Chem.* **2007**, 17, 2607-2615.
- [30] F. Nekelson, H. Monobe, Y. Shimizu, *Chem. Commun.* **2006**, 3874-3876.
- [31] F. Nekelson, H. Monobe, Y. Shimizu, *Mol. Cryst. Liq. Cryst.* **2007**, 479, 205-211.
- [32] *A Lanthanide Lanthology, Vol. I, A - L*, Molycorp, Inc., Mountain Pass, CA, U.S.A., **1993**.

CHAPTER 4

MAGNETIC BEHAVIOR OF THREE REDOX STATES OF A SMM IN SOLUTION

4-1 Introduction

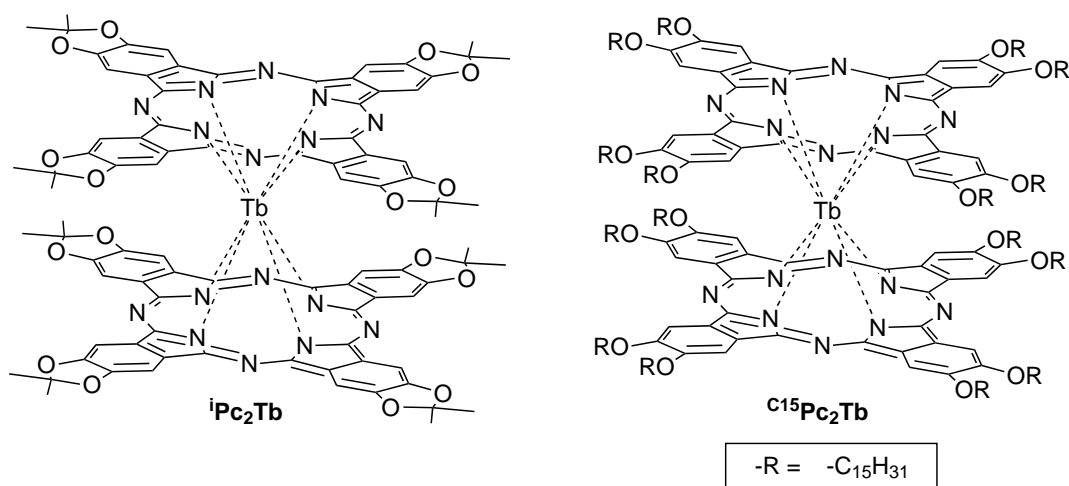
The anionic double-decker phthalocyanine complexes of Tb, Dy and Ho were shown recently to behave as single-molecule magnets based on their ac magnetic susceptibility^[1, 2] and on magnetization hysteresis measurements^[3, 4] performed on dilute solid solutions of the complexes in the isostructural diamagnetic equivalent complex of Y. It was assumed that, because of the dilution in the diamagnetic host, the magnetically active species were sufficiently scattered for the magnetic interactions between them to be discarded. Nevertheless no direct and clear evidence of this fact was given. While efforts have been made to study the magnetic behavior of their one and two electron oxidized forms,^[5, 6] surprisingly, no magnetic hysteresis data have been reported, and no magnetic data have been provided for any oxidation state in dilute solutions in a solvent glass.

Magnetic Circular Dichroism (MCD) spectroscopy is an optical method that consists in recording the difference in absorption of a sample for left and right circularly polarized light in the presence of a magnetic field. Since the intensity of MCD spectra is proportional to the magnetization of the sample, it has been shown to be a powerful tool for the optical detection of the magnetic behavior of Mn₁₂ cluster SMMs.^[7-9] A characteristic of the MCD technique is that it allows one to study the magneto optical

-
- [1] N. Ishikawa, M. Sugita, T. Ishikawa, S.-y. Koshihara and Y. Kaizu, *J. Am. Chem. Soc.* **2003**, *125*, 8694-8695.
- [2] N. Ishikawa, M. Sugita, T. Ishikawa, S.-y. Koshihara and Y. Kaizu, *J. Phys. Chem. B* **2004**, *108*, 11265-11271.
- [3] N. Ishikawa, M. Sugita and W. Wernsdorfer, *J. Am. Chem. Soc.* **2005**, *127*, 3650-3651.
- [4] N. Ishikawa, M. Sugita and W. Wernsdorfer, *Angew. Chem. Int. Ed.* **2005**, *44*, 2931-2935.
- [5] N. Ishikawa, M. Sugita, N. Tanaka, T. Ishikawa, S.-y. Koshihara and Y. Kaizu, *Inorg. Chem.* **2004**, *43*, 5498-5500.
- [6] S. Takamatsu, T. Ishikawa, S.-y. Koshihara and N. Ishikawa, *Inorg. Chem.* **2007**, *46*, 7250-7252.
- [7] E. J. L. McInnes, E. Pidcock, V. S. Oganessian, M. R. Cheesman, A. K. Powell and A. J. Thomson, *J. Am. Chem. Soc.* **2002**, *124*, 9219-9228.
- [8] N. Domingo, B. E. Williamson, J. Gomez-Segura, P. Gerbier, D. Ruiz-Molina, D. B. Amabilino, J. Veciana and J. Tejada, *Phys. Rev. B* **2004**, *69*, 052405.
- [9] P. Gerbier, N. Domingo, J. Gomez-Segura, D. Ruiz-Molina, D. B. Amabilino, J. Tejada, B. E. Williamson and J. Veciana, *J. Mater. Chem.* **2004**, *14*, 2455-2460.

properties of compounds in solution. Another advantage that MCD spectroscopy offers, when compared to standard magnetometric measurements, is its high sensitivity; this allows measurements of the magnetization of a collection of isolated molecules in dilute frozen solutions with diamagnetic solvents, thus minimizing the effect of intermolecular magnetic interactions and facilitating averaged measurements of single-molecules.

In this chapter, the spectroelectrochemical characterization of the anionic, neutral and cationic equivalents of a terbium double-decker complex (${}^i\text{Pc}_2\text{Tb}$) are presented together with a study of the corresponding hysteresis of magnetization and of the magnetization relaxation rates using magnetic circular dichroism (MCD) spectroscopy in frozen dilute solutions at low temperatures (1.5-5 K). Our results show that low temperature MCD spectroscopy is a viable and powerful technique to study the magnetization properties of dilute solutions of this interesting family of compounds. Compound ${}^{C15}\text{Pc}_2\text{Tb}$ was also considered because of its potential greater solubility.



In order to study the behavior of double-decker complexes in solution, the acetal complex ${}^i\text{Pc}_2\text{Tb}$ was used because of its reversible and clear spectroelectrochemical characteristics which are detailed in the following section.

4-2 Redox chemistry of complexes ${}^i\text{Pc}_2\text{Tb}$ and ${}^{C15}\text{Pc}_2\text{Tb}$

Prior to doing the spectroelectrochemistry, it was necessary to determine the half-wave potentials of the double-decker phthalocyanine complexes. The redox properties of the compounds ${}^i\text{Pc}_2\text{Tb}$ and ${}^{C15}\text{Pc}_2\text{Tb}$ were determined by recording their cyclic voltammograms (CV) in solution. The CV of a $4.5 \times 10^{-4} \text{ M}$ solution of ${}^i\text{Pc}_2\text{Tb}$ in CH_2Cl_2 with 0.4 M $[\text{NBu}_4][\text{BF}_4]$ was recorded at 273 K which resulted to be the optimal

temperature for the spectroelectrochemistry measurements. The best results for compound $^{15}\text{C}^{15}\text{Pc}_2\text{Tb}$ were obtained with a $7.5 \times 10^{-5}\text{M}$ solution in THF with 0.5 M $[\text{NBu}_4][\text{BF}_4]$ at 273 K.

The voltammogram of complex $^i\text{Pc}_2\text{Tb}$ (see Figure 4-1) shows four reversible electrochemical processes: one oxidation process, at $E_{1/2}$ 0.45 V vs. SCE, and three reduction processes at $E_{1/2}$ 0.09, -1.16 and -1.45 V vs. SCE, respectively, which are in good agreement with the electrochemical potentials of previously reported double-decker lanthanide phthalocyanine complexes. [10-12]

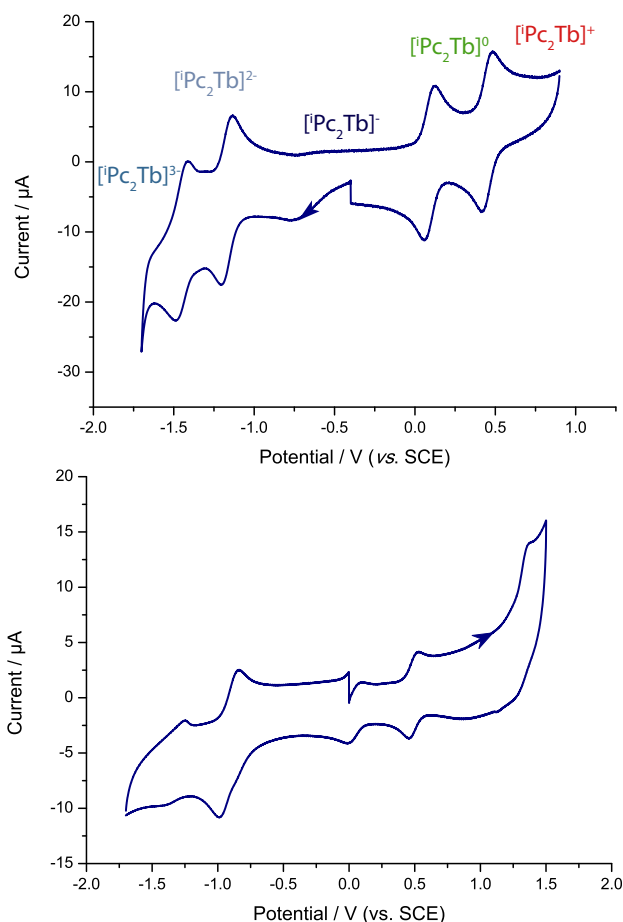


Figure 4-1. Cyclic voltammetry of a $4.5 \times 10^{-4}\text{M}$ solution of $^i\text{Pc}_2\text{Tb}$ in CH_2Cl_2 (above) and a $7.5 \times 10^{-5}\text{M}$ solution of $^{15}\text{C}^{15}\text{Pc}_2\text{Tb}$ in THF (below) with 0.4 M $[\text{NBu}_4][\text{BF}_4]$ recorded at $0.1\text{V}\cdot\text{s}^{-1}$. The potentials are given versus SCE.

[10] K. M. Kadish, T. Nakanishi, A. Gurek, V. Ahsen and I. Yilmaz, *J. Phys. Chem. B* **2001**, *105*, 9817-9821.

[11] P. Zhu, F. Lu, N. Pan, Dennis P. Arnold, S. Zhang and J. Jiang, *Eur. J. Inorg. Chem.* **2004**, *2004*, 510-517.

[12] A. V. Ivanov, P. A. Svinareva, L. G. Tomilova and N. S. Zefirov, *Russ. Chem. Bull. Int. Ed.* **2006**, *55*, 281-286.

The large separation of these electrochemical processes allowed an in depth study of electrogenerated species derived from ${}^1\text{Pc}_2\text{Tb}$ by spectroelectrochemistry. The CV curve of the electrochemical process observed at lowest potentials is not as neat as that of the other four processes. For instance, a plateau can be observed around -1.3 V vs. SCE. This fact, combined with the very negative value associated to this redox couple made us suspect that it might not be a totally reversible process.

As for compound ${}^{15}\text{Pc}_2\text{Tb}$, the measurement was first tried in CH_2Cl_2 but upon dissolution of the compound in CH_2Cl_2 containing the electrolyte, the solution rapidly turned red and was discarded for electrochemical experiments. THF was used instead of CH_2Cl_2 , and the CV characteristics of compound ${}^{15}\text{Pc}_2\text{Tb}$ (see Figure 4-1) showed three reversible processes: one oxidation process centered at 0.48 V vs. SCE and two reduction processes centered at 0.05 V and -0.91 V. As for the third reduction process, it was not well resolved in these conditions. The origin of the bad electrochemical behavior of compound ${}^{15}\text{Pc}_2\text{Tb}$ in these conditions remains unknown.

4-2-1 Spectroelectrochemistry of complex ${}^1\text{Pc}_2\text{Tb}$ (${}^1\text{Pc}_2\text{Tb}$)

The spectroscopic changes in absorption spectra were recorded using a transparent electrode ^[13] (see Figure 4-2) for a 1.48×10^{-4} M solution of ${}^1\text{Pc}_2\text{Tb}$ in CH_2Cl_2 containing 0.4 M $[\text{NBu}_4][\text{BF}_4]$.



Figure 4-2. Representation of the cell used for spectroelectrochemical characterizations using a transparent Pt/Rh electrode.^[13]

All the measurements were recorded successively on the same sample solution. Since the UV-Vis absorption bands broaden with increasing temperature, the measurements were all performed at a reasonably low stabilized temperature of 273 K in order to obtain sharp spectra.

The cationic complex $[\text{Pc}_2\text{Tb}]^+$ was electrogenerated from the neutral complex $[\text{Pc}_2\text{Tb}]^0$ applying a fixed potential of 0.59 V vs. SCE (see Figure 4-3).

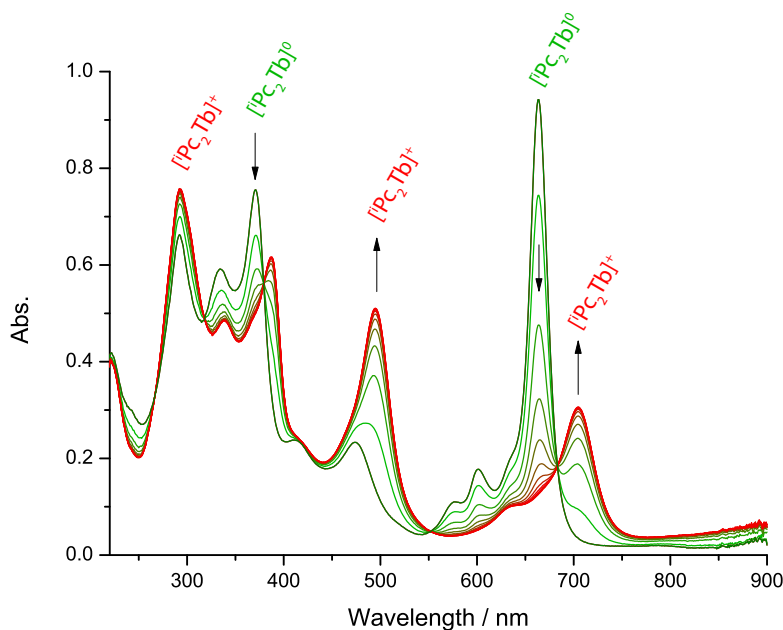


Figure 4-3. Successive absorption spectra recorded at intervals of 2 minutes during the electrogeneration of the cationic form of Pc_2Tb from the neutral species at a potential of 0.59 V vs. SCE and at 273 K.

The reversibility of the process was demonstrated by subsequent regeneration of the neutral complex applying a potential of 0.28 V vs. SCE (see Figure 4-4).

In both processes, tight isosbestic points were observed at 268, 318, 379, 552, and 683 nm, indicating a clean interconversion of both species. Upon oxidation, the neutral Soret band at 371 nm gradually disappears to be replaced by the red-shifted Soret band of the cation. The π -radical band also shifts to higher wavelength (from 474 nm in the neutral complex to 494 nm in the cation) and increases dramatically in intensity. The vibronic bands of the neutral complex disappear and finally the Q-band of the neutral

^[13] S. A. Macgregor, E. McInnes, R. J. Sorbie and L. J. Yellowlees, *Molecular Electrochemistry of Inorganic, Bioinorganic and Organometallic Compounds*, Kluwer Academic Publishers, **1993**.

complex at 663 nm is also shifted to lower energy of about 40 nm and is much less intense in the oxidized complex than in the neutral form.

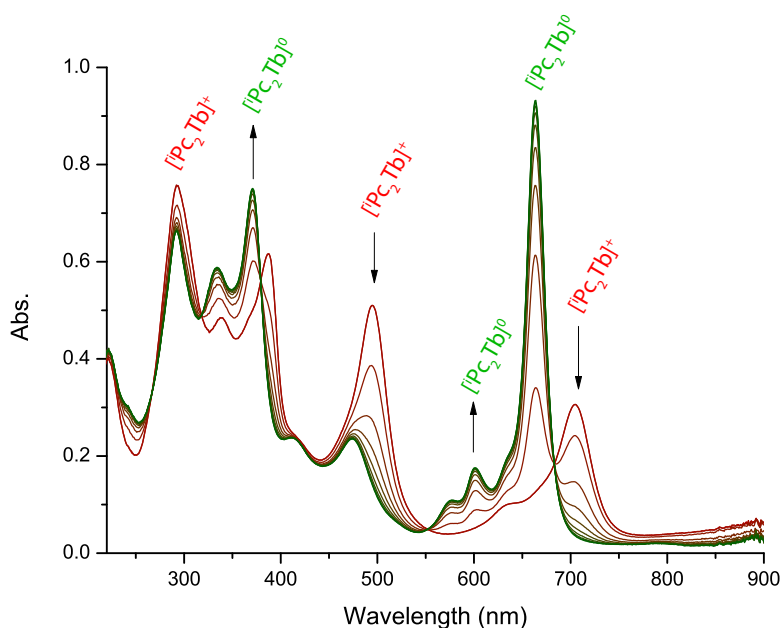


Figure 4-4. Successive absorption spectra recorded at intervals of 2 minutes during the regeneration of the neutral form of ${}^1\text{Pc}_2\text{Tb}$ from the electrogenerated cationic species at a potential of 0.28 V vs. SCE and at 273 K

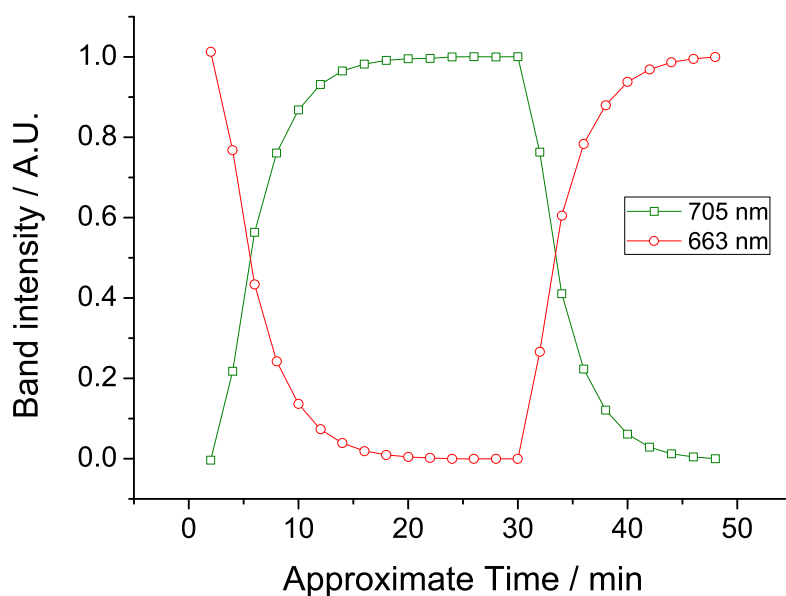


Figure 4-5. Time dependent evolution of the absorbance of a $1.48 \times 10^{-4}\text{M}$ solution of compound ${}^1\text{Pc}_2\text{Tb}$ during the oxidation at 0.59 V vs. SCE of the neutral complex to the cationic species (0-30 min) and the subsequent reduction at 0.28 V vs. SCE to the neutral complex (30-48min)

The normalized absorption intensities (0 for the saturation minimum and 1 for the saturation maximum) for the 663 nm band which is characteristic of the neutral complex and the 705 nm band, characteristic of the cationic species, were also plotted as a function of time (see Figure 4-5) for the oxidation of the neutral complex to the cationic species and the subsequent reverse process. The starting values are clearly identical to the final saturation values after one complete cycle, which demonstrates a complete reversibility.

The anionic species was obtained from the neutral form of ${}^1\text{Pc}_2\text{Tb}$ applying a fixed potential of -0.15 V vs. SCE (see Figure 4-6).

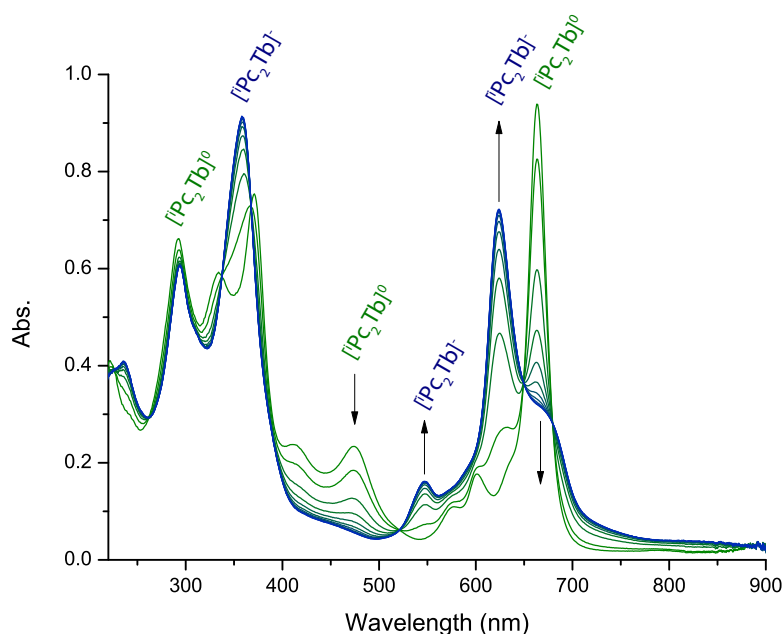


Figure 4-6. Successive absorption spectra recorded at intervals of 2 minutes during the reduction of the neutral form of ${}^1\text{Pc}_2\text{Tb}$ to the anionic species at a potential of -0.15 V vs. SCE and at 273 K

The reverse process yielded again the neutral complex applying a potential of 0.28 V vs. SCE (see Figure 4-7). Both electrochemical conversions proceeded with tight isosbestic points at 261, 337, 367, 521, 649 and 680 nm. Upon reduction, the split Soret bands of the neutral complex (334 and 371 nm) fuse to a single absorption band (358 nm), the π -radical band gradually disappears which is to be expected since in this oxidation state the two ligands are formally closed-shell.

The normalized absorption intensities for the 663 nm band, which is characteristic of the neutral complex, and the 624 nm band, which is characteristic of the anionic complex, were plotted against time (see Figure 4-8) for the reduction of the neutral

complex to the anionic species and the subsequent reverse process. Comparing the starting values and the final saturation values, the complete reversibility of this process was also demonstrated.

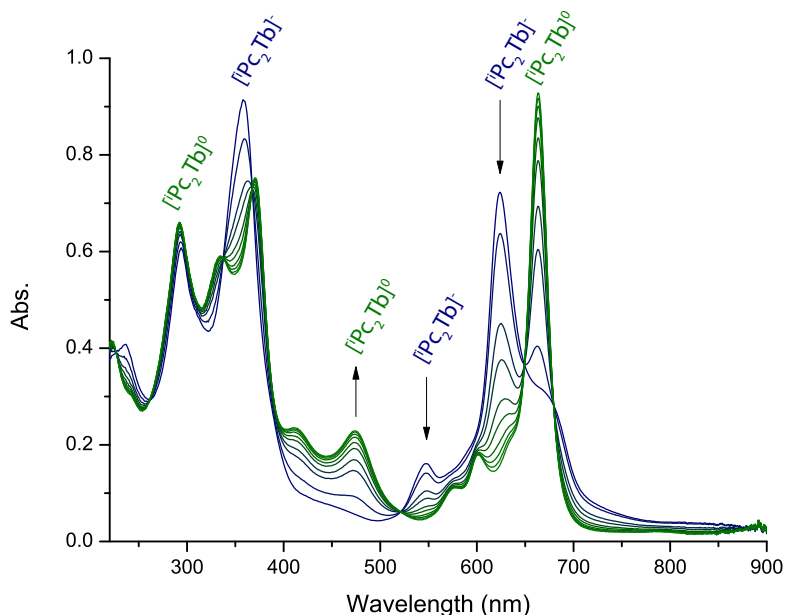


Figure 4-7. Successive absorption spectra recorded at intervals of 2 minutes during the regeneration of the neutral form of ${}^i\text{Pc}_2\text{Tb}$ from the electrogenerated anionic species at a potential of 0.28 V vs. SCE and at 273 K

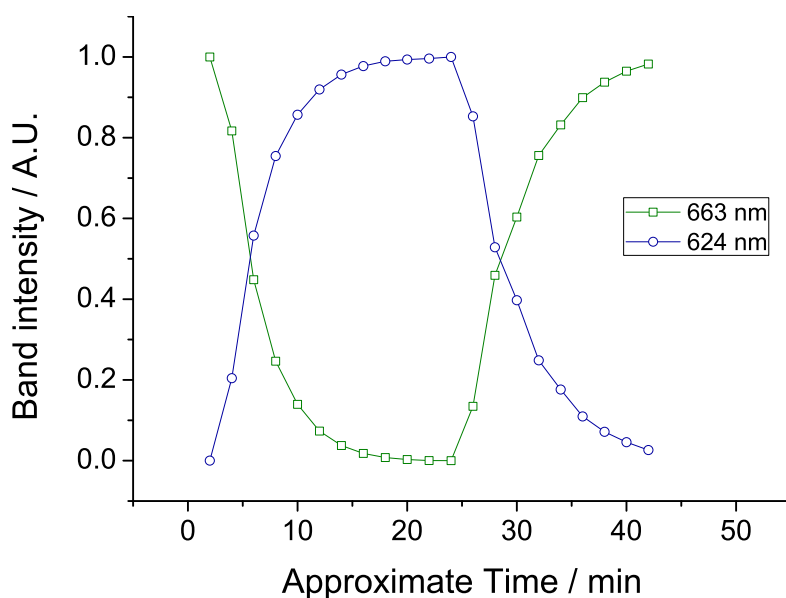


Figure 4-8. Time dependent evolution of the absorbance of a $1.48 \times 10^{-4}\text{M}$ solution of compound ${}^i\text{Pc}_2\text{Tb}$ during the reduction at -0.15 V vs. SCE of the neutral complex to the anionic species (0-24 min) and the subsequent oxidation at 0.28 V vs. SCE to the neutral complex (24-42min)

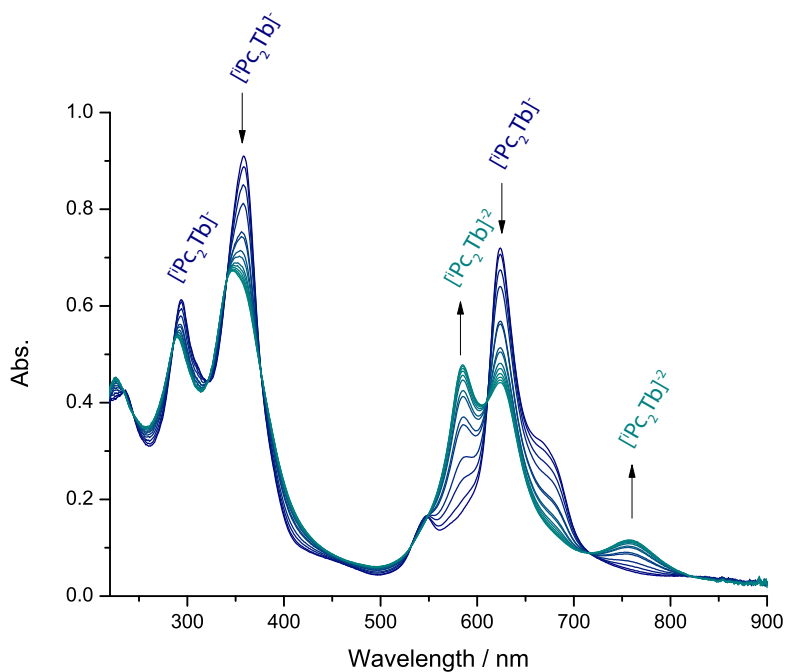


Figure 4-9. Successive absorption spectra recorded at intervals of 2 minutes during the reduction of the anionic form of ${}^1\text{Pc}_2\text{Tb}$ to the dianionic species at a potential of -1.29 V vs. SCE and at 273 K

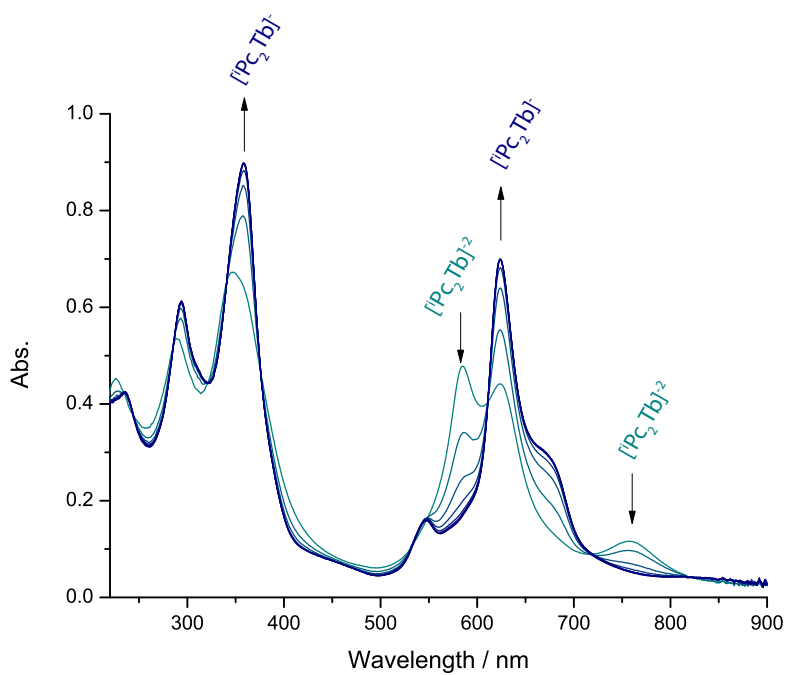


Figure 4-10. Successive absorption spectra recorded at intervals of 2 minutes during the regeneration of the anionic form of ${}^1\text{Pc}_2\text{Tb}$ from the electrogenerated dianionic species at a potential of -0.15 V vs. SCE and at 273 K

The reduction of the anionic species to the dianionic equivalent was done by applying a potential of -1.29 V vs. SCE (see Figure 4-9). The conversion was shown to be reversible by applying again a potential of -0.15 V vs. SCE which quantitatively regenerated the anionic species (see Figure 4-10).

The normalized absorption intensities for the 624 nm band, which is characteristic of the anionic complex, and the 584 nm band, which is characteristic of the dianionic complex, were plotted against time (see Figure 4-11) for the reduction of the anionic complex to the dianionic species and the subsequent reverse process. The starting values and the final saturation values are not identical but still very similar, which tends to demonstrate a reversibility of this process.

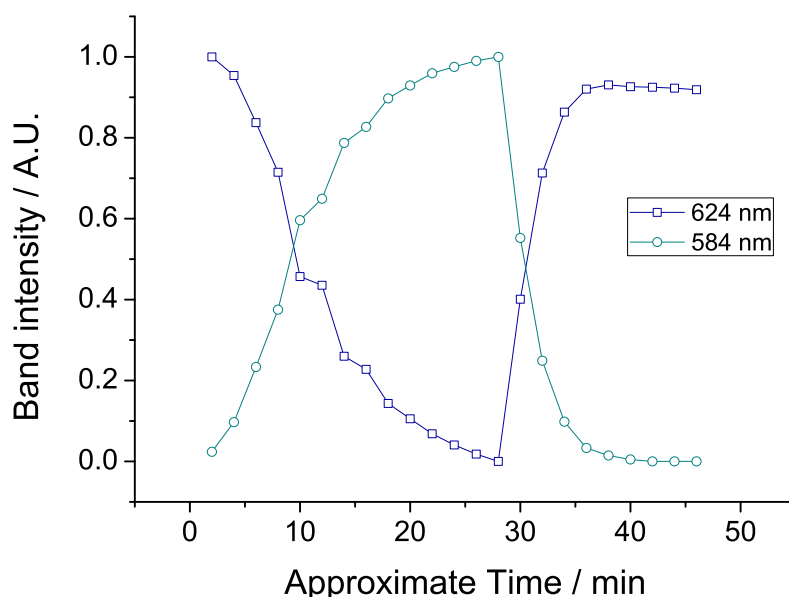


Figure 4-11. Time dependent evolution of the absorbance of a 1.48×10^{-4} M solution of compound ${}^1\text{Pc}_2\text{Tb}$ during the reduction at -1.29 V vs. SCE of the anionic complex to the dianionic species (0-28 min) and the subsequent oxidation at -0.15 V vs. SCE to the anionic complex (24-46min)

Also, tight isosbestic points were observed at 233, 244, 286, 321, 341, 376, 532, 549, 610, 716 and 823 nm. The dianionic complex exhibits a split Q-band (584 and 624 nm) and shows no trace of a vibronic band around 550 nm. Its Soret band is similar to that of the anionic complex, but of lower intensity. Upon reduction of the anionic form to its dianionic equivalent, a new band appears at 760 nm.

Finally, the trianionic species could also be generated electrochemically from its dianionic equivalent at a potential of -1.60 V vs. SCE (see Figure 4-12).

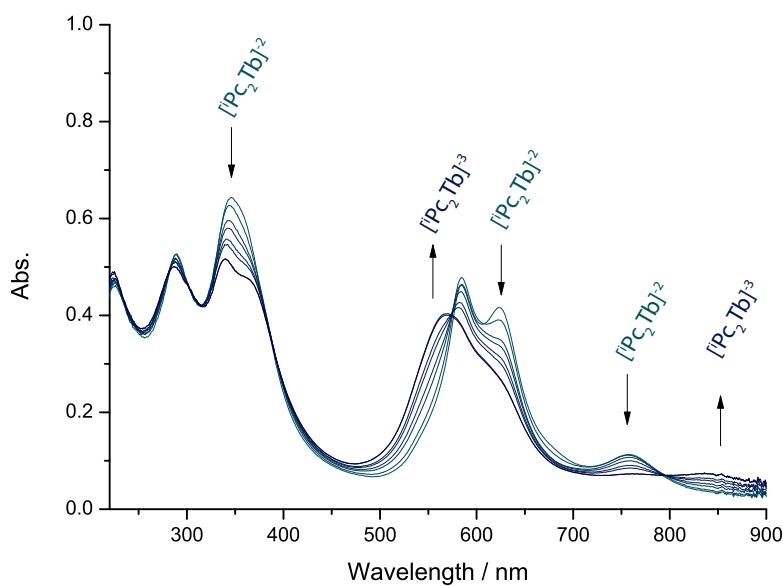


Figure 4-12. Successive absorption spectra recorded at intervals of 2 minutes during the reduction of the dianionic form of ${}^1\text{Pc}_2\text{Tb}$ to the trianionic species at a potential of -1.60 V vs. SCE and at 273 K

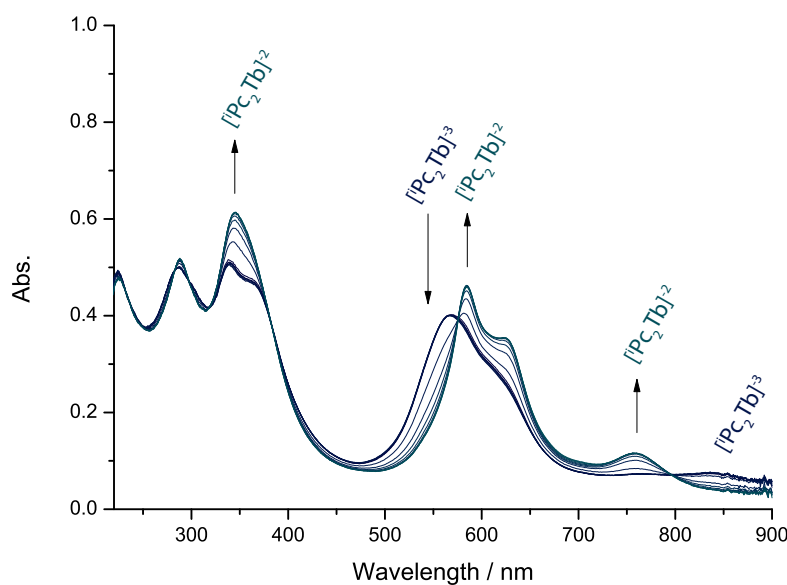


Figure 4-13. Successive absorption spectra recorded at intervals of 2 minutes during the regeneration of the dianionic form of ${}^1\text{Pc}_2\text{Tb}$ from the electrogenerated trianionic species at a potential of -1.29 V vs. SCE and at 273 K

Nevertheless, this time the oxidation process was not totally reversible. The spectrum of the sample regenerated at -1.29 V vs. SCE (see Figure 4-13) was not superimposable to the one of the starting dianionic complex, but it was nevertheless very similar. Again, the normalized absorption intensities were plotted against time for the 584 nm band,

characteristic of the dianionic complex, and the 569 nm band, characteristic of the trianionic complex, for the reduction of the dianionic complex to the trianionic species and the subsequent reverse process (see Figure 4-14). The poor reversibility of this process was evidenced in the irregular shape of the absorption curves and the lack of symmetry of the same for the two bands.

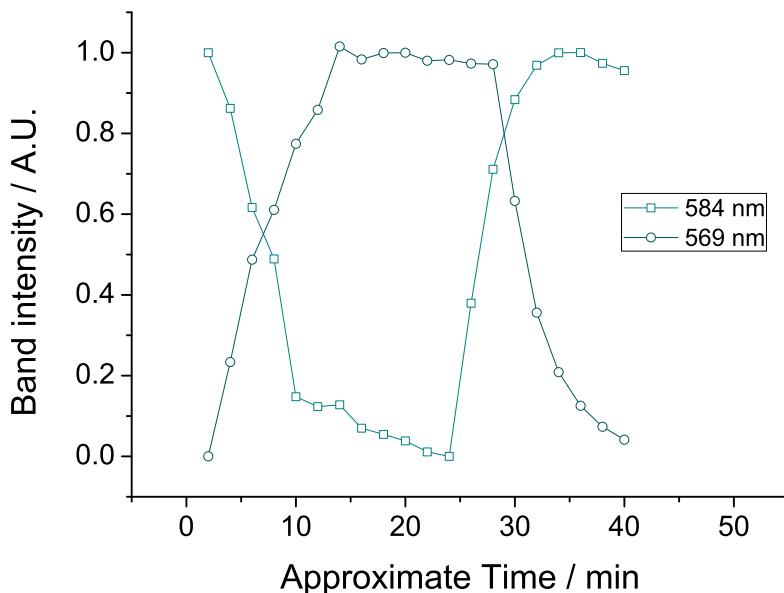


Figure 4-14. Time dependent evolution of the absorbance of a $1.48 \times 10^{-4} \text{M}$ solution of compound ${}^1\text{Pc}_2\text{Tb}$ during the reduction at -1.60 V vs. SCE of the dianionic complex to the trianionic species (0-24 min) and the subsequent oxidation at -1.29 V vs. SCE to the dianionic complex (24-40min)

The split Q-band of the dianionic moiety disappeared to give rise to a single broad band at 569 nm with a small shoulder band at 624 nm upon oxidation to the trianionic complex. Interestingly, the 760 nm band of the dianionic complex vanishes upon oxidation to the trianionic form of complex ${}^1\text{Pc}_2\text{Tb}$, but a new band appears around 850 nm which could correspond to a charge transfer band.

As a conclusion to this set of experiments, all five oxidation states could be electrogenerated and characterized by UV-Vis absorption spectroscopy (see Figure 4-15). All the studied processes were shown to be quantitatively reversible except for the generation of the trianionic complex which is expected to be quite unstable due to the very negative value of the redox potential associated to this couple.

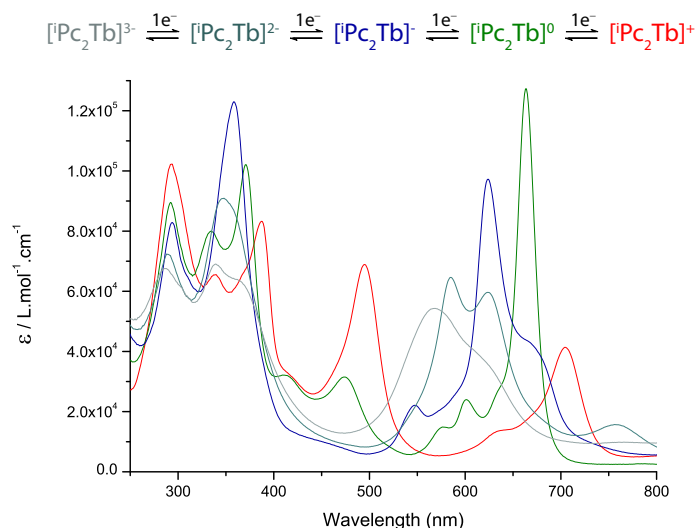


Figure 4-15. UV/Vis absorption spectrum of electrochemically generated species derived from complex ${}^1\text{Pc}_2\text{Tb}$, in CH_2Cl_2 with 0.4 M $[\text{NBu}_4][\text{BF}_4]$. All spectra recorded at 273 K.

4-2-2 Spectroelectrochemistry of complex ${}^{\text{C}15}\text{Pc}_2\text{Tb}$

Despite the apparent poor characteristics of the cyclic voltammogram of compound ${}^{\text{C}15}\text{Pc}_2\text{Tb}$ below -0.5 V vs. SCE, the electrochemical process centered at 0.05 V vs. SCE was studied by spectroelectrochemistry on a 1.1×10^{-4} M solution of ${}^{\text{C}15}\text{Pc}_2\text{Tb}$ in THF containing 0.5 M $[\text{NBu}_4][\text{BF}_4]$. After stabilizing the sample by applying a constant potential of 0.26 V vs. SCE (corresponding to the range of potential where only the neutral species should be present), a potential of -0.13 V vs. SCE was applied, which should have been enough to quantitatively reduce the neutral species to the corresponding anionic form of complex ${}^{\text{C}15}\text{Pc}_2\text{Tb}$. Unexpectedly, the band evolution being abnormally slow, the potential was lowered to first -0.18 V vs. SCE and further down to -0.23 and -0.31 V vs. SCE to reach almost completion of the reduction process (see Figure 4-16).

Despite not reaching the complete reduction to the anionic species (the π -radical band at 482 nm was very weak in the final solution but was still present) and despite the anomalies during the reduction, the reverse process was probed anyway applying a potential of 0.26 V vs. SCE to regenerate the neutral species. As can be seen on Figure 4-17, the solution was partially oxidized back to the neutral complex ${}^{\text{C}15}\text{Pc}_2\text{Tb}$ but at equilibrium, the spectra do not correspond to the initial neutral absorption spectrum. Notably, where the spectrum of the solution of the neutral form of ${}^{\text{C}15}\text{Pc}_2\text{Tb}$ presents only a very weak shoulder band between the vibronic bands (581 and 606 nm) and the

Q-band (670 nm), the obtained spectrum after a full cycle of oxidation and reduction shows a persistent band at 626 nm that coincides with the position of the Q-band of the anionic complex.

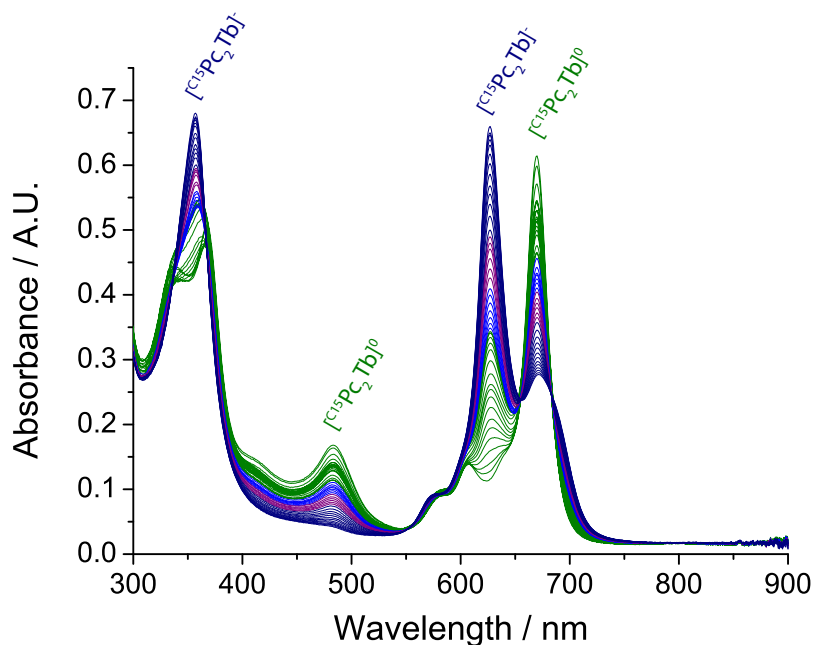


Figure 4-16. Successive absorption spectra recorded at intervals of 2 minutes during the reduction of the neutral form of $^{15}\text{C}_2\text{Pc}_2\text{Tb}$ to the anionic species at a potential of -0.13 V vs. SCE (green) and then at potentials of -0.18 (blue), -0.23 (purple) and -0.31 (dark blue) V vs. SCE and at 273 K

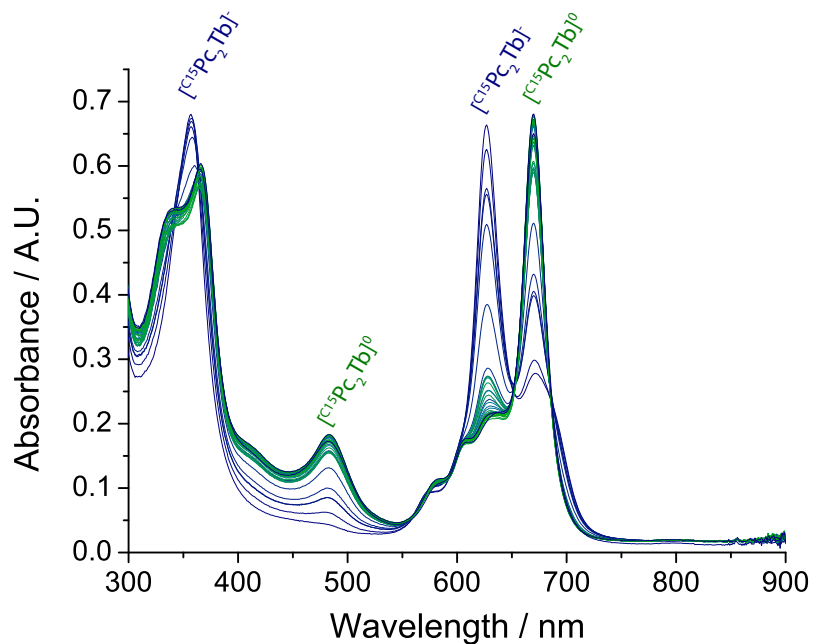


Figure 4-17. Successive absorption spectra recorded during the oxidation of the anionic form of $^{15}\text{C}_2\text{Pc}_2\text{Tb}$ to the neutral species at a potential of 0.26 V vs. SCE and at 273 K

The origin of the difficulties in oxidizing and reducing this double-decker phthalocyanine terbium complex remains unknown to date.

Given the non reversibility of the bulk electrochemical conversion of the neutral to the anionic species, no further spectroelectrochemical studies were done on this compound.

4-3 Magnetic circular dichroism set-up

The magnetization behavior of the frozen solutions of the diluted electrogenerated species, derived from complex ${}^1\text{Pc}_2\text{Tb}$, in CH_2Cl_2 , were studied via magnetic circular dichroism (MCD) spectroscopy. To do this, we used the home made MCD setup designed by Jonathan McMaster and Stephen Davies at the School of Chemistry of the University of Nottingham (UK).

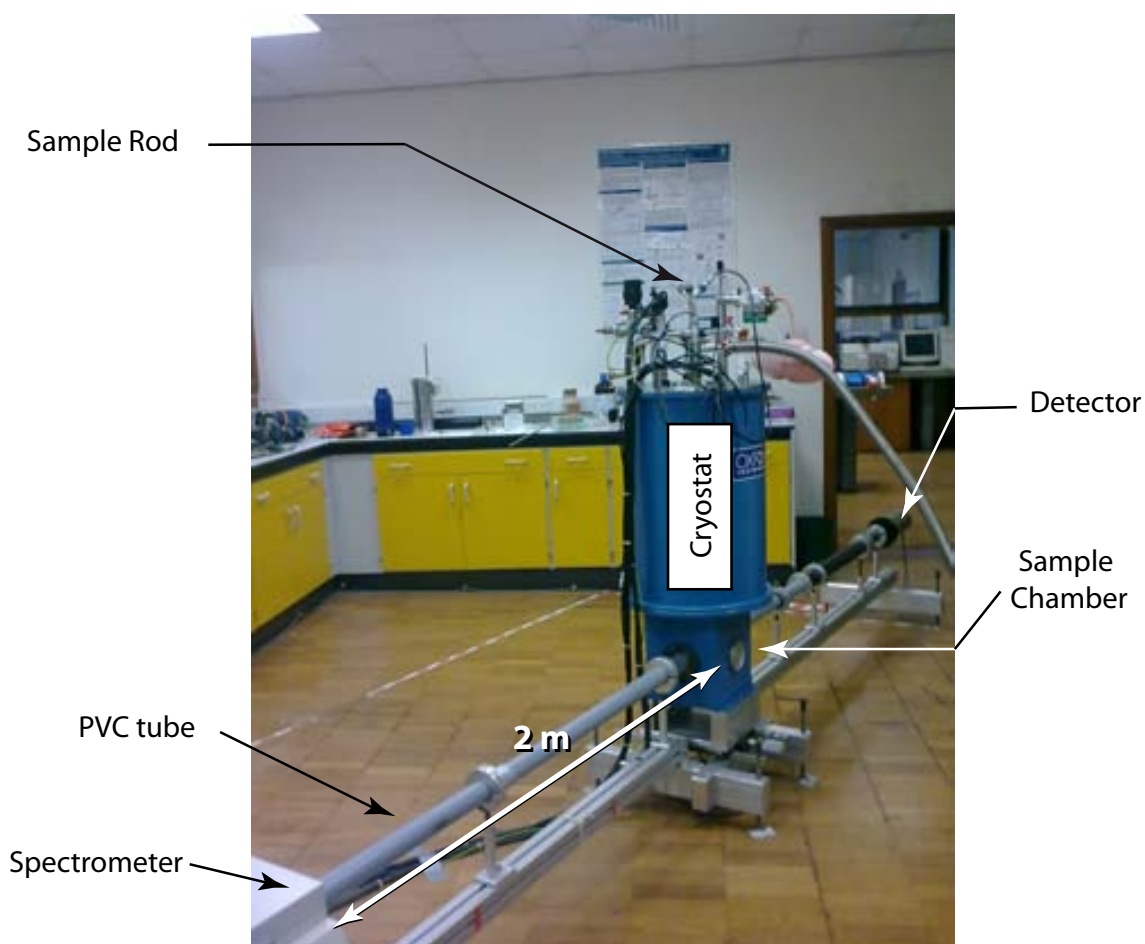


Figure 4-18. Photograph of the experimental setup showing the 7 T cryostat and the detector.

The set-up is based on an Oxford Instrument 0-8 T superconducting magnet operating in the temperature range of 1.5-300 K (see Figure 4-18) and a JASCO 810 spectropolarimeter. The spectropolarimeter is used as a source of polarized UV-Vis radiations which are emitted 2 m away from the magnet (to avoid perturbations of the polarimeter due to the intense magnetic field) and focused on the sample via a set of lenses. The detector is placed on the opposite side of the sample chamber, at 2 m of distance (for the same reasons) and the signal is acquired and processed via the standard JASCO software. The sample temperature and the magnetic field strength are regulated by a control unit (see Figure 4-19).



Figure 4-19. JASCO 810 spectropolarimeter (left) and control unit of the 8 T superconducting magnet (right)

On the other hand, the sample holder is also home-made. The holder's body is made out of a copper block and a copper lid (see Figure 4-20). The cell itself is made out of two quartz disks, sandwiched between the holder and the lid, and separated by a 2 mm soft spacer. The whole system is held in place by four screws.

Initially, the soft spacer used to build up the cell was a Viton o-ring, but, systematically, after injection, the cationic and neutral sample solutions of ${}^1\text{Pc}_2\text{Tb}$ were slightly reduced to the neutral and anionic species, respectively (see Figure 4-21). The observed instability in CH_2Cl_2 might be due to chemical impurities in the rubber o-ring which slowly diffuse in the MCD cell and affect the redox state of the sample. The obtained mixtures of oxidation states were not suitable for quality MCD measurements and the o-ring was replaced by a 2mm thick Teflon spacer which solved the problem.

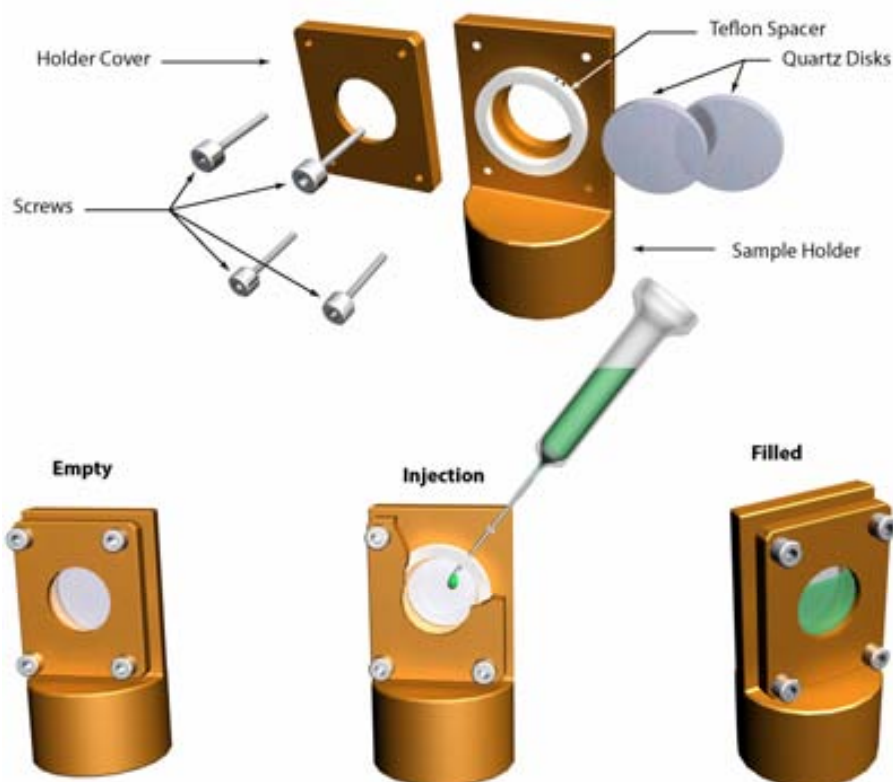


Figure 4-20. View of the different parts of the sample holder (above) and injection in the mounted sample holder through the Teflon spacer (below)

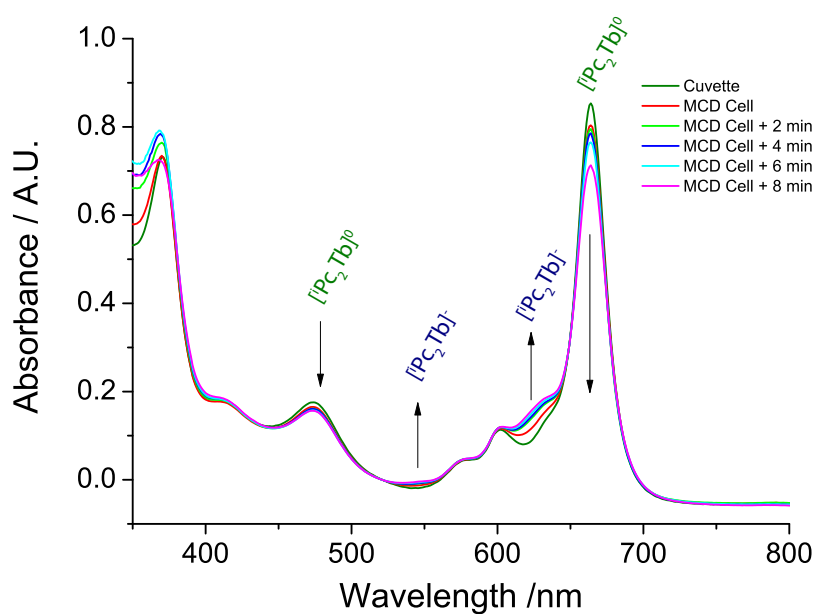


Figure 4-21. Comparison of the room temperature UV-Vis absorption spectra of a 9.0×10^{-5} M solution of a neutral sample of $^1\text{Pc}_2\text{Tb}$ in freshly distilled and neutralized CH_2Cl_2 , and of the evolution of the UV-Vis absorption spectrum of the same solution when injected in the Teflon o-ring MCD cell.

Once the cell is built-up, it is purged with argon, and the sample solution of the oxidation state to be studied is injected with a syringe through the Teflon spacer (see Figure 4-20) and the holder is frozen rapidly in liquid nitrogen to afford a transparent quenched solvent glass. It is then mounted on the sample rod and inserted inside the cryostat all the way down to the sample chamber in which it is aligned (minimizing the background signal) before doing the measurements.

4-4 Magnetic circular dichroism measurements

4-4-1 Preparation and characterization of the samples

The MCD experiments were performed on solutions of species derived from complex ${}^1\text{Pc}_2\text{Tb}$. The dianionic $[\text{}^1\text{Pc}_2\text{Tb}]^{2-}$ and trianionic species $[\text{}^1\text{Pc}_2\text{Tb}]^{3-}$ were too unstable to be transferred to the MCD cell without partial oxidation. For practical reasons, the MCD experiments were therefore limited to the more stable redox states that are the anionic $[\text{}^1\text{Pc}_2\text{Tb}]^-$, neutral $[\text{}^1\text{Pc}_2\text{Tb}]^0$, and cationic $[\text{}^1\text{Pc}_2\text{Tb}]^+$ species. As for the choice of the solvent, CH_2Cl_2 containing 0.8 M $[\text{NBu}_4][\text{BF}_4]$ as an electrolyte was employed, because it provides nice transparent solvent glasses and because its solubilizes well all three oxidation states of complex ${}^1\text{Pc}_2\text{Tb}$.

A 1.11×10^{-4} M solution of $[\text{}^1\text{Pc}_2\text{Tb}]^0$ in CH_2Cl_2 containing 0.8M $[\text{NBu}_4][\text{BF}_4]$ was used directly for MCD experiments while an aliquot of the same solution was quantitatively electrochemically reduced to provide a 1.11×10^{-4} M solution of the anionic complex $[\text{}^1\text{Pc}_2\text{Tb}]^-$. Unfortunately, all the attempts to use an aliquot of the same solution to provide a 1.11×10^{-4} M solution of the cationic complex $[\text{}^1\text{Pc}_2\text{Tb}]^+$ by an electrochemical oxidation failed because this complex was unstable when transferred to the MCD cell. In order to overcome this problem, a 1.16×10^{-4} M solution of the cationic complex in CH_2Cl_2 containing 0.8 M $[\text{NBu}_4][\text{BF}_4]$ was chemically generated by addition of a 3.75×10^{-2} M solution of bromine in CH_2Cl_2 and 0.8 M $[\text{NBu}_4][\text{BF}_4]$ to a solution of neutral complex until the UV-Vis characteristics matched that of a pure cationic sample.

The samples for MCD measurements were frozen in liquid nitrogen, which afforded glasses of suitable quality for optical measurements. In situ absorption spectra were always recorded to check the absence of any aggregation (see Figures 4-22, 4-23 and 4-24), which would translate in the broadening of the spectrum.^[14] A strong in-situ baseline distortion was observed in the region of 300-450 nm and 750-900 nm, which is

essentially due to the lamp baseline and the solvent glass, but besides this, the in situ absorption spectra are quasi identical to the room temperature reference spectra.

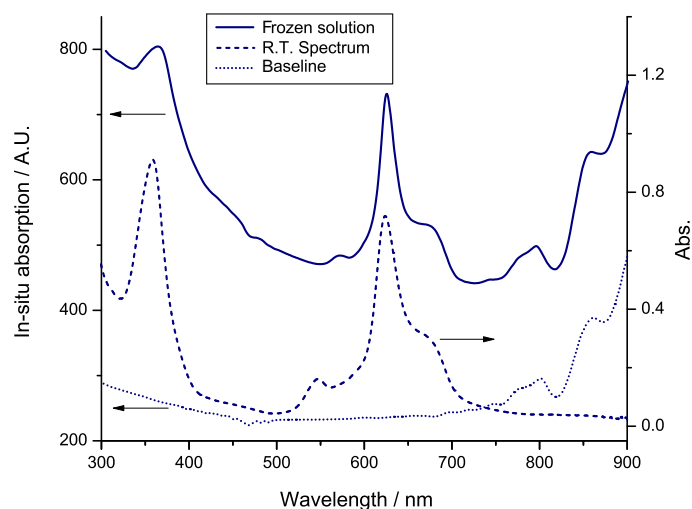


Figure 4-22. Comparison of the UV-Vis spectrum of the anionic complex $[{}^1\text{Pc}_2\text{Tb}]^-$ measured with a UV-Vis spectrometer at room temperature, the spectrum of a frozen solution of the same in CH_2Cl_2 containing 0.8 M $[\text{NBu}_4][\text{BF}_4]$ recorded with the MCD spectrometer at 1.5 K, and the baseline of the equipment at 1.5 K.

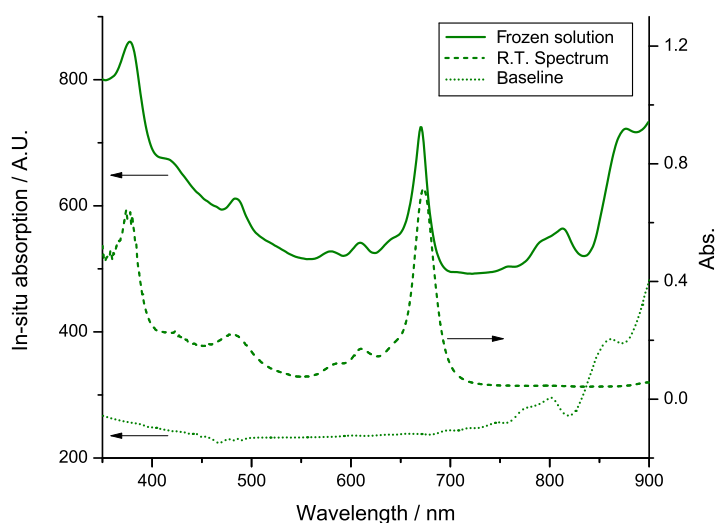


Figure 4-23. Comparison of the UV-Vis spectrum of the neutral complex $[{}^1\text{Pc}_2\text{Tb}]^0$ measured with a UV-Vis spectrometer at room temperature, the spectrum of a frozen solution of the same in CH_2Cl_2 containing 0.8 M $[\text{NBu}_4][\text{BF}_4]$ recorded with the MCD spectrometer at 1.5 K, and the baseline of the equipment at 1.5 K.

The main observed difference was the width of the absorption bands which appear somewhat sharper at low temperature which is to be expected since the energy levels follow a Boltzmann distribution in relation with the torsional degrees of freedom.

Importantly, there is no sign of appearance of an aggregate band in any of the three samples since no additional absorption bands were observed and no broadening of the bands was observed either.

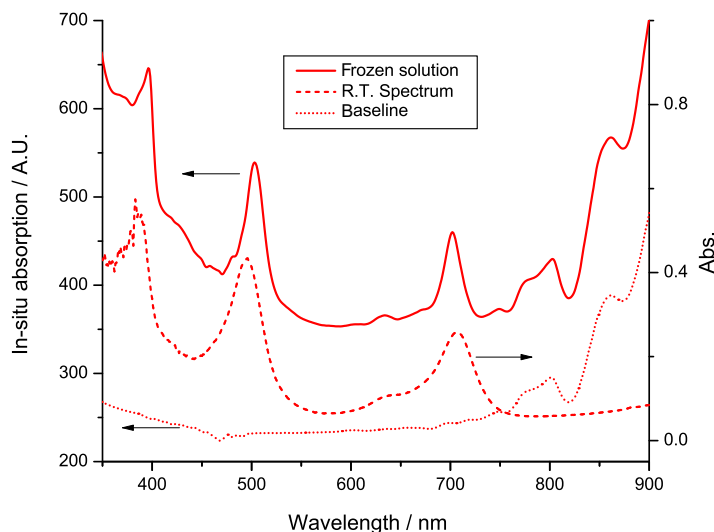


Figure 4-24. Comparison of the UV-Vis spectrum of the cationic complex $[\text{Pc}_2\text{Tb}]^+$ measured with a UV-Vis spectrometer at room temperature, the spectrum of a frozen solution of the same in CH_2Cl_2 containing 0.8 M $[\text{NBu}_4][\text{BF}_4]$ recorded with the MCD spectrometer at 1.5 K, and the baseline of the equipment at 1.5 K.

The absence of signs of aggregation demonstrates that the species are present as isolated molecules in a frozen glass solution, and therefore the magnetic measurements should give information on the averaged magnetic behavior of individual molecules. This situation permits the effective removal of possible perturbations induced by intermolecular magnetic interactions.

4-4-2 MCD spectra of three redox states of complex ${}^1\text{Pc}_2\text{Tb}$

MCD spectra of solutions of anionic, neutral and cationic species of complex ${}^1\text{Pc}_2\text{Tb}$ were recorded from 1.5 K to 88 K for all three samples applying an external magnetic field of ± 7.0 T. Doing this, a complete set of MCD spectra were obtained as a function of magnetic field and temperature. This data set is important in order to assign the different components of the MCD spectra (see Appendix I), named A, B and C terms, which arise from the Zeeman splitting of an orbitally degenerate excited state, second order effects and a Boltzmann distribution across the degenerate ground state. ^[15]

^[15] N. Kobayashi and K. Nakai, *Chem. Commun.* **2007**, 4077-4092.

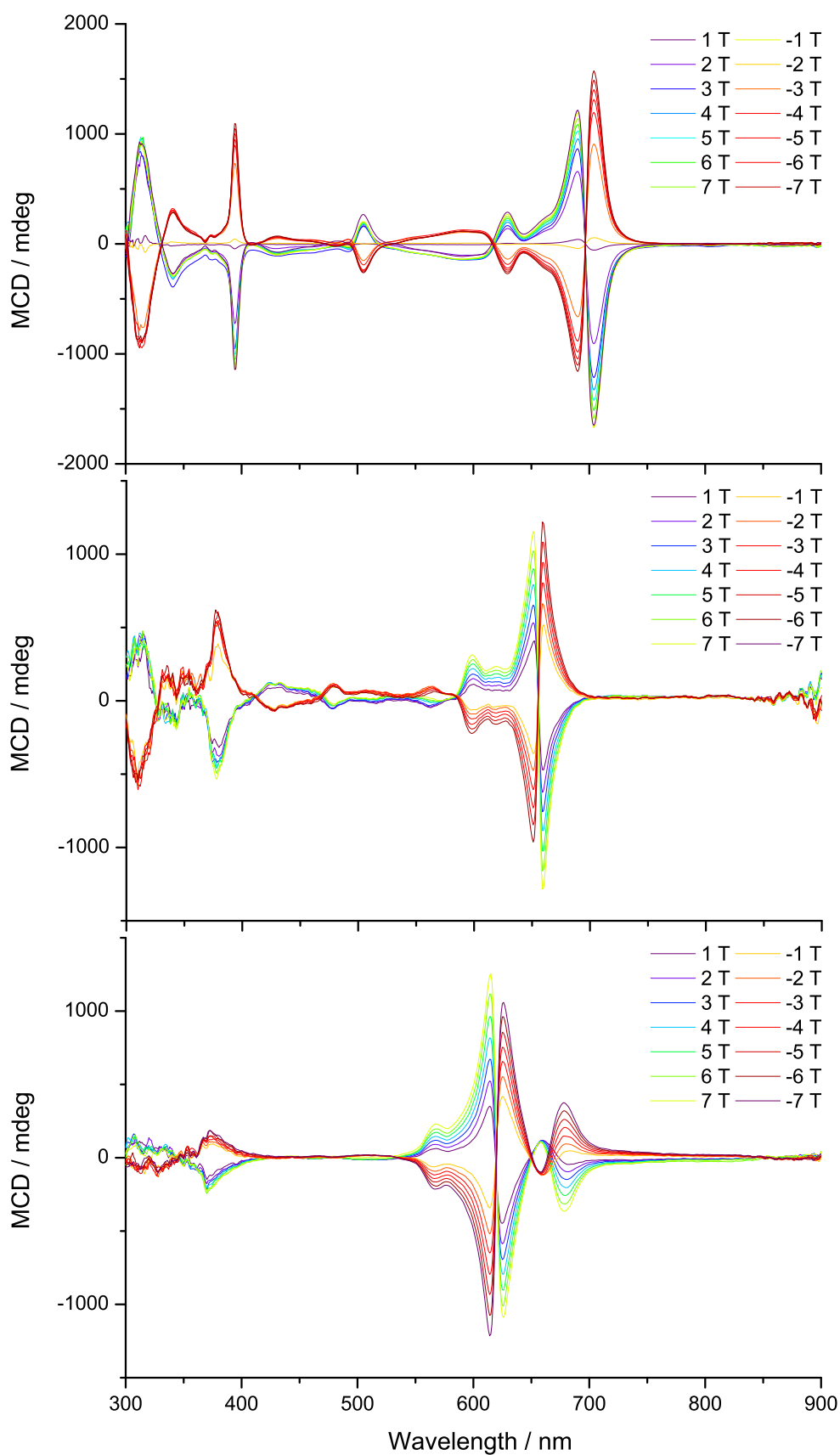


Figure 4-25. MCD spectra of $[^1\text{Pc}_2\text{Tb}]^+$ (above) $[^1\text{Pc}_2\text{Tb}]^0$ (middle) and $[^1\text{Pc}_2\text{Tb}]^-$ (below) for an applied field of -7 to 7 T at 1.5 K

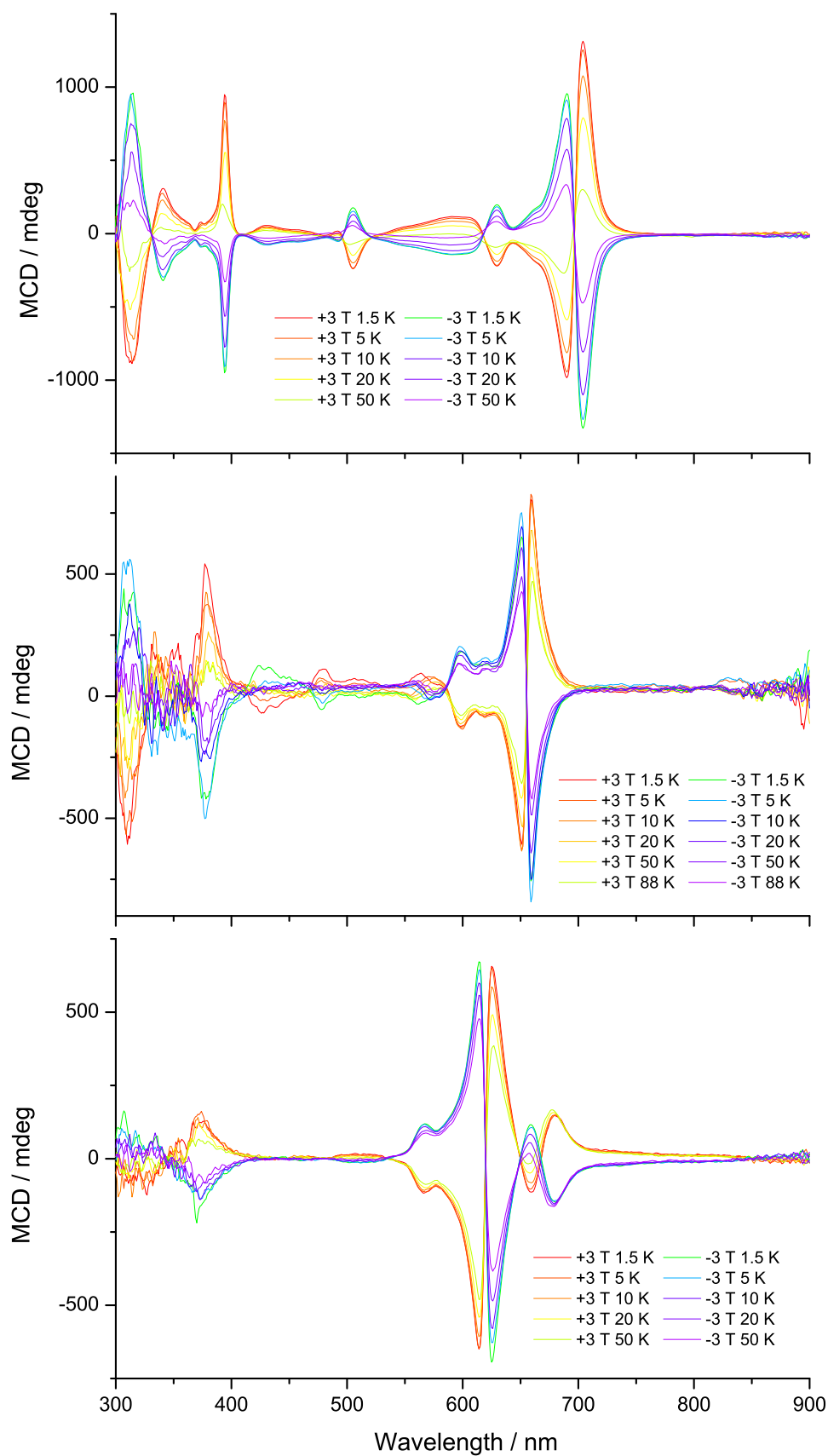


Figure 4-26. MCD spectra of $[^1\text{Pc}_2\text{Tb}]^+$ (above) $[^1\text{Pc}_2\text{Tb}]^0$ (middle) and $[^1\text{Pc}_2\text{Tb}]^-$ (below) for an applied field of ± 3 T at temperatures between 1.5 and 88 K.

Figure 4-25 shows the obtained MCD spectra for all three oxidation states recorded at 1.5 K for magnetic fields between -7 and +7 T while Figure 4-26 shows the obtained MCD spectra for a magnetic field of ± 3 T and temperatures between 1.5 and 88 K. The MCD spectra of the cationic, neutral and anionic complexes contain prominent temperature and field dependent pseudo-A terms at 701, 660 and 624 nm, respectively, (Figure 4-25) that correspond to the intense Q-band features in the UV/Vis absorption spectra (Figure 4-15). In addition, the fingerprint π -radical band of the neutral and the cationic complex show MCD bands of opposite sign at 484 and 510 nm, respectively.

A detailed analysis combined with DFT calculations should allow to determine the electronic structure of all three complexes although this is still a work in progress.

4-4-3 Magnetization data from MCD measurements

The MCD signal is proportional to the magnetization of the sample, and therefore it is possible to image the field or time dependency of the magnetization of the collection of isolated molecules via monitoring its MCD signal intensity. Using this technique one can do mainly two things: a) Extract the magnetization hysteresis curve by recording the MCD intensity while sweeping the magnetic field maintaining a constant temperature, and b) Extract the relaxation time of the complexes by monitoring the decay of the MCD intensity at a given wavelength as a function of time after switching-off the magnetic field and maintaining a constant temperature.

4-4-3-1 Magnetization hysteresis of three redox states of complex ${}^1\text{Pc}_2\text{Tb}$ studied by MCD

Due to experimental limitations, it was only possible to record the magnetization hysteresis while sweeping the field at $1 \text{ T}\cdot\text{min}^{-1}$. Since it is impossible to monitor in real time the MCD signal of the whole spectrum, since they take 3 min to record, the MCD vs. field curves were recorded at a fixed wavelength. In order to check the response of the different bands on the hysteresis curves, the MCD intensity vs. field curves were measured for each oxidation state at two different fixed wavelengths, belonging to the Q-band and the Soret band regions. The experiments were done at 1.5, 2 and 5 K for the neutral $[\text{}^1\text{Pc}_2\text{Tb}]^0$ and cationic $[\text{}^1\text{Pc}_2\text{Tb}]^+$ species and only at 1.5 and 5 K for the anionic species $[\text{}^1\text{Pc}_2\text{Tb}]^-$.

The MCD intensity was monitored for the Q-band region at 705, 664 and 631 nm for the cationic, neutral and anionic complexes, respectively; while for the Soret bands, the

MCD intensity was monitored at 383 and 375 nm for the neutral and anionic species, respectively, and finally at 510 nm for the π -radical band of the cationic species. All the measurements were performed over a ± 2 T field range at a sweep rate of $1 \text{ T}\cdot\text{min}^{-1}$ and plotted as magnetization hysteresis curves, given by either the MCD signal intensity or the opposite of the same, in order to have a positive signal at positive fields.

As a general observation regarding these measurements, the obtained magnetization hysteresis curves have very similar shapes from one band to the other, but some differences can nevertheless be noticed (see Figures 4-27, 4-28 and 4-29). Thus, for all three oxidation states, the Q-band signal is of higher intensity than the higher energy term (Soret or π -radical band). For this reason, the signal to noise ratio is much better for the Q-band region. As could be expected, upon decreasing the temperature, the hysteresis loops broaden, showing larger coercive fields and bigger remnant magnetizations.

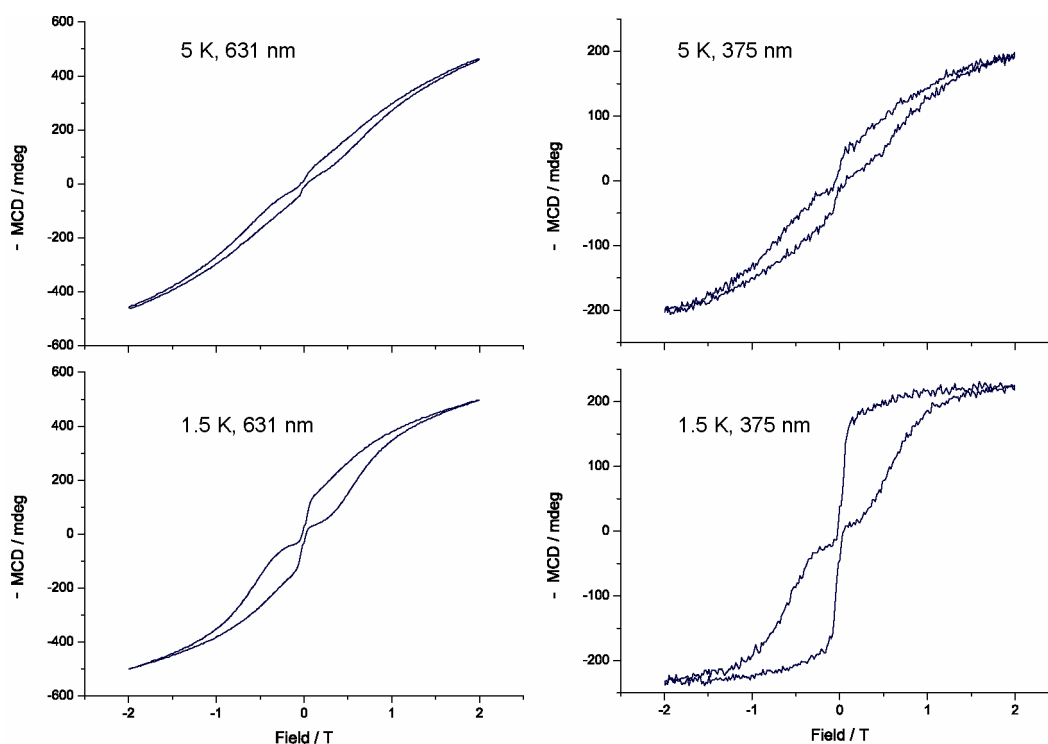


Figure 4-27. MCD intensity versus field for the anionic $[\text{Pc}_2\text{Tb}]^-$ complex measured at 5 K (above) and 1.5 K (below) for the Q-band (left) and the Soret band (right).

In the following, only the analysis and discussion of the MCD intensity hysteresis curves at 1.5 K for the Q-band of each complex are given.

The field dependent MCD intensity of solutions of cationic $[\text{Pc}_2\text{Tb}]^+$ and anionic $[\text{Pc}_2\text{Tb}]^-$ forms of the complex (Figure 4-27 and Figure 4-28) both present butterfly-shaped hysteresis curves that are almost saturated at $H = \pm 2$ T, with an abrupt drop/increase at $|H| < 0.09$ T. These data are similar to the hysteresis curves obtained by magnetometry on dilute solid solutions of the complex $[\text{NBu}_4][\text{Pc}_2\text{Tb}]$ in the isostructural diamagnetic $[\text{NBu}_4][\text{Pc}_2\text{Y}]$ host,^[4] suggesting that MCD is a viable probe of the magnetic properties of isolated double-decker phthalocyanine complexes in frozen solutions. The principal differences between the responses for cationic and anionic double-decker phthalocyanine complexes include a larger coercive field (0.071 T compared to 0.023 T) and a stronger remnant signal (0.198 as compared to 0.065 of the saturated signal intensity) for the cationic species.

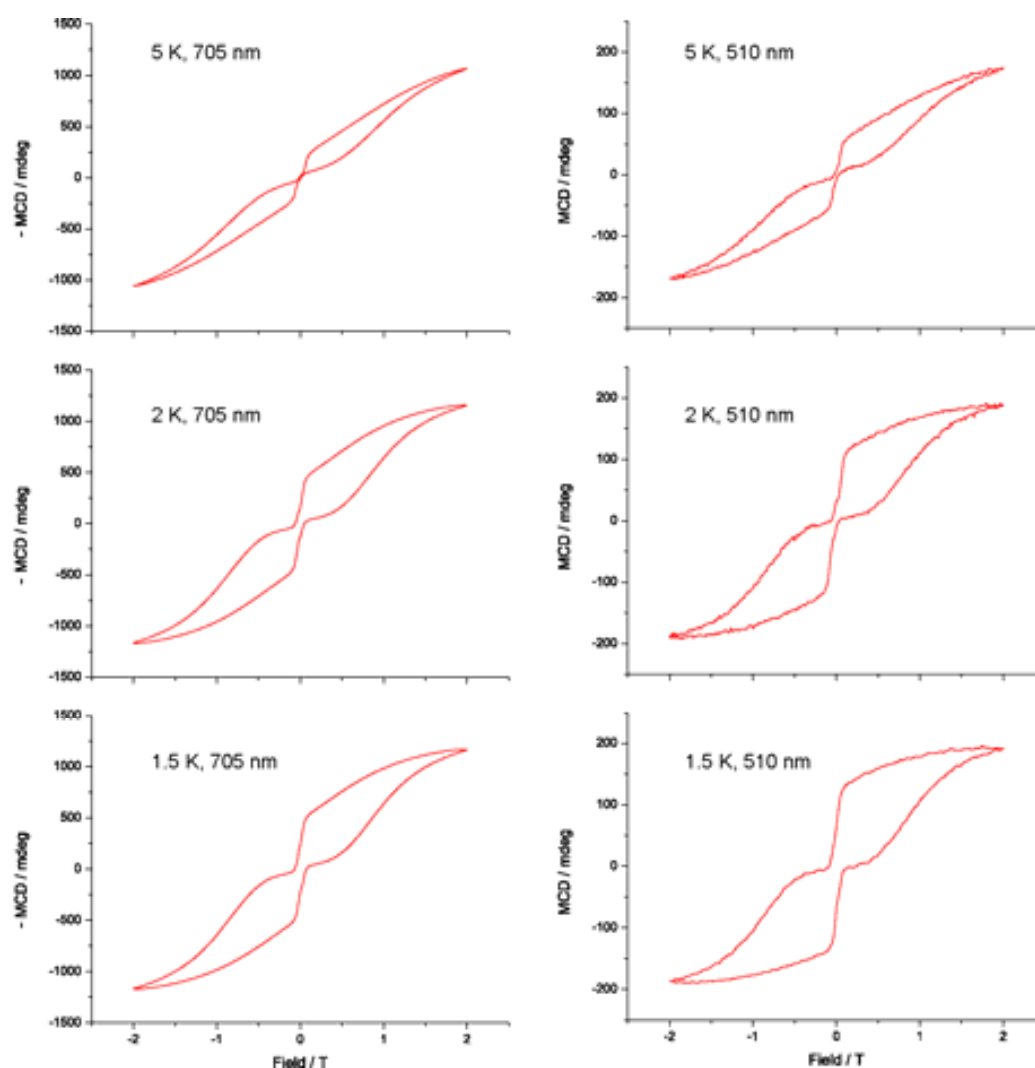


Figure 4-28. MCD intensity versus field for the cationic complex $[\text{Pc}_2\text{Tb}]^+$ measured at 5 K (above), 2 K (middle) and 1.5 K (below) for the Q-band (left) and the π -radical band (right).

The sharp drop/increase in magnetization at $|H| < 0.09$ T for the dilute solid solutions of $[\text{Pc}_2\text{Tb}]$ has been assigned to the eight $|J_z\rangle$ $|I_z\rangle$ states which are brought to resonance by the Zeeman splitting,^[2, 3] as it was schematically depicted in Figure 1-24 and 1-25. This resonance only occurs at low field because of the small energy differences between these states.

The very similar behaviors observed in the MCD of frozen solutions of the anionic and cationic forms of complex $^1\text{Pc}_2\text{Tb}$, especially the coincidence of the change in magnetization around $H = \pm 0.09$ T, suggests that the source of their dynamic magnetic behaviors is closely related. The difference in the width of their hysteresis curves above approximately 0.2 T suggests that the $|J_z\rangle$ multiplet splitting is larger for the cationic species than for the anionic complex.

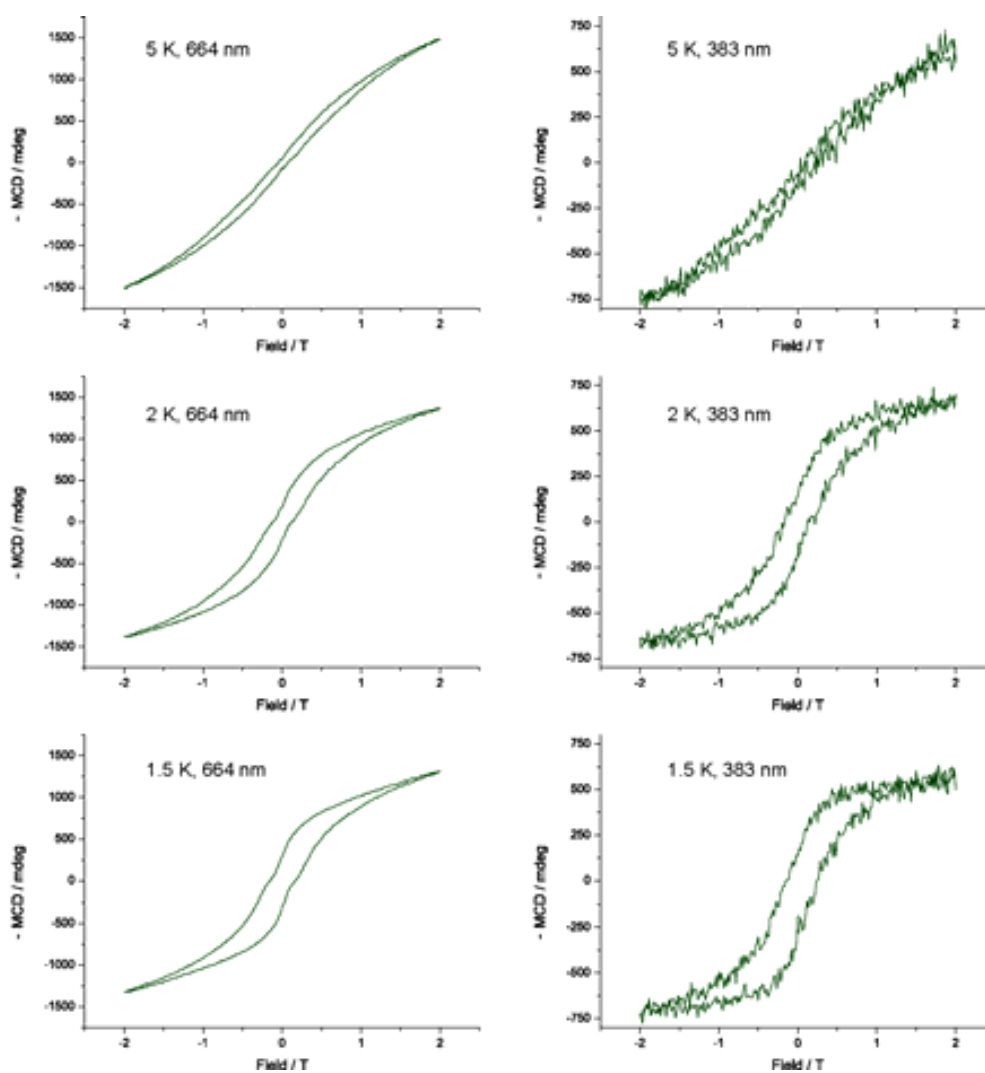


Figure 4-29. MCD intensity versus field for the neutral complex $[\text{Pc}_2\text{Tb}]^0$ measured at 5 K (above), 2 K (middle) and 1.5 K (below) for the Q-band (left) and the Soret band (right).

This is consistent with the temperature dependence of the maximum in the imaginary component of the ac-susceptibility measurements previously reported for these two oxidation states.^[6]

The field dependent MCD of the neutral complex $[\text{Pc}_2\text{Tb}]^0$ (see Figure 4-29) exhibits a different hysteresis behavior as compared to those recorded for the other two oxidation states. Notably, the hysteresis is maintained over the whole range of magnetic field, between ± 1.5 T, and does not narrow at low fields around $H = 0$ T. Consequently, the coercive field is larger for the neutral form (0.16 T) than for the cationic or anionic species in these frozen solutions. The relatively smooth profile of the hysteresis of $[\text{Pc}_2\text{Tb}]^0$ suggests that tunneling is not dominant in this complex when compared to $[\text{Pc}_2\text{Tb}]^{+/-}$. This strong difference is yet to be rationalized, and it is expected that the electronic structure of the compounds should provide more insight into the origin of the different behavior of $[\text{Pc}_2\text{Tb}]^0$.

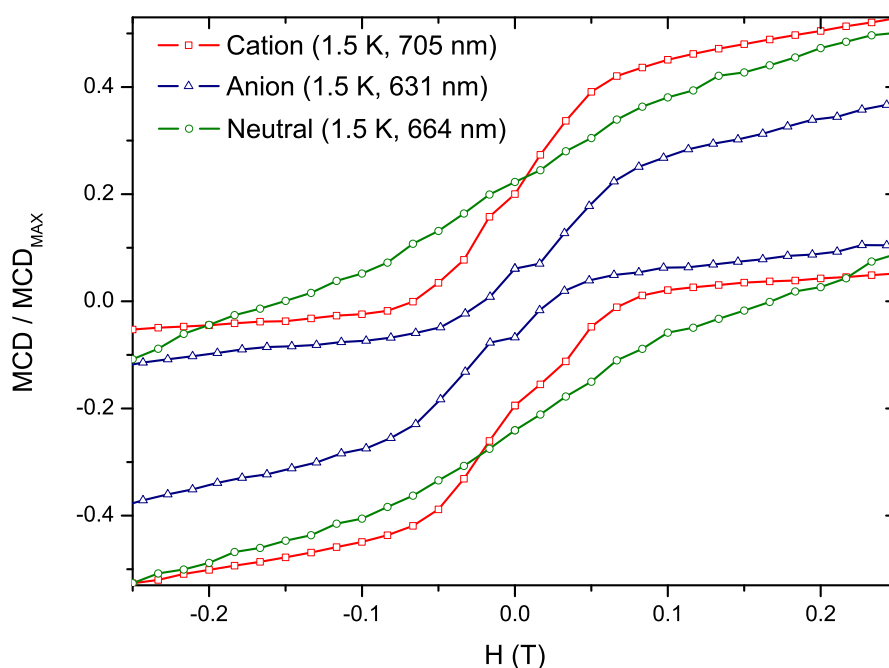


Figure 4-30. Magnification of the MCD hysteresis curve for the Q bands of $[\text{Pc}_2\text{Tb}]$, $[\text{Pc}_2\text{Tb}]^0$ and $[\text{Pc}_2\text{Tb}]^+$ around $\mu_0 H = 0$ T

A closer examination of the MCD hysteresis curve of the three complexes close to zero field reveals an interesting feature. Indeed, when approaching $\mu_0 H = 0$ T, there is a sudden change in behavior of the MCD vs. field curve in the demagnetization part (decreasing values of $|H|$) of the curve which is clearly visible for the two charged

complexes (see Figure 4-30). Namely, the MCD signal settles to a short plateau before it starts to decrease again while crossing $\mu_0 H = 0$ T. The effect is very pronounced for the anionic species. It can also be noticed in the characteristics of the cationic species, but not for the neutral complex. In order to check if this behavior is a common tendency of all three oxidation states, the derivatives of their hysteresis cycles were plotted against the magnetic field (see Figure 4-31).

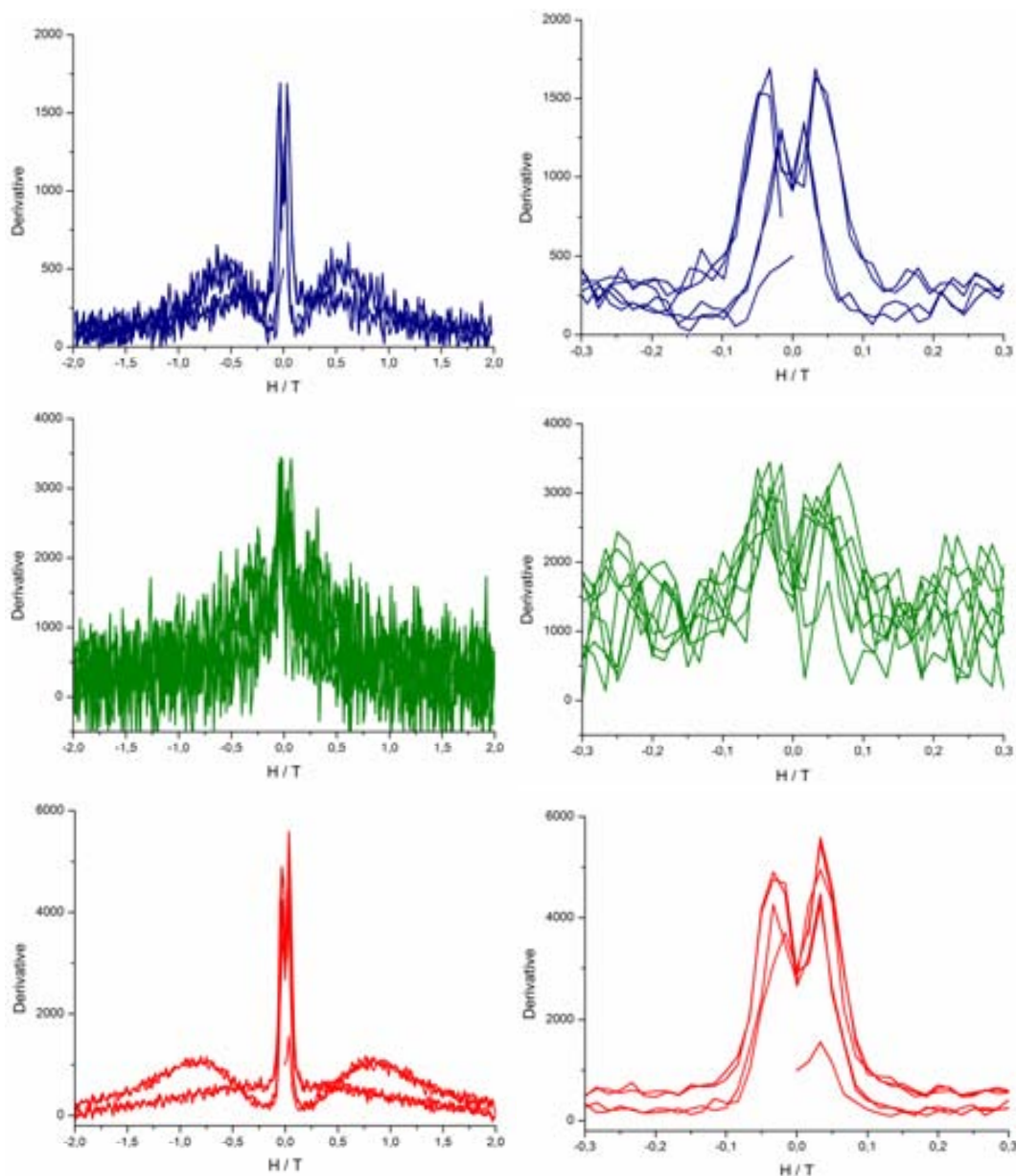


Figure 4-31. Derivative of the hysteresis curve of the normalized MCD intensity vs. H (left) and enlargement of the same (right) for $[^1\text{Pc}_2\text{Tb}]^-$ (above) $[^1\text{Pc}_2\text{Tb}]^0$ (middle) and $[^1\text{Pc}_2\text{Tb}]^+$ (below).

Logically, the plateaus observed in Figure 4-30 translate into drops in the derivative curve as can be seen in Figure 4-31. This behavior is also clearly seen in the derivative of the MCD hysteresis curves of the cationic complex. For the neutral complex, however, the derivatives are more noisy and do not show such a clear behavior as that observed for the other oxidation states. A similar trend can nevertheless be observed, with two peaks at $\mu_0H = 0.04-0.05$ T, and a noisy, yet reproducible decrease of the gradient around $\mu_0H = 0$ T.

Therefore, all three oxidation states show features at ca. $\pm 0.04-0.05$ T that may arise from quantum tunneling effects involving nuclear spin, and the sharp decrease in the gradient at 0 T strongly indicates that in all three systems there is relatively little tunneling at zero field. This is to be expected, at least in the case of the anionic complex, since the avoided level crossing at zero field^[4] correspond to forbidden tunneling transitions involving the inversion of both nuclear and electronic spin.

4-4-3-2 Magnetic relaxation of three redox states of complex ${}^i\text{Pc}_2\text{Tb}$ studied by MCD

Using the same experimental setup, one can also get information on the magnetic relaxation by monitoring the decay of magnetization over time. To do so, one must apply a magnetic field, switch it off and monitor the decay of the magnetization versus time.

The relaxation was monitored for all three oxidation states of ${}^i\text{Pc}_2\text{Tb}$ after completing the hysteresis cycles. For the neutral species, despite its relatively high remnant magnetization, it was only possible to obtain magnetic relaxation curves at 1.5, 2 and 5 K for the intense Q-band (see Figure 4-32), because the Soret band was too weak to provide a good profile of the relaxation.

The data obtained could not be fitted by a normal exponential, but they could be fitted by a Kohlrausch stretched exponential using the following formula:

$$M = y_0 + M_0 e^{-(t/\tau)^\alpha}$$

This equation takes into account the dispersion of the relaxation rate parameter and provides here a better fit. The relaxation rates can be extracted from the fit, and the obtained values of τ^{-1} are shown in Table 4-1 for the neutral complex $[{}^i\text{Pc}_2\text{Tb}]^0$.

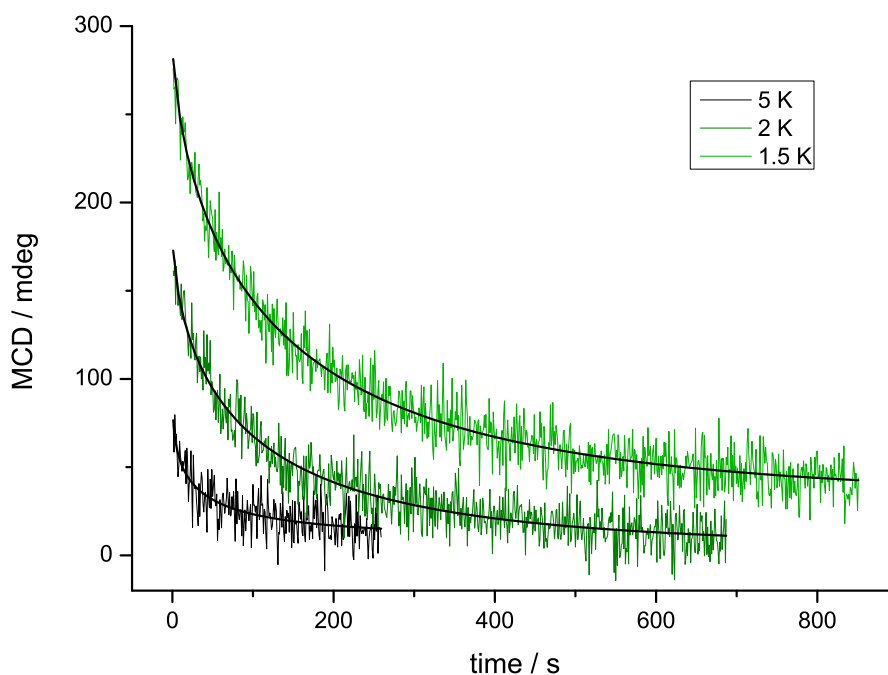


Figure 4-32. MCD detected magnetic relaxation curves for the neutral complex $[{}^1\text{Pc}_2\text{Tb}]^0$, measured at 5, 2 and 1.5 K via monitoring the MCD intensity of the Q-band at 664 nm. The solid lines are best fits to a Kohlrausch model.

The resulting parameter α should be temperature independent. Here, it is indeed found not to vary significantly with temperature, which tends to validate the model used for the fitting of the experimental curves.

Table 4-1. Comparison of the relaxation rates (τ^{-1}) of the neutral complex $[{}^1\text{Pc}_2\text{Tb}]^0$ as a function of temperature

$[{}^1\text{Pc}_2\text{Tb}]^0$	τ^{-1} (s^{-1})	α
5 K	25×10^{-3}	0.634
2 K	10×10^{-3}	0.627
1.5 K	7.4×10^{-3}	0.646

As explained in Chapter 1, the relaxation rate (τ^{-1}) of double-decker phthalocyanine compounds usually shows a crossover from a thermally activated Orbach process at $T > 20$ K approximately, to a direct spin-phonon coupling at lower temperature. In the present case, $1.5 \text{ K} < T < 5 \text{ K}$, it is therefore expected that the relaxation rate occurs through a direct spin-phonon coupling process, for which which in a first approximation

the relaxation time should obey $\tau \propto 1/T$,^[†] rather than a thermally activated Orbach process for which $\ln(\tau) \propto 1/T$. This hypothesis is strongly supported by the two graphs corresponding to these models shown in Figure 4-33.

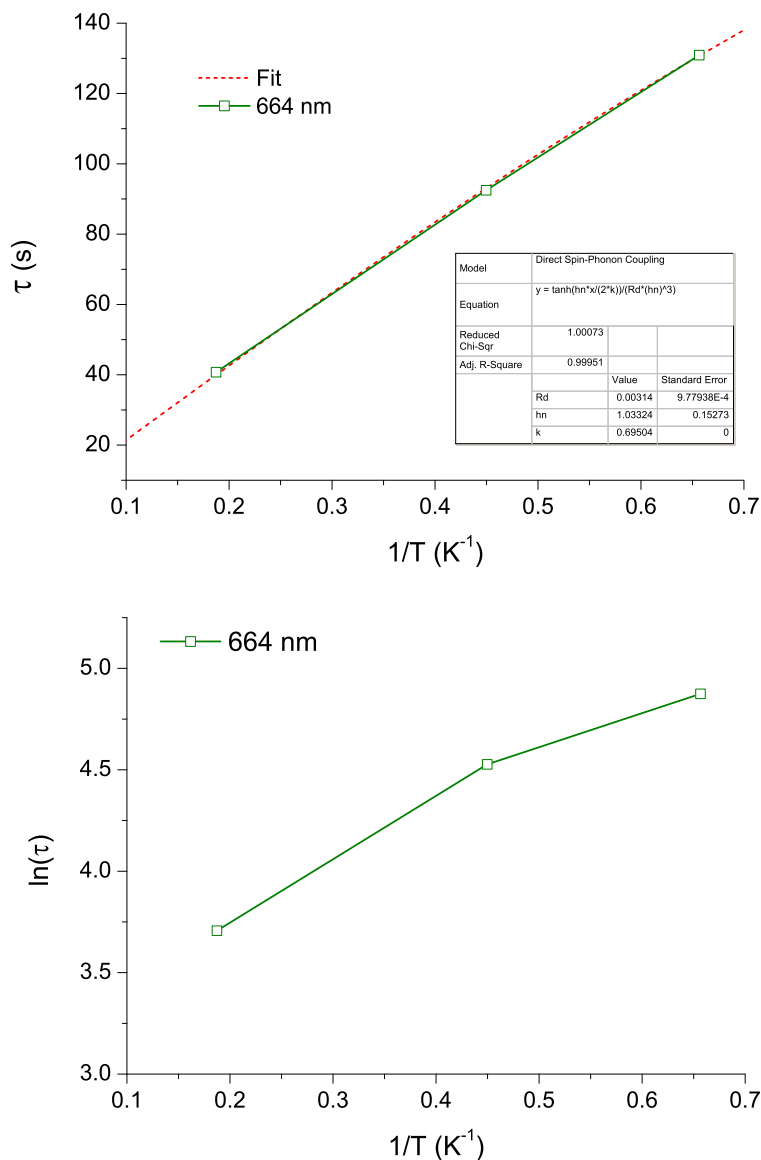


Figure 4-33. Representation of the relaxation time τ (above) and its natural logarithm $\ln(\tau)$ as a function of the inverse temperature $1/T$ for $[^1\text{Pc}_2\text{Tb}]^0$.

The Orbach process has to be discarded since the graph of $\ln(\tau)$ vs. $1/T$ is clearly not linear, whereas the quasi linearity of τ vs. $1/T$ indicates that the direct spin-phonon

[†] The first term of the equation on page 26 describing the direct spin phonon-coupling, $\tau^{-1} = R_d (\hbar\nu)^3 \coth(\hbar\nu/2kT)$ or $\tau = \tanh(\hbar\nu/2kT) / (\hbar\nu)^3$, approximates to $\tau = 1/T$ for $\hbar\nu \gg kT$.

coupling seems to be the dominating relaxation mechanism for $[\text{Pc}_2\text{Tb}]^0$ in solution at $T < 5$ K. Moreover, the plot of τ vs. $1/T$ can be nicely fitted to a hyperbolic tangent function.

A similar analysis was applied to the magnetic relaxation of the anionic complex $[\text{Pc}_2\text{Tb}]^-$. In this case, the very small remnant magnetization made it impossible to monitor the relaxation at 5 K, and in this case, the study was limited only to 1.5 K using both Soret and Q-bands.

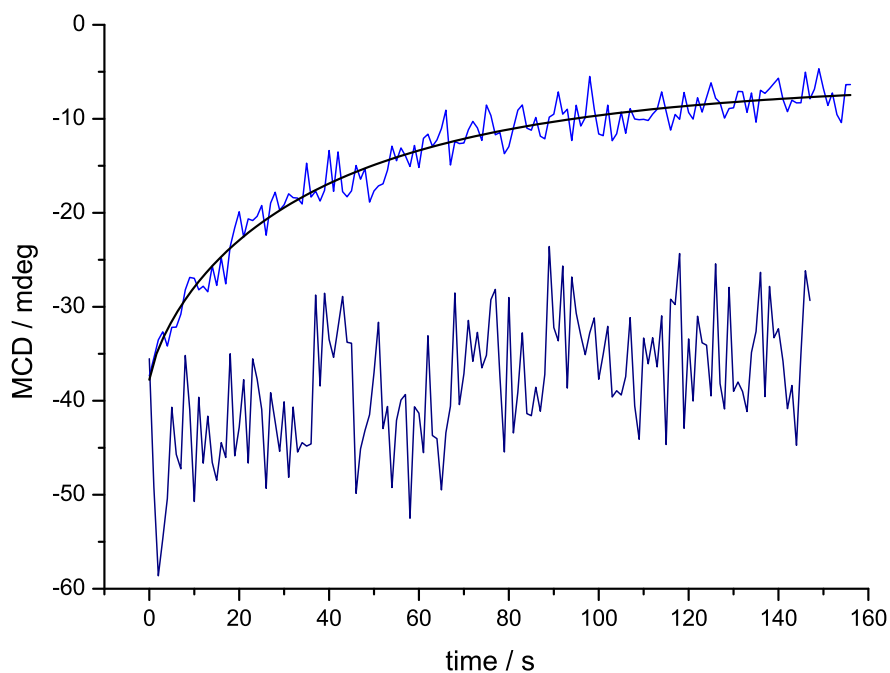


Figure 4-34. MCD detected magnetic relaxation curves for the anionic complex $[\text{Pc}_2\text{Tb}]^-$ measured at 1.5 K by monitoring the Q-band at 631 nm and Soret band at 375 nm MCD intensity. The solid line is a best fit to a Kohlrausch model.

The Soret MCD signal was too noisy to allow a proper fit (see Figure 4-34), but the Q-band afforded a nice stretched exponential type decay which could be fitted and provided the following parameters:

Table 4-2. Fitted relaxation rate (τ^{-1}) and distribution parameter (α) of the anionic complex $[\text{Pc}_2\text{Tb}]^-$ at 1.5 K.

$[\text{Pc}_2\text{Tb}]^-$	τ^{-1} (s^{-1})	α
1.5 K	27×10^{-3}	0.763

Finally, the cationic complex $[\text{Pc}_2\text{Tb}]^+$ was studied in the same way but with this species it was possible to obtain good quality relaxation curves for both the π -radical band and the Q-band at 1.5, 2 and 5 K.

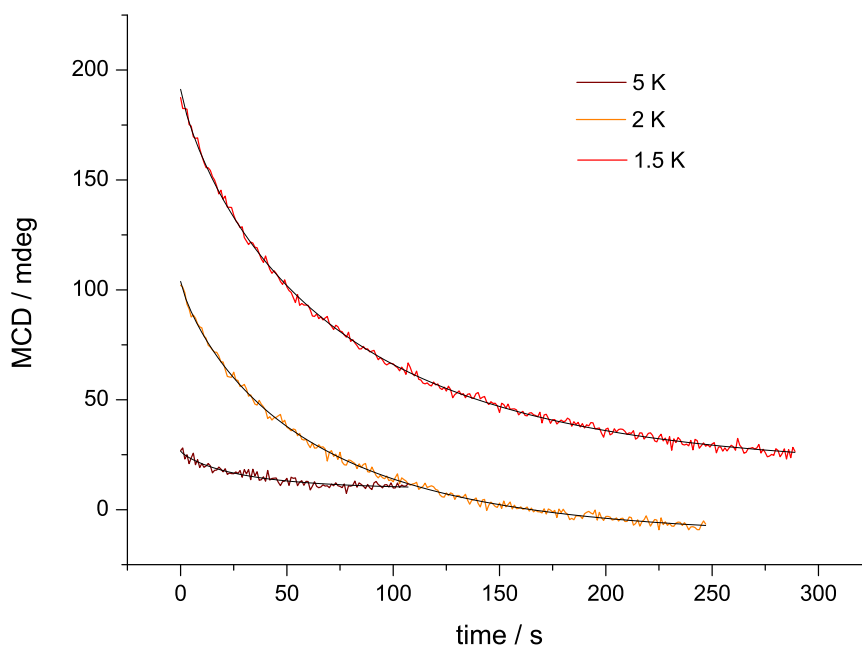


Figure 4-35. MCD detected magnetic relaxation curves for the cation $[\text{Pc}_2\text{Tb}]^+$ measured at 1.5, 2 and 5 K by monitoring the Q-band at 705 nm MCD intensity. The solid lines are best fits to a Kohlrausch model.

The good signal to noise ratio allowed a proper fitting of the relaxation curves to a Kohlrausch model at all three temperatures. Also, like in the case of the neutral complex, the resulting parameter α was found to be temperature independent with a value of approximately 0.83, providing a good confidence on the reliability of the fitted relaxation rates τ^{-1} that are given in Table 4-3 below.

Table 4-3. Comparison of the fitted relaxation rates (τ^{-1}) of the cation $[\text{Pc}_2\text{Tb}]^+$ as a function of temperature, obtained from the MCD signal of the Q-band at 705 nm.

$[\text{Pc}_2\text{Tb}]^+$	τ^{-1} (s^{-1})	α
5 K	34×10^{-3}	0.839
2 K	16×10^{-3}	0.825
1.5 K	14×10^{-3}	0.823

The magnetization decay was also probed by monitoring the MCD intensity of the π -radical band of the cation (see Figure 4-36)

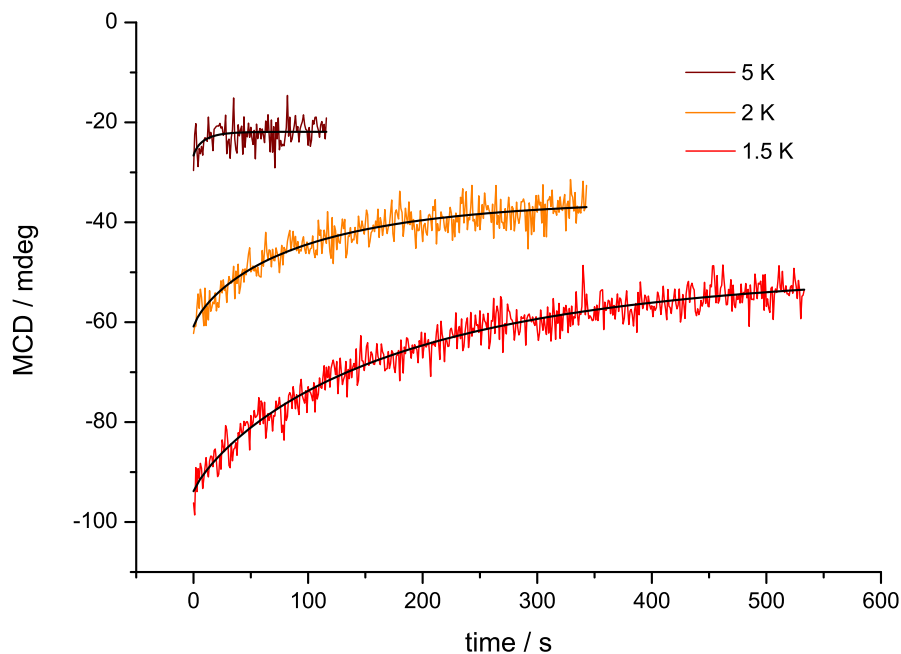


Figure 4-36. MCD detected magnetic relaxation curves for the cationic complex $[^1\text{Pc}_2\text{Tb}]^+$ measured at 1.5, 2 and 5 K by monitoring the π -radical band MCD intensity at 510 nm. The solid lines are best fits to a Kohlrausch model.

With this band, the relaxation rates could again be extracted from the 1.5, 2 and 5 K experiments. The values are given in Table 4-4.

Table 4-4. Comparison of the fitted relaxation rates (τ^{-1}) of $[^1\text{Pc}_2\text{Tb}]^+$ as a function of temperature, obtained from the MCD signal of the π -radical band at 510 nm.

$[^1\text{Pc}_2\text{Tb}]^+$	τ^{-1} (s^{-1})	α
5 K	110×10^{-3}	0.830
2 K	11×10^{-3}	0.791
1.5 K	5.5×10^{-3}	0.834

Again, the distribution parameter α coincides roughly for the two different temperatures, but it also coincides with the experiments performed on the other band. This validates again the quality of the fitting.

As for the relaxation mechanism, the non linearity of the plots of $\ln(\tau)$ vs. $1/T$ and the quasi linearity of the plots of τ vs. $1/T$ for both the Q-band at 705 nm and the π -radical band at 510 nm, indicate that, for this species also, the magnetic relaxation at $T < 5$ K is governed by a direct spin-phonon coupling process (see Figure 4-37).

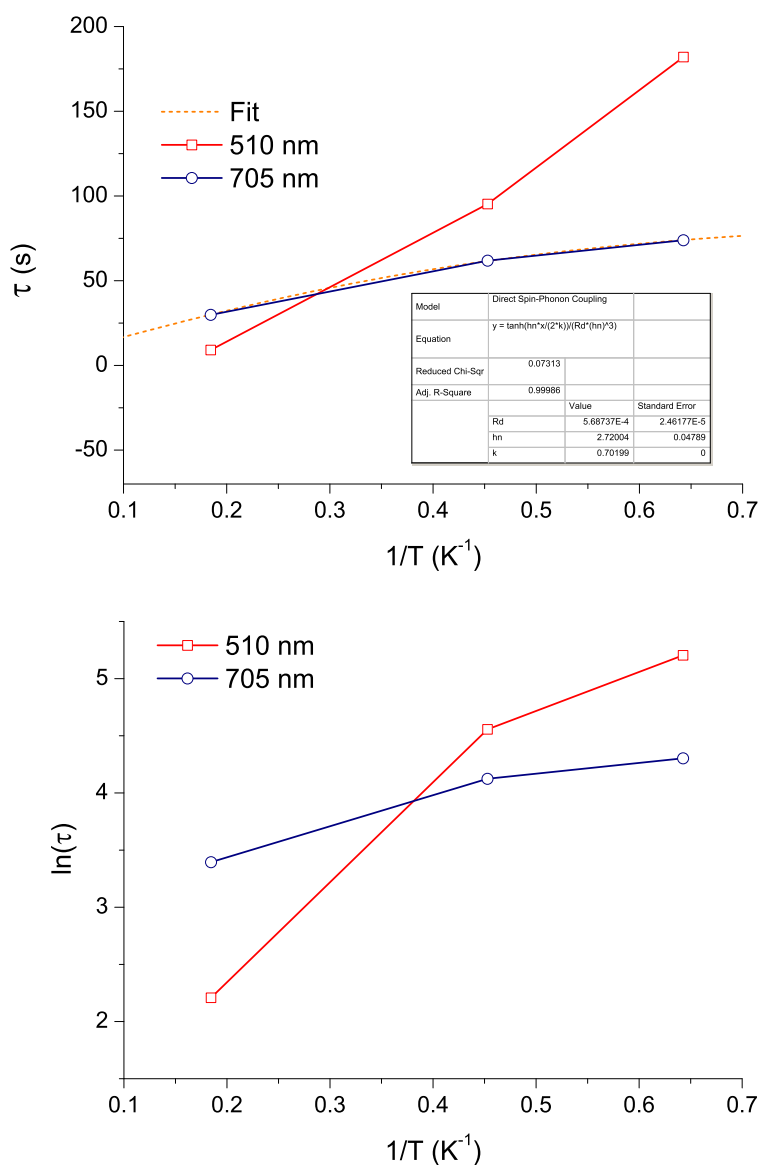


Figure 4-37. Representation of the relaxation time τ (above) and its natural logarithm $\ln(\tau)$ as a function of the inverse temperature $1/T$ for $[^1\text{Pc}_2\text{Tb}]^+$.

In the case of the Q band at 705 nm, the measured relaxation times can be fitted to a hyperbolic tangent function while for the π -radical this cannot be done. Indeed, the linear extrapolation of the relaxation time for this band give negative values for $1/T < 0.15$ which does not make any physical sense. It is also worth noting that the relaxation rates estimated from the Q-band MCD signal decay (Table 4-3) are considerably smaller than those extracted from the π -radical band experiments (Table 4-4). For both of these reasons, the results puts in evidence that some additional parameter should be taken into account when discussing the MCD detected spin dynamics of these complexes.

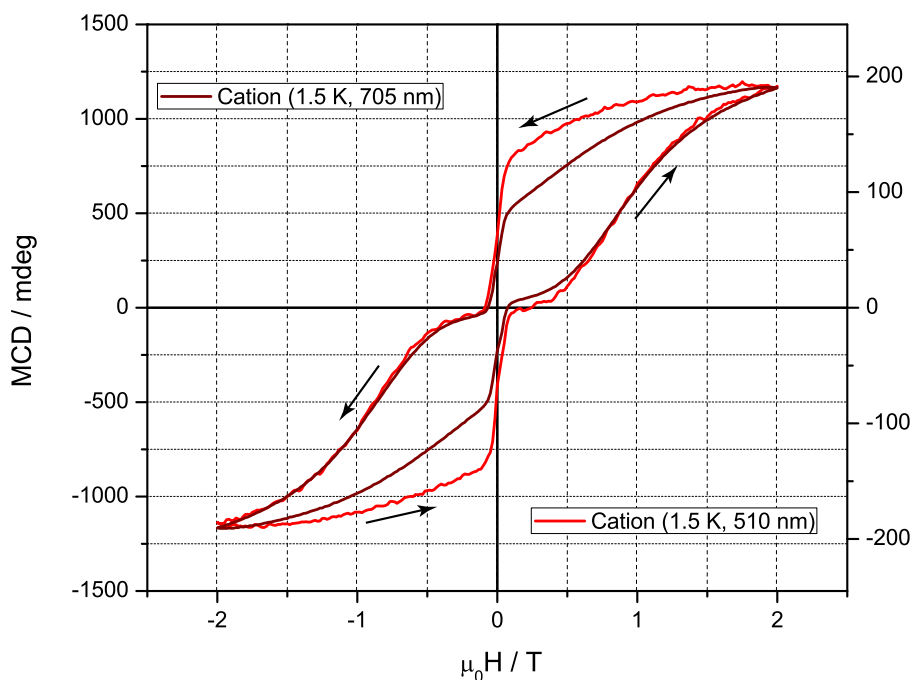


Figure 4-38. Comparison of the MCD hysteresis curve of $[^1\text{Pc}_2\text{Tb}]^+$ at 1.5 K for the two different bands. The magnetization parts coincide but the relaxing parts differ strongly.

Comparing again the MCD detected hysteresis curves obtained for the two different bands for the cationic complex $[^1\text{Pc}_2\text{Tb}]^+$, it appears that the magnetization parts of the hystereses, with increasing values of $|\mu_0H|$, from $\mu_0H = 0$ to $\mu_0H = \pm 2$, coincide for the two different bands, but the relaxation parts, with decreasing values of $|\mu_0H|$, from $\mu_0H = \pm 2$ to $\mu_0H = 0$, indeed do not.

The main difference in the demagnetization parts of the hystereses of all three oxidation states is a slower demagnetization of the higher energy band before reaching the low field tunneling regime. The reason for these differences is probably found in the relative polarizations of the observed transitions. This is a known effect in

dodecamanganese clusters,^[7] and a further analysis of these differences requires an in depth study of the polarization of the different transitions of the MCD spectra. This study is a work in progress.

4-5 Conclusions

Unlike previously reported experiments, the optical MCD technique used here for the characterization of bis(phthalocyaninato)lanthanide-based SMMs does not rely on the preparation of solid solutions and on the identification of suitable isostructural diamagnetic hosts to minimize intermolecular magnetic interactions. Furthermore, the MCD method can be used to probe the magnetic properties of a range of different redox states of the same complex under essentially the same frozen solution conditions. A whole picture of the magnetic behaviour of three oxidation states of the same complex could be obtained, and the respective magnetic relaxation rates could be extracted. While data from magnetic susceptibility studies suggest that the cationic double-decker phthalocyanine complex is more attractive for SMM applications,^[6] we show that, under the conditions of our experiment, the neutral complex, has a greater coercive field than the oxidized or reduced states. A more detailed analysis of the MCD spectra is in progress, and should allow us to assign the polarization of each transition and therefore account for the observed differences in magnetization curves.

Bibliography

- [1] N. Ishikawa, M. Sugita, T. Ishikawa, S.-y. Koshihara, Y. Kaizu, *J. Am. Chem. Soc.* **2003**, *125*, 8694-8695.
- [2] N. Ishikawa, M. Sugita, T. Ishikawa, S.-y. Koshihara, Y. Kaizu, *J. Phys. Chem. B* **2004**, *108*, 11265-11271.
- [3] N. Ishikawa, M. Sugita, W. Wernsdorfer, *J. Am. Chem. Soc.* **2005**, *127*, 3650-3651.
- [4] N. Ishikawa, M. Sugita, W. Wernsdorfer, *Angew. Chem. Int. Ed.* **2005**, *44*, 2931-2935.
- [5] N. Ishikawa, M. Sugita, N. Tanaka, T. Ishikawa, S.-y. Koshihara, Y. Kaizu, *Inorg. Chem.* **2004**, *43*, 5498-5500.
- [6] S. Takamatsu, T. Ishikawa, S.-y. Koshihara, N. Ishikawa, *Inorg. Chem.* **2007**, *46*, 7250-7252.
- [7] E. J. L. McInnes, E. Pidcock, V. S. Oganessian, M. R. Cheesman, A. K. Powell, A. J. Thomson, *J. Am. Chem. Soc.* **2002**, *124*, 9219-9228.
- [8] N. Domingo, B. E. Williamson, J. Gomez-Segura, P. Gerbier, D. Ruiz-Molina, D. B. Amabilino, J. Veciana, J. Tejada, *Phys. Rev. B* **2004**, *69*, 052405.

- [9] P. Gerbier, N. Domingo, J. Gomez-Segura, D. Ruiz-Molina, D. B. Amabilino, J. Tejada, B. E. Williamson, J. Veciana, *J. Mater. Chem.* **2004**, *14*, 2455-2460.
- [10] K. M. Kadish, T. Nakanishi, A. Gurek, V. Ahsen, I. Yilmaz, *J. Phys. Chem. B* **2001**, *105*, 9817-9821.
- [11] P. Zhu, F. Lu, N. Pan, Dennis P. Arnold, S. Zhang, J. Jiang, *Eur. J. Inorg. Chem.* **2004**, *2004*, 510-517.
- [12] A. V. Ivanov, P. A. Svinareva, L. G. Tomilova, N. S. Zefirov, *Russ. Chem. Bull. Int. Ed.* **2006**, *55*, 281-286.
- [13] S. A. Macgregor, E. McInnes, R. J. Sorbie, L. J. Yellowlees, in *Molecular Electrochemistry of Inorganic, Bioinorganic and Organometallic Compounds* (Eds.: A. J. L. Pombeiro, J. A. McCleverty), Kluwer Academic Publishers, **1993**, pp. 503-518.
- [14] S. Wang, M. S. Wemple, J. Yoo, K. Folting, J. C. Huffman, K. S. Hagen, D. N. Hendrickson, G. Christou, *Inorg. Chem.* **2000**, *39*, 1501-1513.
- [15] N. Kobayashi, K. Nakai, *Chem. Commun.* **2007**, 4077-4092.

CHAPTER 5

MAGNETIC BEHAVIOR OF A DOUBLE-DECKER COMPLEX ON GRAPHITE

5-1 Introduction

Since SMMs typically present nanometric dimensions, they are potential candidates for high density data storage bringing the opportunity to achieve the ultimate goal of storing 1 bit of information per molecule,^[1] or for molecular spintronics applications.^[2, 3] Nevertheless, some significant issues need to be addressed for them to be technologically exploitable, like their very low blocking temperature and the difficulties to organize and address individual molecules.^[4] While a lot of effort has been dedicated over the last few years to the preparation of new SMMs, trying to push-up their blocking temperatures (typically of the order of 5 K for the best compounds), very little has been done towards organizing and addressing arrays of independent magnetic molecules. It is even more important, as a first step towards any technological application, to check that the properties of SMMs can be preserved when deposited on a surface, which has been the subject of a very limited amount of publications,^[5, 6] and is one of the goals of the present thesis.

The double-decker phthalocyanine complexes of some lanthanides (Pc_2Ln) have been shown recently to behave, either in bulk or in dilute solid solutions, as single-molecule magnets.^[7-9] On the other hand, some functionalized Pc_2Ln complexes were

[1] M. Cavallini, J. Gomez-Segura, D. Ruiz-Molina, M. Massi, C. Albonetti, C. Rovira, J. Veciana and F. Biscarini, *Angew. Chem. Int. Ed.* **2005**, *44*, 888-892.

[2] M. Affronte, *J. Mater. Chem.* **2009**, *19*, 1731-1737.

[3] L. Bogani and W. Wernsdorfer, *Nat. Mater.* **2008**, *7*, 179-186.

[4] D. Gatteschi, A. Cornia, M. Mannini and R. Sessoli, *Inorg. Chem.* **2009**, *48*, 3408-3419.

[5] L. Vitali, S. Fabris, A. M. Conte, S. Brink, M. Ruben, S. Baroni and K. Kern, *Nano Lett.* **2008**, *8*, 3364-3368.

[6] M. Mannini, F. Pineider, P. Sainctavit, C. Danieli, E. Otero, C. Sciancalepore, A. M. Talarico, M.-A. Arrio, A. Cornia, D. Gatteschi and R. Sessoli, *Nat. Mater.* **2009**, *8*, 194-197.

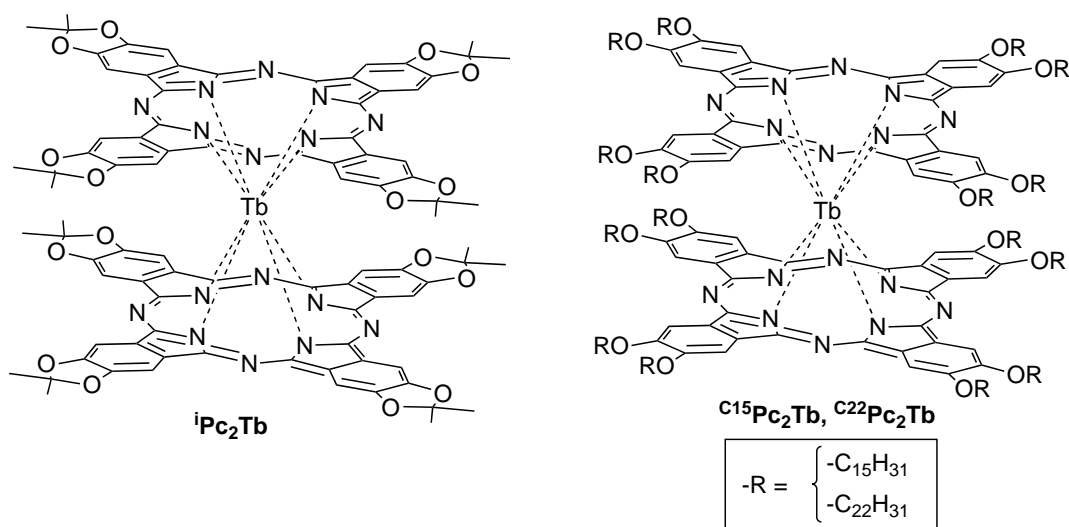
[7] N. Ishikawa, M. Sugita, T. Ishikawa, S.-y. Koshihara and Y. Kaizu, *J. Phys. Chem. B* **2004**, *108*, 11265-11271.

[8] N. Ishikawa, M. Sugita and W. Wernsdorfer, *Angew. Chem. Int. Ed.* **2005**, *44*, 2931-2935.

[9] N. Ishikawa, *Polyhedron* **2007**, *26*, 2147-2153.

also shown to form well ordered self-assembled domains when deposited on highly oriented pyrolytic graphite (HOPG).^[10, 11]

Earlier studies showed that complexes bearing peripheral butoxy substituents formed nicely ordered two-dimensional arrays on graphite, but that the stability of those assemblies was limited to a few hours because the structured monolayers collapsed overnight.^[10] For this reason we chose to prepare long alkoxy chain substituted double-decker complexes, in order to increase the number of van der Waals interactions between the molecule and the substrate, so as to stabilize the monolayers.



The acetal protected complex ${}^1\text{Pc}_2\text{Tb}$ was prepared along with the alkoxy derivatives with pentadecyl and docosyl chains, $\text{C}^{15}\text{Pc}_2\text{Tb}$ and $\text{C}^{22}\text{Pc}_2\text{Tb}$, respectively. The known compound ${}^1\text{Pc}_2\text{Tb}$,^[12] was envisaged initially as a protected reaction intermediate towards a variety of alkoxy terminated phthalocyanines, while the latter have multiple very long chains which should anchor them to a graphite surface. In this chapter, the self assembly of the obtained complexes on graphite is described, together with the magnetic behavior of submonolayers of one of them, the ${}^1\text{Pc}_2\text{Tb}$ complex, which was characterized by X-ray magnetic circular dichroism (XMCD) and compared to its bulk magnetic properties.

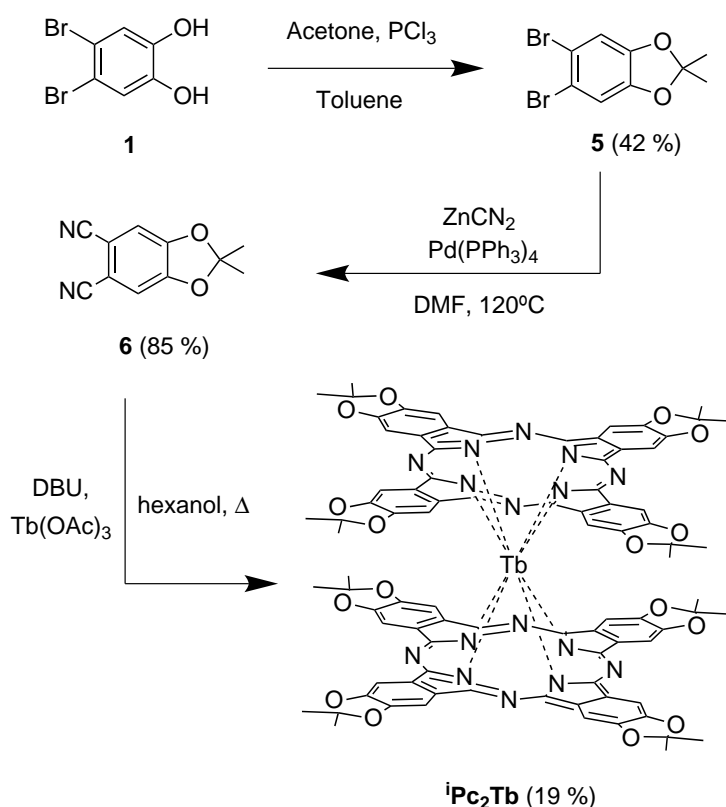
^[10] J. Gomez-Segura, I. Diez-Perez, N. Ishikawa, M. Nakano, J. Veciana and D. Ruiz-Molina, *Chem. Commun.* **2006**, 2866-2868.

^[11] A. S. Klymchenko, J. Slevin, K. Binnemans and S. De Feyter, *Langmuir* **2006**, *22*, 723-728.

^[12] A. V. Ivanov, P. A. Svinareva, L. G. Tomilova and N. S. Zefirov, *Russ. Chem. Bull. Int. Ed.* **2006**, *55*, 281-286.

5-2 Synthesis of the double-decker complexes $^1\text{Pc}_2\text{Tb}$, $^{15}\text{Pc}_2\text{Tb}$ and $^{22}\text{Pc}_2\text{Tb}$

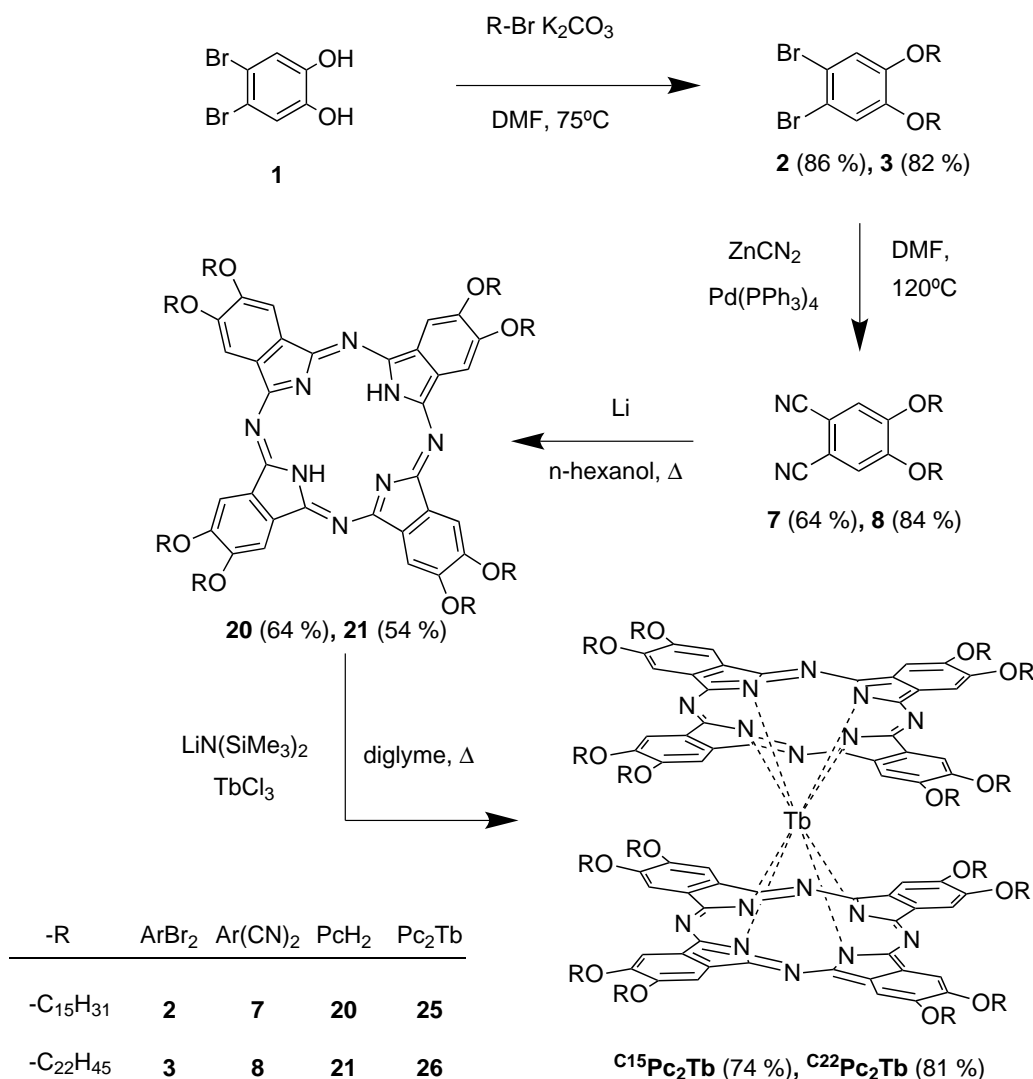
As it was already mentioned in Chapter 3, the isopropylidene-dioxy substituted double-decker terbium complex $^1\text{Pc}_2\text{Tb}$ was prepared in four steps from 4,5-dibromocatechol with small changes from an established method.^[12] The precedent method consisted in first preparing an acetal from acetone and catechol, followed by a bromination of the obtained product. For practical reasons, it was found more convenient to invert these two steps (see Scheme 5-1) since in this way all of the intermediates were solids.



Scheme 5-1. Modified synthesis of $^1\text{Pc}_2\text{Tb}$ in three steps from 4,5-dibromocatechol **1** using a one-step methodology from the corresponding phthalonitrile **6**.

Thus compound **5** was prepared from a solution of compound **1** in toluene (instead of benzene) with a stoichiometric amount of acetone by the dropwise addition of a solution of PCl_3 in toluene. The corresponding phthalonitrile **6** was prepared in high yield by a tandem zinc-palladium catalyzed cyanation of **5**, instead of employing the literature method which was the classical Rosenmund-von Braun conditions. The acetal free base phthalocyanine ($^1\text{PcH}_2$), proved to be quite insoluble in a variety of solvent and it was

judged more convenient to proceed via a one-step methodology, with the direct synthesis of the double-decker complex from the corresponding phthalonitrile. This was achieved by reacting compound **6** with terbium (III) acetate in the presence of DBU in refluxing *n*-hexanol.



Scheme 5-2. Synthesis of $C^{15}Pc_2Tb$ and $C^{22}Pc_2Tb$ in four steps from 4,5-dibromocatechol (**1**) using a two-steps methodology from the corresponding phthalonitriles **7** and **8**.

The bis(octakis-alkoxy-phthalocyaninato) terbium (III) complexes $C^{15}Pc_2Tb$ and $C^{22}Pc_2Tb$, with 15 and 22 carbon linear alkoxy chains respectively, were prepared in four steps from compound **1** (see Scheme 5-2). After preparing the alkoxy substituted dibromo aryls **2** and **3**, they were subjected to a tandem zinc-palladium cyanation to afford the corresponding phthalonitriles **7** and **8**, respectively. In this case, the alkoxy substituents provided a good solubility of all the intermediates, and the preferred

synthetic route was found to be a two-step method. The alkoxy substituted free base phthalocyanines **20** and **21** were first prepared following the original method of Linstead,^[13] in which the phthalonitriles **7** and **8** were reacted with a solution of lithium hexanolate in *n*-hexanol, and then the double-decker complex was prepared by reaction of ^{C15}PcH₂ or ^{C22}PcH₂ with anhydrous terbium (III) chloride and lithium bis trimethylsilylamide in refluxing diglyme, as described elsewhere for other double-decker phthalocyanine complexes with modifications, as mentioned in Chapter 3.^[14]

5-3 Dropcasting the double-decker complexes ¹Pc₂Tb, ^{C15}Pc₂Tb and ^{C22}Pc₂Tb on graphite

The surface self-assembly properties of the obtained complexes were studied by a variety of scanning probe techniques after dropcasting from dilute solutions of complexes ¹Pc₂Tb, ^{C15}Pc₂Tb and ^{C22}Pc₂Tb on freshly cleaved highly oriented pyrolytic graphite (HOPG), which can be an extremely effective way of forming monolayers of compounds or nanoscopic films.^[15-17]

5-3-1 Dropcasting of ¹Pc₂Tb from toluene

In order to screen the behavior of the protected acetal complex ¹Pc₂Tb over graphite, a variety of experimental conditions were tried, changing the concentration of the solution and the drying conditions.

A 10⁻⁶M solution of ¹Pc₂Tb in toluene at room temperature was dropcast on HOPG, allowed to dry in ambient conditions and the resulting organization studied by atomic force microscopy (AFM) in acoustic mode (oscillating tip). This deposition method gave a very irregular morphology, showing a disordered sub-monolayer coverage in some areas, along with big aggregates in some other areas (see Figure 5-1). The lumps seen in this sample could be a result of particles of the compound existing in the solution prior to casting.

[13] R. P. Linstead and M. Whalley, *J. Chem. Soc.* **1952**, 4839-4846.

[14] T. Gross, F. Chevalier and J. S. Lindsey, *Inorg. Chem.* **2001**, *40*, 4762-4774.

[15] S. Furukawa, N. Crivillers, A. Minoia, A. Ver Heyen, M. Mas-Torrent, C. Sporer, M. Linares, A. Volodin, C. Van Haesendonck, M. Van Der Auweraer, R. Lazzaroni, S. De Feyter, J. Veciana and C. Rovira, *J. Am. Chem. Soc.* **2009**, *131*, 6246-6252.

[16] P. Iavicoli, M. Simon-Sorbed and D. B. Amabilino, *New J. Chem.* **2009**, *33*, 358-365.

[17] M. Linares, P. Iavicoli, K. Psychogyiopolou, D. Beljonne, S. De Feyter, D. B. Amabilino and R. Lazzaroni, *Langmuir* **2008**, *24*, 9566-9574.

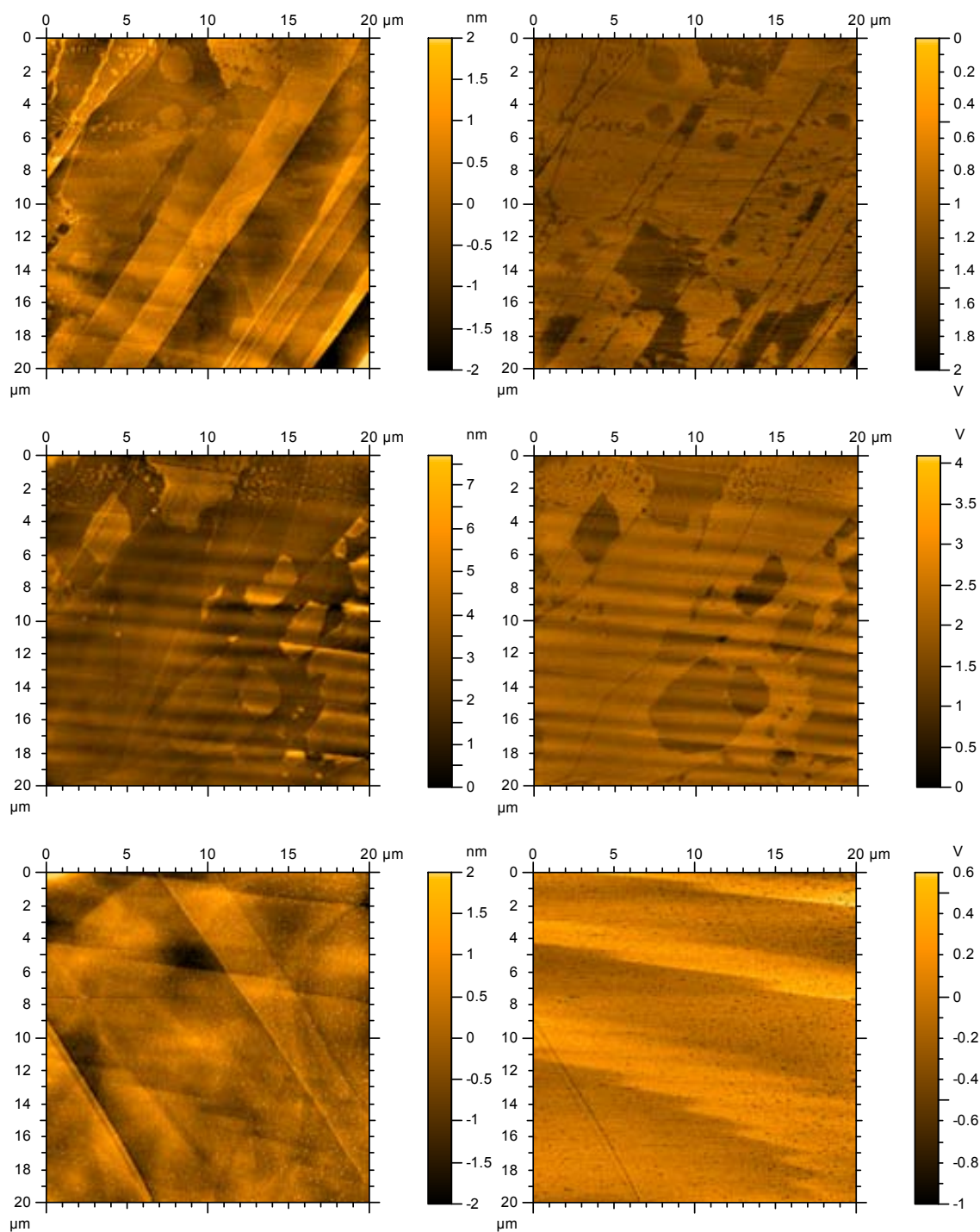


Figure 5-1. Topography (left) and phase (right) AFM images of the irregular morphologies obtained when dropcasting a 10^{-6} M room temperature solution of **28** on HOPG and letting it dry in ambient conditions.

Increasing the concentration of ${}^1\text{Pc}_2\text{Tb}$ by one order of magnitude, a warmed-up 10^{-5} M solution was dropcasted onto freshly cleaved HOPG at room temperature and covered with a Petri dish while drying, which again gave very irregular aggregates.

A mixture of platelets and big molecular aggregates was observed, depending on the scanned areas (see Figure 5-2).

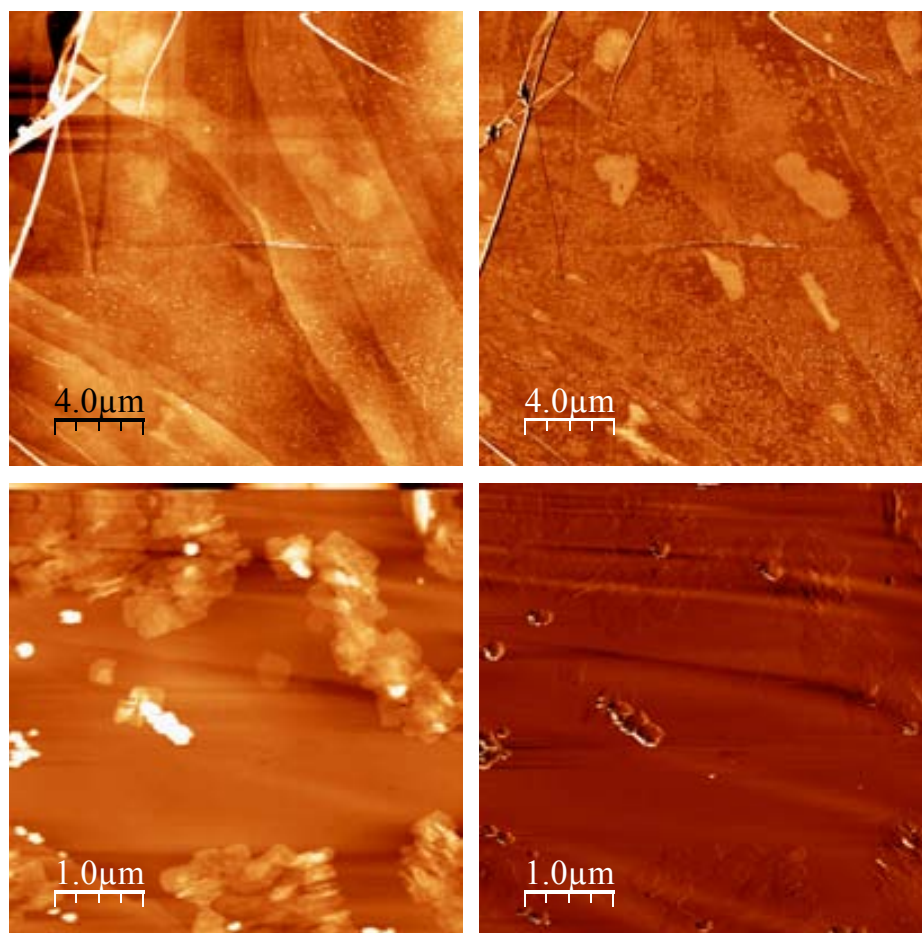


Figure 5-2. Topography (left) and phase (right) AFM images of the samples obtained when dropcasting a 10^{-5} M solution of **28** in toluene under controlled conditions.

The platelets observed in Figure 5-2 have relatively well-defined edges. Having a closer look, it seems like the platelets are made of coalesced crystals. Nevertheless, they do not reach the required regularity of crystal form.

Finally, in order to obtain a slower approach to supersaturation upon drying, the concentration was lowered again and a 10^{-6} M solution of ${}^i\text{Pc}_2\text{Tb}$ in toluene was warmed up with a heat gun, to ensure proper dissolution of the compound, and dropcast onto freshly cleaved HOPG. The drop sample was then covered with a Petri dish and allowed to dry at room temperature, in order to achieve a slower and regular evaporation of the solvent. Complex ${}^i\text{Pc}_2\text{Tb}$ formed highly regular anisotropic bar-shaped islands of a few hundreds of nanometers long and approximately fifty nanometers wide (see Figure 5-3). It is also worth stressing that these bar-shaped islands are not randomly distributed on

the graphite. Indeed they are disposed in such a way that they form angles of about 120° between themselves which is a strong indication that the growth of these domains happens along one of the three main graphite symmetry directions. The anisotropy of these bars can be explained by a difference in the kinetics of crystallization along and across the graphite main axes. Namely, the crystallization rate is higher along the substrate's main axes while the lateral growth seems to be less favored. The height or thickness of the self-assembled nanoislands, as detected by AFM, was of approximately 1.1-1.3 nm, as shown in Fig. 5-3C and 5-3D. The tops of the bars are relatively smooth, indicating a high degree of structural order, as it is expected for a crystalline material.

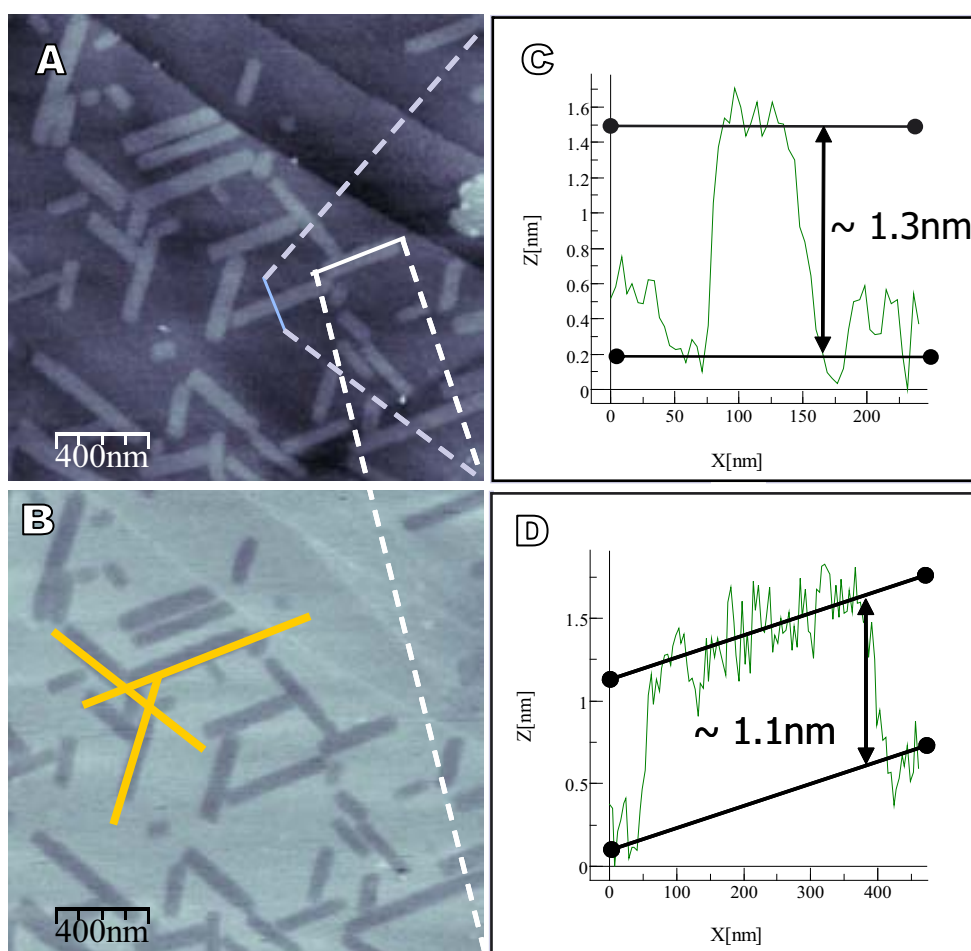


Figure 5-3. (A) Topography and (B) phase AFM images of the self-assembled bar-shaped islands formed by ${}^1\text{Pc}_2\text{Tb}$ on HOPG as dropcast from a 10^{-6}M solution in toluene under slow evaporation conditions. In (B) in yellow are depicted the three different orientation of the islands. In (C) and (D) are shown two height profiles showing the regular thickness of the islands in figure (A).

Ideally, the expected height of a monolayer of molecules of ${}^1\text{Pc}_2\text{Tb}$ can be estimated by summing the interplanar distance of the two phthalocyanine rings, two times the

distance of the outer hydrogen atoms from the mean plane of the phthalocyanine ligands, and two times the van der Waals radius of H atom (see Figure 5-4).

The interplanar distance of the complex was estimated to be of 3.9-4.0 Å from the X-ray crystal structure of another neutral double-decker phthalocyanine complex.^[18] The distance of the outer hydrogen atoms from the mean plane of the phthalocyanines was estimated to be of approximately 2.0 Å from the crystal structures of other benzodioxole compounds^[19] and later on confirmed by PM3 molecular mechanics calculations performed on 2,2-dimethyl-benzodioxolane. Finally, a value of 1.1 Å was used as the van der Waals radius of hydrogen.^[20]

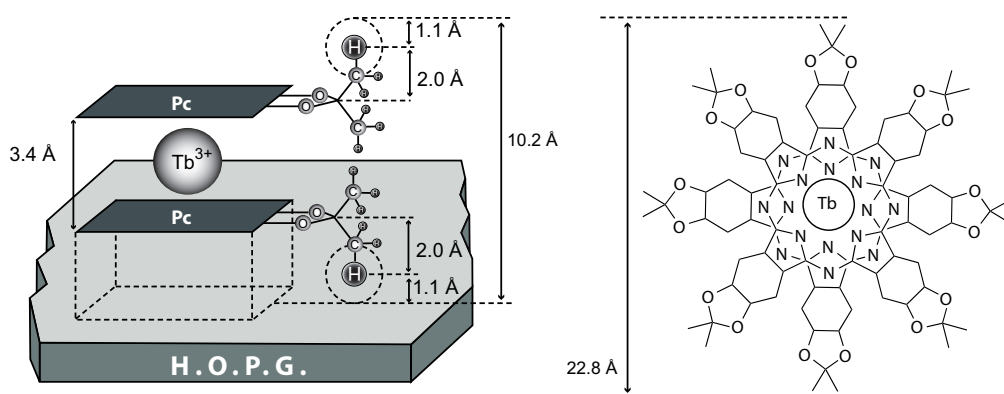


Figure 5-4. Schematic representation of complex ¹Pc₂Tb on top of the graphite (left) and lateral dimension of the complex (right)

The total estimated height of the monolayers on graphite is then 10.1-10.2 Å, i.e. 1.0 nm. On the other hand, the diameter of the complex was estimated to be of approximately 22.8 Å or 2.3 nm, i.e. 20.6 Å plus two times the van der Waals radius of hydrogen. The size distribution of the nanoislands was estimated by measuring 170 islands, the obtained histograms are shown in Figure 5-5. The width of the nanocrystals was thus estimated to be of $w = 70 \pm 30$ nm and their length $l = 250 \pm 150$ nm. All the estimated dimensions suggest therefore strongly that the double-decker molecules should lay flat on the surface, and that they correspond to 2D crystals composed of approximately $1 \times 30 \pm 13 \times 108 \pm 65$ molecules. This morphology could be seen over large areas on the sample, in different locations of the graphite and on different samples. The observation of bars for the 10^{-6} M solution implies a surface-mediated

[18] A. G. Gurek, T. Basova, D. Luneau, C. Lebrun, E. Koltsov, A. K. Hassan and V. Ahsen, *Inorg. Chem.* **2006**, *45*, 1667-1676.

[19] D. Sun, S. V. Rosokha and J. K. Kochi, *J. Phys. Chem. B* **2007**, *111*, 6655-6666.

[20] R. S. Rowland and R. Taylor, *J. Phys. Chem.* **1996**, *100*, 7384-7391.

crystallization, whereas in the more concentrated solution, nucleation may take place inside the bulk of the solvent drop before interacting with the HOPG substrate because of super-saturation occurring quickly.

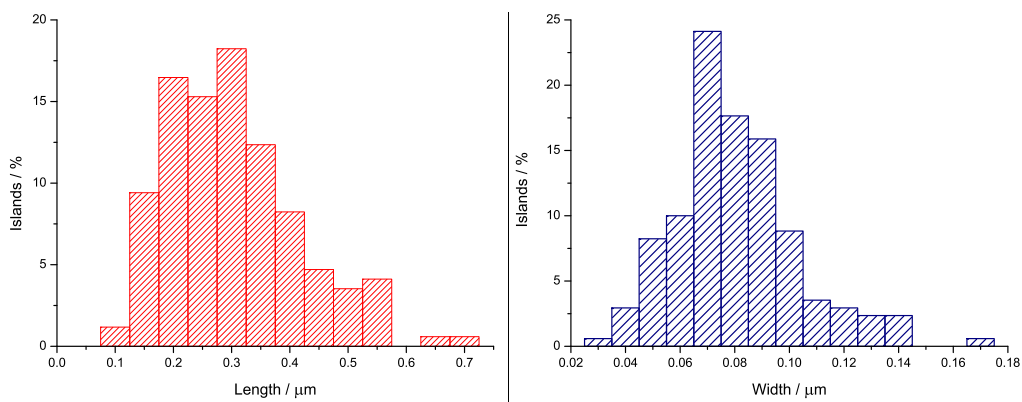


Figure 5-5. Histograms of the length (left) and width (right) distribution of the bar-shaped islands of $[\text{Pc}_2\text{Tb}]$ on top of HOPG.

The layers formed upon dropcasting of a 10^{-5}M solution of the anionic complex $[\text{Pc}_2\text{Tb}]$ in acetone was also characterized (see Figure 5-6).

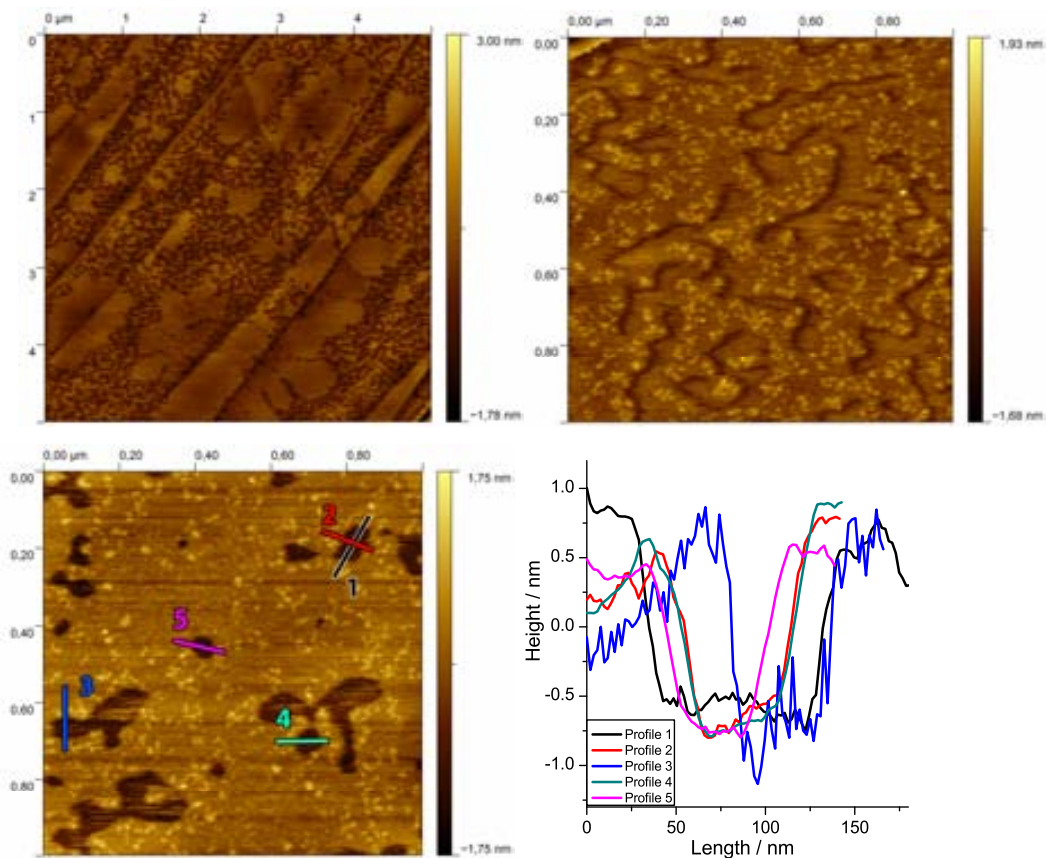


Figure 5-6. Topography AFM images of the discontinuous layer formed by $[\text{Pc}_2\text{Tb}]$ on HOPG as dropcast from a 10^{-5}M solution in acetone and height profiles measured on one of them.

A discontinuous layer was formed of a homogeneous height of approximately 1.2-1.3 nm was characterized which is in good agreements with the size of the molecules. Over this flat layer lay some small aggregates of approximately 1 nm in height which could be due to the packing of a second layer of molecules. This morphology was observed in different areas of the sample. The difference in the various observed areas lay mainly in the different relative coverage from one area to the other as can be appreciated in Figure 5-6.

5-3-2 Surface deposition of $^{15}\text{C}_2\text{Tb}$

The pentadecyloxy substituted complex $^{15}\text{C}_2\text{Tb}$ was also dropcast onto freshly cleaved HOPG from toluene and observed in acoustic mode by AFM. The best images (see Figure 5-7) were obtained this time with a concentration of 10^{-5}M in toluene.

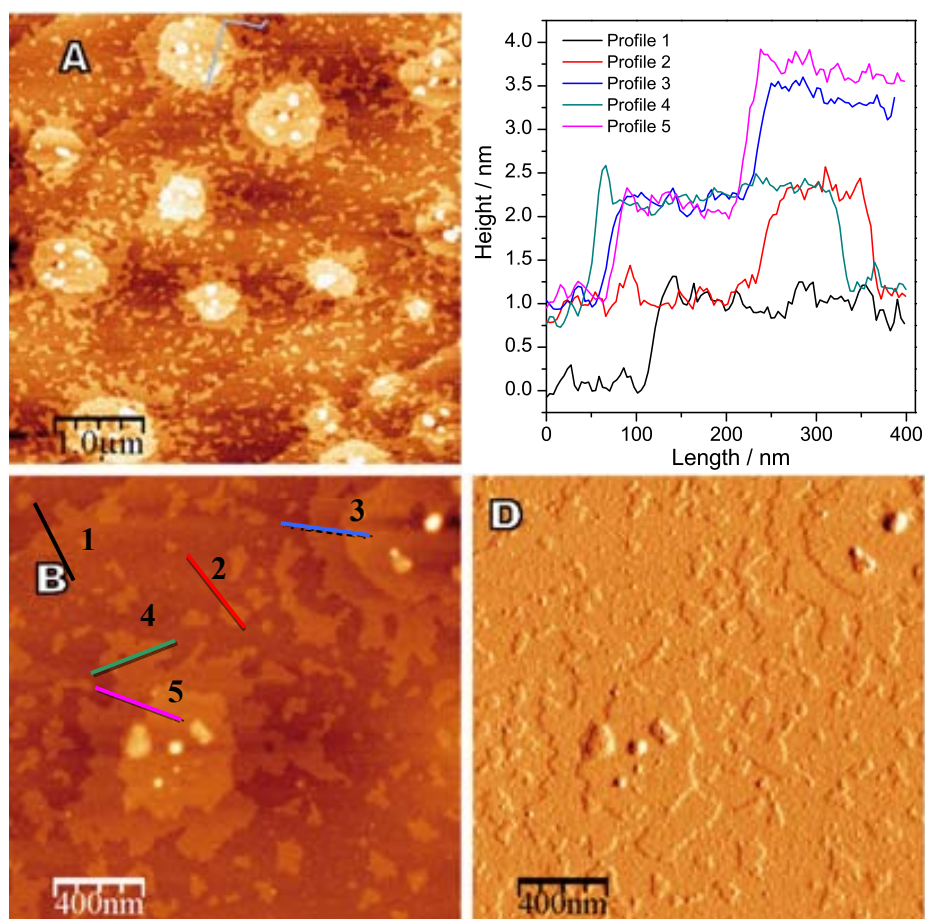


Figure 5-7.(A) and (B) Topography AFM images of the self-assembled terraces of $^{15}\text{C}_2\text{Tb}$ on HOPG. The bigger islands show a multilayer structure. The overall structure shows no preferential orientation. In (C) the height profiles showing the dimensions of the observed terraces is shown. In (D) is depicted the amplitude AFM image corresponding to image (B).

The morphology of the self-assembled layer showed multilayered flat terraces of up to four different levels. Apart from an overall round shape, probably due to the formation of droplets of solvent during the evaporation process, the terraces show no preferential distribution or orientation, and their edges are quite disordered. The height of the observed steps is of the order of 1.2 nm which is commensurate with the height of one molecule and much smaller than the width of one molecule. Despite the layered aspect of the thin film, there is apparently no long range ordering in the xy plane. The compound seems to be distributed in a rather random pattern which could have been governed by the evaporation of the solvent and molecule-molecule interactions rather than by the molecule-substrate interactions which were the determining interaction in the formation of the nanocrystals observed for compound ${}^1\text{Pc}_2\text{Tb}$.

As for the coverage of the surface, is it not clear whether the multilayer islands lay directly on the graphite surface or on a continuous layer of complex ${}^{\text{C}15}\text{Pc}_2\text{Tb}$. Indeed, the large steps that could correspond to the graphite are not very straight and look more like a continuation of the base layer of ${}^{\text{C}15}\text{Pc}_2\text{Tb}$ as can be seen in Fig. 5-7. The four main terraces that can be seen are all prolonged into the lower one, which should imply that none of them is the actual edge of the graphite substrate. The observed morphology in this area of the sample corresponds therefore to a multilayer film of more than four superimposed layers.

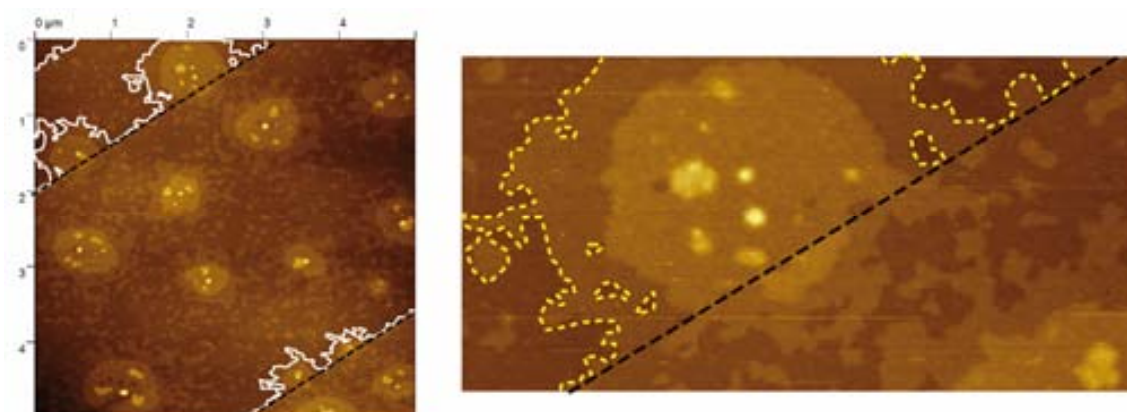


Figure 5-8. Topography AFM image of the multilayer of ${}^{\text{C}15}\text{Pc}_2\text{Tb}$ on HOPG (left) and close-up of the same (right).

Alternative solvents were also tried for organizing ${}^{\text{C}15}\text{Pc}_2\text{Tb}$ on HOPG by dropcasting, obtaining organizations with poor long-range order. For instance, when a 10^{-5}M solution of compound ${}^{\text{C}15}\text{Pc}_2\text{Tb}$ in chloroform was dropcast onto HOPG under

ambient conditions (without covering it with a Petri dish), a totally different morphology was observed (see Figure 5-9).

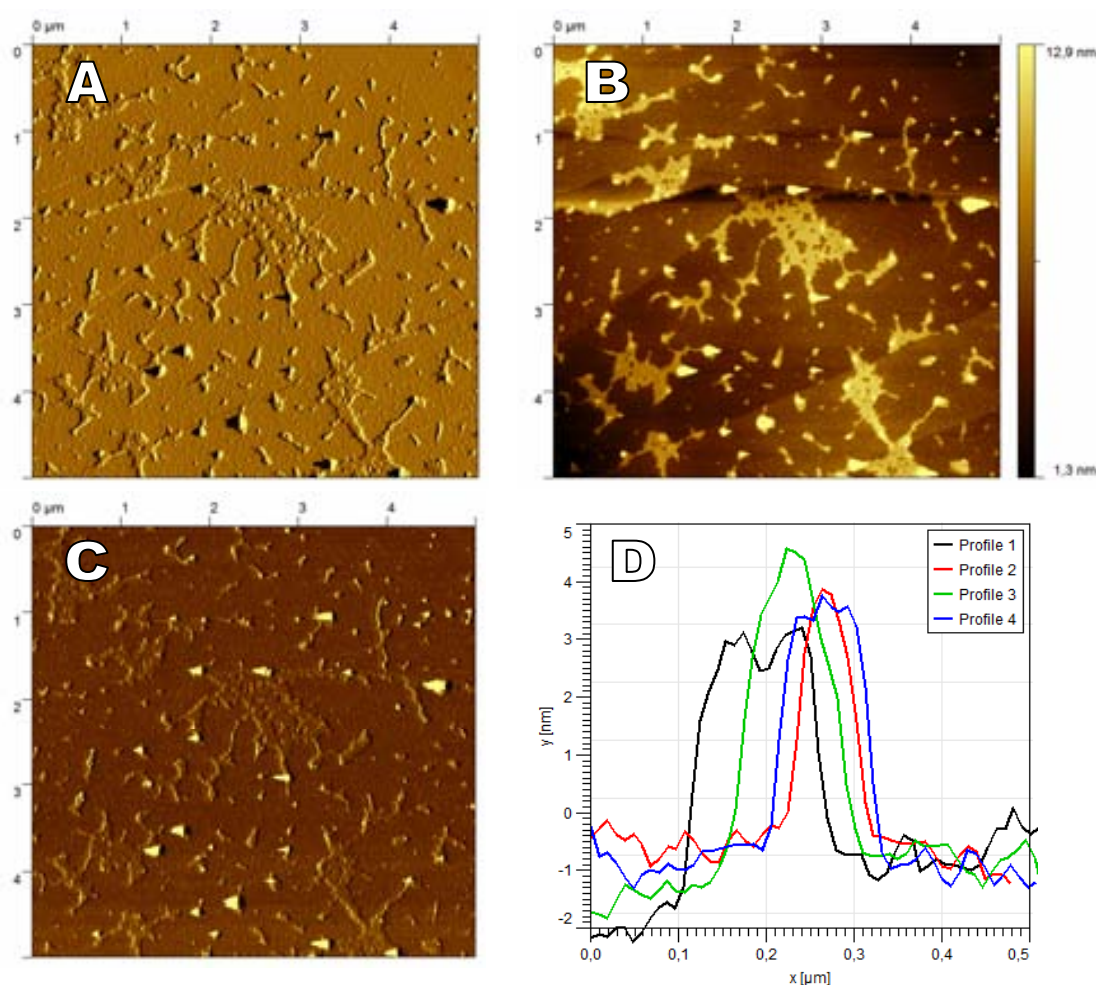


Figure 5-9. Amplitude (A) topography (B) and phase (C) AFM images of $C^{15}Pc_2Tb$ as dropcasted from a $10^{-5}M$ solution in $CHCl_3$, and topographical profiles (D) of the same.

Two types of phases were evident in this experiment. An underlying rough layer topped by some apparently disordered thick dewetting structures. The thick features were about 4-6 nm in height and of variable shapes (see Figure 5-10). It appears that the rough bottom layer presents some holes (probably due to the drying of the material) and that the thick layer shows a fibril-like structure quite similar to previously reported films of double-decker phthalocyanine complexes of samarium and gadolinium.^[18]

^[18] A. G. Gurek, T. Basova, D. Luneau, C. Lebrun, E. Koltsov, A. K. Hassan and V. Ahsen, *Inorg. Chem.* **2006**, *45*, 1667-1676.

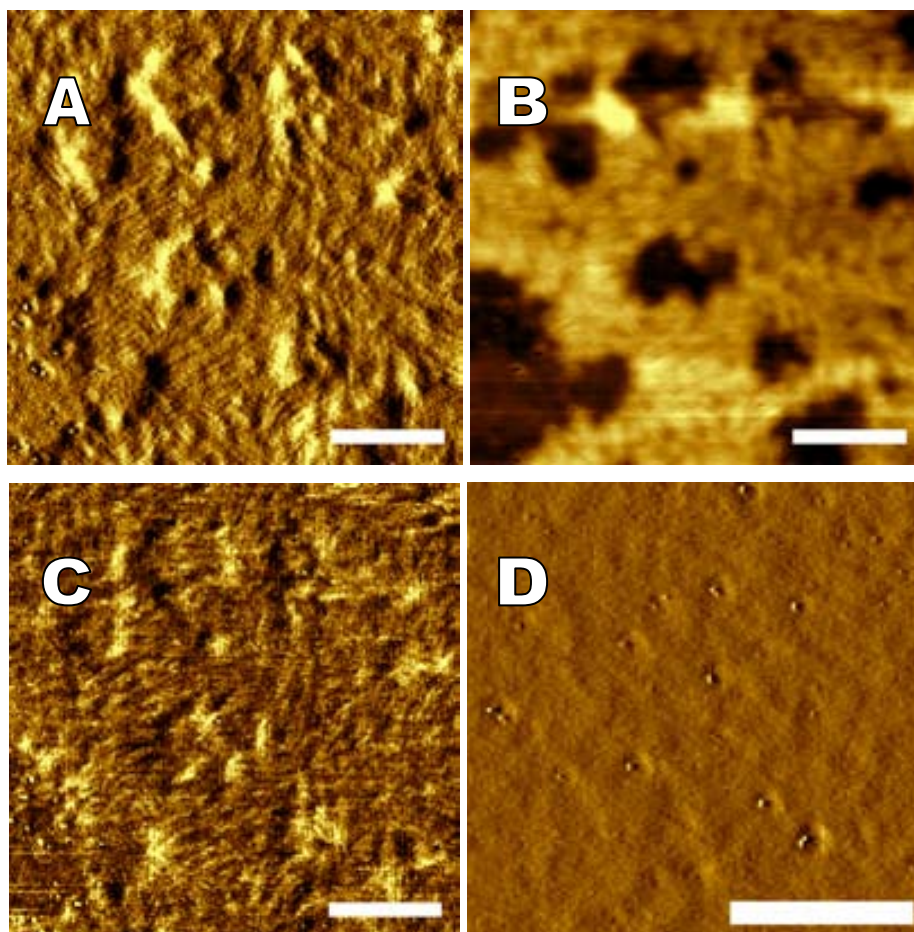


Figure 5-10. Amplitude (A), topography (B) and phase (C) AFM images showing the thick fibril-like patterns of $^{15}\text{Pc}_2\text{Tb}$ and amplitude AFM image (D) showing the holes in the bottom layer. The scale bars represent 100nm.

5-3-3 Surface deposition of $^{22}\text{Pc}_2\text{Tb}$

Complex $^{22}\text{Pc}_2\text{Tb}$, that is the docosyloxy substituted double-decker phthalocyanine terbium complex, is, amongst the synthesized complexes, the one presenting the higher number of methylene groups and was therefore expected to be the one having the stronger van der Waals interaction with the HOPG substrate. It was deposited by dropcasting onto HOPG, employing a 10^{-6}M solution in toluene, in the conditions described earlier for compounds $^{15}\text{Pc}_2\text{Tb}$ and $^i\text{Pc}_2\text{Tb}$.

5-3-3-1 Atomic force microscopy measurements on a monolayer of $^{22}\text{Pc}_2\text{Tb}$ on HOPG

Complex $^{22}\text{Pc}_2\text{Tb}$ was also dropcast on HOPG from a 10^{-6}M solution in toluene. The obtained sample showed a very irregular pattern with big molecular aggregates of several nm in height and an underlying rough film with a surface roughness of

approximately 6 Å, but the height of the layer could not be estimated since it was not possible to distinguish clearly the HOPG surface from the molecular layer.

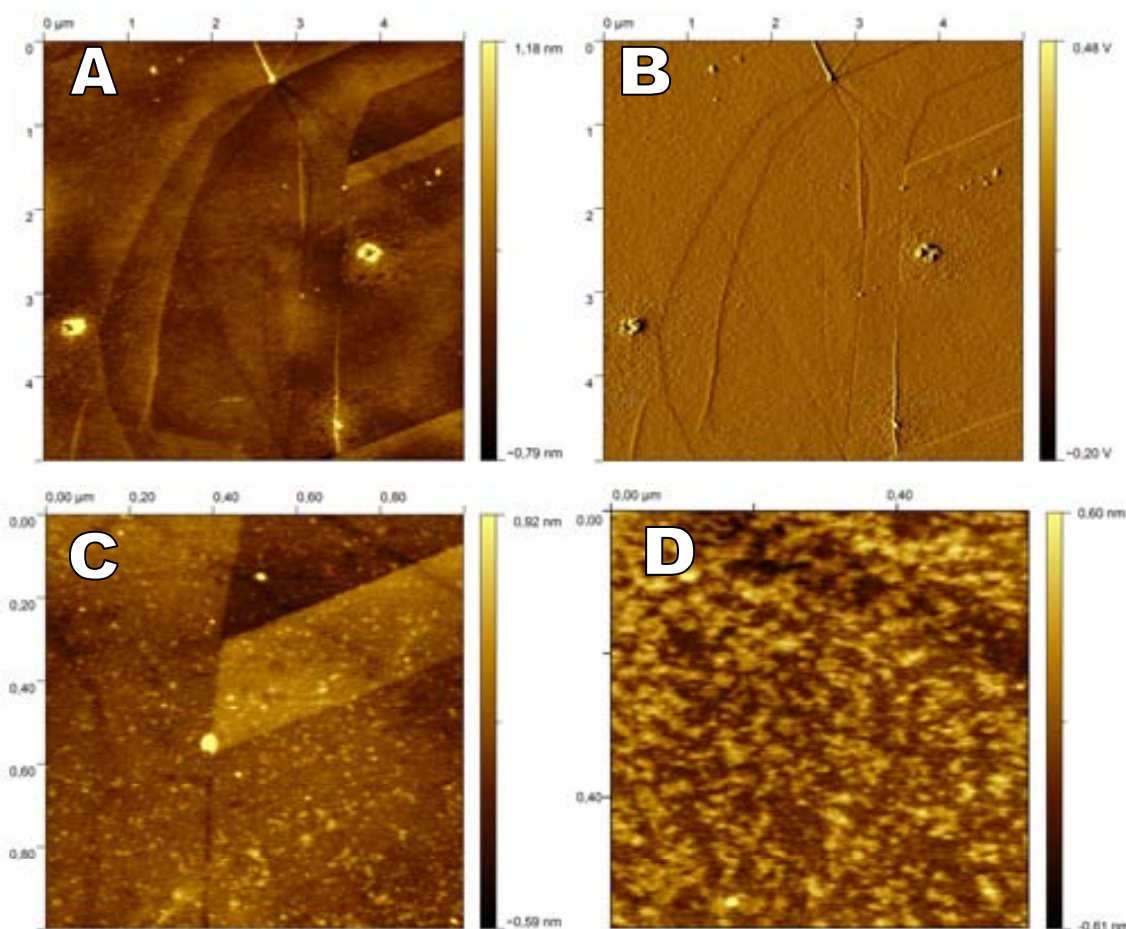


Figure 5-11. Topography (A, C and D) and amplitude (B) AFM images showing the rough layer of $C^{22}Pc_2Tb$ when dropcast from a 10^{-6} M solution in toluene onto HOPG.

This very irregular surface could be due to the lower solubility of $C^{22}Pc_2Tb$ when compared to $C^{15}Pc_2Tb$ due to the very long alkyl chains. Therefore it is possible that upon slow evaporation of the solvent, the compound formed aggregates in the bulk of the drop of solvent that were deposited as a rough film of molecular aggregates.

5-3-3-2 Magnetic force microscopy measurements on a monolayer of $C^{22}Pc_2Tb$ on HOPG

After characterizing the compound by tapping mode AFM, it was studied by magnetic force microscopy (MFM) in order to see if any magnetic contrast could be observed by this technique at room temperature, between the graphite substrate and the areas covered by a layer of $C^{22}Pc_2Tb$. This experiment consists in doing a double scan of the surface, using a Co-Cr coated tip. The first scan is done in a standard tapping mode,

affording the topography and amplitude images similar to those obtained with AFM but with a lower spatial resolution due to the coarse size of the magnetic tip. The obtained images are formally due to a combination of the van der Waals and magnetic forces. Nevertheless, the magnetic forces are negligible with respect to the van der Waals ones. The obtained topography and amplitude images are thus almost unaffected. The second scan is done also in oscillating mode but this time it is done at a fixed height (with respect to the previously established topography) away from the surface in order to get rid of the van der Waals interactions and to image only the magnetic contribution. The phase image is recorded during that second scan and gives a picture of the magnetic interaction between the coated tip and the magnetically active material on the sample.

In the present case, some aggregates of about 10 nm in size could be seen in the topography images. The MFM scans were therefore performed at 50 nm above the sample surface. The morphology of obtained the sample is shown in Figure 5-12.

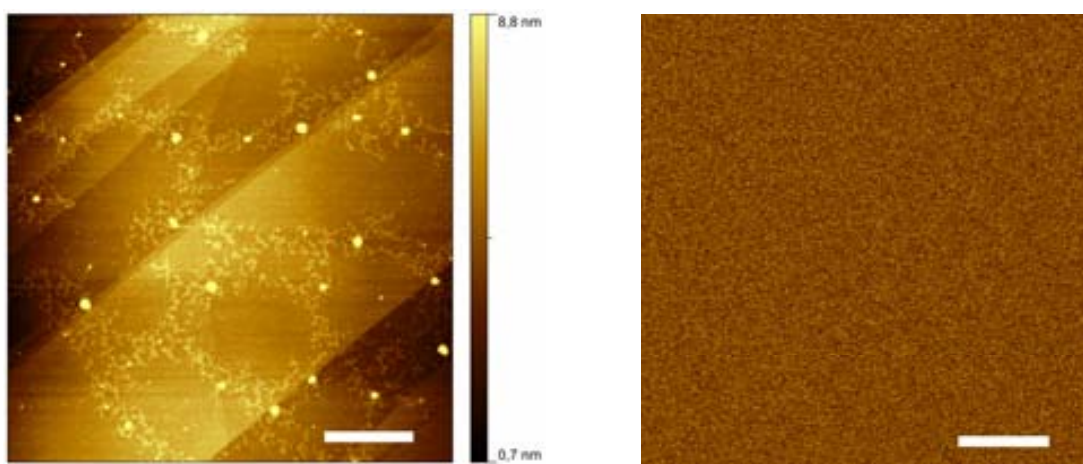


Figure 5-12. Topography (left) and MFM phase image (right) of $C^{22}Pc_2Tb$ on HOPG.

As can be seen on the above figure, the morphology of the film deposited from a 10^{-6} M solution of $C^{22}Pc_2Tb$ in toluene on HOPG is composed of big aggregates (bright dots) and a dewetting film which is roughly consistent in height (1.1 nm in average) with the height of one molecule (see Figure 5-13).

On the other hand, the MFM phase image shows no contrast whatsoever. Not only is it impossible to see contrasts inside the domains of $C^{22}Pc_2Tb$ but these can not even be distinguished from the graphite areas, and the phase image shows only the background noise of the experiment.

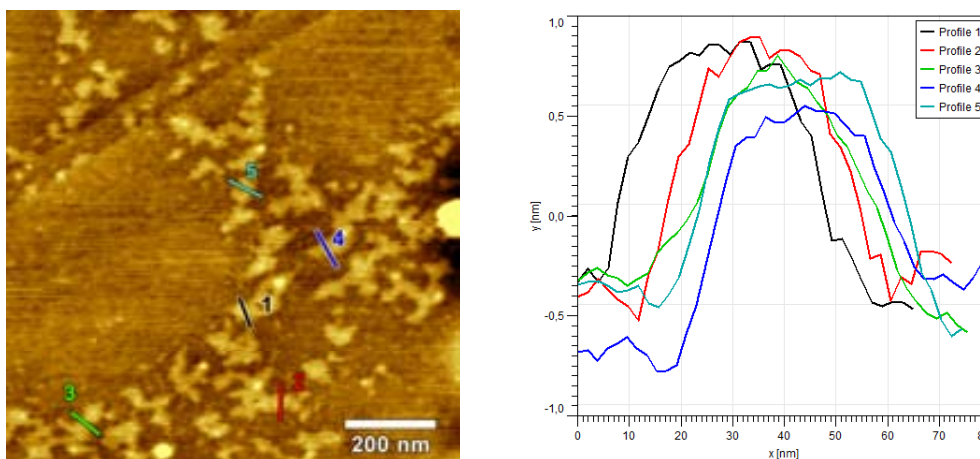


Figure 5-13. Close up of the topography of the sample (left) and height profiles of the observed structures (right).

This means that the magnetic force exerted on the cantilever during the scan is not strong enough to give a signal above the noise level of the experiment. Several reasons could explain this lack of response. First, since the experiment is done at room temperature, it is possible that the complexes flip their magnetization fast enough for the magnetic interaction between tip and sample to be averaged to zero. Also, given the apparent lack of organization of the film, it could be expected that the sample would present an isotropic distribution of the anisotropy axes. Given the small size of the complexes and the big size of the tip, the probe is thus probably sensing a great number of complexes at once with different orientations, for which the resulting averaged magnetic moment might be negligible. It is also possible that the strong diamagnetism be much stronger than the paramagnetism of the complexes and would therefore mask it. Finally, the magnitude of the magnetic interaction between tip and sample decays exponentially with the distance between them. It is therefore also possible that the lack of MFM signal be due to the fact that the measurement was done too far away from the sample (50 nm) to detect any appreciable tip-sample interaction.

5-4 Magnetic characterizations of double-decker terbium complexes deposited on HOPG

Because the unique double-decker terbium complex that exhibits a supramolecular organization on HOPG showing a good crystalline order is ${}^1\text{Pc}_2\text{Tb}$, we limited the magnetic characterization to organizations of ${}^1\text{Pc}_2\text{Tb}$ on graphite. The first magnetic

characterization that was used was spin-polarized scanning tunneling microscopy (SP-STM) at low temperature and in ultra-high vacuum (UHV).

These experiments were attempted at the Materials Physics and Chemistry Institute in Strasbourg in the group of Prof. Jean-Pierre Bucher. The supramolecular organization of bar-shaped aggregates on graphite was reproduced in Strasbourg before introducing it into the UHV-STM chamber. While the AFM images do not reach the same quality as those measured in Barcelona, perhaps due to the change of AFM machine or tip, it is nevertheless clear that the 2D-nanocrystals were successfully reproduced (see Figure 5-14). The phase images of the two newly prepared samples reproduced quite well the results obtained earlier. On the contrary, the topography images, this time, could not be resolved satisfactorily, perhaps due to the change of AFM equipment. The sample obtained in Strasbourg (Figure 5-14-*right*) was then inserted in the UHV chamber.

Unfortunately, due to several experimental problems with the equipment it could only be imaged after 3 days inside the setup and after having been subjected to several drastic changes in pressure and temperature (from ambient conditions of temperature and pressure down to 4 K and approximately 10^{-6} mbar).

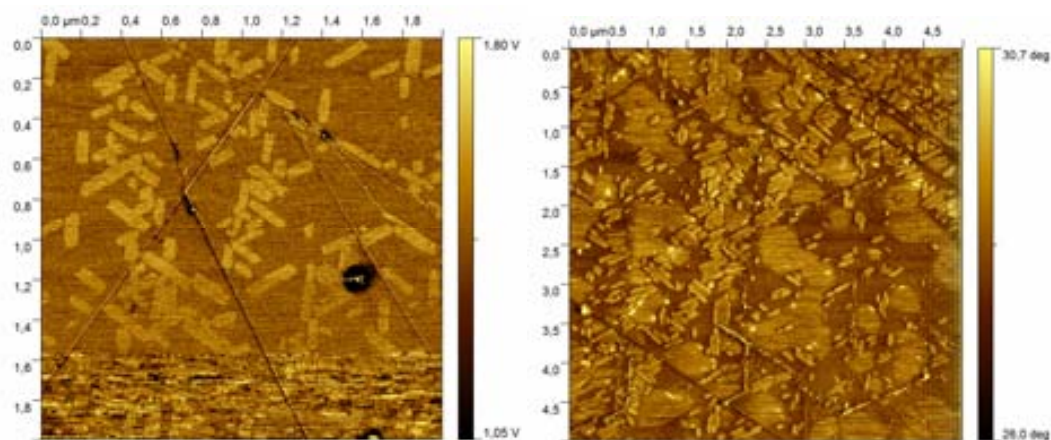


Figure 5-14. Phase AFM images of the samples reobtained in Barcelona (left) and in Strasbourg before inserting in the UHV-STM chamber (right).

The observed sample after 3 days did not allow to characterize the morphology of the sub-monolayers by either STM or AFM, and it was therefore not possible to study the compound by SP-STM either. Due to time limitations with the use of the equipment, it was not possible to prepare a fresh sample, and the magnetic characterization with this technique was given up. We decided therefore to move on to another magnetic

characterization allowing to characterize the magnetic behavior of these SMMs on a surface. The chosen method was X-ray magnetic circular dichroism spectroscopy (XMCD), but before studying the magnetic behavior of ${}^1\text{Pc}_2\text{Tb}$ with this technique, we decided to characterize the magnetic behavior of a bulk sample of ${}^1\text{Pc}_2\text{Tb}$.

5-4-1 Magnetic behavior of a bulk sample of ${}^1\text{Pc}_2\text{Tb}$

The dynamic magnetic behavior of a bulk sample of complex ${}^1\text{Pc}_2\text{Tb}$ was characterized by ac-magnetic susceptometry (see Figure 5-15). The blocking temperature of complex ${}^1\text{Pc}_2\text{Tb}$ at 997 Hz was found to be 41 K which is significantly smaller than the literature value (49 K) for the unsubstituted neutral double-decker terbium complex at the same frequency.^[21] Indeed it means that the relaxation time of ${}^1\text{Pc}_2\text{Tb}$ at 49 K is of approximately 3.4×10^{-5} s, thirty times smaller than the literature value of 1×10^{-3} s for Pc_2Tb .

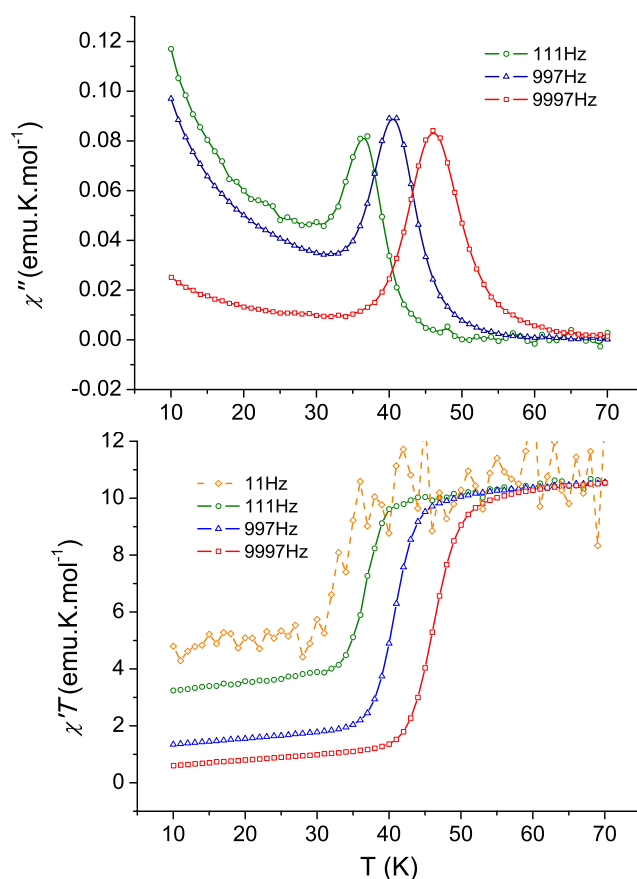


Figure 5-15. Temperature and frequency dependence of the out of phase (above) and in-phase (below) ac magnetic susceptibility of a bulk sample of complex ${}^1\text{Pc}_2\text{Tb}$.

^[21] N. Ishikawa, M. Sugita, N. Tanaka, T. Ishikawa, S.-y. Koshihara and Y. Kaizu, *Inorg. Chem.* **2004**, *43*, 5498-5500.

While the 11 Hz imaginary part χ'' was too noisy to allow extraction of any data, the real component $\chi'T$ still allowed a determination of the blocking temperature at this frequency.

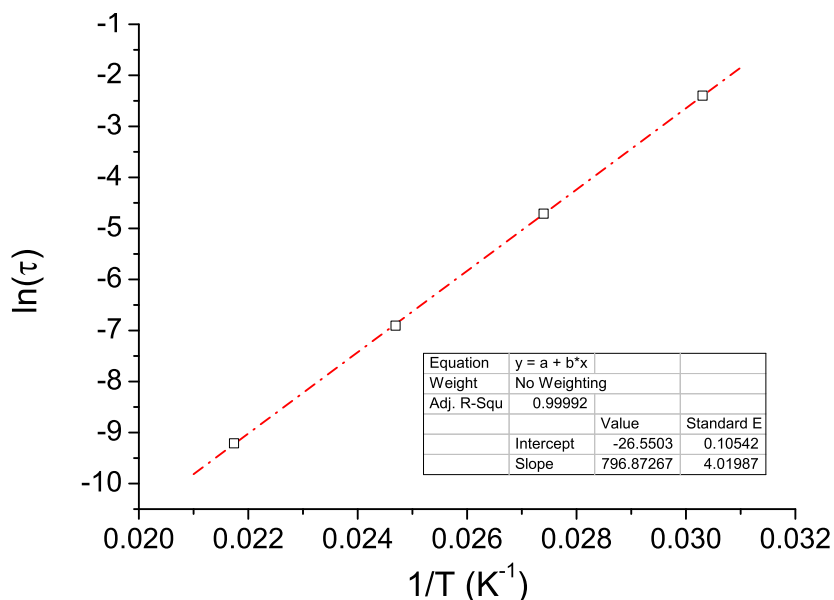


Figure 5-16. Arrhenius plot of the relaxation time τ versus the inverse of the temperature $1/T$ for a bulk sample of ${}^1\text{Pc}_2\text{Tb}$. The data are extracted from the observed blocking temperatures in the $\chi'T$ vs. T plots

The Arrhenius analysis (see Figure 5-16) shows that the relaxation of compound ${}^1\text{Pc}_2\text{Tb}$ in a bulk sample follows a thermally activated process with a pre-exponential factor of $\tau_0^{-1} = 3.39 \times 10^{11} \text{ s}^{-1}$ and an effective barrier height of $\Delta = 553 \text{ cm}^{-1}$. These values are both significantly higher than those found for a powder sample of the unsubstituted neutral double-decker phthalocyanine complex of terbium, $6.8 \times 10^8 \text{ s}^{-1}$ and 410 cm^{-1} , respectively, explaining the apparent different relaxation rates exhibited by both SMMs.

The hysteresis of magnetization of a bulk sample of compound ${}^1\text{Pc}_2\text{Tb}$ was first recorded with a quantum design MPMS equipped with a SQUID sensor. The experiment was done leaving the signal to equilibrate at each field value, and the obtained magnetization versus field curve showed almost no hysteresis. Indeed, the system relaxes so fast that the equilibration time at each field value is so long that the signal decays significantly even at 2 K (see Figure 5-17). This demonstrates that at this temperature, the Orbach process is not predominant since with the above determined parameters the relaxation time at 2 K should be of $1.74 \times 10^{16} \text{ s}$, which is obviously not

the case. Therefore, the magnetic relaxation at 2 K must then occur via an alternative process which can be either direct phonon-coupling or a Raman process.^[7]

The hysteresis measurement was done again at 2 K, but using this time a Quantum Design PPMS magnetometer equipped with a vibrating sample magnetometer (VSM) which allows to have a good sensitivity while scanning at a constant sweep rate of 1 T.min⁻¹.

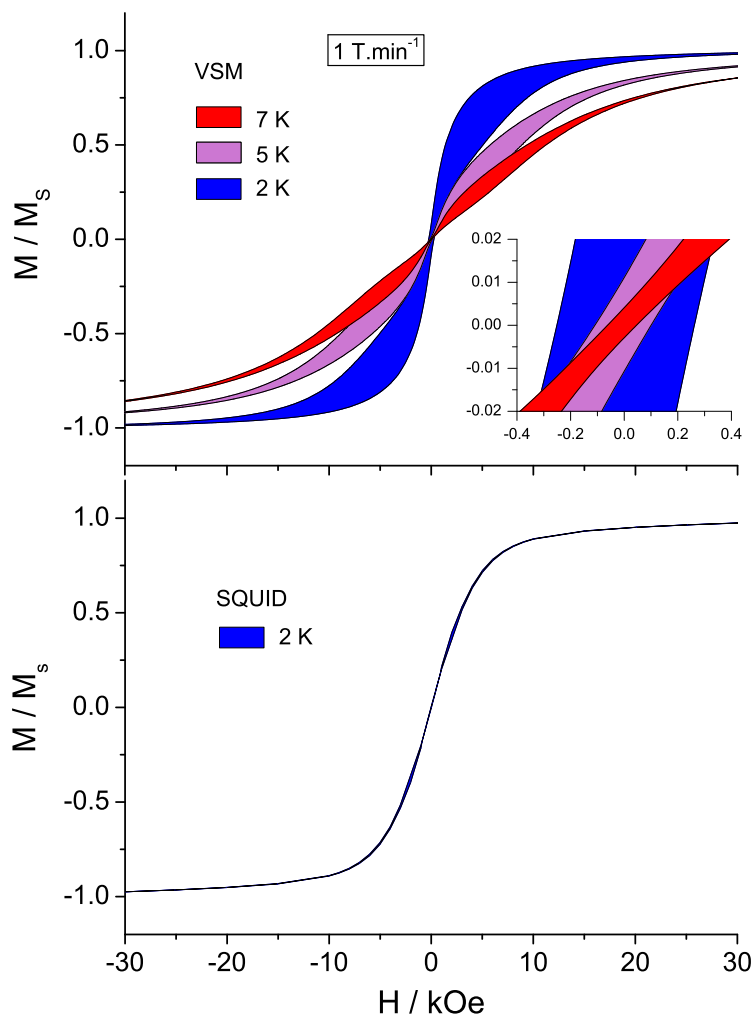


Figure 5-17. Bulk magnetization hysteresis of a sample of ¹Pc₂Tb measured at 2, 5 and 7 K using a PPMS equipped with a VSM sensor (above) and measured at 2 K with a MPMS equipped with a SQUID sensor (below). Inset: a zoom of the center region of the hysteresis curves showing the different coercive fields.^[†]

^[†] Note on magnetic units:

The magnetic field B and the magnetizing field H are related by the formula: $B = \mu_0 H$ in vacuum. Formally speaking, H is expressed in oersted (Oe) while B is expressed in teslas (T) in the SI units system or in gauss (G) in the CGS units system. Nevertheless, in CGS units $\mu_0 = 1$ and a magnetic field B of 1 T or 10 000 G corresponds to a magnetizing field of 10 000 Oe. In practice, many authors express either H or B in T or Oe indistinctively.

The obtained magnetization hysteresis curve at 2 K is shown in Figure 5-17, exhibiting a butterfly-shaped hysteresis,^[22] which is the typical one for these complexes.^[8] The measurement was repeated at 5 and 7 K allowing to compare the apparent coercive fields. As can be seen, while the magnetization hysteresis curve at 7 K is quite thin, even when measured with the VSM sensor at a sweeping rate of 1 T.min⁻¹, it broadens upon lowering the temperature, and the coercive field (see inset in Figure 5-17) is tripled by going from 7 K to 5 K and tripled again by lowering the temperature to 2 K, although even here it only reaches 0.4 kOe.

5-4-2 Magnetic behavior of a monolayer of ⁱPc₂Tb deposited on HOPG

The well defined morphology of the sub-monolayers of complex ⁱPc₂Tb, are a good example of a low dimensional assembly of independent magnetic centers. For this reason, the magnetic behavior of these 2D crystals is very interesting from the magnetic point of view. It is worth mentioning that all molecules of complex ⁱPc₂Tb lay directly on the graphite surface and therefore all of them should be affected by it, being of great importance knowing whether the molecules retain their SMM behavior under such conditions.

X-ray magnetic circular dichroism spectroscopy (XMCD) was used to characterize the magnetic behavior of complex ⁱPc₂Tb in such an organization. In this technique, two X-ray absorption spectra (XAS) are recorded with the helicity of the incident radiation parallel and antiparallel to the applied magnetic field. The difference of these two spectra provides the XMCD spectrum which is proportional to the magnetization of the sample. For a more detailed explanation of this technique, see Appendix II.

5-4-2-1 Magnetic behavior of the neutral complex [ⁱPc₂Tb]⁰ on HOPG

In order to characterize the magnetic properties of the neutral complex ⁱPc₂Tb when deposited on a HOPG surface, two samples were prepared: a submonolayer sample named ^{ML}[ⁱPc₂Tb]⁰ prepared using the dropcasting conditions described earlier and a thick layer sample, called ^{TL}[ⁱPc₂Tb]⁰, prepared by repeating ten times the previous dropcasting procedure. The differences between samples ^{ML}[ⁱPc₂Tb]⁰ and ^{TL}[ⁱPc₂Tb]⁰ should indicate the influence of the surface on the magnetic behavior of the molecules. Indeed, while the submonolayer ^{ML}[ⁱPc₂Tb]⁰ must be strongly influenced by the interaction of all the molecules with the surface, the thick layer should behave

essentially like the bulk compound in which the majority of molecules only feel the neighboring analogous molecules. The XAS spectra of the ${}^{\text{TL}}\text{Pc}_2\text{Tb}$ complexes is produced by the Tb^{3+} ion in which the energy of the incident X-ray radiations excite a 3d core electron to the 4f level and therefore it gives information about the 4f electronic structure governing the magnetic properties of the terbium ion.

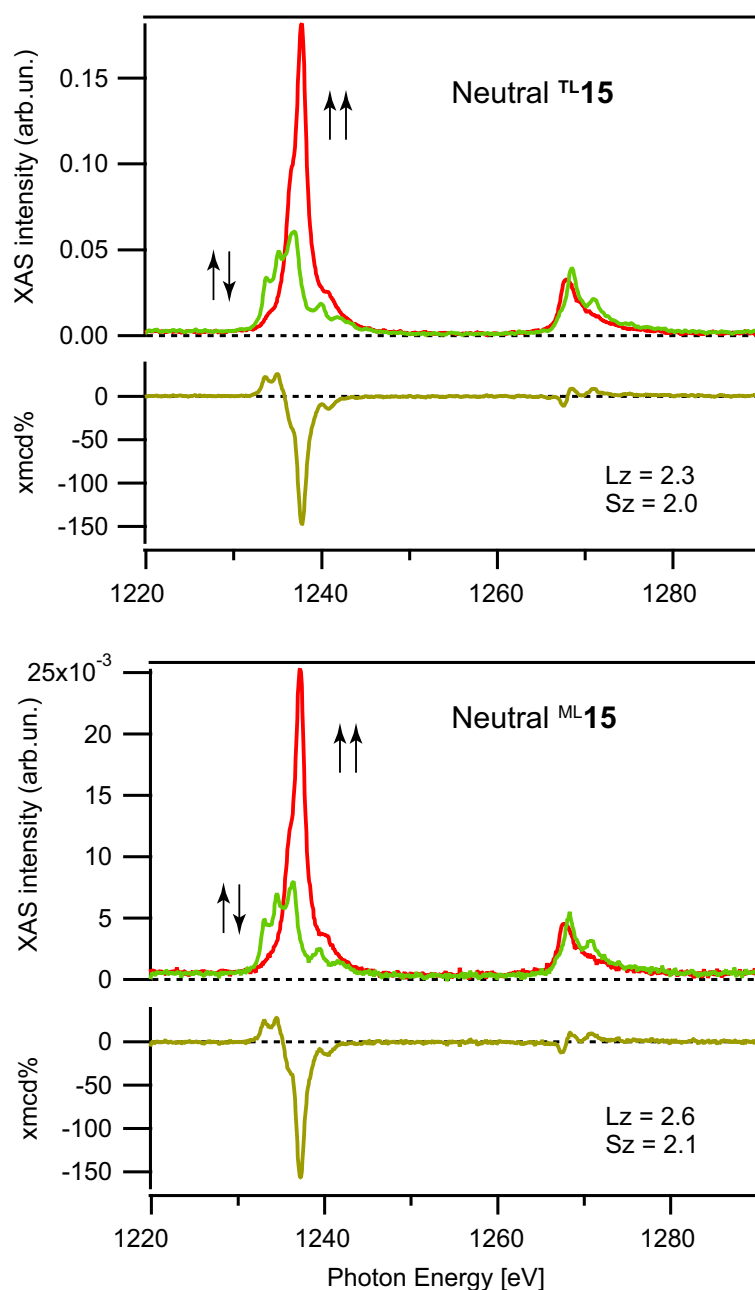


Figure 5-18. XAS spectra at the $M_{4,5}$ edge of Tb of a thick layer of the neutral complex ${}^{\text{TL}}[\text{Pc}_2\text{Tb}]^0$ (above), and a submonolayer of the same complex, ${}^{\text{ML}}[\text{Pc}_2\text{Tb}]^0$ (below) on HOPG, with helicities parallel ($\uparrow\uparrow$) and antiparallel ($\uparrow\downarrow$) to an applied magnetic field of 5 T at 7 K and the resulting XMCD spectra given by their difference.

The obtained spectral multiplet is split in the M_4 and M_5 bands around 1270 and 1240 eV respectively.^[23] At first glance, in the present experiment, there is qualitatively not much difference in the spin polarized XAS spectra of both monolayer and thick layer samples of compound ${}^i\text{Pc}_2\text{Tb}$ (see Figure 5-18).

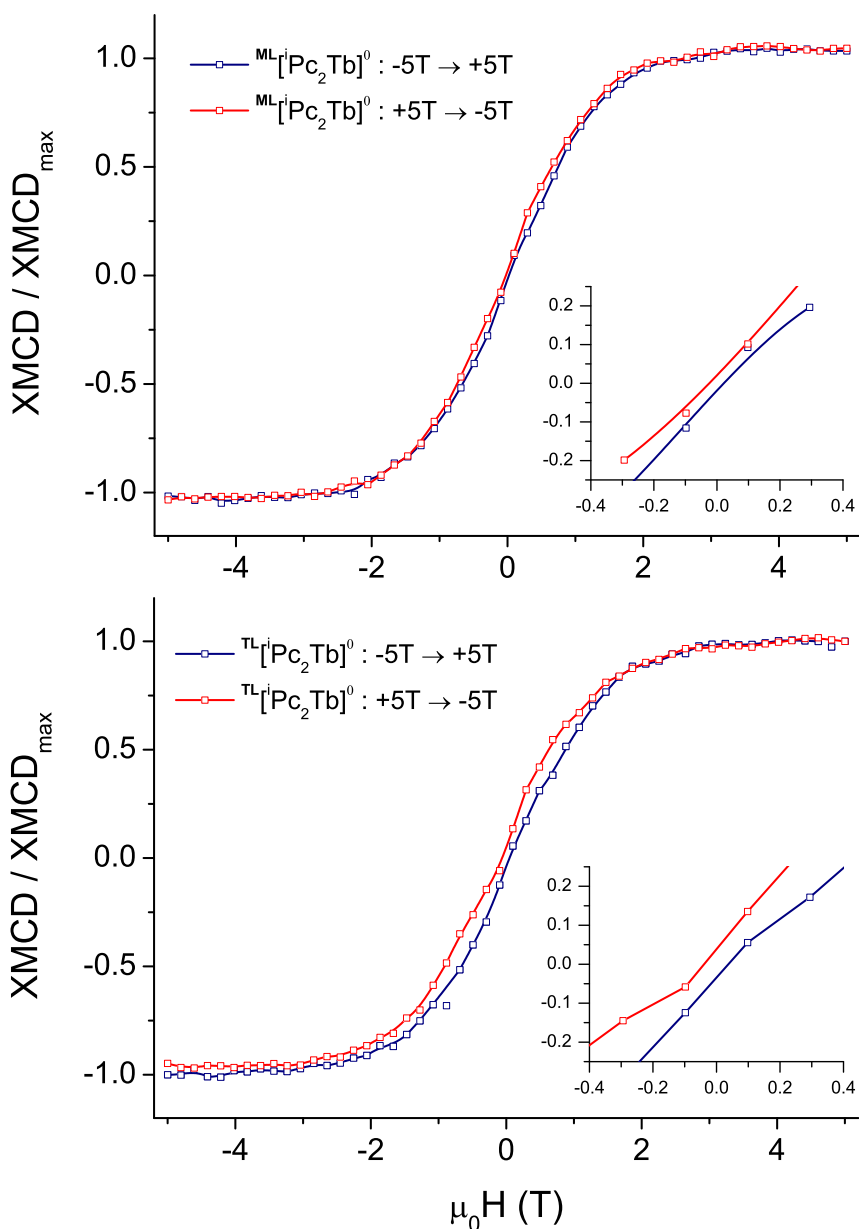


Figure 5-19. XMCD detected hysteresis of magnetization for a submonolayer $\text{ML}^i\text{Pc}_2\text{Tb}^0$ (above) and a thick layer $\text{TL}^i\text{Pc}_2\text{Tb}^0$ (below) of the neutral form of compound ${}^i\text{Pc}_2\text{Tb}$ on HOPG measured at 7 K and $dH/dt = 1 \text{ T}\cdot\text{min}^{-1}$. The insets show enlargements of the central part of both hystereses.

^[23] G. van der Laan, J. C. fuggle, M. P. van Dijk, A. J. Burggraaf, J. M. Esteva and R. Karnatak, *J. Phys. Chem. Solids* **1986**, 47, 413-416.

Also, when computing the XMCD spectra, they look quite similar both in shapes and intensities. This means that the surface is not affecting much the 4f electronic structure of the Tb ion, which is responsible for its magnetic behavior, since both samples present the same features.

The XMCD spectra also permit measurement of the hysteresis curves, which are recorded in two passes for practical reasons. First, the XMCD intensity at a given wavelength is monitored while sweeping the magnetic field from -60 kOe to +60 kOe, and the second part is recorded by sweeping the magnetic field from +60 kOe to -60 kOe. For this experiment, the measurement was done monitoring the XMCD intensity of the M_5 band at 7 K, at a field sweeping rate of $1 \text{ T}\cdot\text{min}^{-1}$. The resulting XMCD detected magnetization hysteresis curves are given in Figure 5-19.

At first glance, the two hysteresis curves look quite similar in shape. However, it is worth noting that the butterfly loops are more open for the thick layer sample $^{TL}[\text{}^i\text{Pc}_2\text{Tb}]^0$ than for the submonolayer sample $^{ML}[\text{}^i\text{Pc}_2\text{Tb}]^0$. There is almost no remnant magnetization for either of the two samples in these conditions, and the coercive field of the submonolayer sample (see inset in Figure 5-19) is not significantly different from zero, which is to be expected at this temperature (see the 7 K bulk measurement inset in Figure 5-17). While they differ slightly from one another, the hysteresis curves of the thick layer and the submonolayer of the neutral complex $^i\text{Pc}_2\text{Tb}$ on HOPG are both very similar to the bulk measurement made in the same conditions (7 K , $1 \text{ T}\cdot\text{min}^{-1}$), which means that the magnetic behavior of $[\text{}^i\text{Pc}_2\text{Tb}]^0$ is essentially preserved when deposited on the graphite surface. As it appears, there is therefore not much influence of the surface on the magnetization hysteresis.

5-4-2-2 Magnetic behavior of the anionic complex $[\text{}^i\text{Pc}_2\text{Tb}]^-$ on HOPG

The anionic form of complex $^i\text{Pc}_2\text{Tb}$, $[\text{}^i\text{Pc}_2\text{Tb}]^-$, is stable in degassed acetone or THF over several days. A 10^{-5}M solution of the anionic complex in degassed acetone was prepared, and deposited by dropcasting on HOPG first once and then repeating the deposition ten times so as to obtain a monolayer anionic sample $^{ML}[\text{}^i\text{Pc}_2\text{Tb}]^-$ and a thick layer anionic sample $^{TL}[\text{}^i\text{Pc}_2\text{Tb}]^-$, respectively. These samples were again characterized at the $M_{4,5}$ edge of Tb by XMCD just like for the samples of the neutral complex.

The results (see Figure 5-20) show that the monolayer sample of the anionic form of complex $[\text{}^i\text{Pc}_2\text{Tb}]^-$ on HOPG behaves just like the neutral form in the same conditions,

as can be seen in the XMCD curves in Figure 5-20, while the thick layer has different characteristics. The main difference from one sample to the other resides in the intensity of the XMCD spectra. One could think that the reason for such a big difference is the instability of the anionic form in ambient conditions, but this is not the case here as will be shown later on.

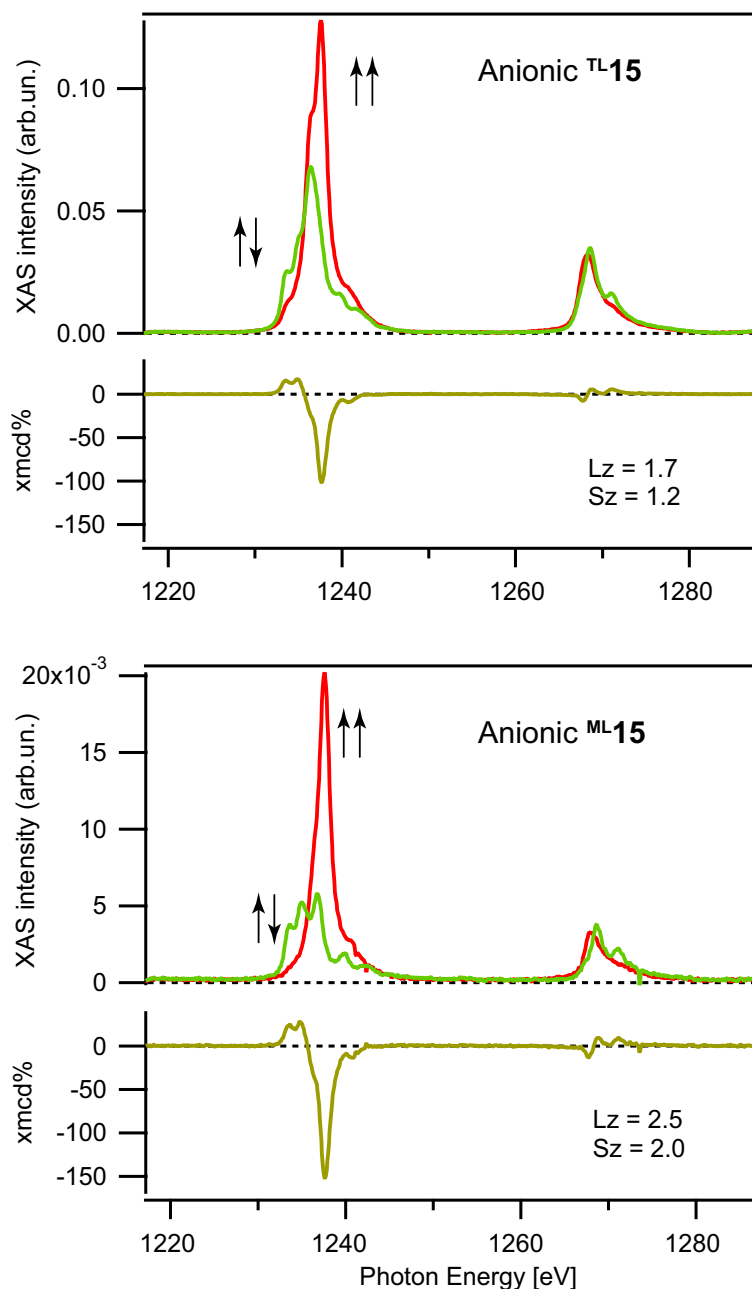


Figure 5-20. XAS spectra at the M_{4,5} edge of Tb of a thick film of the anionic complex, ^{Tl}[ⁱPc₂Tb]⁻ (above), and a thin film of the same, ^{Ml}[ⁱPc₂Tb]⁻ (below), on HOPG, with helicities parallel and antiparallel to an applied magnetic field of 5 T at 7 K and the resulting XMCD spectra given by their difference.

As explained in more details in appendix II, the XMCD experiments can be done in several ways, since one can: a) monitor directly the X-ray absorption or b) measure the X-ray fluorescence or c) measure the flow of photoelectrons from the ground to the sample. The latter type of experiment, namely using the total electron yield as a detection method, are advantageous for the characterization of complex ${}^i\text{Pc}_2\text{Tb}$, since this detection method is a sensitive and selective probe of the outermost layers of compound,^[24] because the electrons are only emitted by the first 50-65 Å of the material. Therefore, with this detection method, in both thick and thin layer samples, the outermost sensitive layer is always in contact with the ambient atmosphere. The thick layer and monolayer samples should therefore provide identical XMCD spectra if an apparent oxidation were caused by the ambient oxygen. Since it is not the case, it is possible to exclude the oxidation of the outermost layer of double-decker complexes with air as a cause of the observed difference of behavior between ${}^{\text{ML}}[{}^i\text{Pc}_2\text{Tb}]^-$ and ${}^{\text{TL}}[{}^i\text{Pc}_2\text{Tb}]^-$.

An alternative explanation would be that the oxidation of the anionic molecules is a result of a surface effect at the interface between the graphite and the double-decker molecules. In the monolayer sample, we supposedly have a sub-monolayer coverage of the graphite, which means that in an ideal case, all of the complexes are in interaction with the graphite surface, which means that all of the anionic molecules are oxidized to the neutral species and sensed as such by XMCD. In the thick layer structure, only the bottom layer of molecules is interacting with the surface and is consequently oxidized by it. The next layers are formed by unaffected anionic complexes (see Figure 5-21), and therefore the resulting XMCD spectra would be dominated by these unaffected anionic molecules.

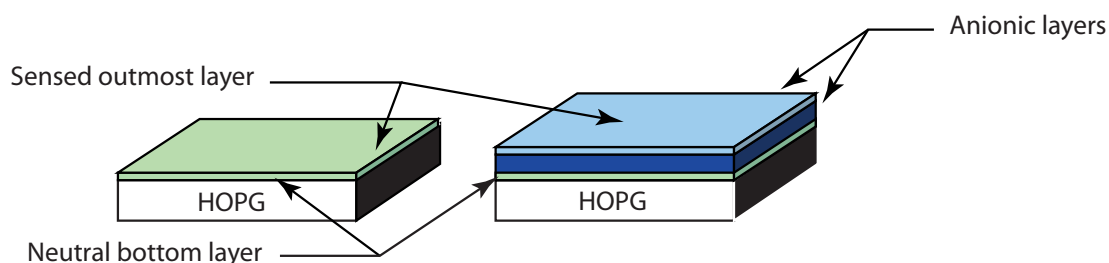


Figure 5-21. Schematic representation of the monolayer (left) and thick layer (right) structures formed by the anionic compound ${}^i\text{Pc}_2\text{Tb}]^-$ deposited on HOPG from a 10^{-5}M solution in acetone.

^[24] T. Funk, A. Deb, S. J. George, H. Wang and S. P. Cramer, *Coord. Chem. Rev.* **2005**, *249*, 3-30.

The XMCD detected hysteresis of magnetization recorded for the thick and monolayer of the anionic form of complex ${}^i\text{Pc}_2\text{Tb}$ are shown in Figure 5-22.

For the monolayer sample, the saturation values overlap well, and it presents a relatively thin hysteresis curve which resembles that of the thin submonolayer sample of the neutral complex, which is in good agreement with the apparent similarity of the XMCD curves of ${}^{\text{ML}}[{}^i\text{Pc}_2\text{Tb}]^0$ and ${}^{\text{ML}}[{}^i\text{Pc}_2\text{Tb}]^-$ and supports the hypothesis that the compound is oxidized on the graphite surface in sample ${}^{\text{ML}}[{}^i\text{Pc}_2\text{Tb}]^-$.

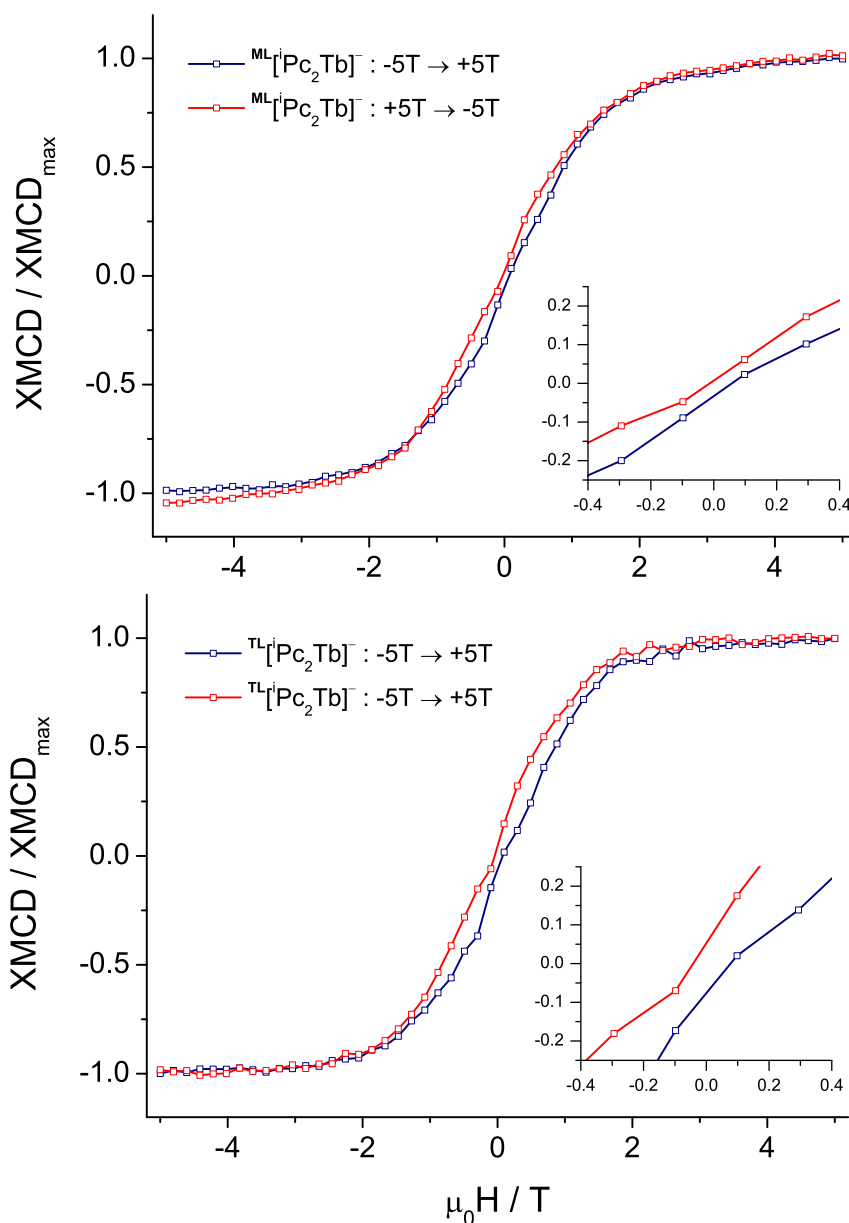


Figure 5-22. XMCD detected hysteresis of magnetization for a submonolayer ${}^{\text{ML}}[{}^i\text{Pc}_2\text{Tb}]^-$ (above) and a thick layer ${}^{\text{TL}}[{}^i\text{Pc}_2\text{Tb}]^-$ (below) of the anionic form of compound ${}^i\text{Pc}_2\text{Tb}$ on HOPG measured at 7 K and $dH/dt = 1 \text{ T}\cdot\text{min}^{-1}$. The insets show the enlargement of the central part of both hystereses.

In the case of the thick layer sample, the saturation of the XMCD signal at both negative and positive field values coincide, which puts in evidence the good quality of the measurement. The resulting hysteresis curve of magnetization also presents a butterfly-shape which is typical of those compounds, and the hysteresis loops of ${}^{\text{ML}}[\text{}^{\text{i}}\text{Pc}_2\text{Tb}]^-$ appear slightly more opened than in the case of sample ${}^{\text{ML}}[\text{}^{\text{i}}\text{Pc}_2\text{Tb}]^0$.

5-5 Conclusions

XMCD was used as a successful tool to record the magnetization hysteresis of a submonolayer of two redox states of a double-decker phthalocyanine lanthanide complex ${}^{\text{i}}\text{Pc}_2\text{Tb}$ in the vicinity of a surface.

Magnetization hysteresis had been previously reported only for the double-decker phthalocyanine complexes of some lanthanides in dilute solid solutions in a diamagnetic matrix of the isomorphous Yttrium complex, and we have shown in Chapter 4 how dilute solutions of the anionic, neutral and cationic redox states of complex ${}^{\text{i}}\text{Pc}_2\text{Tb}$ all present magnetization hysteresis in a frozen dilute solvent glass. Nevertheless, to the best of our knowledge, it is the first time that magnetization hysteresis is observed for a double-decker phthalocyanine lanthanide complex in the vicinity of a surface. Importantly, the slow magnetic relaxation rate, characteristic of these compounds is still present in a submonolayer sample of the neutral and anionic double-decker terbium complexes $[\text{}^{\text{i}}\text{Pc}_2\text{Tb}]^0$ and $[\text{}^{\text{i}}\text{Pc}_2\text{Tb}]^-$, and the behavior of the samples is not very different from the bulk complex measured in the same conditions.

Unlike the previously described Fe_4 on gold,^[6] it is important to notice that here the terbium complexes are not wired covalently to the surface by a long alkyl chain but are on the contrary lying directly on top of the graphite surface. The perturbation induced by the surface on the SMM could have been higher and destroyed the SMM properties, but the experiment showed that this is not the case.

Bibliography

- [1] M. Cavallini, J. Gomez-Segura, D. Ruiz-Molina, M. Massi, C. Albonetti, C. Rovira, J. Veciana, F. Biscarini, *Angew. Chem. Int. Ed.* **2005**, *44*, 888-892.
- [2] M. Affronte, *J. Mater. Chem.* **2009**, *19*, 1731-1737.
- [3] L. Bogani, W. Wernsdorfer, *Nat. Mater.* **2008**, *7*, 179-186.
- [4] D. Gatteschi, A. Cornia, M. Mannini, R. Sessoli, *Inorg. Chem.* **2009**, *48*, 3408-3419.
- [5] L. Vitali, S. Fabris, A. M. Conte, S. Brink, M. Ruben, S. Baroni, K. Kern, *Nano Lett.* **2008**, *8*, 3364-3368.
- [6] M. Mannini, F. Pineider, P. Sainctavit, C. Danieli, E. Otero, C. Sciancalepore, A. M. Talarico, M.-A. Arrio, A. Cornia, D. Gatteschi, R. Sessoli, *Nat. Mater.* **2009**, *8*, 194-197.
- [7] N. Ishikawa, M. Sugita, T. Ishikawa, S.-y. Koshihara, Y. Kaizu, *J. Phys. Chem. B* **2004**, *108*, 11265-11271.
- [8] N. Ishikawa, M. Sugita, W. Wernsdorfer, *Angew. Chem. Int. Ed.* **2005**, *44*, 2931-2935.
- [9] N. Ishikawa, *Polyhedron* **2007**, *26*, 2147-2153.
- [10] J. Gomez-Segura, I. Diez-Perez, N. Ishikawa, M. Nakano, J. Veciana, D. Ruiz-Molina, *Chem. Commun.* **2006**, 2866-2868.
- [11] A. S. Klymchenko, J. Sleven, K. Binnemans, S. De Feyter, *Langmuir* **2006**, *22*, 723-728.
- [12] A. V. Ivanov, P. A. Svinareva, L. G. Tomilova, N. S. Zefirov, *Russ. Chem. Bull. Int. Ed.* **2006**, *55*, 281-286.
- [13] R. P. Linstead, M. Whalley, *J. Chem. Soc.* **1952**, 4839-4846.
- [14] T. Gross, F. Chevalier, J. S. Lindsey, *Inorg. Chem.* **2001**, *40*, 4762-4774.
- [15] S. Furukawa, N. Crivillers, A. Minoia, A. Ver Heyen, M. Mas-Torrent, C. Sporer, M. Linares, A. Volodin, C. Van Haesendonck, M. Van Der Auweraer, R. Lazzaroni, S. De Feyter, J. Veciana, C. Rovira, *J. Am. Chem. Soc.* **2009**, *131*, 6246-6252.
- [16] P. Iavicoli, M. Simon-Sorbed, D. B. Amabilino, *New J. Chem.* **2009**, *33*, 358-365.
- [17] M. Linares, P. Iavicoli, K. Psychogiopoulou, D. Beljonne, S. De Feyter, D. B. Amabilino, R. Lazzaroni, *Langmuir* **2008**, *24*, 9566-9574.
- [18] A. G. Gurek, T. Basova, D. Luneau, C. Lebrun, E. Koltsov, A. K. Hassan, V. Ahsen, *Inorg. Chem.* **2006**, *45*, 1667-1676.
- [19] D. Sun, S. V. Rosokha, J. K. Kochi, *J. Phys. Chem. B* **2007**, *111*, 6655-6666.
- [20] R. S. Rowland, R. Taylor, *J. Phys. Chem.* **1996**, *100*, 7384-7391.
- [21] N. Ishikawa, M. Sugita, N. Tanaka, T. Ishikawa, S.-y. Koshihara, Y. Kaizu, *Inorg. Chem.* **2004**, *43*, 5498-5500.
- [22] I. Chiorescu, W. Wernsdorfer, A. Müller, H. Bögge, B. Barbara, *Phys. Rev. Lett.* **2000**, *84*, 3454.
- [23] G. van der Laan, J. C. fuggle, M. P. van Dijk, A. J. Burggraaf, J. M. Esteva, R. Karnatak, *J. Phys. Chem. Solids* **1986**, *47*, 413-416.
- [24] T. Funk, A. Deb, S. J. George, H. Wang, S. P. Cramer, *Coord. Chem. Rev.* **2005**, *249*, 3-30.